The synthesis of novel single source precursors for the CVD of fluorine-doped tin oxide

Stanley, Joanne Elizabeth

Award date:
1997

Awarding institution:
University of Bath

THE SYNTHESIS OF NOVEL SINGLE SOURCE PRECURSORS FOR THE CVD OF FLUORINE-DOPED TIN OXIDE

submitted by Joanne Elizabeth Stanley

for the degree of PhD
of the University of Bath
1997

ProQuest LLC
789 East Eisenhower Parkway
P.O. Box 1346
Ann Arbor, MI 48106-1346

ABSTRACT

The research described in this thesis has been concerned with the synthesis and characterisation of a range of novel single source precursors for the CVD of fluorine-doped tin oxide. Three classes of compound have been investigated; perfluoroalkyltin compounds, fluorinated organotin carboxylates and fluorinated organotin alkoxides.

Chapter One - Introduction - provides information regarding the applications of tin oxide thin films and the various deposition techniques available. Chemical vapour deposition (CVD) is then discussed, followed by a survey of the current precursors used for the CVD of tin oxide and fluorine-doped tin oxide thin films. The chemistry of organotin(IV) compounds is also included to provide basic information regarding the chemistry of the compounds discussed in subsequent chapters.

Chapter Two - Perfluoroalkyltin Compounds - describes the synthesis and characterisation of a range of perfluoroalkyltin compounds containing a variety of alkyl and fluorinated groups. Compounds have been characterised by Mössbauer and NMR spectroscopy, and subsequently tested as CVD precursors. Conditions used for the deposition experiments are described, followed by analysis to identify the quality of the films obtained.

Chapter Three - Organotin Carboxylates - details the synthesis and characterisation of a range of fluorinated organotin carboxylates containing a variation in the alkyl and fluorinated groups. Compounds have been characterised by infra-red, Mössbauer and NMR spectroscopy, with single crystal X-ray diffraction characterisation for $Et_3SnO_2CC_2F_5$ and $Me_2Sn(O_2CCF_3)_2(OH_2)$. Details of the conditions and subsequent film analysis for the CVD of a selection of compounds is then discussed.

Chapter Four - Organotin Alkoxides - details the synthesis and characterisation of a range of fluorinated tributyltin alkoxides containing a variation in the fluorinated alkoxide ligand. Compounds have been characterised by Mössbauer and NMR

spectroscopy, and subsequently tested as CVD precursors. Details of the CVD conditions used and the film analysis are included.

A brief conclusion follows to compare the three classes of compound investigated, and highlight the main discoveries. Appendices provide information regarding the source of the starting materials, along with the crystallographic data and details of the instrumentation. Details of the CVD reactor are also included and a numerical list of all of the compounds prepared.

ACKNOWLEDGEMENTS

Firstly, I would like to thank my supervisor, Dr. Kieran Molloy for his guidance throughout the project, and especially for his support during the writing of this thesis. I would also like to thank Dr. Mary Mahon for the crystallographic material included in this work. Financial support from the E.P.S.R.C. and Pilkington plc is gratefully acknowledged.

I would also like to thank the technical staff, Robert, Ahmed and Sheila for their help and co-operation during the laboratory work, and Alan Carver, Dave and Harry for the microanalysis and NMR spectroscopy.

I must also extend my gratitude to my colleagues in the laboratory for making my time at Bath an enjoyable one. Particular thanks go to Mike Hill, Rob Harker, John McGinley, Dave Smith, Tim Paget (and Ronnie, even though she wasn't actually in my lab!) Chris Rainford, Phil Wright, Mike Maxwell, Virginie Ogrodnik and Paul Williams. I know there are lots of other people who have come and gone, but I wanted to keep the thesis short! Thanks folks, it wouldn't have been as much fun without you lot!

Finally, I would like to thank the three most important people in my life, my mother, my sister Catherine and of course my husband. I would like to thank my mother for her fantastic support and belief in my ability to succeed, and my sister for being a wonderful friend, and buying me lots of lunches! For my husband Paul, I am extremely grateful for his support and patience throughout this work, and of course for the succession of improved vehicles with which I was provided!

ABBREVIATIONS

Ac	:	Acetate	NMR	:	Nuclear Magnetic Resonance
b.p.	:	boiling point	Ph	:	Phenyl
bipy	:	bipyridyl	ppm	:	parts per million
Bu	:	Butyl	^{i}Pr	:	Isopropyl
^{t}Bu	:	Tertiary Butyl	py	:	pyridyl
CVD	:	Chemical Vapour Deposition	q	:	quartet
DBTD	:	Dibutyltin Diacetate	QS	:	Quadrupole Splitting
DMF	:	Dimethylformamide	quin	:	quintet
DMT	:	Dimethyltin Dichloride	r.t.	:	room temperature
dt	:	doublet of triplets	R_f	:	Fluorinated Alkyl Group
Et	:	Ethyl	s	:	singlet
FTIR	:	Fourier Transform Infra-Red	SEM	:	Scanning Electron Microscopy
HPz	:	Pyrazole	sept	:	septet
IR	:	Infra-Red	Std.	:	Standard
IS	:	Isomer Shift	t	:	triplet
L	:	Ligand	terpy	:	terpyridyl
m	:	multiplet	THF	:	Tetrahydrofuran
m.p.	:	melting point	TMT	:	Tetramethyltin
Me	:	Methyl	tt	:	triplet of triplets
Mes	:	Mesityl	XRD	:	X-Ray Diffraction
MOCVD	:	Metal-Organic CVD	XRF	:	X-Ray Fluorescence

CONTENTS

Chapter One

Introduction

1.1 TIN(IV) OXIDE THIN FILMS

1.1.1 Background

Transparent conducting oxides are a very important group of materials due to the wide range of their possible applications in both industry and research. There are several review articles which discuss the vast number of materials studied.[1-3] Of these, tin(IV) oxide[4-5] is extremely important as it is the first transparent conductor to have received significant commercialisation, and due to the nature of this thesis will be discussed at greater length. Throughout the content of this thesis, the tin oxide described will refer to tin(IV) oxide (SnO_2). Tin oxide crystallises with the tetragonal rutile structure. The unit cell contains six atoms, two tin and four oxygen as illustrated in Figure 1.1.

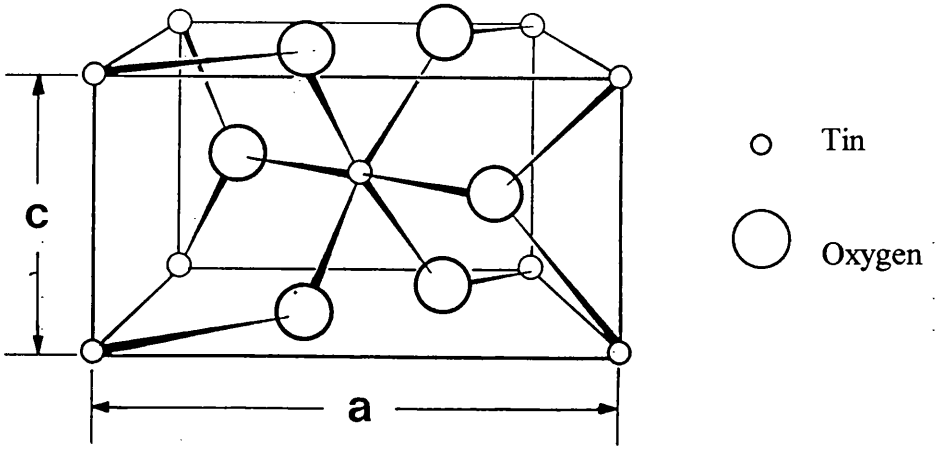

Figure 1.1 The Unit Cell of Tin Oxide

Each tin atom is at the centre of six oxygen atoms placed approximately at the corners of an octahedron, and every oxygen atom is surrounded by three tin atoms approximately at the corners of an equilateral triangle.

Tin oxide is an insulator in its stoichiometric form, but in practice the non-stoichiometric form is always encountered and therefore it acts as an n-type, wide band gap (> 3.5 eV) semiconductor. It is an ionic compound for which the conduction band is

formed predominantly from the metal orbitals, while the oxygen orbitals make up most of the filled valence band. However, the transition from the uppermost valence band into the lowest conduction band is *dipole forbidden* so that the gap is so referred.[6]

1.1.2 Doping of Tin Oxide

Tin oxide can be made to be a conductor without affecting its visible transmission (hence the name *transparent conductor*) by making it non-stoichiometric or by adding suitable dopants.[7] Doping tin oxide to introduce a surplus of electrons is the preferred method, as it is difficult to control the concentration of oxygen vacancies in pure non-stoichiometric SnO_2. The two most commonly used elements are antimony,[8-13] which substitutes tin, and fluorine, substituting oxygen. They both provide an extra electron to the lattice which increases the n-type conductivity of tin oxide. Other less recognised dopants include arsenic,[14] phosphorus,[15] and a number of transition metals such as platinum[16] and vanadium.[17]

1.1.2.1 n and p Type Doping

There are two doping mechanisms which can have the effect of increasing the conductivity, n-type and p-type doping. These techniques are illustrated in Figure 1.2.

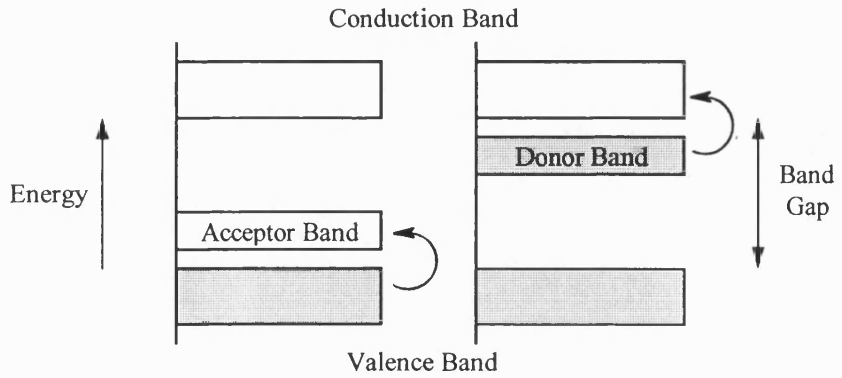

(a) p-type doping (b) n-type doping

Figure 1.2 p-type and n-type Doping

A dopant with fewer electrons than its host can form a narrow band that accepts electrons from the valence band [Figure 1.2 (a)]. The holes in the band are mobile which gives rise to *p-type semiconductivity*, the p indicating that the holes are relatively positive with respect to the electrons in the band.

A dopant with more electrons than its host forms a narrow band that can supply electrons to the conduction band [Figure 1.2 (b)]. The electrons it supplies are mobile which gives rise to *n-type semiconductivity*, where n denotes the negative charge of the carriers. This is the mechanism which occurs in the doping of tin oxide.

1.1.2.2 Fluorine-Doped Tin Oxide

Due to its widespread use, there are many articles in the literature which discuss fluorine as a dopant.[18-34] There has also been a limited amount of research on the effect of doping with another element in addition to fluorine, such as phosphorus[35] or antimony.[36]

When doping tin oxide with fluorine, the added dopant carries an extra electron to its host oxygen which enhances the n-type conductivity as previously discussed. The properties of the fluorine-doped tin oxide films are strongly dependent on the content and distribution of the fluorine. To be effective, the fluorine must be incorporated in oxygen vacancies. A halogen substituting for oxygen has the effect of disturbing the filled valence band of tin oxide, and only slightly disturbs the electrons in the conduction band.

Substituting a tin atom for a dopant such as antimony however, has the effect of inducing a large amount of disorder in the conduction band. This reduces the mobility of the electrons, which has the subsequent effect of deteriorating the conductivity and transparency of the material. Fluorine is therefore more appealing as a dopant, and produces coatings of a higher conductivity, optical transmittance, and infrared reflectance than antimony-doped films. It is possible to use other halogens as dopants but heavier halogens are so large that they distort the lattice and cause additional

electron scattering. Fluorine causes the least scattering of all the halogens, and fluorine doping produces tin oxide films with the highest conductivity and transparency.[37]

1.1.2.3 Indium Tin Oxide

Thin film tin-doped indium oxide (ITO) is another extremely important material, and due to its highly conductive and transparent nature is used in a wide range of applications.[38-45] The high conductance is generated by a high level of tin dopants and oxygen vacancies in the In_2O_3 lattice. The major use is found in solar cell applications due to its extremely high optical transmittance, wide bandgap and low electrical resistivity (10^{-4} Ω cm). As ITO exhibits such excellent optical and electrical properties, alternative dopants to tin appear to be rather rare, although the effect of sulphur has been explored.[46]

Although ITO has superior optical and electrical properties, tin oxide films exhibit more stable mechanical and chemical properties, so the two materials find optimum use in different applications. Another major advantage of tin oxide is the substantially lower cost of this material.

1.2 APPLICATIONS OF TIN OXIDE THIN FILMS

Tin oxide has some very important properties, such as high electrical conductivity, high transparency in the visible region, high reflectivity in the IR region, good adhesion to the substrate, and very good chemical stability and mechanical resistance. These properties make tin oxide a suitable material for a vast number of applications, which will be briefly discussed below.

1.2.1 Transparent Heat Reflecting Films

An extremely important application of conducting tin oxide is as a coating for windows.[47-49] It is only over the past thirty years that thin films have been used to enhance the thermal performance of window glazings. The solar spectrum is shown in Figure 1.3 in which the three important regions of the electromagnetic spectrum are indicated, and that of a blackbody.

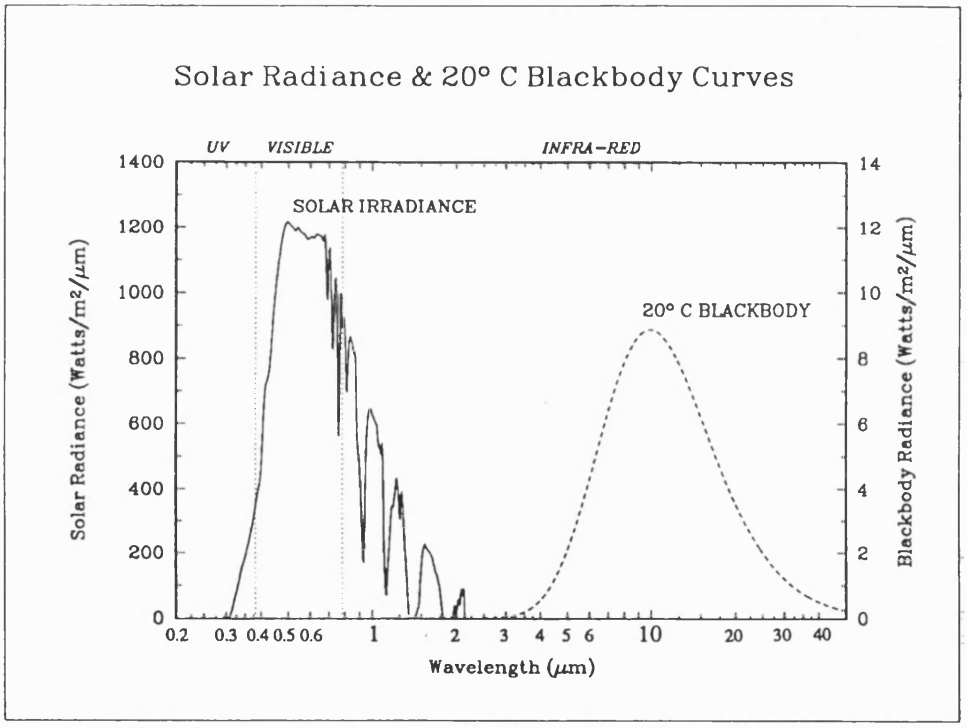

Figure 1.3 The Solar Spectrum and that of a Blackbody

A surface of standard soda-lime float glass facing air has a high emissivity of approximately 0.85,[50] which means that 85% of the blackbody infra-red radiation is lost to the outdoors. In winter, windows are major sources of heat loss by conduction, convection and also radiation due to the high emissivity value of glass. Conduction and convection losses can be drastically reduced by the use of multiple glazings, but heat losses by radiation emittance remain. To prevent these unwanted effects, a fluorine-doped tin oxide film can be applied to the glass to act as a spectrally selective coating.

Energy Advantage Low *E* (low emissivity) glass was introduced in 1990 to perform this function.[51] It is a high performance, near colour neutral, pyrolytically low emissivity product specifically developed for residential and commercial applications. The effect of the coating can clearly be seen in Figure 1.4 which shows the spectrally selective nature of the coated glass.

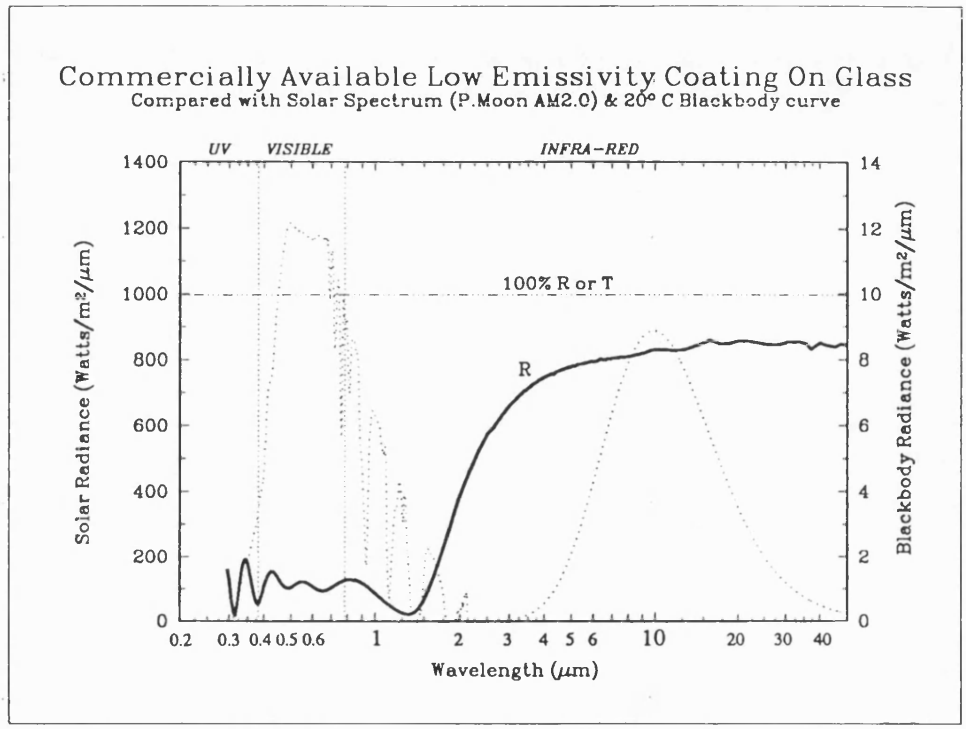

Figure 1.4 The Effect of Fluorine-Doped Tin Oxide Coated Glass

In practice, low *E* films are applied to one of the inner surfaces of an insulating glass unit which allows most of the sun's short wavelength energy to penetrate the home. This absorbed energy is subsequently re-irradiated at longer wavelengths, and due to the infrared reflectance property of the film is reflected back into the home. Potential heat loss through the windows of a warm home to colder air outside is therefore dramatically reduced.

In summer, the installation of uncoated windows leads to a different undesired effect. In warmer climates, the high transmittance of the whole solar range leads to overheating of buildings because all the energy transmitted inwards through the glass is

then blocked. This is the "greenhouse effect". One can prevent overheating by fitting windows that are transparent for visible light and reflecting for infrared solar radiation.

The installation of windows containing the appropriate spectrally selective coating can therefore be a great advantage economically, by reducing the costs of heating and air conditioning systems.

1.2.2 Solar Cells

Heterojunction solar cells consisting of a wide bandgap semiconductor (usually an oxide semiconductor) mated to a much narrower bandgap (active) semiconductor have gained considerable interest over many years. The choice of the top oxide layer depends on its work function and the nature of the electron affinity of the base semiconductor.

The conducting transparent film permits the transmission of solar radiation directly to the active region with little or no attenuation. These solar cells have therefore improved sensitivity in the high-photon-energy portion of the solar spectrum.

Although tin oxide can be utilised in solar cell applications,[52-53] alternative materials exhibiting superior efficiencies are now more commonly used. Examples include silicon[54] and InGaP/GaAs tandem solar cells.[55]

1.2.3 Gas Sensors

The structure of a semiconductor makes it a good design for the role of a gas sensor. The conductance changes in semiconductor materials are large and are caused primarily by changes in carrier concentration due to charge exchange with the species adsorbed from the gas phase. The electron concentration in semiconductor sensors can vary in the conduction band approximately linearly with pressure, while variations in the carrier mobility are generally small. This large and reversible variation in conductance

with active gas pressure makes semiconductors such as tin oxide attractive as materials for gas sensing devices.[56-59]

Of the semiconductors, tin oxide-based gas sensors have found the most widespread use, both in research and commercially, because they have the advantages of relatively low operating temperature, low cost, and long-term stability. Tin oxide has been used as a gas sensor for hydrogen,[60-63] oxygen,[63] nitrous oxide,[63] hydrogen sulphide[63-64] and alcohol.[65] It has been shown that the addition of a small amount of silver as a surface additive can enhance the sensor performance of tin oxide.[66]

1.2.4 Protective Coatings

A metallic oxide coating on a glass substrate reduces appreciably the coefficient of friction of a glass surface so can reduce damaging of glass objects during manufacture or filling. Usually, the tin oxide film is present between the glass surface and a lubricating layer such as silicone which is applied after cooling and annealing.

1.2.5 Other Applications

There are several other applications for transparent conducting oxides such as tin oxide. One important function is in de-misting and de-icing glass for such items as mirrors, refrigerator door glass and automotive glass. Another application is found in space as a surface layer of orbiting satellites, to combat the problem of non-uniform electric charge build-up on the exterior surface.[67] Other applications include light-transmitting electrodes in optoelectronic devices[68-69] and laser-damage resistant coatings in high power laser technology.[40]

1.3 METHODS OF FILM DEPOSITION

There are a large number of deposition techniques available for producing tin oxide films, each with certain advantages and disadvantages.[70-71] Due to the nature of this thesis, chemical vapour deposition (CVD) will be discussed in detail, and other deposition techniques mentioned briefly.

1.3.1 Chemical Vapour Deposition

Chemical vapour deposition (CVD) may be simply defined as a process in which gaseous species are employed in the formation of solid state materials. The CVD process has developed into an extremely important deposition technique, and has found an enormous amount of widespread use. There are numerous reviews in the literature which thoroughly explain the process of CVD.[72-76] Basically, the CVD process consists of a series of steps (Figure 1.5) :

(i) *Mass transport of the precursor from the reactor inlet to the deposition site.*
(ii) *Gas-phase reactions, leading to the formation of film precursors and by-products.*
(iii) *Mass transport of the precursor to the substrate.*
(iv) *Adsorption of the precursor on the substrate surface.*
(v) *Surface diffusion of the precursor to the growth site.*
(vi) *Surface reactions and incorporation of the film constituents into the growing film.*
(vii) *Desorption of by-products.*
(viii) *Mass transport of by-products from the reactor.*

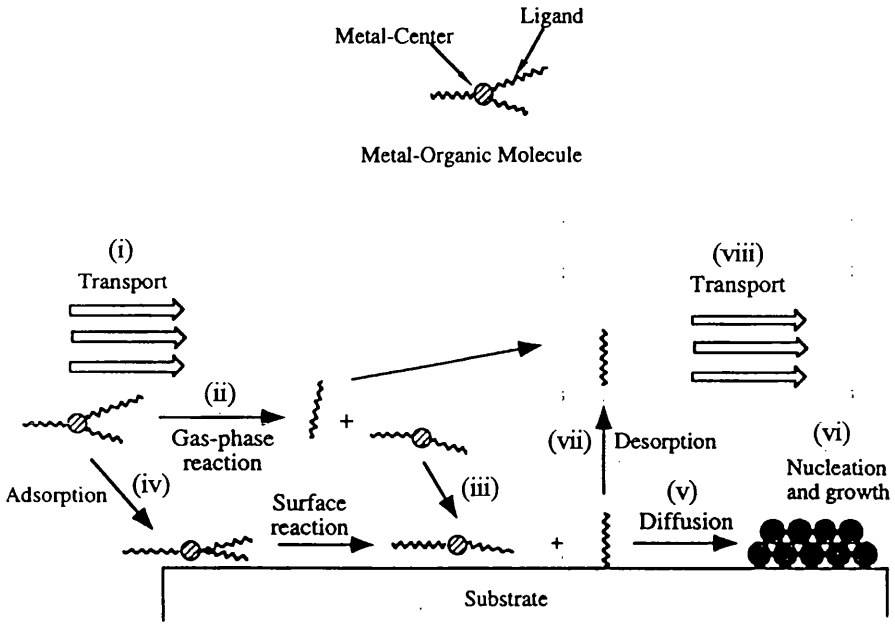

Figure 1.5 Important Steps of the CVD of a Metal-Containing Film from a Metal-Organic Precursor

To be useful, a CVD process must produce thin films with reproducible and controllable properties including purity, composition, thickness, adhesion, microstructure, and surface morphology.

1.3.1.1 CVD Growth Processes

The most common rate-limiting step in CVD growth processes is the gas-phase transport and adsorption of the organometallic precursor to the substrate. Once adsorbed on the surface, the precursor molecule or fragment may diffuse to a growth site. The growth of metal containing films usually occurs by one of three growth processes (Figure 1.6):

(a) Layer or Franck-van der Merwe.

(b) Layer Plus Island or Stranski-Krastanov.

(c) Island or Volmer-Weber.

The resultant process is dictated primarily by the nature of the interaction between the growing film and the substrate, the thermodynamics of adsorption, and the kinetics of crystal growth.

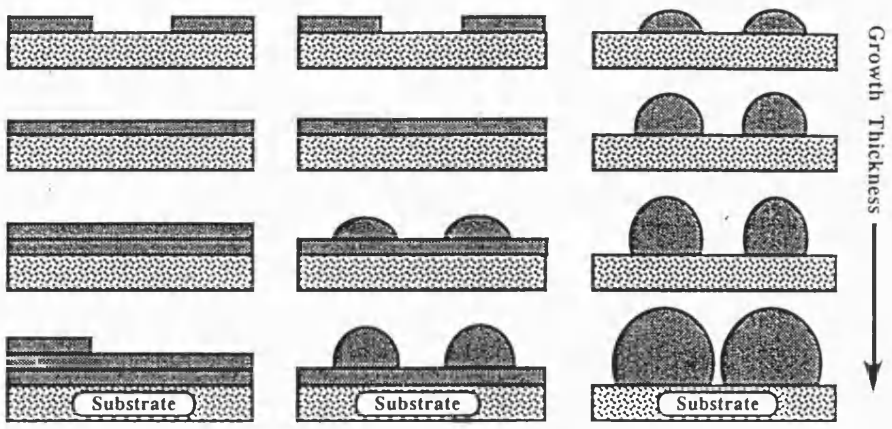

(a) Layer (b) Layer plus Island (c) Island

Figure 1.6 CVD Growth Modes

In growth mode (a) the deposited atoms are more strongly bound to the substrate than each other. This growth process is referred to as "simultaneous multilayer growth" and its occurrence depends on the relative rates of nucleation and growth of the deposition.

For growth mode (b) a layer type growth is initially exhibited, but islands subsequently form on the previously deposited layers as continued layer growth is unfavourable. This type of growth is common when the molecular orientation of the organometallic precursor prevents the formation of successive layers due to the production of highly strained intermediate monolayers.

Growth mode (c) takes place when small droplets or clusters initially nucleate on the surface, and subsequent growth occurs on these island sites. This process transpires when the depositing atoms bind more strongly to each other than to the substrate.

1.3.1.2 Reactor Design

The design of a CVD reactor is extremely important and can have a profound effect on the nature and quality of the material deposited. CVD reactors may be considered to be of two general types, (a) hot-wall reactors, and (b) cold-wall reactors. The systems are basically self-explanatory as hot-wall reactors contain an external heat source surrounding the reaction chamber, and cold-wall systems maintain the reactor walls at relatively cool temperatures.

The major problem with hot-wall systems is that deposition can occur not only on the substrate but also on the reactor walls. This can cause two undesired effects :

(i) *The deposits can eventually fall off the surface and contaminate the growing film on the substrate.*
(ii) *The consumption of precursor is large due to deposition over a larger area.*

Although cold-wall reactor systems provide the greatest degree of control over the deposition, they are much more sensitive to secondary-flow effects and turbulence than hot-wall systems.

1.3.1.3 Advantages for CVD

CVD has a number of key advantages in depositing metal-containing films compared to other thin film deposition techniques. These advantages include :

(i) *Conformal coverage, i.e. the ability to coat a surface with complex topography with a layer of uniform thickness.*
(ii) *Selective deposition, i.e. the ability to deposit a coating on a specific surface, and not on the undesired area.*
(iii) *Low deposition temperature, which can be vital for thermally sensitive substrates.*
(iv) *High deposition rates.*

(v) *Formation of high purity materials*

(vi) *Facility for large scale production.*

(vii) *Low cost.*

Metallic oxides are usually deposited by the vaporisation of a suitable metal-bearing compound and its *in situ* oxidation with an appropriate oxidising agent.[77] A reasonably inert material such as nitrogen or argon is generally used as carrier gas. Due to the large number of variables (precursor temperature, substrate temperature and gas flows), a large number of runs are necessary in order to ascertain the ideal conditions to achieve a coating exhibiting optimum properties.

Due to the advantages of CVD, it is an extremely common technique for the deposition of tin oxide thin films.[78-81] Although the CVD process is quite general, there are a wide range of specialised techniques available which involve variations in the method used for the precursor delivery. Examples include laser-induced CVD,[82] plasma-enhanced CVD,[83] and aerosol CVD.[84]

1.3.2 Other Deposition Techniques

There are a number of alternative techniques available for the deposition of tin oxide thin films. The methods mentioned below are some of the most common.

1.3.2.1 Sputtering

Sputtering is a process operating on an atomic or molecular scale whereby an atom or molecule which is part of a surface is ejected when the surface is struck by a fast incident particle. The momentum of the incident atom is transferred to the atoms in the target material and this momentum transfer can often lead to the ejection of a surface atom - the sputtering process.

There are many different sputtering techniques, such as ion beam sputtering, DC or RF sputtering,[85] and magnetron sputtering. RF magnetron sputtering can be used to

prepare tin oxide coatings on low temperature substrates[86] which is an advantage over high temperature processes such as CVD.

Sputtering is one of the most extensively used techniques for the deposition of transparent conducting oxide films. Sputtering methods produce high quality films but the apparatus required is expensive and their low production rate makes them less useful for mass production. Sputtered films usually need further annealing to stabilise their characteristics.

1.3.2.2 Evaporation

In evaporation, there are three general steps :

(i) *A vapour is generated by boiling or subliming a source material.*
(ii) *The vapour is transported from the source to the substrate.*
(iii) *The vapour is condensed to a solid film on the substrate surface.*

There are many evaporation methods, including vacuum evaporation, electron-beam evaporation and reactive evaporation.[87-88] They have the same disadvantages for mass production as sputtering methods.

1.3.2.3 Spray Pyrolysis

The spray pyrolysis technique involves the application of a fine mist of very small droplets containing the reactants onto a hot glass substrate. The substrate temperatures are usually similar to those used in CVD, about 300-500°C. Due to the simplicity of the apparatus, this method is an inexpensive procedure and is suitable for large scale applications. The only limitation is the low deposition efficiency, defined as the ratio of atoms effectively deposited to those supplied.

The quality of these films depends on parameters such as the spray rate, the substrate temperature, and the ratio of the various constituents in the solutions. In order

to obtain films with good electrical properties, an appropriate reducing agent is required to avoid complete oxidation of the metal.

Spray pyrolysis is a very common method for depositing tin oxide.[89-91] In the vast majority of cases the tin precursor is $SnCl_4$,[92] although $SnCl_2$ has also been tried due to its lower cost.[93] Doped tin oxide films have also been prepared via spraying methods.[94]

1.3.2.4 Sol-Gel Methods

The sol-gel process is a dipping technique which involves the preparation of a solution containing the desired material - the "sol" - into which the substrate is dipped, then subsequently dried to give the coated material. This method is used extensively for the production of tin oxide films[95-97] and has many advantages over other techniques.

(i) *Low temperature processing.*
(ii) *Precise control of the doping level.*
(iii) *Simple, inexpensive equipment.*
(iv) *Excellent homogeneity of films.*
(v) *Easy control of film thickness.*
(vi) *Ability to coat large and complex shapes.*
(vii) *Ability to produce ultrafine films.*

In the vast majority of cases, the tin precursor used is an alkoxide due to the fact that alkoxides can be obtained with a high degree of purity and can easily be hydrolysed to form the oxide.[98]

$$Sn(OR)_4 + 2H_2O \longrightarrow SnO_2 + 4ROH \qquad [1.1]$$

1.4 METAL ORGANIC CVD (MOCVD)

Metal-organic compounds are used extensively as molecular precursors for the CVD of tin oxide, and hence the abbreviation MOCVD. The precursor can be designed in such a way as to be specific for the target material, so decomposition occurs to produce the desired film with loss of unwanted organic ligands.

In conventional MOCVD the precursor is heated in a stainless steel bubbler assembly to generate a saturated vapour of the complex. A carrier gas sweeping the bubbler is used to deliver the gaseous precursor into the deposition chamber.

1.4.1 Pre-requisites of a Good Precursor for MOCVD

There are many crucial design requirements that must be satisfied in order for a metal-organic compound to be suitable as a precursor for MOCVD.[72,74,99] These can be summarised as follows :

(i) *It should have good volatility to enable transport to the reactor and achieve high deposition rates.*

(ii) *It must have good thermal stability during its evaporation and transport in the gas phase.*

(iii) *It should decompose cleanly on pyrolysis without contamination of the growing film.*

(iv) *It should have a high level of purity.*

(v) *It is an advantage if it is non-toxic and non-pyrophoric, to enable easier handling.*

(vi) *It is also an advantage if it is stable, to enable easier storage.*

(vii) *Liquid precursors are the most favourable to ensure reproducible delivery rates.*

(viii) *Availability in consistent quantity and quality at low cost is also advantageous.*

1.4.1.1 Volatility

Volatility is one of the most important properties of a precursor for MOCVD. It is extremely important to achieve a reasonably high volatility otherwise adequate transport of the precursor to the deposition zone will be practically impossible. A sufficient concentration of the precursor in the vapour phase is also essential to achieve a reasonable deposition rate. Although a higher concentration of precursor can be achieved by raising the bubbler temperature, premature decomposition must be avoided.

Enhancement of the volatility requires a minimisation of the polarisability, dipoles, and especially interactions between molecules of the precursor in the condensed state, *e.g.* suppression of hydrogen bonds. Obviously, ionic and covalent intermolecular bonds must be avoided as they will diminish the volatility.

There are several adaptations that can be performed to enhance the volatility. For example, for non-polar compounds, smaller size is associated with higher vapour pressure. Also, substitution of fluorine for hydrogen increases the volatility due to the diminished number of hydrogen bonds, and the difficulty to polarise fluorides due to the minimising of dipole-dipole interactions between molecules.

Inorganic complexes often exhibit low vapour pressures as a result of aggregation. For example, although the formula weight of $SnCl_2$ is lower than that of $SnCl_4$, the vapour pressure of $SnCl_4$ is higher because the tin centre is more coordinatively saturated and therefore exhibits a lower tendency towards aggregation compared to $SnCl_2$.

Aggregation can also be a problem for metal-organic complexes, but such compounds have much more scope for adaptation to engineer a higher volatility. For example, chelating ligands such as β-diketonates are more easily derivatised to alter volatility and melting point than inorganic compounds such as metal halides.

1.4.1.2 Control of Impurity Incorporation

A significant problem with the use of organometallic compounds for CVD is that it can result in unwanted impurities in the deposited film. The biggest problem is carbon, as the precursor usually contains a high proportion of this element.

An attractive route to avoiding carbon contamination of the film is the design of a precursor able to undergo a clean removal of its ligands by, for example, intramolecular mechanisms. In such a molecule, the ligands should have a high kinetic lability and they should be removed rapidly from the deposition chamber to prevent unwanted side decomposition of by-products leading to carbon incorporation. This is possible when the ligand itself is a stable molecule which can be released after cleavage of the metal-ligand bond, since this is generally the weakest bond in the molecule. Examples of such ligands include alkenes and carbon monoxide.

Another approach to minimise carbon incorporation is to use ligands where a reaction pathway exists in which volatile products are formed which desorb easily from the surface. The well known β-hydride elimination is an example of a mechanism which cleaves the metal-carbon bond, and ligands which undergo this mechanism can be chosen, such as ethyl or tertiary butyl.

Overall, rough guidelines can be derived for choosing the organic portion of an organometallic precursor. In general, as the metal-carbon bond order increases in organometallic compounds, the chances for carbon incorporation are increased due to the increased strength of the metal-carbon bonding, *i.e.* metal alkene ≈ metal alkyne ≤ metal alkyl < metal (η^3-allyl) < metal carbonyl < metal cyclopentadienyl < metal arene. Carbon incorporation can also be minimised by the use of precursors with fewer metal-carbon bonds, purely due to the smaller carbon content.

Contamination can also be controlled to a certain extent by the choice of atmosphere in the deposition chamber. The use of a reducing gas such as hydrogen can

prevent unwanted carbon inclusion by, for example, reducing a methyl group to methane, and hence removing the organic ligands cleanly.

1.4.1.3 Liquid Precursors

Liquid source precursors are the most desirable for several reasons.

(i) *They generally have good volatility, so transport is relatively easy.*

(ii) *They are preferred to solids because when a solid reagent is used, the pick-up is variable during the run because of the changing surface area of the solid as it is consumed.*

(iii) *Some problems encountered with solids are eliminated, such as sublimation onto reactor components.*

There is one possible disadvantage for attempting to synthesise a liquid precursor. Purification can be difficult as distillation is the only method available, and problems may arise if the material has a high boiling point, or is difficult to separate from by-products.

1.5 THE CVD OF TIN OXIDE

The CVD of tin oxide has been performed at temperatures ranging from 300 to 700°C, depending on the desired result. Lower temperatures can produce films of higher crystallinity, but higher temperatures significantly raise the deposition rate.

1.5.1 Current Precursors

There are many precursors currently in use for the CVD of tin oxide thin films. The most common compounds are discussed briefly below.

1.5.1.1 Inorganic Precursors

By far the most common precursor encountered is tin tetrachloride ($SnCl_4$) which has received a large amount of attention.[78, 79, 100, 101]

The reaction of $SnCl_4$ with oxygen in the formation of tin oxide can be represented by :

$$SnCl_4\,(g) + O_2\,(g) \longrightarrow SnO_2\,(s) + 2Cl_2\,(g) \qquad [1.2]$$

Tin oxide can also be formed by hydrolysis of $SnCl_4$.

$$SnCl_4\,(g) + 2H_2O\,(g) \longrightarrow SnO_2\,(s) + 4HCl\,(g) \qquad [1.3]$$

$SnCl_2$ dissolved in methanol has also been tested as a precursor due to the lower cost of this material.[101]

These inorganic precursors are in widespread use due to their availability and relatively low cost, although deposition does have some problems. Chloride-based precursors generally yield films with good electrical resistivities, but only mediocre optical transmittance. There is usually some chloride incorporation into the film due to incomplete oxidation of the chloride precursor which can enhance the conductivity by acting as a dopant.

Alkoxides are another group of compounds which have received a significant amount of research for the deposition of tin oxide films. Fully substituted tin precursors are usually chosen which have the advantages of good volatility and high purity levels. This group of precursors are generally used to produce tin oxide films via the sol-gel technique.[98, 102] However, there has been a minimal amount of research on the potential of alkoxides as CVD precursors. An example of a tin alkoxide precursor that has been used for CVD is $Sn(O^tBu)_4$.[16]

Nitrogen-containing precursors have received little attention for use in this application, which is probably due to the added complication of potential nitrogen contamination of the deposited film. Tin amido compounds have been synthesised as possible precursors where it was found that it was possible to produce films comparable to coatings obtained from halide and alkyl precursors.[103] The tin compound that has been investigated in this case is $Sn(NMe_2)_4$, which is a suitable precursor as it is a thermally stable liquid with only moderate air sensitivity.

1.5.1.2 Organometallic Precursors

Due to the reasons previously discussed (Section 1.4) there has been a lot of interest in the development of effective metal-organic precursors for the CVD of tin oxide thin films. However, the amount of published material regarding organotin precursors is considerably less than that of $SnCl_4$. Organotin-based precursors generally produce films with excellent optical transmittance but rather low electrical conductivity.

The most studied organotin compound appears to be tetramethyltin (TMT).[104-106] Although it has a reasonably high vapour pressure, it has a rather high level of toxicity so does present some handling difficulties. Some kinetic modelling studies have recently been conducted[107] to try to determine the nature of the decomposition mechanisms in the reactor. Overall, the reaction can be represented as :

$$Sn(CH_3)_4\,(g) + 8O_2\,(g) \longrightarrow SnO_2\,(s) + 6H_2O\,(g) + 4CO_2\,(g) \qquad \textbf{[1.4]}$$

Dimethyltin dichloride (DMT) has also been studied as a precursor for MOCVD, although the amount of literature concerning this material appears to be rather scarce. As for TMT, there have been some kinetic modelling studies performed.[108]

The third organotin compound which has been used as a precursor for tin oxide films is dibutyltin diacetate (DBTD) in both CVD[109-110] and spraying[111] processes. Dibutyltin diacetate has been used because it has a reasonable volatility, is air-stable, non toxic, and is readily available at a low cost.

Although the vast majority of research has been conducted on tin(IV) compounds, there has been a limited amount of investigation on the capability of tin(II) derivatives. Examples are tin(II) acetate[112] and tin(II) acetylacetonate.[113]

There are several reasons why tin(IV) compounds are chosen in preference to tin(II) analogues. The most important is that the synthesis of tin(IV) compounds is generally less complicated that that of the tin(II) analogues due to their higher degree of stability. Another significant reason is that organotin(IV) precursors tend to exhibit a higher degree of volatility due to the coordinative saturation of the tin environment. Coordinatively unsaturated tin(II) compounds are more likely to exhibit strong intermolecular bonding, which results in high melting, involatile solid compounds. Also, it seems unnecessary to perform a more difficult tin(II) synthesis if the target is a tin(IV) material.

1.6 THE CVD OF FLUORINE-DOPED TIN OXIDE

There are currently a variety of precursors in operation for the production of fluorine-doped tin oxide thin films by CVD. The accepted method of manufacture involves the use of a tin-containing precursor as the tin source, with the fluorine introduced from a separate source by a fluorine-containing compound. In the vast majority of cases the oxidising agent is oxygen gas. This method requires careful control to ensure that the dopant is added in the precise quantity and by use of exact conditions in order to obtain a quality film, which are quite difficult procedures.

It is very important to incorporate a specific quantity of fluorine in order to achieve optimum film properties. Studies on the effect of the fluorine level on resultant film properties have been performed which suggest that a level of fluorine of around 1-2 atom% produces the optimum results. [19,25,28] However, the definitive amount has not been confirmed because it will depend upon how effectively the incorporated fluorine contributes to the carrier concentration (the *doping efficiency*). Heavily doped films

have been shown to contain pits in the surface which leads to an increase in the electrical resistivity. This observation is due to the additional fluorine diffusing to interstitial positions,[28] and therefore not contributing to the conductivity.

The tin precursors used for the production of fluorine-doped tin oxide are extremely similar to those discussed previously for undoped films. Again, $SnCl_4$ appears to be the most common tin precursor in use, which is probably due to its low cost and availability. The most frequently encountered fluorinating agent is hydrofluoric acid (HF), [18,19,20] presumably for similar reasons. There are, however, several other fluorine dopants which have been used in conjunction with $SnCl_4$ in the CVD method, such as ammonium fluoride,[21] fluorine gas,[22] and F^+ ions.[23]

TMT has also been used for depositing fluorine-doped tin oxide films. Fluorine dopants used with this precursor have included HF[24] and bromotrifluoromethane (a Freon) which is an attractive fluorine dopant as it is a stable, non-toxic gas.[25] DBTD has found use as a precursor, with trichloro-trifluoroethane (Freon 113) as a dopant.[114]

The use of fluorine-containing precursors is extremely rare, with very little research reported in the literature. Until very recently the only material tested appeared to be tin(II) bis-trifluoroacetate.[26] However, a tin(II) alkoxide complex $Sn[OCH(CF_3)_2]_2(HNMe)_2$ using hexafluoroisopropoxide as the fluorine containing organic ligand has recently been synthesised,[115] with CVD experiments performed.[116] The films were grown by low-pressure CVD and were found to be non-conductive, showing that any fluorine incorporated was not effective. A tin(IV) derivative $Sn[OCH(CF_3)_2]_4(HNMe_2)_2$ has also been synthesised and subsequently tested by low-pressure CVD, [116] and has been found to produce films with a resistivity of 2.1×10^{-3} Ω cm.

Table 1.1 shows fluorine-doped tin oxide films that have been derived from separate tin and fluorine sources.

Table 1.1 Fluorine-Doped Tin Oxide Films from Published Precursors

TIN PRECURSOR	Fluorine Dopant	Deposition Temp. (°C)	Thickness (Å)	Sheet Res. (Ω/□)	Ref.
$SnCl_4$	HF	570-600	7,200	5.0	18
$SnCl_4$	NH_4F	450	12,500	4.9	21
$SnCl_4$	F_2 gas	550	6,550	4.0	22
$SnCl_4$	F^+ ions	-	-	-	23
$SnMe_4$	HF	360	20,000	1.8	24
$SnMe_4$	$BrCF_3$	570	10,500	3.0	25
$Sn(CF_3CO_2)_2$	-	400	12,600	4.7	26
$Sn[OCH(CF_3)_2]_4(HNMe)_2$	-	200-450	4800-6000	-	116

It can be seen that the sheet resistance is highly dependent on the film thickness, with thicker films generally producing films with lower resistance.

From the published literature, it appears that the choice of precursor is governed by cost and availability, even for research purposes. There have been very few tin precursors tested, with fluorine dopants suffering from either severe handling difficulties in the case of HF, or potential damage to the environment in the case of freons. Considering the vast number of conceivable tin compounds, there appears to be minimal research into new precursors which could rule out the handling problems, and potentially produce higher quality films.

1.6.1 Industrial Production of Fluorine-Doped Tin Oxide

The deposition of fluorine-doped tin oxide has been developed into a large scale process in the production of Low *E* coated glass for use in windows, as previously discussed (Section 1.2.1). In industry, the coating is achieved by a CVD reaction

directly on a float glass production line, *i.e.* the thin film is deposited onto the glass while it is being manufactured, prior to being cut into the required sizes.

This process is known as *on-line filming* whereas in contrast, *off-line filming* processes deposit thin films onto previously manufactured glass which has earlier been cut into customer desired sizes. A typical Low *E* glass is obtained by depositing a very thin film of silicon dioxide followed by the thin film of fluorine-doped tin oxide. The SiO_2 layer acts as a diffusion barrier[117] to prevent the migration of sodium ions into the tin oxide coating which could cause a deterioration of electrical properties.

Due to the temperature restriction of the float glass production line and the necessity for a fast deposition rate during on line filming, the CVD process occurs at a high temperature of $\approx$ 600°C.

1.7 PROPERTIES AND ANALYSIS OF FLUORINE-DOPED TIN OXIDE THIN FILMS

The resultant properties exhibited by a fluorine-doped tin oxide film can be tailored to a certain extent by the deposition parameters chosen. To determine the quality of a fluorine-doped tin oxide thin film there are a number of important measurements that must be made. A large variety of analytical techniques are available to perform this operation. The film properties and analytical methods mentioned below are techniques that will be subsequently used and discussed in this thesis.

As the major use of fluorine-doped tin oxide films is in window coatings, the properties important for this application will be discussed. The aim is to achieve a high quality film exhibiting a good overall set of properties without significant deterioration of any particular characteristic.

1.7.1 Film Thickness

In general, the thickness governs the optical and electrical properties of the film.[118] Electrical properties such as resistivity will improve with increasing thickness, but optical properties such as haze and emissivity will deteriorate. For spectrally selective coatings, an ideal thickness is ≈ 3000 Å as this achieves a film exhibiting a good overall set of properties without the deterioration of any specific feature for this application.[51]

1.7.2 Haze

The haze is a measure of the degree of light scattering exhibited by the glass. To the naked eye, a high haze measurement results from a piece of glass with a milky appearance, which is not very appealing to a prospective customer. A low haze measurement is therefore the desired target, as the glass will appear transparent. The haze is highly dependent on the thickness, with a thinner film generally exhibiting lower haze. A good fluorine-doped tin oxide film approximately 3000 Å in thickness will produce a haze measurement of < 0.4%.

1.7.3 Emissivity

The emissivity is a measure of the ability of materials to reradiate absorbed energy into a colder environment. Hence, for window applications a very low value is desirable to prevent unwanted heat loss. This can be obtained with a thick film, but will have the undesired effect of an increase in the haze as previously mentioned. A very low emissivity of < 0.15 is indicative of a good quality coating for a film in the 3000 Å thickness range.

1.7.4 Sheet Resistance

Low resistance is the required property, as this is a result of good conductivity. This property is measured in units of Ω/□ as the value will be identical regardless of the area measured, *i.e.* the film has a square shape irrespective of the dimensions. As for emissivity, a thicker film will exhibit a lower resistance, but for a film 3000 Å in thickness 15-16 Ω/□ is a good result.

1.7.5 Resistivity

The resistivity of a film is directly proportional to the conductivity, where the greater the conductivity, the lower the resistivity. Conductivity is a function of the thickness and sheet resistance, and can be calculated by :

$$\sigma = 1/Rd \qquad [1.5]$$

where σ = conductivity, R = sheet resistance and d = thickness.

The conductivity is the inverse of the resistivity, so to calculate the resistivity R^* :

$$R^* = 1/\sigma \qquad [1.6]$$

A low value in the region of $< 0.5 \times 10^{-3}$ Ω cm indicates a good conducting coating for the thickness in question.

1.7.6 X-Ray Diffraction

X-ray diffraction (XRD) can be used to determine the composition and preferred orientation of the film. The X-rays decelerate as they plunge into the tin oxide film and generate radiation with a continuous range of wavelengths. Superimposed on the continuum are a few high-intensity, sharp peaks which arise from the interaction of the

incoming electrons with the electrons in the inner shells of the atoms. The positions of these sharp peaks will be characteristic of a tin oxide film, so the spectrum obtained can be used to confirm the film composition provided it is crystalline.

1.7.7 Fluorine Content

Obviously this is a very important measurement to see how much fluorine has been incorporated in the film during the deposition process. In order for the fluorine to induce an effect on the conductivity of the tin oxide film, it must be *active fluorine*. The fluorine must occupy the oxygen positions in order to be effective. If fluorine incorporation has occurred through inclusion of organic radicals such as CF_3 it will be inactive and have no positive effect on the conductivity.

Fluorine content can be accurately measured by X-Ray Fluorescence (XRF). Industrially produced films from separate dopants typically contain $\approx$ 1-2 atom% fluorine.

1.8 SINGLE SOURCE PRECURSORS

The concept of the single source precursor is a relatively recent one, with research only increasing significantly over the last five year period. The idea is relatively simple and has an enormous amount of potential for future applications. The precursor contains all the required film constituents, and during the CVD process all unwanted material is lost to leave the coating in the required stoichiometry, hence the term *single source*. The use of a single source precursor is very appealing and has several advantages for film deposition.

(i) *Separate dopants are not required, which therefore simplifies the procedure as there are less parameters to perfect.*

(ii) *More reproducible films are feasible.*

(iii) *The cost can be reduced as less material is required.*

(iv) *The precursor can be engineered to produce a specific film, rather than relying on separate dopants to achieve the correct dopant concentration.*

There are however some possible problems with designing new single source precursors.

(i) *It may not be possible to synthesise a compound containing all the required elements in their specific quantities.*

(ii) *Precursor composition does not always transfer directly to resultant film stoichiometry.*

(iii) *It would be extremely expensive to adapt existing large scale production plants to a new technology.*

For the CVD of fluorine-doped tin oxide, simple organotin fluorides are not viable as single source precursors due to the common occurrence of strong intermolecular bonding which leads to polymeric structures and hence low volatility. Table 1.2 illustrates the physical properties of a variety of triorganotin fluorides.

Table 1.2 Physical Properties of Triorganotin Fluorides

COMPOUND	Structure	Melting Point (°C)	Ref.
Me_3SnF	Polymeric *trans*-R_3SnX_2	> 360	119
Ph_3SnF	Polymeric *trans*-R_3SnX_2	357	120
$(c\text{-}C_6H_{11})_3SnF$	Tetrahedral R_3SnX	260	121
$(Mes)_3SnF$	Tetrahedral R_3SnX	-	122
$Me_2[(Me_3Si)_3C]SnF$	Tetrahedral R_3SnX	313	123

It can clearly be seen that the triorganotin fluorides are not viable as CVD precursors due to their extremely low volatility. Although the melting point of $(Mes)_3SnF$ is not reported, the bromide analogue $(Mes)_3SnBr$ is quoted as 177-178°C,[122] which suggests an extremely high value for the fluoride. Therefore, even with bulky ligands to prevent the formation of the polymeric arrangement the melting points are far too high, and transport of such compounds in the vapour phase would be practically impossible.

There has been a vast increase in the amount of research conducted on single source precursors in recent years, with a wide range of compounds developed. Examples of thin films for which single source precursors have been explored recently include gallium nitride,[124] copper sulphide,[125] zinc sulphide,[126] and indium sulphide.[127] Other materials which have attracted the attention of single source methods are metal chalcogenide complexes,[128-129] and Group 13-Antimonides.[130] Heterobimetallic complexes have also been developed as single source precursors to both mixed metal[131] and mixed metal oxide[132] films. It can therefore be seen how diverse the concept has become, and what enormous potential there is for the future in this exciting new field of chemistry.

1.9 CHEMISTRY OF ORGANOTIN COMPOUNDS

Organotin research is an extremely interesting and diverse field of chemistry. There are a number of books[133-136] and comprehensive reviews[137-140] which thoroughly survey the whole field of tin chemistry.

1.9.1 Background

Tin metal has a $5s^2 5p^2$ electronic configuration which enables the formation of compounds in both the +2 and +4 oxidation states. It is possible to prepare organotin compounds, defined as containing at least one tin-carbon bond in the molecule, in both

oxidation states. However, organotin(IV) compounds are much more numerous due to their higher degree of stability.

Most organotin compounds do not present major handling difficulties. They are generally stable in air, insensitive to moisture, and can be stored for long periods of time. They are soluble in ordinary organic solvents and insoluble in water.

However, most organotin compounds are toxic to some extent, with the toxicity highly dependent on the nature of the substituents. Maximum toxicity is observed with small alkyl groups such as methyl and ethyl, and the toxicity level decreases as the length of the alkyl chain increases, so larger groups such as butyl are more attractive in terms of toxicity. In the series R_nSnX_{4-n} the toxicity decreases with a decreasing number of alkyl groups, and inorganic tin compounds are generally non-toxic.

1.9.1.1 Bonding in Tin(IV) Compounds

The most common form of tin in organotin(IV) compounds is tetravalent with sp^3 hybridisation. Whereas tin(II) compounds do not appear to utilise the 5*d* orbitals except in the possible cases of π-bonding in donor-acceptor complexes, tin(IV) compounds make extensive use of 5*d* orbitals. When the tin atom is attached to electronegative ligands its Lewis acidity increases and coordination with electron-rich sites leads to the hypervalent form of sp^3d (trigonal bipyramid) or sp^3d^2 (octahedral). Tin has a large covalent radius and bonds to the tin atom are long and mostly covalent with facile polarisability.

The tin-carbon bond dissociation energy is relatively low ($\approx$ 210 kJ mol^{-1}) and therefore organotin compounds exhibit reasonably high levels of reactivity. Tin is considered hard, but is softer than silicon. It can therefore associate with hard bases such as fluoride, but is also able to associate with softer bases such as sulphides.

1.9.2 Coordination Geometries of Tin Complexes

Organotin(IV) compounds exhibit a large number of possible coordination numbers, which range from two to seven. Examples are shown in Table 1.3.

Table 1.3 Coordination Geometries Exhibited by Organotin Compounds

COORDINATION NUMBER	Geometry	Example	Ref.
2	Bent	$Sn[CH(SiMe_3)_2]_2$ (in gas phase)	141
3	Trigonal Planar	$(Me_3Si)_2C(B^tBu)_2C{=}SnR''_2$	142
	Pyramidal	$Sn[CH(SiMe_3)_2]_2$	141
4	Tetrahedral	Ph_4Sn	143
5	Trigonal Bipyramidal	Me_3SnCl	144
	Square Pyramidal	$\{Sn[S_2(CH_2)_2]Ph\}^-Et_4N^+$	145
6	Octahedral	$[(4\text{-}FC_6H_4)_2SnCl_2(C_2H_4SO)_2]$	146
	Skew Trapezoidal	$Bu_2Sn(O_2CCH_2SC_6H_5)_2$	147
7	Pentagonal Bipyramidal	$Me_2Sn(NCS)_2{\cdot}terpy$	148

R'' = 2-^{t}Bu-4,5,6-Me_3C_6H

By far the most common coordination numbers observed are 4, 5, and 6, with the majority of common tin(IV) compounds exhibiting either tetrahedral (**I**), trigonal bipyramidal (**II**) or octahedral (**III**) geometry.

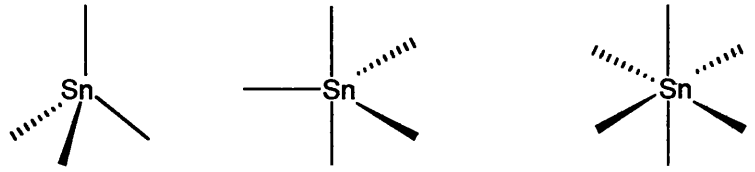

(I) (II) (III)

In general, the coordination number tends to rise as the number of tin-carbon bonds diminishes due to an increase in Lewis acidity.

1.9.2.1 Four-Coordinate Organotin Compounds

Compounds containing four bonds to carbon are almost without exception four-coordinate and tetrahedral, although bond distances exhibit a large degree of variation. Bonds to electronegative organic ligands are generally longer and weaker, and therefore more susceptible to cleavage. For example, the tin-carbon bond distances in $Sn(CF_3)_4$ are lengthened by 6 pm compared with those in $SnMe_4$.

In the case of R_4Sn compounds, both symmetrical structures such as Ph_4Sn[143] and asymmetric examples such as Ph_3SnCH_2I[149] are commonly encountered.

As the number of tin-carbon bonds decreases, the tendency for the coordination number to rise becomes progressively more likely. This is due to the replacement of the R group with more electronegative substituents and an increase in the Lewis acidity.

To prevent this occurrence for R_3SnX compounds, bulky R groups can be employed, as, for example, in $Me_2[(PhMe_2Si)_3C]SnNCS$ (Figure 1.7).[150]

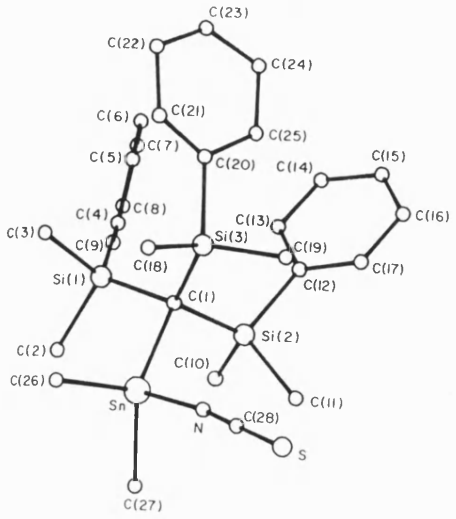

Figure 1.7 The Molecular Structure of $Me_2[(PhMe_2Si)_3C]SnNCS$[150]

Another way to maintain a four-coordinate tin is to use a ligand with a low electronegativity for X, *e.g.* $(2\text{-}MeOC_6H_4)_3SnI$.[151] This strategy can also be used to preserve tetrahedral geometry in R_2SnX_2 compounds, for example, Ph_2SnI_2.[152]

As expected, there are very few incidences of tetrahedral $RSnX_3$ compounds. One example is CH_3SnI_3 which has been shown to consist of discrete, loosely-packed monomer units.[153]

1.9.2.2 Five-Coordinate Organotin Compounds

There are only two possible geometries for five-coordinate organotin compounds, trigonal bipyramidal and square pyramidal. Although the two geometries are close in energy[154-155] and readily convertible via the Berry mechanism (Figure 1.8),[156] the vast majority are trigonal bipyramidal in shape.

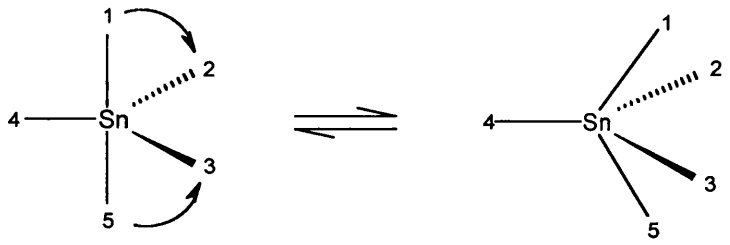

Figure 1.8 The Berry Mechanism

Triorganotin compounds R_3SnX_2 are the most likely to be found with this geometry, with three possible isomers, *trans* (**IV**), *cis* (**V**) and *mer* (**VI**).

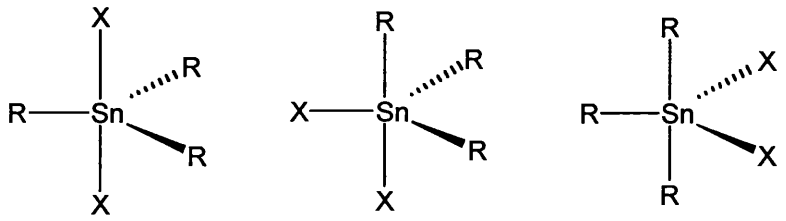

(IV) **(V)** **(VI)**

The *trans* isomer (**IV**) is the most commonly encountered form, with the *mer* isomer (**VI**) yet to be confirmed crystallographically, although Mössbauer studies have suggested its existence.[157] The *trans* arrangement commonly occurs as a result of bridging interactions giving rise to polymeric structures, as in, for example, tribenzyltin acetate[158] and trimethyltin chloride.[144] Monomeric species are less frequently encountered but do exist, *e.g.* $Me_3SnCl.py$.[159]

Examples of five-coordinate tetraorganotin compounds R_4SnX are rare due to their preference for tetrahedral geometry. There is one example which appears to adopt a structure between the two, {C, N-[3-(2-pyridyl)-2-thienyl]}tri(*p*-tolyl)tin.[160]

At the other extreme, five-coordinate diorganotin compounds R_2SnX_3 are also rather infrequent, as there is a strong tendency to increase the coordination number to six. All reported examples are *cis* and *mer*, with organic groups occupying equatorial sites, *e.g.* dichloro(1-hydroxymethylpyrazole)dimethyltin(IV).[161] As expected, five-coordinate $RSnX_4$ species are equally as rare, although examples do exist, *e.g.* $Me_2N(CH_2)_3Sn(SPh)_3$ (Figure 1.9).[162]

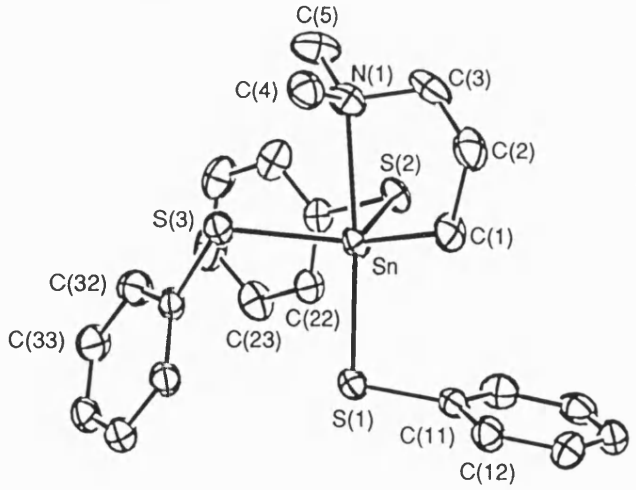

Figure 1.9 The Molecular Structure of $Me_2N(CH_2)_3Sn(SPh)_3$[162]

1.9.2.3 Six-Coordinate Organotin Compounds

Six is most commonly found as the coordination number for diorganotin compounds R_2SnX_4, with *cis* (**VII**) and *trans* (**VIII**) isomers possible for the octahedral geometry.

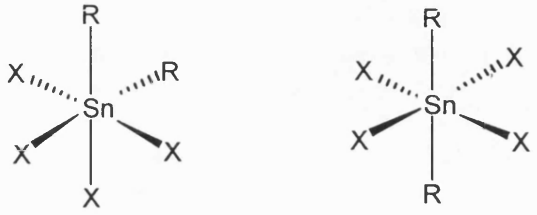

(VII) **(VIII)**

Trans isomers (**VIII**) are the most common, with both monodentate and bidentate chelating ligands. Respective examples are dichlorobis(imidazole)dimethyltin[163] and diphenylbis[1-phenyl-3-methyl-4-(4-bromobenzoyl)-pyrazolon-5-ato]tin (Figure 1.10).[164] The latter can be abbreviated to $Ph_2Sn(Q_{Br})_2$ and its molecular structure is illustrated below.

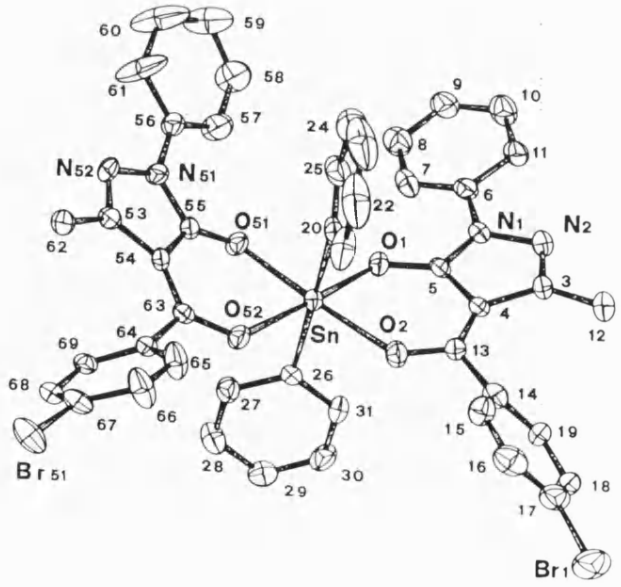

Figure 1.10 The Molecular Structure of $Ph_2Sn(Q_{Br})_2$[164]

Stable *cis* geometry has been observed, in, for example, dimethyltin bis-(8-hydroxyquinolate)[165] but the structure is severely distorted.

There are certain compounds which can be described as distorted octahedral or *skew trapezoidal*. This geometry results from chelating ligands acting in an anisobidentate fashion, which causes a significant reduction in the perfect octahedral bond angle of 180° between the two axial ligands. Certain diorganotin carboxylates have been shown to adopt this geometry[147,166] where the carboxylate groups are asymmetrically chelating, and create a much reduced C-Sn-C bond angle. An example of the skew trapezoidal geometry is illustrated by $Bu_2Sn(O_2CCH_2SC_6H_5)_2$ (Figure 1.11)[147] where the bond angle has been reduced to 140.7°.

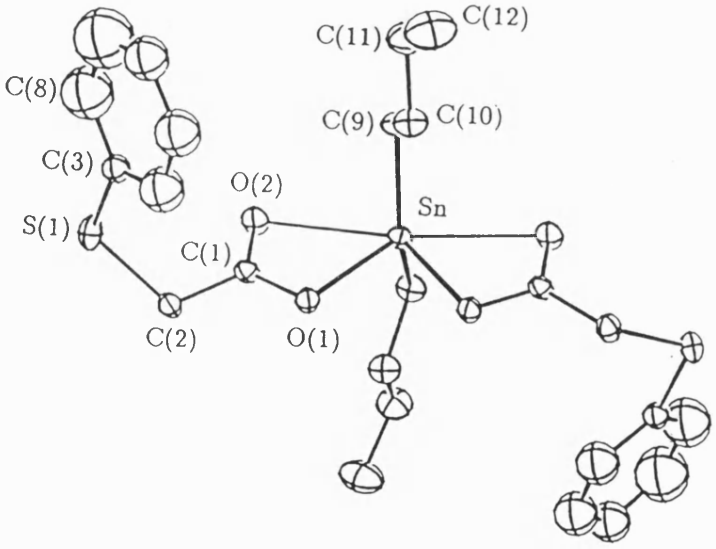

Figure 1.11 The Molecular Structure of $Bu_2Sn(O_2CCH_2SC_6H_5)_2$[147]

A coordination number of six is much less frequently encountered with other organotins. An example of a six-coordinate tetraorganotin is known, the compound being bis[3-(2-pyridyl)-2-thienyl-*C*,*N*]diphenyltin,[167] but this appears to be a unique case. Octahedral triorganotin compounds R_3SnX_3 are also relatively rare, an example being tris(pyrazolyl)borate(trimethyl)tin.[168] However, occurrence of octahedral monoorganotin complexes is more frequent with strongly Lewis acidic compounds, *e.g.* $[SnPhCl_3(HPz)_2]$[169] and butylchlorobis(8-quinolinate)tin(IV).[170]

1.9.2.4 Polymeric Organotin Compounds

The structures illustrated in the previous sections were mainly examples of organotin compounds exhibiting monomeric arrangements. Organotin compounds also commonly form oligomeric and polymeric structures in certain circumstances.

Triorganotin species of the general formula R_3SnX commonly crystallise as infinite one-dimensional polymeric networks (**IX**). The X ligands bond in a bridging fashion which results in a *trans*-R_3SnX_2 repeat unit. Examples of this arrangement include Me_3SnF[119] and Me_3SnN_3.[171]

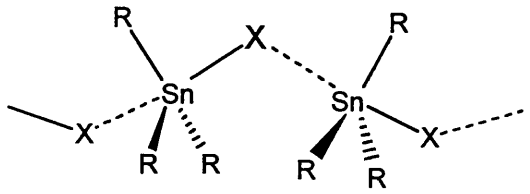

(IX)

Several diorganotin compounds of the general formula R_2SnX_2 also form similar one dimensional chains. In this arrangement, doubly-bridged X ligands result in the tin exhibiting *trans*-octahedral R_2SnX_4 geometry (**X**). Examples of this include Et_2SnCl_2[172] and Et_2SnBr_2.[172]

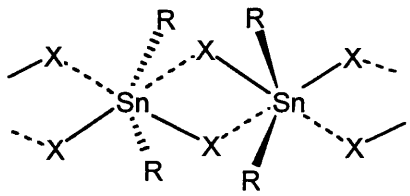

(X)

The Lewis acidity of the tin atom is the usual reason for the polymerisation of an organotin compound, although steric interactions of the organic ligands can influence the type of structure that is formed. For example, sterically demanding ligands can increase the likelihood of a monomeric arrangement, as, for example, in $(Me_3Si)_3CSnPh_2F$.[123]

1.9.3 Reactions of Tin(IV) Compounds

The chemistry of organotin(IV) compounds is extremely diverse with a wide range of reaction types known. The reaction scheme below gives a general idea of the synthesis of a wide range of common organotin(IV) compounds.

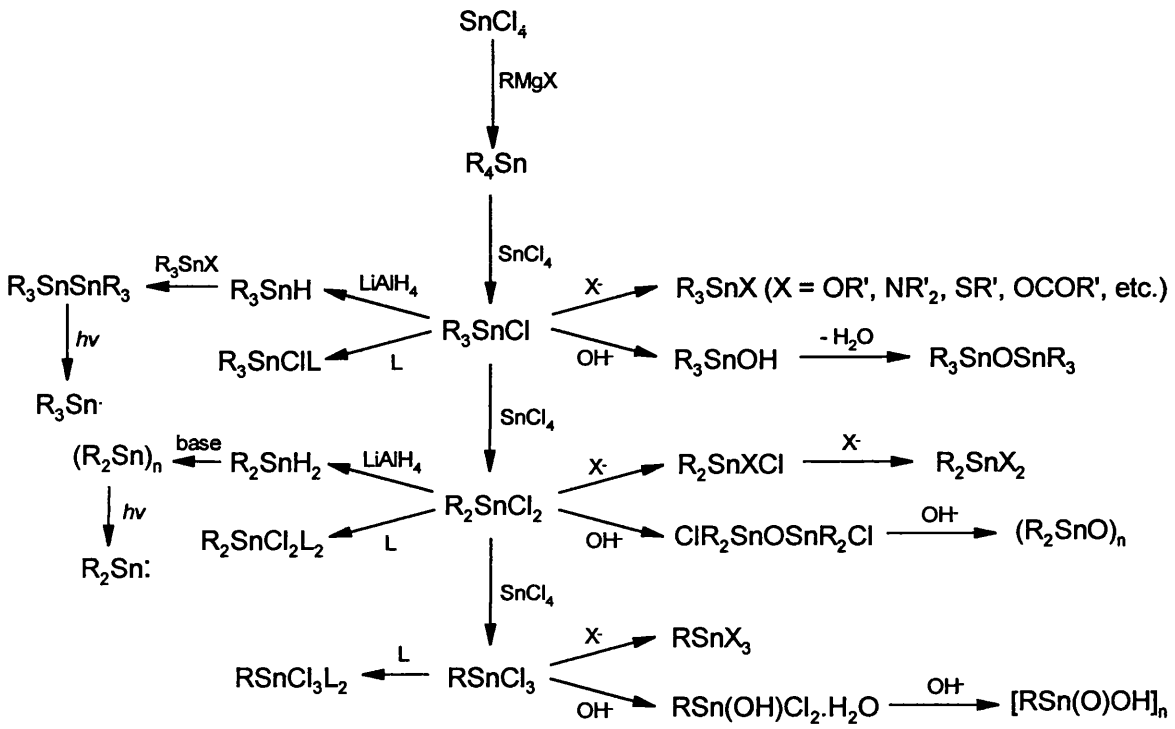

Scheme 1.1 Common Reactions of Organotin(IV) Compounds

1.9.3.1 Grignard Reagents and Organolithiums

Grignard and organolithium reagents are used extensively for the formation of the tin-carbon bond. Due to the availability and low cost of tin tetrachloride this is the most commonly used tin reagent.

$$SnCl_4 + 4LiR \longrightarrow SnR_4 + 4LiCl \qquad [1.7]$$

$$SnCl_4 + 4RMgX \longrightarrow SnR_4 + 4MgXCl \qquad [1.8]$$

Steric hindrance affects these reactions considerably, and yields decrease as the R group becomes more bulky, *i.e.* yields from secondary and tertiary alkyl groups are poor. Only three tertiary butyl groups may be attached to a tin atom due to the steric bulk of the ligand, and the reaction proceeds in a very poor yield.

To ensure the absence of organotin halide by-products, the Grignard or organolithium reagent is usually used in excess. It is likely that unwanted products such as $RSnCl_3$, R_2SnCl_2 or R_3SnCl will be formed otherwise, and separation of the products can present some difficulties. However, these compounds can be produced in very good yield by further reaction of SnR_4 with $SnCl_4$ in the correct stoichiometric quantities. The reactions take place in the absence of solvent at 200°C.

$$3SnR_4 + SnCl_4 \longrightarrow 4R_3SnCl \qquad [1.9]$$

$$SnR_4 + SnCl_4 \longrightarrow 2R_2SnCl_2 \qquad [1.10]$$

$$SnR_4 + 3SnCl_4 \longrightarrow 4RSnCl_3 \qquad [1.11]$$

Other functional groups are introduced by nucleophilic substitution of the chloride, and it is possible to prepare a wide range of organotin compounds in this fashion, as illustrated in Scheme 1.1. The scheme demonstrates the enormous variety of organotin compounds that can be derived from the series R_nSnCl_{4-n}.

1.10 SPECTROSCOPY OF ORGANOTIN COMPOUNDS

There are a large number of general and more specific analytical techniques available for the characterisation and structural classification of organotin compounds. Infra-red,[173-174] ^1H NMR[175] and ^{13}C NMR[176] spectroscopy are extremely useful techniques for providing information regarding the ligand structure. The ^1H and ^{13}C NMR studies can also supply structural information regarding the tin centre by the observation of ^1J and ^2J coupling constants. For definitive structural information

concerning the tin centre, the nucleus-specific techniques of ^{119m}Sn Mössbauer and ^{119}Sn NMR are indispensable. These spectroscopic techniques will be utilised in this thesis and therefore discussed in greater depth.

1.10.1 Mössbauer Spectroscopy

Mössbauer spectroscopy is a specialised technique, and is a very useful method for investigating the nature and stereochemistry of the tin centre in organotin compounds. It can be described by its alternative title of nuclear gamma resonance spectroscopy, as the Mössbauer effect is the resonant absorption of γ-rays. There are many books[177-178] and general reviews[179-180] which thoroughly explain the principles of Mössbauer spectroscopy, and only a general outline summarising the major points is given here.

Gamma emission occurs when a nucleus, the *source*, drops from an excited state to one of lower energy. The source is a metastable ^{119m}Sn isotope which must have an accessible excited state, preferably by the spontaneous decay of a parent isotope with a reasonably long half-life. If these emitted γ-rays now fall on a nucleus of the same isotope which is in the lower state, the γ-photon may be absorbed and the second nucleus excited. This procedure is shown in Figure 1.12.

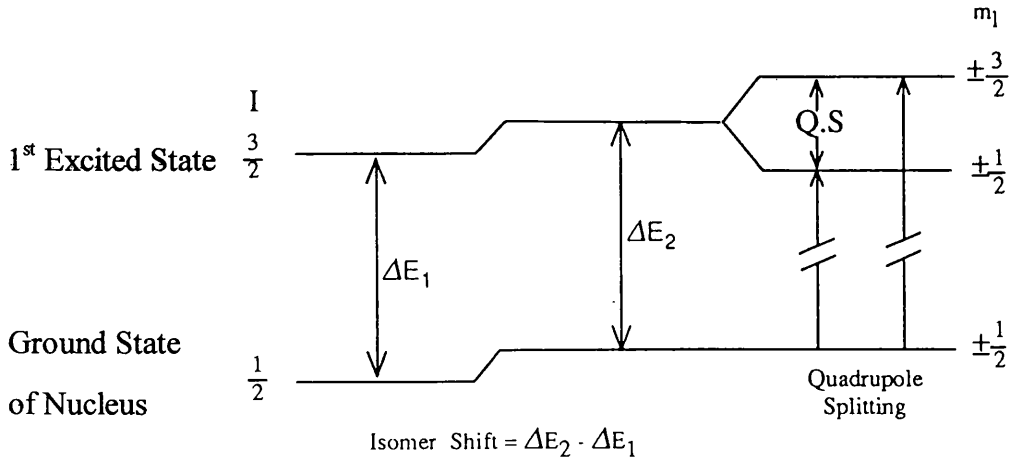

Figure 1.12 The Mössbauer Effect, with $I_{gr} = {}^1/_2$, $I_{ex} = {}^3/_2$

However, usually there is a mismatch in energy between the nuclear excitation energy and the energy of the incident γ-photon, related to the *recoil energy*. In order to obtain resonant absorption, the emitting and absorbing nuclei must be bound in solid lattices for which the lowest vibrational excitation energy is greater than the recoil energy. There will then be a fraction of the nuclei which will emit or absorb without any recoil at all. In order to obtain a significant recoil-free fraction, samples must be in the solid state, and it is this recoil-free fraction which gives rise to the observed spectrum.

For tin Mössbauer studies, the sample is maintained at liquid nitrogen temperature (80 K), and the technique therefore requires studies to be carried out on solid samples either as the pure materials or incorporated in a particular matrix.

There are two important parameters which can be determined by the use of Mössbauer spectroscopy, the *isomer shift*, and the *quadrupole splitting* parameter. The energy scale of a Mössbauer spectrum is a velocity scale and energies are quoted in mm s^{-1}, the energy difference between pairs of nuclear energy levels (ΔE_1, ΔE_2) being necessarily small.

1.10.1.1 The Isomer Shift

The isomer shift δ is due to the mismatch between source and absorber of the ground and first excited nuclear energy levels (ΔE_1 - ΔE_2 in Figure 1.12) and provides information regarding the oxidation state of the tin. It is dependent upon the *s*-electron density at the ^{119}Sn nucleus, and falls in the range ±5 mm s^{-1} for all tin compounds. A positive δ value corresponds to an increase in nuclear *s*-electron density at the tin atom. Since the electron density at the tin nucleus is related to the *s*-electron density in the valence shell of the tin atom, δ varies with the polarity of the tin-ligand bonds. One observation is that an increase in the electronegativity of an attached halogen produces a steady reduction in the nuclear s-electron density, with a corresponding drop in the value of δ. For example, the replacement of the chlorine atom in $K_2\{BuSnF_4Cl\}$ with a fifth fluorine atom corresponds to a reduction in the isomer shift from 0.47 mm s^{-1} to 0.27 mm s^{-1}.[181]

Similarly, the isomer shift value will increase in accordance with the electron donating power of an attached alkyl group. Phenyltin derivatives usually exhibit lower isomer shift values than their aliphatic counterparts due to the strong electron-withdrawing power of the phenyl group.

The isomer shift parameter is also affected by a change in the coordination number or stereochemistry at the tin atom. An increase in the coordination number will cause an increase in the use of tin's 5*d*-orbitals for bonding, which results in a reduction in the 5*s*-electron density at the tin nucleus and hence a corresponding drop in δ. A change in stereochemistry will also have an influence on the value of δ usually by altering the amount of *s*-character of the tin-carbon bonds.

Organotin(II) compounds show much higher values of δ than organotin(IV) derivatives due to the presence of a lone pair of formally 5*s* electrons. In general, the value of δ usually falls in the range of -0.50 mm s^{-1} to +2.70 mm s^{-1} for tin(IV) compounds, with tin(II) derivatives exhibiting a higher value, although there is some area for crossover due to possible structural variations described above.

1.10.1.2 The Quadrupole Splitting Parameter

The quadrupole splitting parameter arises from an asymmetry in the electron cloud around the tin nucleus, and provides information regarding the geometry of the tin atom. If the tin atom has a perfectly spherical symmetry, as in, for example, a tetraorganotin compound such as Me_4Sn, then only a single line is observed in the Mössbauer spectrum, a *singlet*. Any deviation of the ^{119}Sn nuclear charge from cubic results in two lines in the spectrum known as a *doublet*. The magnitude of the line separation is measured in mm s^{-1} and has the symbol ΔE_Q.

Essentially, the principal cause of any asymmetry in the ^{119}Sn nuclear charge is an imbalance in the 5*p* valence electrons of the tin atom. This is affected mainly by the spatial arrangements of the organic groups surrounding the metal. The ΔE_Q values are specific for a particular tin atom stereochemistry, particularly for di- and tri-organotin

compounds so the quadrupole splitting parameter is a very useful tool for the assignment of stereochemistry in organotin chemistry. Table 1.4 shows how the values of ΔE_Q vary with different stereochemistries.

Table 1.4 The Effect of Stereochemistry on ΔE_Q (mm s^{-1})

COMPOUND	Stereochemistry	ΔE_Q Range
R_3SnX	Tetrahedral	1.00 - 2.40
R_2SnX_2	Tetrahedral	1.00 - 2.40
R_3SnX_2	*trans*-Trigonal Bipyramidal	3.00 - 4.00
R_3SnX_2	*cis*-Trigonal Bipyramidal	1.70 - 2.40
R_2SnX_4	*trans*-Octahedral	$\approx$ 4.00
R_2SnX_4	*cis*-Octahedral	$\approx$ 2.00

Five-coordinate triorganotin complexes R_3SnX_2 may exist in three trigonal bipyramidal isomeric forms (**IV**), (**V**), and (**VI**), and the magnitude of ΔE_Q can be used to decipher which isomer is present. The *trans* isomer is the most common, and can easily be distinguished from the *cis* isomer as it gives much higher values of ΔE_Q. An increasing difference in the two axial Sn-X bond lengths causes a corresponding increase in value of ΔE_Q. The *mer* form is extremely rare, but ΔE_Q values are estimated to fall in the range of 3.50 to 4.10 mm s^{-1}.[182]

Octahedral *cis* and *trans* isomers of diorganotin compounds (**VII**) and (**VIII**) are also easily distinguishable by the ΔE_Q parameter, as the value for the *trans* isomer is double that of the *cis* isomer regardless of the nature of the X groups. The ΔE_Q values actually increase smoothly with increasing C-Sn-C bond angle.[183]

1.10.2 ^{119}Sn NMR Spectroscopy

Only three of the ten naturally occurring isotopes of tin have a nuclear spin I = ½, these being ^{115}Sn, ^{117}Sn and ^{119}Sn. This makes study by NMR spectroscopy possible, but not facile. In practice, the isotope chosen is usually ^{119}Sn, due to its slightly higher abundance and greater sensitivity to NMR detection. Various books[184-185] are available for reference which thoroughly describe the ^{119}Sn NMR technique.

1.10.2.1 ^{119}Sn Chemical Shifts

^{119}Sn chemical shifts, $\delta(^{119}Sn)$, of organotin compounds cover a large range of over 600 ppm and are quoted relative to tetramethyltin which is referenced at 0 ppm. Downfield shifts from the reference compound have a positive sign as in other NMR studies. The position of the observed signal is influenced by a number of factors, so the NMR technique is an extremely useful tool in assignment of the structure of the compound under investigation.

The value of $\delta(^{119}Sn)$ is largely affected by the nature of the alkyl groups surrounding the tin nucleus. As the electron-releasing power of the alkyl group increases, the tin atom becomes progressively more shielded and the $\delta(^{119}Sn)$ value moves to higher field. Unsaturated substituents such as vinyl or allyl cause the chemical shifts to move markedly upfield which is probably due to the increased polarisability of these groups. Inorganic ligands also influence the value of $\delta(^{119}Sn)$, with the chemical shift moving more downfield as the electronegativity of the ligand increases. The effects of varying the nature and number of alkyl groups in the series R_nSnCl_{4-n} are shown in Table 1.5.

Table 1.5 ^{119}Sn NMR Chemical Shifts (ppm) of the Series R_nSnCl_{4-n} with Varying R Group

R	$RSnCl_3$	R_2SnCl_2	R_3SnCl
Me	+20	+141	+164
Et	+6.5	+126	+155
Bu	+6.0	+122	+141
^{t}Bu	-	+52	+50
Ph	-6.3	-32	-48

An important property of $\delta(^{119}Sn)$ is that an increase in coordination number of the tin atom usually results in a large upfield shift. This may occur by the addition of a complexing solvent to a solution of the organotin compound in a non-coordinating solvent. For example, if Me_3SnCl is mixed with pyridine in carbon tetrachloride, the ^{119}Sn chemical shift moves remarkedly upfield which is consistent with the increase in coordination number.

A decrease in coordination number will hence cause the opposite effect of a downfield shift. This can occur if the solvent has the effect of decreasing the number of tin bonds, by, for example, breaking up a polymeric arrangement. For example, the chemical shift of $(c\text{-}C_6H_{11})_3SnOH$ is seen to change from -217 ppm in the solid to +11.6 ppm in solution as the compound becomes monomeric and hence exhibits a lower coordination number.

1.10.2.2 Coupling Constants Involving ^{119}Sn

^{119}Sn can couple to other NMR active nuclei and the resulting spin-spin coupling constant J can usually be measured. Coupling constants are related via the Fermi contact term to the *s* electron density in the bond, and their magnitudes can therefore be used to infer valence electron distribution and hence bonding and structure. The most detailed

studies have been carried out on couplings involving tin and hydrogen $^{2}J(^{119}Sn\text{-}^{1}H)$ and tin and carbon $^{1}J(^{119}Sn\text{-}^{13}C)$, and correlations of their magnitudes with stereochemistry are often informative. For example, tin-hydrogen couplings for tetrahedral trimethyltin compounds are lower than those for pentacoordinate trimethyltin complexes. Also, tin-carbon couplings show an increase with increasing coordination number of the tin atom.

The magnitudes of $^{2}J(^{119}Sn\text{-}^{1}H)$ and $^{1}J(^{119}Sn\text{-}^{13}C)$ have been related in a quantitative manner to the C-Sn-C bond angles in methyl- and butyltin(IV) compounds. The following formulae apply for butyltin(IV)[186] (Formula 1.1) and methyltin(IV)[187] (Formula 1.2) compounds respectively.

$$|\,^{1}J(^{13}C\text{-}^{119}Sn)\,| = (9.99 \pm 0.73)\theta - (746 \pm 100) \qquad \textbf{[Formula 1.1]}$$

$$\theta = 0.0161\,|\,^{2}J(^{1}H\text{-}^{119}Sn)\,|^{2} - 0.799\,|\,^{2}J(^{1}H\text{-}^{119}Sn)\,| + 133.4 \qquad \textbf{[Formula 1.2]}$$

In fluorine-containing organotin compounds, tin-fluorine coupling is readily observed if the fluorine is situated on the α-carbon $[^{2}J(^{119}Sn\text{-}^{19}F)]$, although a coupling constant of a much smaller magnitude can sometimes be seen from fluorine in the β-carbon position $[^{3}J(^{119}Sn\text{-}^{19}F)]$. For example, the respective values found for $Me_3SnCF_2CF_2H$ were 249 Hz and 10 Hz.[188]

1.11 AIMS AND SYNTHETIC STRATEGIES

The aim of this thesis is to describe the attempts to synthesise novel single source precursors for the CVD of fluorine-doped tin oxide. A variety of fluorine-containing organotin(IV) compounds have been synthesised and fully characterised for this purpose.

The single source precursors were designed :

(i) *To be synthesised from relatively cheap starting materials to allow a facile scale-up process in order to obtain sufficient quantities for large scale CVD trials.*

(ii) *To have a sufficient level of volatility to allow easy transport to the reactor.*

(iii) *To achieve volatility by minimising intermolecular interactions.*

(iv) *To locate fluorine on various parts of the ancillary ligands to identify the optimum position, but largely avoiding direct tin-fluorine bonds which are known to diminish volatility.*

CVD experiments have been carried out in order to assess the viability of each precursor in terms of the film characteristics achievable by dual source methods (Section 1.6). A thickness of approximately 3000 Å was desired in order to obtain films which could potentially be used as spectrally selective coatings on windows.

Chapter Two

Perfluoroalkyltin Compounds

2.1 INTRODUCTION

Compounds containing the perfluoroalkyl group (R_f), in which the carbon chain is totally fluorinated, play an important role in fluorine chemistry and in industry because the R_f group has unique properties. These include high electronegativity, stability, lipophilicity, and water and oil repellency.[189] Many reagents have therefore been developed to introduce the R_f group into organic molecules to utilise these properties to full effect. There are several reviews which discuss the various research which has recently been conducted in this field of chemistry.[190-191]

Perfluoroalkyltin compounds are potential single source precursors for the CVD of fluorine-doped tin oxide for several reasons.

2.1.1 Advantages and Disadvantages

There are many clear advantages for compounds of the type $R_{(4-n)}Sn(R_f)_n$ for use as CVD precursors.

(i) *They are unlikely to exhibit any strong intermolecular bonding and should therefore have a good level of volatility.*
(ii) *They are likely to be liquids.*
(iii) *The fluorine could be positioned very close to the tin which should encourage facile fluorine transfer during decomposition in the CVD reactor.*

There are, however, some inevitable potential problems which could be encountered.

(i) *Synthesis could be difficult as there are relatively few perfluoroalkyltin compounds known.*
(ii) *Starting materials are expensive.*

(iii) *There are a limited number of readily available starting materials, restricting the development of a wide range of compounds.*

One of the main reasons for exploring compounds of the formula $R_{(4-n)}Sn(R_f)_n$ is the potentially favourable fluorine arrangement which can be achieved in the precursor. It was envisaged that a β-fluoride elimination could take place during the CVD of compounds containing fluorine in the appropriate position (Scheme 2.1).

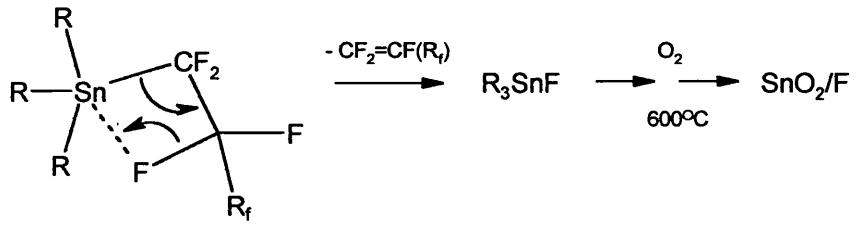

Scheme 2.1 β-Fluoride Elimination Mechanism

This process could be favourable, so compounds containing such an arrangement could be effective single source precursors for the CVD of fluorine-doped tin oxide.

This chapter will briefly describe the structural chemistry and various synthetic routes currently known for this class of compound. The introduction will be followed by details of the synthesis, characterisation and CVD testing of a series of novel perfluoroalkyltin compounds produced for this thesis.

2.2 STRUCTURAL CHEMISTRY

With the exception of certain phenyltin derivatives, the vast majority of perfluoroalkyltin compounds are liquids so there is very little structural chemistry documented in the literature. All compounds of the type $R_{(4-n)}Sn(R_f)_n$ contain four tin-carbon bonds and therefore exhibit tetrahedral geometry. One compound for which

there has been a crystal structure determined is 2,4,6-$(CF_3)_3C_6H_2SnPh_3$[192] (Figure 2.1) which displays the expected tetrahedral arrangement.

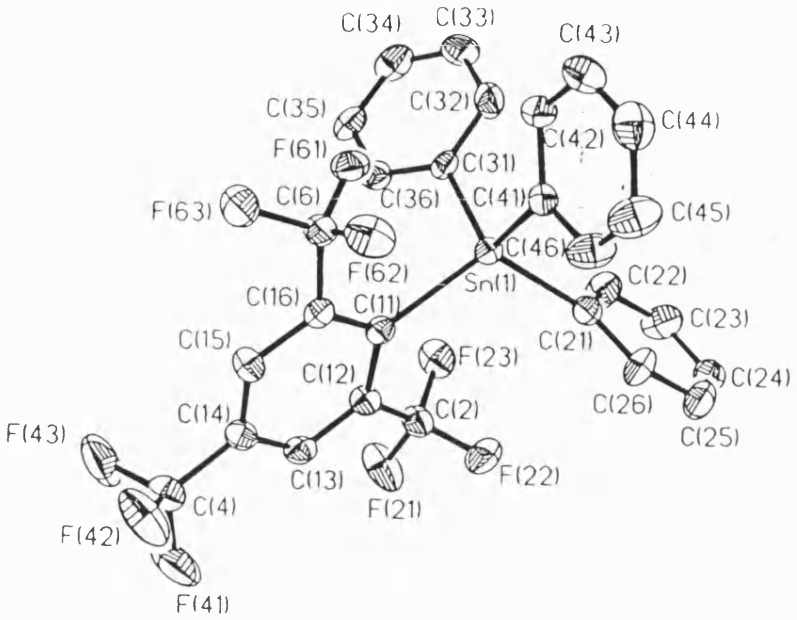

Figure 2.1 The Molecular Structure of 2,4,6-$(CF_3)_3C_6H_2SnPh_3$[192]

2.3 SYNTHETIC ROUTES

The synthesis of perfluoroalkyltin compounds is associated with a reasonable degree of difficulty and has caused many problems over the years. The difficulties arise because fluorocarbons are reluctant to coordinate to metal centres and are resistant to chemical attack.[193] This is a consequence of the great strength of the C-F bond and the high electronegativity of fluorine.

There are currently several routes available for the synthesis of perfluoroalkyltin compounds, each being associated with certain difficulties. A reasonable amount of research into such syntheses took place in the late 1960's when several methods were identified, but only mediocre success achieved. In general, complex product mixtures were obtained and yields were rather low. To date, relatively little progress has been

accomplished, and the synthesis of such compounds still appears to be rather underdeveloped. The vast majority of known compounds contain only one fluorinated group and therefore have the R_3SnR_f arrangement, with very few examples of compounds containing additional R_f groups. Information regarding the methods used, compounds produced and brief comments concerning the experimental conditions are summarised in Table 2.1. The table includes compounds containing aliphatic R and R_f groups with relevant equations and further details given in the following text.

Table 2.1 Synthetic Routes Used for the Preparation of Perfluoroalkyltin Compounds

COMPOUND	Synthesis[a]	Comments	Yield	Ref.
Me_3SnCF_3		Reaction involves Carius tube,	42	194
$Me_3SnC_2F_5$	2.1	difficult to separate complex	17	195
$Me_3SnCF(CF_3)_2$		product mixture.	42	195
$Me_2Sn(C_2F_5)_2$			34	196
$Bu_2Sn(C_2F_5)_2$	2.2 - 2.3	Slow reaction, low yields.	16	196
$Bu_3SnC_2F_5$			48	196
$Sn(C_3F_7)_4$		Good method provided careful	19	197
$MeSn(C_3F_7)_3$	2.5 - 2.7	control of low temperature is	11	197
$Me_2Sn(C_3F_7)_2$		maintained.	82	197
$Bu_3SnC_4F_9$	2.8 - 2.9	Method unreliable, complex product mixture.	28	198

[a] Equation numbers given

The first accepted method involved the reaction of a hexaorganoditin compound with the appropriate perfluoroalkyl iodide, in which the tin-tin bond is cleaved by the iodide.

$$R_3Sn\text{-}SnR_3 + R_fI \xrightarrow{\text{heat or hv}} R_3SnI + R_3SnR_f \qquad [2.1]$$

This method was originally used to synthesise trimethyltrifluoromethyltin Me_3SnCF_3,[199] and has since been used to prepare a wide range of perfluoroalkyltin compounds (Table 2.1).[194-195] However, this method is not very attractive due to a difficult synthetic procedure which involves irradiation in a sealed vessel for a period of *ca.* 24 hours. The reaction also produces a mixture of products and the perfluoroalkyltin compound is generally recovered in a low yield. It is also only possible to incorporate one fluorinated group into the tin compound via this method and hexaorganoditin starting materials are rather limited and expensive. This method is generally found in older literature, and alternative synthetic routes have been developed more recently.

The more recent synthetic methods involve the use of a variety of organometallic reagents,[200] the most common being organolithium and Grignard reagents. There are problems with these methods due to the high electronegativity of the fluorines, and hence the difficulty in incorporating a lithium or magnesium atom into the organofluorine compound.

There has been a considerable amount of research conducted on the synthesis of perfluoroaliphatic Grignard reagents, R_fMgX. There have been several modifications to the synthetic procedure over the years as the properties of this group of compounds has become clearer.

The first technique involved the standard Grignard reaction in which elemental magnesium is reacted with the appropriate iodide to produce the Grignard reagent. This is subsequently reacted with the corresponding organotin halide to produce the perfluoroalkyltin compound.

$$Mg + R_fI \xrightarrow[\text{r. t.}]{\text{THF}} R_fMgI \qquad [2.2]$$

$$nR_fMgI + R_{(4-n)}SnX_n \xrightarrow[\text{40°C, 15 hr}]{\text{THF}} R_{(4-n)}Sn(R_f)_n + nMgIX \qquad [2.3]$$

This synthetic method has been used to produce a range of perfluoroalkyltin compounds (Table 2.1), with products obtained in low yields (16-48%).[196]

It has since been discovered that the intermediate fluorinated Grignard reagent has a very low thermal stability, and the outcome is improved by maintaining the reagent at a low temperature. Several perfluorovinyltin compounds have been prepared in this fashion,[201] in which the magnesium is preactivated by the addition of bromoethane and the Grignard reagents are subsequently prepared at a temperature of -20°C.

By far the best synthetic route concerning perfluoroalkyl Grignard reagents involves the use of a preformed simple Grignard reagent to subsequently form the fluorinated Grignard reagent by an exchange reaction. A generalised reaction is given by Equation 2.4.

$$RMgX + R_fI \longrightarrow R_fMgX + RI \qquad [2.4]$$

The production of perfluoroaliphatic Grignard reagents in this fashion was first discovered in 1953[202] and has since been developed into a successful method for the synthesis of such compounds.[203,204] It has been found that EtMgBr and PhMgBr are effective for producing the fluorinated Grignard reagent with good exchange with R_fI at -70°C in diethyl ether. Experimental conditions have been found to have a pronounced effect on the yield. For example, using freshly distilled perfluoroalkyliodide is found to increase the yield significantly, and only perfluoroalkyl iodides are effective with very little exchange achieved from bromides and chlorides.

Although a good method for the synthesis of perfluoroaliphatic Grignard reagents was established several decades ago, subsequent reactions using them as intermediates as a route to new perfluoroalkyltin compounds have only appeared very recently. Seyferth *et al*, have recently reported the successful synthesis of a range of perfluoropropyltin compounds using this method.[197] For these reactions isopropyl chloride was found to be a good starting material for forming the initial Grignard reagent and hence the subsequent fluorinated compound.

$$^{i}PrCl + Mg \xrightarrow[r.t.]{Et_2O} {}^{i}PrMgCl \qquad [2.5]$$

$$^{i}PrMgCl + R_fI \xrightarrow[-78°C]{Et_2O} R_fMgCl + {}^{i}PrI \qquad [2.6]$$

$$nR_fMgCl + R_{(4-n)}SnX_n \xrightarrow[-40°C]{Et_2O} R_{(4-n)}Sn(R_f)_n + nMgClX \qquad [2.7]$$

The conversion to the fluorinated compound proceeds very well at very low temperatures (*ca.* -78°C), and the subsequent reaction with the tin halide is found to benefit from the slightly elevated temperature of -40°C. The yields of the perfluoropropyltin compounds in this case are very good (11-82%), but are found to generally decrease as more fluorinated ligands are incorporated.

The Grignard method is generally a very good synthetic route for the preparation of the perfluoroalkyltin compounds provided the reaction conditions are carefully monitored. It is an appealing method due to the capability of producing compounds containing one to four fluorinated groups, and it generally proceeds in higher yields than other methods. One drawback is the relatively high cost of the fluorinated iodides and the limited number available. Also, trifluoromethyl and pentafluoroethyl iodides are gases increasing the difficulty of the synthesis of derivatives containing these groups via this route. However, the Grignard method appears to be one of the chosen routes for the recent synthesis of compounds, for example $[C_6F_{13}(CH_2)_2]_3SnPh$.[205]

The second class of organometallic reagent which have been utilised in the synthesis of perfluoroalkyltin compounds are the organolithiums. In general, the reagent chosen is methyllithium due to the relatively high reactivity of this reagent. Again, a very low temperature is required to prevent decomposition of the intermediate fluorinated lithium reagent.

$$MeLi + R_fI \xrightarrow[-90°C]{Et_2O} R_fLi + MeI \qquad [2.8]$$

$$R_{(4-n)}SnX_n + nR_fLi \xrightarrow[-90°C]{Et_2O} R_{(4-n)}Sn(R_f)_n + nLiX \qquad [2.9]$$

This method has been used to prepare tributyl(perfluorobutyl)tin $Bu_3SnC_4F_9$[198] where the organometallic reagent used was methyllithium-lithium bromide. Following distillation under reduced pressure, the isolated product was found to be a mixture of compounds including unreacted Bu_3SnCl, and also Bu_3SnMe and Bu_3SnBr as by-products. This was due to the similarity in boiling points of the tributyltin compounds, and a clean method of separation was not reported for this reaction. The synthetic route using an organolithium reagent has also been used to prepare a range of allyltin compounds[206] and more recently, tributyl(trifluorovinyl)tin.[207]

There are also a variety of less common preparations which are documented in the literature. A powerful fluoroalkylating agent that has been discovered is bis(trifluoromethyl)cadmium·glyme (glyme = dimethoxyethane) which has been used to synthesise the fully substituted tetrakis-(trifluoromethyl)tin.[208] The cadmium reagent is formed from bis(trifluoromethyl)mercury and dimethylcadmium in glyme, and the subsequent reaction with $SnBr_4$ yields $Sn(CF_3)_4$. Although this method is successful, it is limited for the preparation of trifluoromethyl derivatives and is rather unattractive due to the high level of toxicity of the mercury and cadmium reagents.

There are two methods documented in the literature which could potentially lead to the production of perfluoroalkyltin compounds. One such method involves the initial conversion of a tin(II) halide to a tin(IV) species by an oxidative addition reaction.

$$R_fI + SnX_2 \xrightarrow[r.t.]{DMF} R_fSnX_2I \qquad [2.10]$$

A variety of compounds of this nature have been prepared,[209] but it was found to be impossible to isolate them in a pure form. It should be possible to use such a compound as an intermediate, and perform a subsequent Grignard reaction to replace the halide groups with alkyl substituents. However, this method would be restricted to the preparation of compounds containing one fluorinated ligand only, R_3SnR_f.

Another synthetic route which has been used to prepare compounds of a different nature, but could potentially be a route to the targeted perfluoroalkyltin compounds

involves the synthesis of organosilver compounds. There is a significant amount of material in the literature which reports the synthesis of a variety of perfluoroalkylsilver compounds, although the majority is rather old.[210-213] The reaction involves the addition of silver fluoride across the double bond of a fluorinated olefin to produce the perfluoroalkylsilver compound.

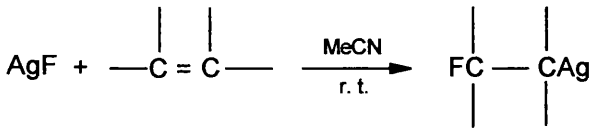

[2.11]

Problems with the perfluoroalkylsilver compounds have been encountered during the attempted isolation of such species due to their instability to light and heat. However, it would not be necessary to isolate the silver compound therefore eliminating such difficulties. It could therefore be feasible to use a perfluoroalkylsilver compound as an intermediate to the target perfluoroalkyltin compound by reacting it with the appropriate organotin halide to produce the silver halide as a by-product. This method has the advantage of the possible incorporation of different fluorinated groups, as the starting materials are not iodides as in all the other available synthetic methods.

2.3.1 Pyrolysis Studies

Pyrolysis studies of two of the perfluoroalkyltin compounds have been conducted,[195] with results summarised in Table 2.2.

Table 2.2 Pyrolysis Studies of Perfluoroalkyltin Compounds[195]

COMPOUND	Pyrolysis Conditions	% Recovery[a]	Other Products
$Me_3SnC_2F_5$	200°C, 72 hrs	91	C_2F_5H
$Me_3SnCF(CF_3)_2$	150°C, 64 hrs	54	$(CF_3)CF{=}CF_2$, Me_3SnF

[a] Recovered undecomposed reagent

The results show that the compounds have a good level of thermal stability and relatively harsh conditions are required in order to achieve decomposition. The higher level of decomposition observed for the branched compound $Me_3SnCF(CF_3)_2$ implies a lower degree of thermal stability for this material, which could be due to the presence of two β-fluoride sites and hence more facile fluorine elimination. The observation of Me_3SnF as a product of thermal decomposition is very encouraging as it shows the viability of perfluoroalkyltin compounds as potential precursors for fluorine-doped tin oxide.

2.4 RESULTS AND DISCUSSION

2.4.1 Synthesis

A series of perfluoroalkytin compounds $R_{(4-n)}Sn(R_f)_n$ have been prepared with a variation in both the organic group R and the fluorinated component R_f, which has enabled the effects of both constituents to be explored. Also, the number of fluorinated groups incorporated into the molecule has been varied in the fashion R_3SnR_f, $R_2Sn(R_f)_2$ and $RSn(R_f)_3$. The optimum arrangement of a perfluoroalkyltin precursor could therefore be determined.

As previously mentioned, the synthesis of compounds in this class has been met with some degree of difficulty, and several synthetic routes were tried until a suitable method was identified. A method was required for which it was possible to incorporate multiple fluorinated components, hence the method involving hexaorganoditin starting materials was not feasible. Also, a variety of fluorinated components were desired, so the method using the cadmium reagent was also not appropriate. Therefore, it appeared that the best methods available were those involving organometallic lithium or Grignard reagents. The first attempts for all methods used perfluorobutyl iodide as the fluorinated source due to lower cost and easier handling of this fluorinated iodide.

The first method attempted involved a direct Grignard reaction between elemental magnesium and perfluorobutyl iodide, followed by subsequent reaction with tributyltin chloride.

$$Mg + C_4F_9I \xrightarrow[r.t.]{THF} C_4F_9MgI \qquad [2.12]$$

$$Bu_3SnCl + C_4F_9MgI \xrightarrow[40^oC,\ 15\ hrs]{THF} Bu_3SnC_4F_9 + MgICl \qquad [2.13]$$

The Grignard reagent and tributyltin chloride were stirred together at 40°C for 15hr, and the solvent removed by distillation. A mixture of unreacted Bu_3SnCl (155.9 ppm) in addition to a quantity of Bu_3SnI (86.2 ppm) and $Bu_3SnC_4F_9$ (-1.6 ppm) were identified in the crude material by ^{119}Sn NMR spectroscopy. Vacuum distillation of the residue was unsuccessful in yielding a clean product due to the similarity in boiling points of all the tributyltin compounds. Therefore, column chromatography was attempted as it was envisaged that the tetraorganotin species could be isolated in this fashion due to faster movement through the silica gel. It was found that with a very long column (≈ 30 cm) and a non polar solvent, in this case hexane or 40°-60° petroleum ether, separation could be achieved. A very long column was essential in order to achieve complete separation as the triorganotin species moved only slightly slower through the column. However, although the reaction proved successful to a certain extent, the perfluoroalkyltin compound was isolated in a very poor yield (10%), and for CVD use a better method was required due to the volume of material required.

The second method attempted involved an organolithium reagent as it was thought that the greater strength of this reagent may produce better results. The reagent chosen was methyllithium-lithium bromide as this is known to produce the target compound, tributyl(perfluorobutyl)tin.[198]

$$MeLi + C_4F_9I \xrightarrow[-100^oC]{Et_2O} C_4F_9Li + MeI \qquad [2.14]$$

$$C_4F_9Li + Bu_3SnCl \xrightarrow[-100^oC \rightarrow r.t.]{Et_2O} Bu_3SnC_4F_9 + LiCl \qquad [2.15]$$

It was found that an extremely low temperature of -100°C was required to prevent decomposition of the intermediate lithium reagent. Also, as mentioned in the literature[198] it was found to be very difficult to separate the mixture of products. The reaction was found to be rather irreproducible and also proceeded in a low yield (11%), so again was not suitable for adequate scale-up.

The next method which was attempted involved a modification of the Grignard reaction. This utilised a preformed simple Grignard reagent which was subsequently used to form the fluorinated Grignard as published by Seyferth.[197] Isopropyl chloride was found to be a very effective reagent for this purpose, and the target perfluoroalkyltin compound could be produced by subsequent reaction with the appropriate organotin halide.

$$Mg + {}^{i}PrCl \xrightarrow[r.t.]{Et_2O} {}^{i}PrMgCl \qquad [2.16]$$

$$^{i}PrMgCl + R_fI \xrightarrow[-78^{o}C]{Et_2O} R_fMgCl + {}^{i}PrI \qquad [2.17]$$

$$nR_fMgCl + R_{(4-n)}SnCl_n \xrightarrow[-40^{o}C]{Et_2O} R_{(4-n)}Sn(R_f)_n + nMgCl_2 \qquad [2.18]$$

R = Bu, $R_f = C_4F_9$, n = 1 (**1**), n = 2 (**2**), n = 3 (**3**)
R = Bu, $R_f = C_6F_{13}$, n = 1 (**4**)
R = Et, $R_f = C_4F_9$, n = 1 (**5**)

This method was found to be very reliable, and all attempted compounds were produced. The reaction was found to be extremely temperature sensitive due to the instability of the intermediate fluorinated Grignard reagent and care had to be taken to ensure the temperature remained at -78°C during this step. To achieve transfer of the magnesium to the fluorinated compound the reaction mixture had to be stirred at this temperature for at least one hour. 1.5 equivalents of the required Grignard reagents were always used due to the possibility of decomposition, and also to ensure complete replacement of all chloride groups on the tin. This was especially important for the synthesis of compounds in which more than one chloride was to be replaced due to the possibility of a complex product mixture. The reaction of the fluorinated Grignard

reagent with the organotin chloride proceeded better at a slightly elevated temperature of -40°C, but to achieve a reasonable yield this temperature had to be maintained for at least 2 hours.

Despite the use of excess Grignard reagent, there was always some unreacted organotin starting material in the isolated product, and the products could not be separated by even careful vacuum distillation. Therefore, a long column using a non-polar solvent such as hexane was found to be a very good method of separation for all compounds, with the perfluoroalkyltin compound always eluted as the first fraction.

The yields were found to be a vast improvement on the previous two methods tried (> 11%). It was generally found that the yields decreased as more fluorinated groups were introduced, and overall were in the range 18-55%. All compounds are colourless liquids which is a very attractive property for subsequent use as CVD precursors, and microanalysis confirmed that all materials had been produced in a pure form, with good agreement for hydrogen and carbon contents.

The composition of the possible compounds which could be synthesised by this method was restricted by the type of fluorinated iodides commercially available, with the vast majority consisting of simple, linear chains. Therefore, to prepare materials with a variation in the structure of the fluorinated component a different synthetic route was required. It was desired to synthesise some compounds containing branched fluorinated chains which could possibly be a better arrangement for fluorine transfer during the CVD process, and perfluoroalkylsilver compounds were used as intermediates. This method was attractive due to the availability of a number of branched fluorinated olefins which could potentially lead to the production of the corresponding branched perfluoroalkyltin compounds.

The first attempted synthesis used perfluoro-2-methyl-2-pentene as the fluorinated olefin. This compound was chosen due to its attractive properties of cheap availability, ease of handling as it is a liquid rather than a gas, and presence of fluorine atoms in a potentially effective position.

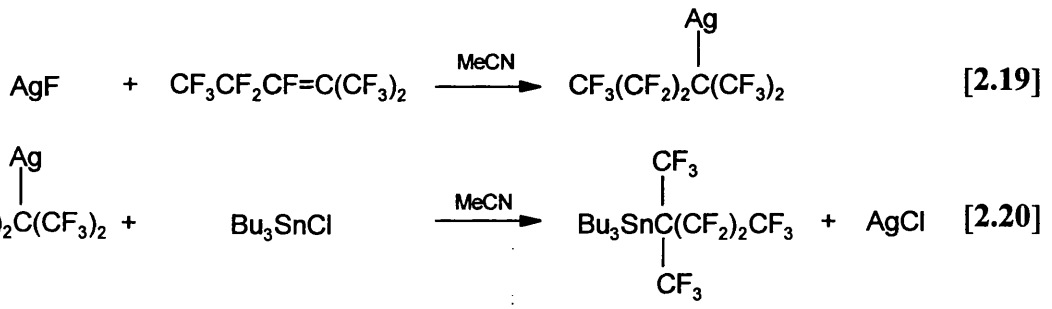

$$AgF + CF_3CF_2CF{=}C(CF_3)_2 \xrightarrow{MeCN} CF_3(CF_2)_2C(CF_3)_2(Ag) \quad [2.19]$$

$$CF_3(CF_2)_2C(CF_3)_2(Ag) + Bu_3SnCl \xrightarrow{MeCN} Bu_3SnC(CF_2)_2CF_3(CF_3) + AgCl \quad [2.20]$$

The fluorinated olefin was added to the insoluble silver fluoride to form the soluble intermediate perfluoroalkylsilver compound. The reaction mixture was then filtered by use of a canula filter, and the tributyltin chloride added by syringe. On removal of the solvent, a mixture of white solids were isolated. One compound was found to be soluble in hot methanol, which afforded separation of the two products. Following analysis, the soluble product was identified as tributyltin fluoride. Considering that the preparation of the intermediate perfluoroalkylsilver compound is known,[210] it appears that the only conceivable route to the production of tributyltin fluoride is following decomposition of the target compound. Additional evidence for this is supplied by the composition of the insoluble compound, which was identified as silver chloride. Although Bu_3SnF can be formed from the reaction of AgF with Bu_3SnCl this can not have been possible as any unreacted AgF was removed by filtration before the Bu_3SnCl was subsequently added to the filtrate. It therefore appears that the desired compound was temporarily formed, which rapidly decomposed to form the tributyltin fluoride isolated. This observation could possibly be due to the presence of three β-fluoride sites which could cause a rapid elimination, and hence the result obtained.

Therefore, following the successful preparation of the series of unbranched perfluoroalkyltin compounds, and the apparent decomposition of the attempted branched compound above, it was decided to attempt the synthesis of a compound with a structure intermediate to the compounds previously tried. An analogue to the fluorinated olefin was therefore used which contained the double bond in a different position, therefore producing a tin compound with a different fluorine arrangement. In this case, there were two β-fluoride sites which was an intermediate arrangement to the compounds previously tried. An identical reaction to the previous one was attempted.

$$AgF + CF_3CF{=}CFCF(CF_3)_2 \xrightarrow{MeCN} CF_3CF_2\underset{\displaystyle Ag}{\overset{|}{C}}FCF(CF_3)_2 \qquad [2.21]$$

$$CF_3CF_2\underset{\displaystyle Ag}{\overset{|}{C}}FCF(CF_3)_2 + Bu_3SnCl \xrightarrow{MeCN} Bu_3Sn\underset{\displaystyle C_2F_5}{\overset{|}{C}}CF(CF_3)_2 + AgCl \qquad [2.22]$$

(F above the C in the product)

However, the same result was obtained, indicating that only compounds containing straight alkyl chains have a high degree of stability at room temperature. This could explain the apparent lack of examples of perfluoroalkyltin compounds containing branched fluorinated chains. As previously mentioned (Section 2.3.1), pyrolysis has been performed on $Me_3SnCF(CF_3)_2$ which appears to be the only example of compound containing a branched fluorinated ligand. In this latter study, the equivalent Me_3SnF was identified as a product of decomposition, which therefore suggests a low thermal stability for compounds of this composition.

2.4.2 Mössbauer Spectroscopy

All compounds (**1**) - (**5**) were studied as frozen liquids at 78K; data are given in Table 2.3.

Table 2.3 Mössbauer Data for the Perfluoroalkyltin Compounds

COMPOUND		Isomer Shift δ ($mm\ s^{-1}$)	Quadrupole Splitting ΔE_Q ($mm\ s^{-1}$)
$Bu_3SnC_4F_9$	(**1**)	1.39	1.58
$Bu_2Sn(C_4F_9)_2$	(**2**)	1.46	1.75
$BuSn(C_4F_9)_3$	(**3**)	1.44	1.49
$Bu_3SnC_6F_{13}$	(**4**)	1.35	1.57
$Et_3SnC_4F_9$	(**5**)	1.36	1.65

All of the observed isomer shifts are consistent with organotin(IV) compounds as expected. The values obtained for the quadrupole splitting parameter are consistent with those usually observed for regular tetrahedral triorganotin compounds which usually fall in the range 1.00-2.40 mm s^{-1}. However, the perfluoroalkyltin compounds cannot be compared to triorganotin compounds R_3SnX as they are strictly tetraorganotin species containing four tin-carbon bonds. They would therefore be expected to display either a singlet or very narrow doublet in the Mössbauer spectrum. The observation of a considerable quadrupole splitting is therefore the result of the influence of the high electronegativity of the fluorine atoms contained on the R_f ligands. The compounds are tetrahedral, but the difference in electronegativity between the R and R_f groups leads to the rather large ΔE_Q values. Such effects have previously been observed for compounds which contain an electronegative ligand.[214]

The observation of relatively large quadrupole splittings for the compounds prepared in this thesis are consistent with values quoted in the literature for analogous compounds. For example, the quadrupole splitting for Me_3SnCF_3 has been determined as 1.38 mm s^{-1},[215] compared to the observation of a singlet for the hydrogenated equivalent Me_4Sn. The values found in this study are considerably larger than for the trifluoromethyl derivative which can be explained by the longer R_f ligands incorporated and hence the influence of an increased number of electronegative fluorine atoms.

2.4.3 NMR Spectroscopy

For all compounds synthesised, ^{1}H, ^{13}C, ^{19}F and ^{119}Sn NMR spectroscopy studies were performed.

2.4.3.1 ^{1}H, ^{13}C and ^{19}F NMR Spectroscopy

Expected results were observed in the proton and carbon-13 NMR studies, with R groups displayed clearly. Both spectra showed diagnostic chemical shifts for the R groups, with predicted integration and multiplicities evident in the proton spectra. The

one bond tin-carbon coupling constants $^{1}J(^{13}C\text{-}^{119}Sn)$ could be extracted from the carbon-13 spectra and are shown in Table 2.4.

Table 2.4 $^{1}J(C\text{-}^{119}Sn)$ Coupling Constants for the Perfluoroalkyltin Compounds

COMPOUND		$^{1}J(^{13}C\text{-}^{119}Sn)$ (Hz)
$Bu_3SnC_4F_9$	**(1)**	333
$Bu_2Sn(C_4F_9)_2$	**(2)**	358
$BuSn(C_4F_9)_3$	**(3)**	395
$Bu_3SnC_6F_{13}$	**(4)**	329
$Et_3SnC_4F_9$	**(5)**	331

The magnitudes of the coupling constants for all compounds are in the appropriate region for four-coordinate tributyltin species which are usually in the range 327-387 Hz.[216] There is an increase in the value with a corresponding increase in the number of R_f groups incorporated. This is due to the high electronegativity of the R_f ligand which leads to a higher covalent character of the Sn-Bu bond and hence a stronger demand for 5*s*(Sn) character in this bond as the R groups are progressively replaced by R_f ligands.

In the ^{13}C NMR spectra there was an absence of observed resonances for the carbon atoms which contained the fluorines. Therefore, the proton and carbon-13 NMR studies could be used to provide information regarding the R groups and confirmed their presence in the correct quantities. The $^{1}J(^{13}C\text{-}^{119}Sn)$ coupling constants could be used to confirm the coordination number of the tin, showing the compounds to be four-coordinate with tetrahedral geometry as expected.

The fluorine-19 NMR spectra displayed clear resonances for all the fluorine atoms contained on the R_f groups, and confirmed the presence of the appropriate ligand.

2.4.3.2 ^{119}Sn NMR Spectroscopy

The ^{119}Sn NMR studies provided information regarding the environment around the tin atom. This analytical technique was an extremely useful tool for the identification of the mixture of products initially isolated from the reactions. It was then an excellent method for confirming that column chromatography had indeed been successful in attaining a complete separation of the mixture. All perfluoroalkyltin compounds were run as solutions in deuterated chloroform and, following separation, all gave one signal showing that each compound had been produced cleanly.

All compounds showed strong coupling constants to the fluorine atoms on the α-carbon, but there were no couplings displayed with fluorines further from the tin. All data are displayed in Table 2.5.

Table 2.5 ^{119}Sn NMR Data for the Perfluoroalkyltin Compounds

COMPOUND		Chemical Shift (ppm)	Multiplicity	$^{2}J(^{119}Sn-^{19}F)$ (Hz)
$Bu_3SnC_4F_9$	(1)	-1.6	triplet	190
$Bu_2Sn(C_4F_9)_2$	(2)	-56.0	quintet	237
$BuSn(C_4F_9)_3$	(3)	-154.5	septet	300
$Bu_3SnC_6F_{13}$	(4)	-0.6	triplet	191
$Et_3SnC_4F_9$	(5)	3.6	triplet	190

Due to all the compounds containing four tin-carbon bonds, the chemical shifts would be expected to appear around zero ppm. However, the influence of the electronegative fluorines can clearly be seen from the large movement upfield in the series (1) - (3) as the number of R_f groups increases. This observation is consistent with the replacement of R groups with more electronegative constituents, which always results in an upfield shift of the resonance due to tin atom becoming progressively more

shielded. For example, as shown in Table 1.5 (Chapter One, Section 1.10.2) the values of δ for the series Bu_nSnCl_{4-n} decrease from +155 to +6.5 ppm as n reduces from 3 to 1, respectively.

The values found for the series of perfluoroalkyltin compounds are consistent with previously reported derivatives in the literature. For example, the value for $Me_2Sn(C_3F_7)_2$ is quoted as -22.8 ppm with the corresponding tris-compound $MeSn(C_3F_7)_3$ found to be -131 ppm.[197] The shifts for the compounds synthesised for this thesis are found to be slightly further upfield which would be expected as they contain an additional CF_2 and hence the influence of two extra fluorines.

The multiplicities displayed by the ^{119}Sn NMR spectra are consistent with the interaction of the tin nucleus with the surrounding fluorine atoms. It can clearly be seen that all fluorines attached to α-carbons contributed to the resultant multiplicity in the characteristic 2n + 1 fashion, and hence the observation of the triplet, pentet and septet with the presence of 2, 4 and 6 fluorines respectively.

Two-bond tin-fluorine coupling constants $^2J(^{119}Sn\text{-}^{19}F)$ could be measured for all compounds. The value of 190 Hz found for the compounds containing three R groups is consistent with previously reported compounds, for example a value of 187 Hz has previously been quoted for $Bu_3SnC_4F_9$.[198] It can be seen that the coupling constants increase as more R_f groups are introduced, which again is consistent with reports found in the literature. For example, for the perfluoropropyltin compound $MeSn(C_3F_7)_3$ $^2J(^{119}Sn\text{-}^{19}F)$ is quoted as 308 Hz, and the corresponding completely substituted tetrakis derivative $Sn(C_3F_7)_4$ is calculated at the increased value of 387 Hz.[197] A similar pattern has been observed for the $(CF_3)_n(CF_2H)_{4-n}Sn$ derivatives, where it is found that the $^2J(^{119}Sn\text{-}^{19}F)$ coupling constants for both Sn-CF_3 and Sn-CF_2H bonds increase as n increases from 1 to 4.[217] This is due to the lower electronegativity of the CF_2H group relative to a CF_3 group, which leads to a higher covalent character of the Sn-CF_2H bond and thus a stronger demand for 5*s*(Sn) character.

2.5 CVD TESTING OF PRECURSORS

All compounds (**1**) - (**5**) were subsequently tested as CVD precursors, with the testing carried out on a purpose-built atmospheric pressure CVD reactor at the University of Bath. Details of the apparatus are provided in Appendix Five. In all cases, the substrate used was 4 mm glass which had been undercoated with a thin film of SiCO to act as a "blocking layer" to prevent sodium diffusion into the fluorine-doped tin oxide film. This section gives details of the CVD conditions used and results of the film analysis to identify the quality of the films, and therefore allow an assessment of the potential of the perfluoroalkyltin compounds as single source precursors for the CVD of fluorine-doped tin oxide. All film analysis reported in this and subsequent chapters was carried out by Pilkington plc at Lathom, Lancashire.

The series of compounds (**1**) - (**3**) were tested first in order to determine the optimum number of fluorinated groups in the precursor. Following the results obtained from these three precursors, compounds (**4**) and (**5**) were synthesised and subsequently tested to see the effect of alternative R and R_f groups.

2.5.1 Deposition Conditions

Due to the difficulties encountered during the synthesis of the perfluoroalkyltin precursors, it was only possible to carry out deposition using a small quantity of some of the precursors. As the highest yield was obtained from compound (**1**) (8 g), this compound was used to try to ascertain a set of conditions which provided a good starting point for the other compounds, and therefore prevented the waste of the other expensive precursors. Table 2.6 shows the deposition conditions that were used for each precursor.

Table 2.6 Conditions for the CVD of Fluorine-Doped Tin Oxide Using Perfluoroalkyltin Precursors

PRECURSOR	**(1)**	**(2)**	**(3)**	**(4)**	**(5)**
Reactor Temperature (°C)	564	564	564	564	546
Bubbler Temperature (°C)	136	121	109	131	84
Heater Tapes (°C)	200	200	200	200	200
Diluent Flow ($Lmin^{-1}$)	3.00	3.50	3.00	3.00	3.00
Carrier Flow ($Lmin^{-1}$)	1.0	1.0	1.0	1.0	1.0
Oxygen Flow ($ccmin^{-1}$)	600	600	600	600	600
Run Time (min)	15	7	25	25	1

Tin oxide thin films are known to exhibit specific coloured fringes which are characteristic of certain thicknesses, making it possible to estimate the thickness by a visual inspection. The target thickness of ≈ 3000 Å could be identified by the first purple-green fringe from the deposited film, and it was often necessary to perform a substantial number of runs in order to identify a set of conditions which resulted in this characteristic. It was sometimes difficult to achieve this goal due to the small quantity of a number of the precursors, especially compounds (**3**) and (**4**) for which only 2.7 g and 1.7 g were available, respectively. The conditions listed in Table 2.6 correspond to those used which resulted in the best coating from each precursor. All films were found to adhere well to the glass substrate, and could not be removed without relatively harsh treatment.

The reactor temperatures listed in Table 2.6 were found to produce good transparent films. Lower temperatures resulted in a vast decrease in the growth rates, while powdery deposits were obtained at higher temperatures.

As all compounds were liquids, it was hoped that low bubbler temperatures would be sufficient to achieve a good transport of material. To prevent unnecessary use

of vast quantities of material, runs with the first precursor $Bu_3SnC_4F_9$ (**1**) were initially attempted at very low bubbler temperatures of approximately 40°C. The bubbler temperature was then increased gradually by 10°C for each successive run until a good film was obtained.

However, from the bubbler temperatures listed in Table 2.6 it can be seen that reasonably high temperatures were required, suggesting that the compounds were not remarkably volatile. The butyltin derivatives (**1**) - (**4**) were found to require a much higher temperature than the ethyltin compound (**5**) which suggests a higher degree of volatility for the precursor containing the smaller R groups and/or better mass transport of this material. Also, it was observed that the bubbler temperature decreased through the series (**1**) - (**3**) as the number of fluorinated groups increased, showing a greater volatility with additional fluorine incorporation. This is due to weaker intermolecular interactions caused by the minimising of dipole-dipole interactions between molecules.

As all precursors were liquids, excessive temperatures for the heater tapes were not necessary as there were no problems with condensation of precursors within the pipework. Therefore, a consistent temperature of 200°C was found to be satisfactory for the transport of all precursors. Suitable gas flows were also found to be fairly universal for all compounds tested, as those initially determined by precursor (**1**) were found to be adequate for the other materials.

In general, the deposition times were found to diminish as the number of R_f groups increased, which again can be explained by the higher volatility of the more substituted compounds. A longer run time was generally required by the two tributyltin derivatives, (**1**) and (**4**), than the butyltin compounds containing two and three fluorinated groups, (**2**) and (**3**) respectively. A significantly shorter run time was required by the triethyltin derivative (**5**) which is also consistent with a high degree of volatility for this precursor. The drastically reduced run time for this compound suggests that better mass transport of material can be achieved by incorporating small R groups into the precursor.

Films grown from the butyltin compounds (**1**) - (**4**) were found to favour deposition at the front end of the substrate directly after the inlet, and only coated the first 5 - 6 cm of the glass. The film grown from the ethyltin derivative (**5**) had a much more uniform appearance and spanned the total length of the glass. This can be explained by more rapid decomposition occurring for the butyl group due to a weaker tin-carbon bond in this longer hydrocarbon. Also, the β-hydride elimination mechanism is easier for a butyl group as the leaving group is more stable than for the ethyltin analogue.

Therefore, for large scale production where a high growth rate is vital, and also for better film uniformity, small R groups appear to be preferential.

2.5.2 Film Analysis

All coatings produced were subsequently analysed to determine which precursors had been successful in achieving a good fluorine-doped tin oxide film.

2.5.2.1 X-Ray Diffraction

Glancing Angle X-Ray diffraction studies were performed to determine if the films were crystalline, and then confirm the film composition as tin oxide. All the samples showed preferred orientation and were compared to a standard sample of SnO_2. Research has been conducted on the preferred orientation of SnO_2 thin films.[101] It has been shown that SnO_2 films grown along the (200) direction contain less structural defects,[114] and therefore give better performance for such applications as solar cells.[32]

As a means of expressing the degree of orientation, the peak counts of each SnO_2 reflection were summed and a ratio of the peak counts of the (200) reflection to the summed total expressed as a percentage. It should be noted that for a random specimen of SnO_2 the value of this ratio would be 7%. From line broadening measurements of the (110) reflection it was possible to measure the approximate crystallite size of the samples. The X-Ray diffraction data are given in Table 2.7 showing the number of

counts for each orientation, and a diffraction pattern illustrated in Figure 2.2 for the film grown from $Bu_3SnC_4F_9$ (**1**). The top spectrum represents the sample, with the spectrum of standard tin oxide displayed below.

Scanning Electron Microscopy (SEM) was performed on the film deposited from $Bu_3SnC_4F_9$ (**1**) to show the surface of the film where the crystallinity is clearly visible (Figure 2.3). The photographs clearly show the SiCO undercoat on which the fluorine-doped tin oxide coating has subsequently been deposited.

Table 2.7 X-Ray Diffraction Data for the Perfluoroalkyltin Precursors

PRECURSOR		**(1)**	**(2)**	**(3)**	**(4)**	**(5)**
(hkl)	Angle (°)					
(110)	26.6	785	598	594	410	668
(101)	33.9	331	248	482	173	193
(200)	37.9	295	301	477	93	520
(111)	39.0	19	10	23	3	0
(210)	42.6	11	11	15	4	12
(211)	51.7	428	317	571	195	384
(220)	54.8	78	58	86	34	85
(002)	57.8	3	3	0	0	0
(310)	61.9	87	66	119	36	88
(112)	64.7	32	24	38	0	20
(301)	66.0	60	53	74	25	71
Total Counts		2129	1688	2480	973	2042
(200) (Total as %)		13.8	17.8	19.2	9.5	25.5
Crystallite Size (Å)		213	205	264	119	182

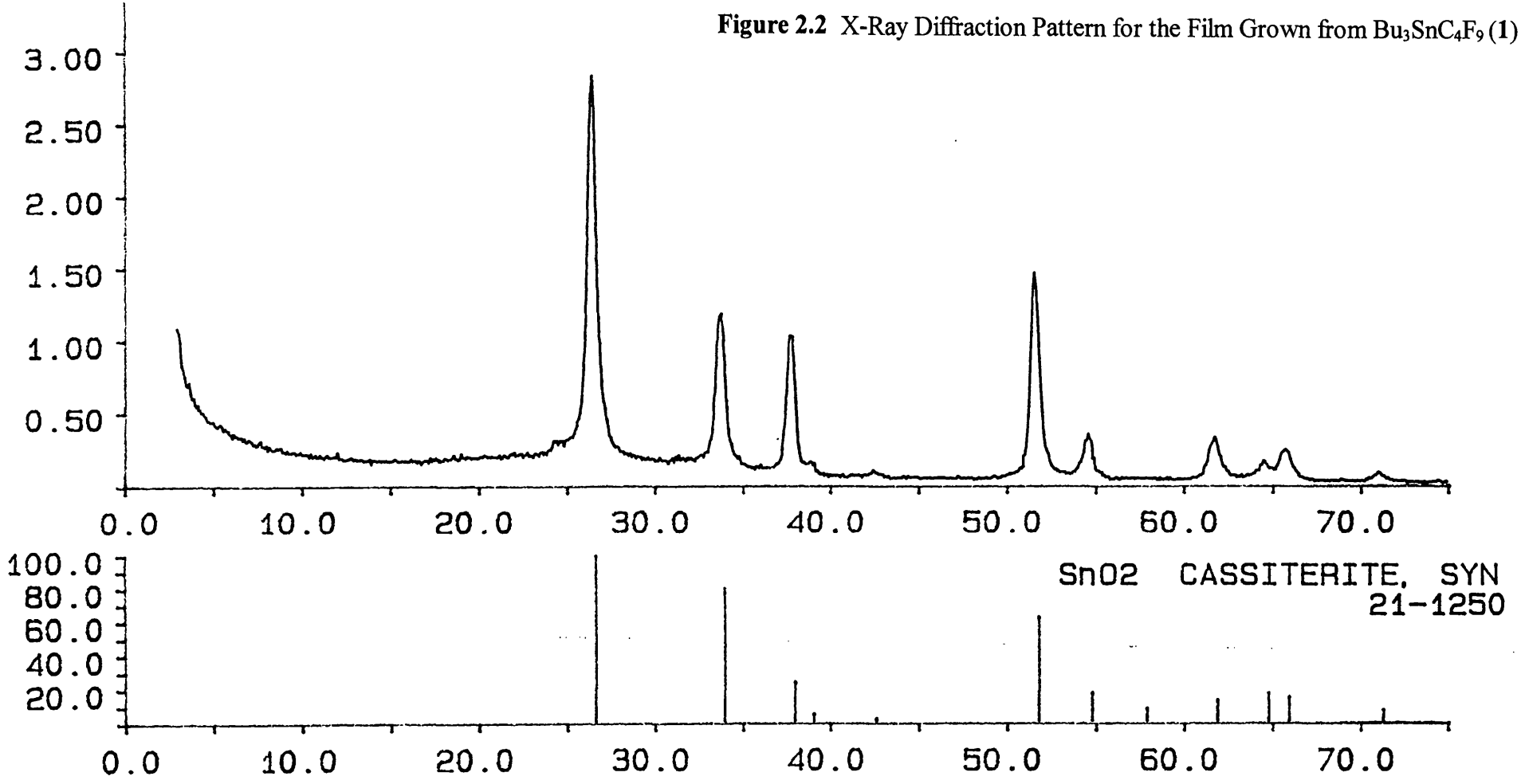

Figure 2.2 X-Ray Diffraction Pattern for the Film Grown from $Bu_3SnC_4F_9$ (**1**)

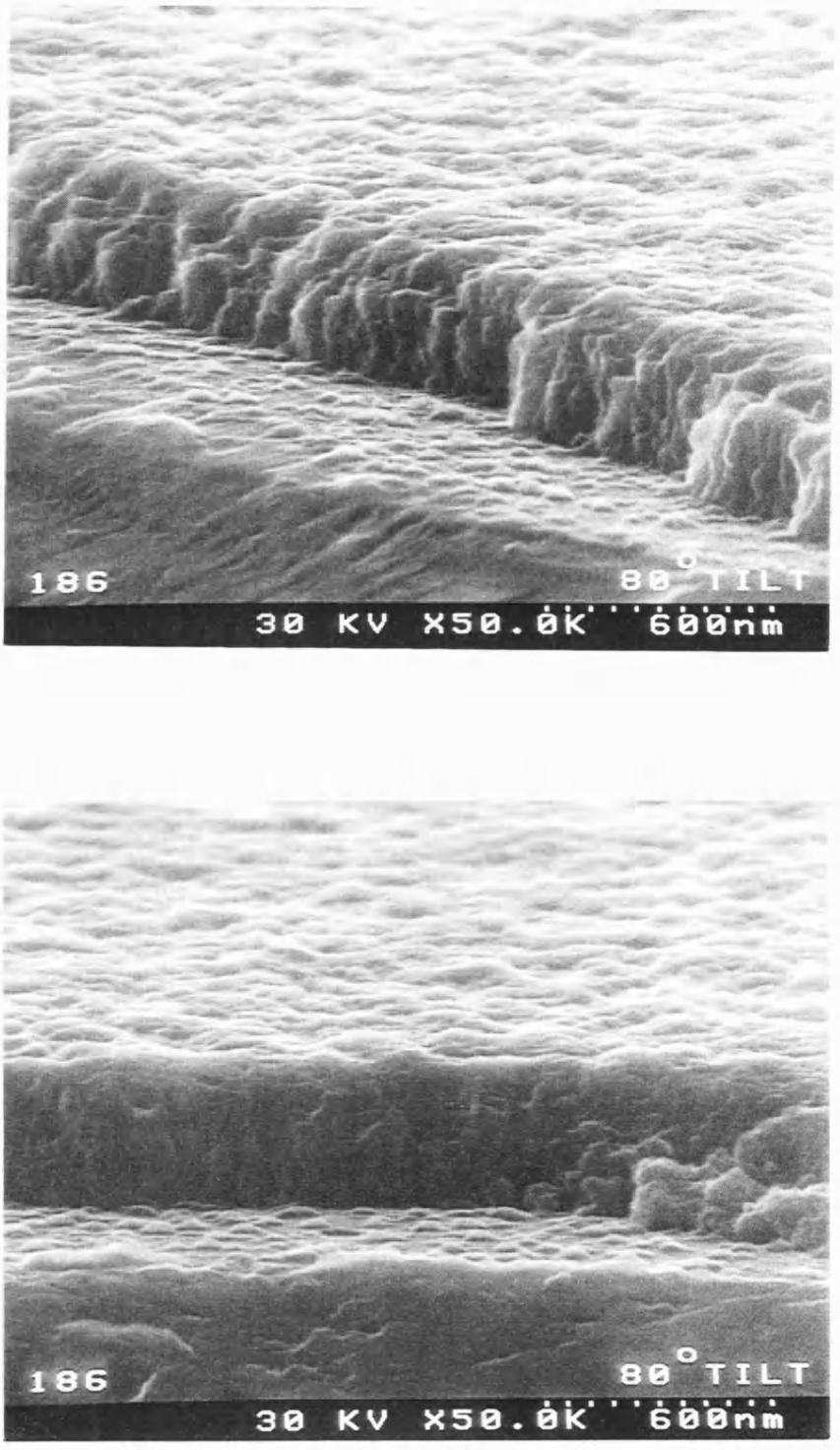

Figure 2.3 Scanning Electron Micrographs of the Film Grown from $Bu_3SnC_4F_9$ (**1**)

It can be seen that all films provided a diffraction pattern, and were therefore crystalline. The peak positions are consistent with those found for standard SnO_2, therefore confirming the expected film composition. Preferred orientations were observed which were found to be similar for all films, these being the (110), (101), (200) and (211) orientations. The proportions found for the (200) reflection were consistently higher than 7%, suggesting that the films contained less structural defects than a random specimen of SnO_2.

2.5.2.2 Film Properties

For all films, thickness, haze, emissivity, sheet resistance, resistivity and fluorine content were measured. The results of the analysis are given in Table 2.8.

Table 2.8 Analysis of Fluorine-Doped Tin Oxide Films from Perfluoroalkyltin Precursors

PRECURSOR	**(1)**	**(2)**	**(3)**	**(4)**	**(5)**	**Std.[a]**
Thickness (Å)	3795	3675	6165	2000	4330	3000
Haze (%)	0.64	0.54	4.10	0.50	1.05	< 0.40
Emissivity	0.220	0.328	0.139	0.655	0.132	< 0.150
Sheet Resistance (Ω/□)	22	58	9	215	11	15
Resistivity ($\times 10^{-3}$ Ω cm)	0.85	2.13	0.58	5.10	0.46	0.50
Fluorine Content (atom%)	1.48	2.02	0.79	< 0.05	1.20	2.00

[a] Typical measurements for a good fluorine-doped tin oxide film derived from separate tin and fluorine sources.

All precursors produced fluorine-doped tin oxide films establishing that the perfluoroalkyltin compounds were capable of acting as single source precursors. Reasonable success was achieved in trying to obtain films of approximately 3000 Å in

thickness from precursors with which there were sufficient quantities to perform several runs, showing that visual inspection could be used as a good estimate of thickness.

Due to the small quantities of precursors (**3**) and (**4**) films of the desired thickness were not obtained. The film derived from precursor (**3**) was extremely thick (6165 Å), and the opposite result of a very thin film (2000 Å) was obtained from precursor (**4**), resulting in the observation of opposite film properties, as expected. It can be seen that good emissivity and resistivity were measured for the thick film grown from precursor (**3**), but a very high haze of 4.10%. In contrast, high emissivity and resistivity were found for the thin film grown from precursor (**4**), although the haze of 0.50% was still reasonably high for a film only 2000 Å in thickness.

Although it is very difficult to predict the properties of a film without obtaining the appropriate thickness, it can be extrapolated that the properties of films grown from precursors (**3**) and (**4**) would not be particularly encouraging if a film of 3000 Å in thickness was achieved. The properties of the film derived from precursor (**3**) are not a sufficient improvement on the measurements given for a standard coating for a thickness of double the intended. The film from precursor (**4**) exhibits a poor overall set of properties, and a film an additional 1000 Å in thickness would be extremely unlikely to display properties rivalling those obtained from dual precursors. Due to the difficult and expensive synthesis of the precursors, and, more importantly, the production of better quality films from other precursors, it was decided not to synthesise additional material in order to perform further runs.

A significant observation can be drawn from the series (**1**) - (**3**) which contained an increasing number of fluorinated groups. It can be seen that the incorporation of additional fluorine into the precursor led to an increase in the quantity of resultant fluorine found in the tin oxide film as the number of R_f groups in the precursor increased from 1 to 2 as expected as shown by precursors (**1**) and (**2**) respectively. However, a reduced fluorine content was observed from $BuSn(C_4F_9)_3$ (**3**) with three fluorinated ligands. It could be the case that a β-fluoride elimination occurs for precursors (**1**) and (**2**) which would explain the increase in resultant fluorine content with a corresponding

increase in the number of β-fluorine sites in the precursor. This does not appear to be the case for precursor (**3**) for which the reason is unclear.

From compounds (**1**) and (**2**), it appears that the incorporation of additional fluorine resulted in a deterioration in the film properties, suggesting that the optimum dopant concentration for this class of compound is relatively low. The films grown from precursors (**1**) and (**2**) were of a very similar thickness, enabling a direct comparison to be made. It could be that a level below that produced by precursor (**1**) is the optimum as the properties of this film are not as good as those for the dual source standard. Although there is more fluorine present in the standard film, it could be that a high proportion is inactive and therefore does not contribute favourably to the film properties. The results obtained from this study indicate a higher proportion of active fluorine incorporation from the single source precursors R_3SnR_f (**1**) and (**5**). The deterioration in emissivity and resistivity with a corresponding increase in dopant concentration suggests that the fluorine content of the film deposited from precursor (**1**) is closer to the optimum. It can therefore be suggested that a lower fluorine content than that incorporated by (**1**) is the optimum amount and could lead to better film properties which would rival the dual source standard. If this is the case, it appears that it is possible to achieve a higher proportion of *active fluorine* from a single source precursor than by dual source methods.

The extremely low fluorine content found in the film deposited from $Bu_3SnC_6F_{13}$ (**4**) was also unexpected, but explains the extremely poor set of properties exhibited by this film. This can be explained by the longer R_f ligand reducing the basicity of the CF_2 group by electron withdrawal. It appears that the decomposition pathway may involve the production of a stable fluorinated species which is transported from the reactor without transferring any fluorine to the tin. Therefore, incorporation of smaller R_f ligands into the precursor could possibly be a more favourable arrangement for fluorine-doping during the CVD of a doped SnO_2 film.

The fluorine content determined for the film grown from precursor (**5**) is similar to that found for (**1**) which was expected as the compounds have the identical R_3SnR_f

arrangement with C_4F_9 as the R_f component. It can therefore be postulated that the same decomposition mechanism holds for each precursor.

FTIR studies have been conducted on $Bu_3SnC_4F_9$ (**1**) in collaboration with P. G. Harrison at the University of Nottingham in an attempt to gain some information regarding the decomposition pathway of this precursor.[218] The decomposition product was found to be Bu_3SnF which was extremely encouraging as it shows that the perfluoroalkyltin compounds can indeed achieve the target of effective fluorine transfer to the tin during thermal decomposition.

However, the conditions used for the FTIR study and those used during the CVD process are very different, particularly with regard to temperature, so the decomposition pathways could vary considerably in each environment. This could explain the rather low fluorine contents determined in the films deposited, as high levels would have been expected due to the apparently facile production of the required Sn-F bond. It therefore appears that a different or competing decomposition pathway occurred in the CVD reactor which resulted in a lower level of fluorine incorporation than expected. This can be explained by the feasibility of a large number of possible decomposition mechanisms at the elevated temperature present in the CVD reactor. For example, although fluorine transfer appeared to occur relatively easily at the temperatures used for the FTIR studies, R groups will be largely unaffected at this temperature. However, at the elevated temperature present in the CVD reactor, mechanisms such as loss of butene become feasible which can influence the subsequent pathway followed. Overall, the harsh reactor conditions of $\approx$ 560°C would be likely to dictate the decomposition pathway taken.

The films grown from precursors (**4**) and (**5**) can be used to determine the effects of alternative R_f and R groups respectively. From the results obtained from the series (**1**) to (**3**) it has been discovered that the best design appears to be a compound containing one fluorinated ligand, therefore the films could be compared with that produced from precursor (**1**). Precursor (**4**) shows the effect of a longer fluorinated group, and it can be concluded with a reasonable amount of confidence that the shorter ligand was favoured.

The very low fluorine incorporation achieved from precursor (**4**) concludes that the longer chain was less effective as a fluorine dopant.

An alternative R group (**5**) did not lead to a vast improvement in film properties. Although better emissivity and resistivity measurements were obtained, these can be explained by the slight increase in thickness, and similarly, the same explanation can be used to justify the increase in haze.

In conclusion, the films produced from the perfluoroalkyltin compounds were reasonably encouraging, and showed that it was possible to grow a fluorine-doped tin oxide film from a single source precursor. Overall, it appears that the best arrangement for a precursor in this class consists of one containing a single fluorinated group as the best film properties are achieved by this arrangement. The length of the fluorinated chain seems to be extremely important as a huge difference was observed from the two R_f groups tried. For effective fluorine-doping a small R_f group appears to be essential as the fluorine incorporation vastly diminished as R_f changed from C_4F_9 (**1**) to C_6F_{13} (**4**). For increased volatility and hence a significantly shorter run time, a vast improvement is achieved by the incorporation of small R groups, although film properties appear to be unaffected by the choice. Although organotin compounds containing small R groups are more expensive and have a higher toxicity than the butyltin compounds, the CVD properties are greatly enhanced.

Therefore, the results obtained from the perfluoroalkyltin precursors were reasonably encouraging, and were a good starting point for this study. The observation of Bu_3SnF as a decomposition product from $Bu_3SnC_4F_9$ (**1**) was particularly encouraging as it proved that fluorine transfer could indeed be achieved. However, improvements were needed to find a group of precursors with an easier synthetic route, cheaper starting materials, and film properties rivalling those produced from separate tin and fluorine sources.

2.6 EXPERIMENTAL

2.6.1 Preparation of Tributyl(perfluorobutyl)tin - $Bu_3SnC_4F_9$ (1)

Isopropyl chloride (3.48 g, 44 mmol) in dry ether (30 ml) was added slowly to magnesium turnings (1.20 g, 50 mmol) to prepare the Grignard reagent isopropylmagnesium chloride. This was transferred by canula into a pressure equalising dropping funnel then added dropwise to freshly distilled perfluorobutyl iodide (15.32 g, 44 mmol) in dry ether (100 ml) at -78°C. The solution was stirred at this temperature for one hour to allow exchange to take place. Tributyltin chloride (9.72 g, 30 mmol) was then added slowly by syringe, the solution warmed to -40°C and stirred at this temperature for two hours. The flask was then allowed to slowly warm to room temperature overnight with stirring, and the solvent removed *in vacuo* to yield an oil and a white solid. The mixture was extracted into 40°-60° petroleum ether and the solid removed by filtration. The solvent was removed *in vacuo* to leave a colourless oil, which by ^{119}Sn nmr was found to be a mixture of tributylperfluorobutyltin and unreacted tributyltin chloride. The mixture was separated by column chromatography using silica gel as the stationary phase and 40°-60° petroleum ether as the eluant. Tributyl(perfluorobutyl)tin was eluted as the first fraction, and removal of the solvent *in vacuo* yielded the product as a colourless oil (8.33 g, 55%).

Analysis : Found (calc. for $C_{16}H_{27}F_9Sn$) : C 37.8 (37.7)%; H 5.37 (5.36)%.

Mössbauer data (mm s^{-1}) : IS = 1.39; QS = 1.58.

^{119}Sn nmr [δ(ppm), $CDCl_3$ soln] : -1.6, t, $^2J(^{119}Sn\text{-}^{19}F)$ = 190 Hz.

^{1}H nmr [δ(ppm), $CDCl_3$ soln] : 0.92 [9H, t, $CH_3(CH_2)_3$], $^3J(^1H\text{-}^1H)$ = 7 Hz; 1.22 [6H, m, C_4H_9]; 1.35 [6H, m, C_4H_9]; 1.60 [6H, m, C_4H_9].

^{13}C nmr [δ(ppm), $CDCl_3$ soln] : 10.5 [$CH_3(CH_2)_3$]; 13.5 [$CH_3(CH_2)_2CH_2$]; 27.1 [$CH_3CH_2(CH_2)_2$]; 28.3 [$CH_3CH_2CH_2CH_2$]. $^1J(^{13}C\text{-}^{119}Sn)$ = 333 Hz. C-F carbons not observed.

^{19}F nmr [δ(ppm), $CDCl_3$ soln] : -126.6 [m, $CF_3CF_2(CF_2)_2$]; -119.2 [m, $CF_3CF_2CF_2CF_2$]; -118.2 [m, $CF_3(CF_2)_2CF_2$]; -81.7 [m, $CF_3(CF_2)_3$].

IR data (NaCl plates, liquid film, cm^{-1}) : 2961, 2928, 2859, 1466, 1420, 1379, 1346, 1235, 1154, 1084, 1007, 961, 793, 743.

2.6.2 Preparation of Dibutyl Bis-(perfluorobutyl)tin - $Bu_2Sn(C_4F_9)_2$ (2)

The method described previously for (**1**) was utilised with isopropyl chloride (54.98 g, 63 mmol) added to magnesium turnings (1.60 g, 66 mmol) in dry ether (30 ml). The Grignard reagent was added dropwise to freshly distilled perfluorobutyl iodide (22.68 g, 66 mmol) at -78°C. Dibutyltin dichloride (6.40 g, 21 mmol) dissolved in dry ether (5 ml) was added slowly by syringe at -78°C, then the flask warmed to -40°C and stirred at this temperature for two hours. Following the previously described work-up procedure, dibutyltin bis-(perfluorobutyl)tin was obtained as a colourless liquid (4.58 g, 32%).

Analysis : Found (calc. for $C_{16}H_{18}F_{18}Sn$) : C 29.6 (28.6)%; H 2.74 (2.71)%.

Mössbauer data ($mm\ s^{-1}$) : IS = 1.46; QS = 1.75.

^{119}Sn nmr [δ(ppm), $CDCl_3$ soln] : -56.0, quin, $^2J(^{119}Sn\text{-}^{19}F)$ = 237 Hz.

^1H nmr [δ(ppm), $CDCl_3$ soln] : 0.94 [6H, t, $CH_3(CH_2)_3$], $^3J(^1H\text{-}^1H)$ = 7 Hz; 1.37 [4H, m, C_4H_9]; 1.60 [8H, m, C_4H_9].

^{13}C nmr [δ(ppm), $CDCl_3$ soln] : 13.3 [$CH_3(CH_2)_3$]; 13.6 [$CH_3(CH_2)_2CH_2$]; 26.9 [$CH_3CH_2(CH_2)_2$]; 27.4 [$CH_3CH_2CH_2CH_2$]. $^1J(^{13}C\text{-}^{119}Sn)$ = 358 Hz. C-F carbons not observed.

^{19}F nmr [δ(ppm), $CDCl_3$ soln] : -126.7 [m, $CF_3CF_2(CF_2)_2$]; -118.4 [m, $CF_3CF_2CF_2CF_2$]; -113.9 [m, $CF_3(CF_2)_2CF_2$]; -81.8 [m, $CF_3(CF_2)_3$].

IR data (NaCl plates, liquid film, cm^{-1}) : 2965, 2932, 2865, 1468, 1348, 1238, 1132, 1071, 1009, 795, 745, 681, 644.

2.6.3 Preparation of Butyl Tris-(perfluorobutyl)tin - $BuSn(C_4F_9)_3$ (3)

The methodology described for (**1**) was repeated with isopropyl chloride (6.44 g, 82 mmol) reacted with magnesium turnings (2.00 g, 82 mmol). The resultant Grignard reagent was added dropwise to freshly distilled perfluorobutyl iodide (29.19 g, 82 mmol) at -78°C. Butyltin trichloride (5.10 g, 18 mmol) was added slowly by syringe then the mixture warmed to -40°C and stirred at this temperature for two hours. Following the work-up procedure described for (**1**), (**3**) was obtained as a colourless liquid (2.74 g, 18%).

Analysis : Found (calc. for $C_{16}H_9F_{27}Sn$) : C 24.5 (23.1)%; H 1.51 (1.09)%.

Mössbauer data ($mm\ s^{-1}$) : IS = 1.44; QS =1.49.

^{119}Sn nmr [δ(ppm), $CDCl_3$ soln] : -154.5, sept, $^2J(^{119}Sn\text{-}^{19}F)$ = 300 Hz.

^1H nmr [δ(ppm), $CDCl_3$ soln] : 0.96 [3H, t, $CH_3(CH_2)_3$], $^3J(^1H\text{-}^1H)$ = 7 Hz; 1.42 [2H, m, C_4H_9]; 1.60 [4H, m, C_4H_9].

^{13}C nmr [δ(ppm), $CDCl_3$ soln] : 13.0 [$CH_3(CH_2)_3$]; 13.2 [$CH_3(CH_2)_2CH_2$]; 26.6 [$CH_3CH_2(CH_2)_2$]; 26.9 [$CH_3CH_2CH_2CH_2$]. $^1J(^{13}C\text{-}^{119}Sn)$ = 395 Hz. C-F carbons not observed.

^{19}F nmr [δ(ppm), $CDCl_3$ soln] : -126.8 [m, $CF_3CF_2(CF_2)_2$]; -117.8 [m, $CF_3CF_2CF_2CF_2$]; -108.6 [m, $CF_3(CF_2)_2CF_2$]; -81.9 [m, $CF_3(CF_2)_3$].

IR data (NaCl plates, liquid film, cm^{-1}) : 2969, 2882, 1470, 1348, 1237, 1134, 1101, 997, 851, 777, 745, 683, 534.

2.6.4 Preparation of Tributyl(perfluorohexyl)tin - $Bu_3SnC_6F_{13}$ (4)

The methodology described for (**1**) was employed with isopropyl chloride (1.89 g, 24 mmol) and magnesium turnings (0.60 g, 25 mmol). The resultant Grignard reagent was added to freshly distilled perfluorohexyl iodide (10.93 g, 25 mmol) at -78°C and stirred at this temperature for one hour. Tributyltin chloride (5.30 g, 16 mmol) was added slowly by syringe then the flask was warmed to -40°C and stirred for a further two hours. Following the work-up procedure described for (**1**), (**4**) was isolated as a colourless liquid (1.70 g, 17%).

Analysis : Found (calc. for $C_{18}H_{27}F_{13}Sn$) : C 35.5 (35.5)%; H 4.45 (4.48)%.

Mössbauer data ($mm\ s^{-1}$) : IS = 1.35; QS = 1.57.

^{119}Sn nmr [δ(ppm), $CDCl_3$ soln] : -0.6, t, $^2J(^{119}Sn\text{-}^{19}F)$ = 191 Hz.

^1H nmr [δ(ppm), $CDCl_3$ soln] : 0.92 [9H, t, $CH_3(CH_2)_3$], $^3J(^1H\text{-}^1H)$ = 7 Hz; 1.21 [6H, m, C_4H_9]; 1.35 [6H, m, C_4H_9]; 1.57 [6H, m, C_4H_9].

^{13}C nmr [δ(ppm), $CDCl_3$ soln] : 10.6 [$CH_3(CH_2)_3$]; 13.5 [$CH_3(CH_2)_2CH_2$]; 27.1 [$CH_3CH_2(CH_2)_2$]; 28.3 [$CH_3CH_2CH_2CH_2$]. $^1J(^{13}C\text{-}^{119}Sn)$ = 329 Hz. C-F carbons not observed.

^{19}F nmr [δ(ppm), $CDCl_3$ soln] : -126.7 [m, $CF_3CF_2(CF_2)_4$]; -123.5 [m, $CF_3CF_2CF_2(CF_2)_3$]; -122.5 [m, $CF_3(CF_2)_2CF_2(CF_2)_2$]; -118.3 [m, $CF_3(CF_2)_3CF_2CF_2$]; -117.9 [m, $CF_3(CF_2)_4CF_2$]; -81.4 [m, $CF_3(CF_2)_5$].

IR data (NaCl plates, liquid film, cm^{-1}) : 2961, 2926, 2857, 1659. 1466, 1360, 1238, 1206, 1144, 1115, 1084, 1017, 882, 735, 652.

2.6.5 Preparation of Triethyl(perfluorobutyl)tin - $Et_3SnC_4F_9$ (5)

The methodology described for (**1**) was followed using isopropyl chloride (2.80 g, 36 mmol) and magnesium turnings (0.90 g, 37 mmol). The resultant Grignard reagent was added to freshly distilled perfluorobutyl iodide (12.18 g, 35 mmol) at -78°C, then triethyltin chloride (5.70 g, 24 mmol) added after stirring for one hour. The flask was warmed to -40°C and stirred for a further two hours at this temperature. The work-up procedure described for (**1**) yielded (**5**) as a colourless liquid (3.68 g, 37%).

Analysis : Found (calc. for $C_{10}H_{15}F_9Sn$) : C 28.4 (28.3)%; H 3.56 (3.57)%.

Mössbauer data ($mm\ s^{-1}$) : IS = 1.36; QS = 1.65.

^{119}Sn nmr [δ(ppm), $CDCl_3$ soln] : 3.6, t, $^2J(^{119}Sn\text{-}^{19}F)$ = 190 Hz.

^{1}H nmr [δ(ppm), $CDCl_3$ soln] : 1.19 [9H, m, CH_3CH_2], $^3J(^1H\text{-}^1H)$ = 7 Hz; 1.27 [6H, m, CH_3CH_2].

^{13}C nmr [δ(ppm), $CDCl_3$ soln] : 10.1 [CH_3CH_2]; 10.3 [CH_3CH_2]. $^1J(^{13}C\text{-}^{119}Sn)$ = 331 Hz. C-F carbons not observed.

^{19}F nmr [δ(ppm), $CDCl_3$ soln] : -126.7 [m, $CF_3CF_2(CF_2)_2$]; -119.5 [m, $CF_3CF_2CF_2CF_2$]; -117.9 [m, $CF_3(CF_2)_2CF_2$]; -81.8 [m, $CF_3(CF_2)_3$].

IR data (NaCl plates, liquid film, cm^{-1}) : 2957, 2878, 1470, 1383, 1348, 1237, 1154, 1084, 1047, 1006, 961, 743, 679, 519.

Chapter Three

Organotin Carboxylates

3.1 INTRODUCTION

Organotin carboxylates are a very important class of compounds, with a wide range of important commercial applications.[137] Examples include industrial uses such as homogeneous catalysts, and the carboxylates are used in considerable quantities in agriculture as biocides. A more recent development is the discovery of their antitumour activity which can be of use in the pharmaceutical industry.

Following the problems encountered with the synthesis of the perfluoroalkyltin compounds, organotin carboxylates were identified as potential single source precursors for the CVD of fluorine-doped tin oxide.

3.1.1 Advantages and Disadvantages

Organotin carboxylates could have many advantages over the previously discussed perfluoroalkyltin precursors.

(i) *Organotin carboxylates R_3SnO_2CR' are known to decompose thermally to R_3SnR' by CO_2 loss, therefore creating the possibility of forming a perfluoroalkyltin compound in situ.*

(ii) *Synthesis is far less complicated than for the perfluoroalkyltin compounds, and products can be obtained in high yield in a relatively pure form.*

(iii) *Possible starting materials are numerous, inexpensive and readily available, making production of sufficient quantities of material a simple task.*

(iv) *There are a vast number of possible starting materials, therefore a potentially large selection of possible precursors.*

(v) *Organotin carboxylates are stable at room temperature with no handling or storage difficulties.*

There are, however, some potential problems which could arise from the use of organotin carboxylates as CVD precursors.

(i) *Organotin carboxylates are solid materials.*

(ii) *Many organotin carboxylates are known to incorporate intermolecular bonds which lead to the formation of polymeric structures, therefore creating the possibility of some volatility problems.*

One of the main reasons for citing organotin carboxylates as precursors was due to the possibility of a decarboxylation process. Decarboxylation has been observed in some organotin carboxylates, for example $Ph_3SnO_2CC_6F_5$,[219] and also some organomercury carboxylates.[220]

$$R_3SnO_2CR' \longrightarrow R_3SnR' + CO_2 \qquad [3.1]$$

The organotin carboxylates could therefore be used as an alternative route to the perfluoroalkyltin precursor as such a species could possibly be formed as an intermediate *in situ* during the CVD process.

This chapter contains a brief description of the structural chemistry of organotin carboxylates and the various synthetic routes available for the formation of such compounds. The introduction will be followed by details of the synthesis, characterisation and CVD testing of a range of organotin carboxylates prepared for this thesis.

3.2 STRUCTURAL CHEMISTRY

Organotin carboxylates have received considerable attention, and their structural chemistry is enormously varied. Due to the important applications and rich structural diversity of this class of compound, the volume of material found in the literature is constantly expanding. The structural chemistry of organotin carboxylates has been thoroughly reviewed by Tiekink[221,222] who describes all possible structural variations in

this extensive field of chemistry. The list has been updated with any new structural types discovered since the latest review.

3.2.1 Mono-Organotin Carboxylates

The mono-organotin carboxylates are the least studied group, with relatively few examples available.[223-226] There are two structural variations displayed by these compounds, with examples given in Table 3.1.

Table 3.1 Structural Variations in Mono-Organotin Carboxylates

STRUCTURE	Formula	Example	Ref.
"Drum"	$[RSn(O)(O_2CR')]_6$	R = Me, R′ = Me	223
"Ladder"	$\{[RSn(O)(O_2CR')]_2[RSn(O_2CR')_3]\}_2$	R = *n*-Bu, R′ = Ph	224

The "drum" variation is illustrated by $[MeSn(O)(O_2CMe)]_6$ (Figure 3.1), and the "ladder" by $\{[(n\text{-}BuSn(O)O_2CPh)_2\text{-}n\text{-}BuSn(O_2CPh)_3]\}_2$ (Figure 3.2).

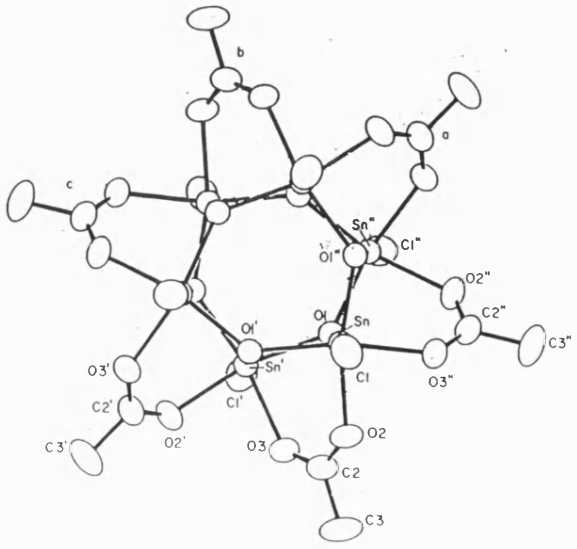

Figure 3.1 Molecular Structure of $[MeSn(O)O_2CMe]_6$[223]

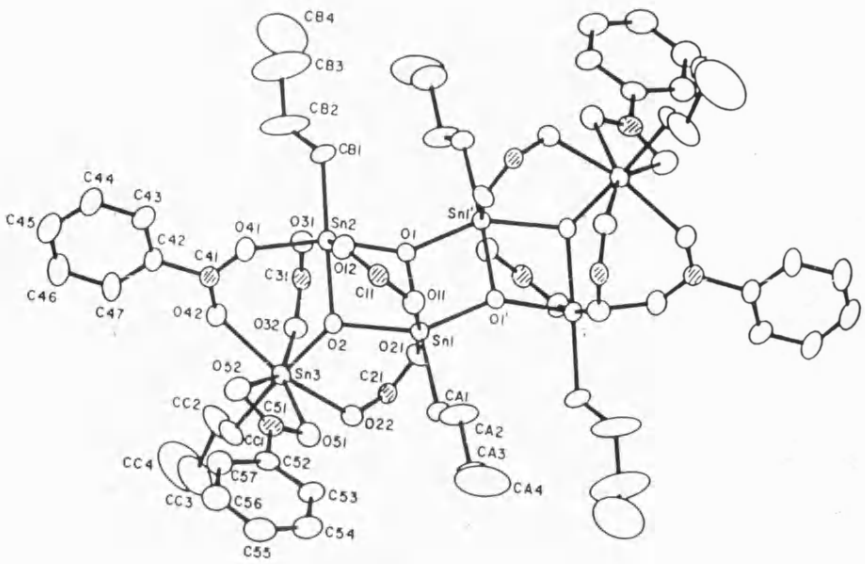

Figure 3.2 Molecular Structure of $\{[(n\text{- BuSn(O)O}_2\text{CPh})_2\text{-}n\text{-BuSn(O}_2\text{CPh)}_3]\}_2$[224]

3.2.2 Diorganotin Carboxylates

The greatest structural diversity among the carboxylates is displayed by the diorganotin derivatives. There are an enormous number of variations, ranging from compounds containing monodentate carboxylate ligands to mixed ligand species. Table 3.2 lists examples of all the major structural categories.

Table 3.2 Structural Variations in Diorganotin Carboxylates

FORMULA	Variation	Example	Ref.
$[R_2Sn(O_2CR')]_2$		$[Me_2Sn(O_2CCCl_3)]_2$	227
$[R_2Sn(O_2CR')]$		$[n\text{-}Bu_2Sn(O_2CCH(^iPr)N{=}C(H)C_6H_4O)]$	228
$[R_2Sn(O_2CR')]_6$		$[n\text{-}Bu_2Sn(O_2CCH_2CH_2S)]_6$	229
$[R_2Sn(O_2CR')X]_n$	Type A[a]	$[Me_2Sn(O_2CMe)Cl]_n$	230
	Type B[b]	$[t\text{-}Bu_2Sn(O_2CMe)OH]_2$	231
	Type C[c]	$[Me_2Sn(O_2CC_5H_4N\text{-}2)Cl]_n$	232
$\{[R_2Sn(O_2CR')]_2O\}_2$	Type A[d]	$\{[n\text{-}Bu_2Sn(O_2CCCl_3)]_2O\}_2$	233
	Type B[e]	$\{[n\text{-}Bu_2Sn(O_2CCH_2C_6H_4F\text{-}p)]_2O\}_2$	234
	Type C[f]	$\{[Me_2Sn(O_2CMe)]_2O\}_2$	235
	Type D[g]	$\{[Ph_2Sn(O_2CCCl_3)]_2O\}_2$	233
	Type E[h]	$\{[n\text{-}Bu_2Sn(O_2CC_5H_4N\text{-}2)]_2O\}_2$	236
$[R_4Sn_2(O_2CR')_3X]$		$[n\text{-}Bu_4Sn_2(O_2CCCl_3)_3(OH)]$	237
$[R_8Sn_4(O_2CR')_6X_2]$		$[Ph_8Sn_4(O_2CCCl_3)_6(OH)_2]$	233
$[R_2Sn(O_2CR')_2]$	Type A[i]	$[Me_2Sn(O_2CC_6H_4OMe\text{-}2)_2]$	238
	Type B[j]	$[Me_2Sn(O_2CH)_2]$	239
	Type C[k]	$[Ph_2Sn(O_2CC_5H_4N\text{-}2)_2]$	240
	Type D[l]	$[Me_2Sn(O_2CC_5H_4N\text{-}2)_2]_n$	241
$[R_2Sn(O_2CR')_2L]$		$[n\text{-}Bu_2Sn(O_2CCH_2C_6H_5)_2(OH_2)]$	242
$[R_2Sn(O_2CR')_2L_2]$		$[(CH_2{=}CH)_2Sn(O_2CCF_3)_2bipy]$	243
$[R_2Sn(O_2CR')_3]^-$		$[(Me_2Sn(O_2CMe)_3]^-$	244
$[R_2Sn((O_2C)_2R')]$		$[n\text{-}Bu_2Sn(O_2CCH_2)_2N(CH_2CH_2OH)]$	245
$[R_2Sn((O_2C)_2R')L]_n$		$\{Me_2Sn[(O_2C)_2C_5H_3N](OH_2)\}_2$	246

[a] Polymeric with bridging acetate groups. [b] Dimeric with hydroxide bridges. [c] Polymeric with bridging carboxylates and bonding from N of pyridine. [d] Bidentate bridging carboxylates. [e] One chelating carboxylate, other links two tins by one oxygen. [f] Two trigonal bipyramidal tins, two octahedral. [g] Endocyclic tins octahedral, exocyclic tins trigonal bipyramidal. [h] As for [d] with interaction of N from pyridine. [i] Bidentate chelating carboxylates. [j] Bidentate bridging carboxylates to form polymer. [k] Chelation from one oxygen and N from pyridine, monomeric [l] Bonding from both oxygens and N from pyridine for one carboxylate, polymeric.

Two of the structural categories will be discussed in greater detail as they have been explored in this thesis.

3.2.2.1 $[R_2Sn(O_2CR')_2]$

As shown in Table 3.2, there are currently four structural types known for this class of compound. These usually arise, however, as a result of additional interactions between atoms in the carboxylate R′ residues and the tin atoms, rather than by different modes of coordination of the simple carboxylate ligands.

In the dominant Type A motif, the carboxylate ligands chelate the tin atom forming disparate Sn-O bond distances, as illustrated by $[Me_2Sn(O_2CC_6H_4OMe\text{-}2)_2]$[238] (Figure 3.3). The geometry about the tin atom is based on a skew trapezoidal bipyramid, with the axial tin-bound organic groups forming a C-Sn-C bond angle of 138.2°.

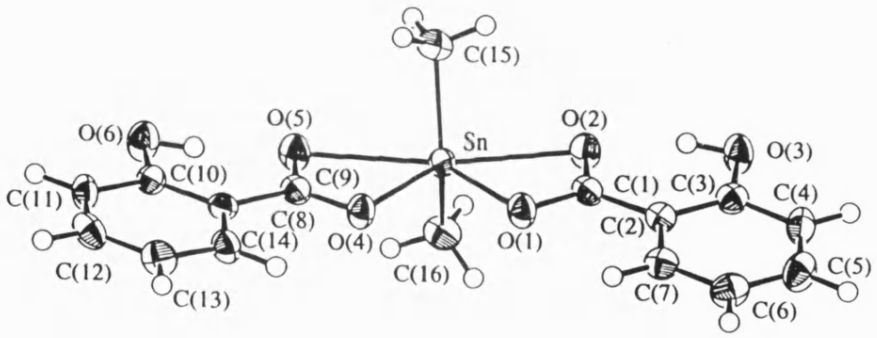

Figure 3.3 Molecular Structure of $[Me_2Sn(O_2CC_6H_4OMe\text{-}2)_2]$[238]

In the Type B variation, the ligands are bidentate bridging rather than bidentate chelating as for the Type A structures. This has the result that infinite two-dimensional sheets are formed in the lattice. The best description of the coordination geometry about the tin atom is one based on a slightly distorted octahedron, and is shown by $[Me_2Sn(O_2CH)_2]_n$[239] (Figure 3.4).

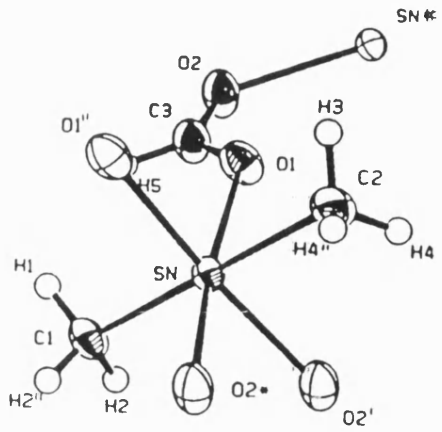

Figure 3.4 Molecular Structure of $[Me_2Sn(O_2CH)_2]_n$[239]

For Type C, different bonding is observed from the carboxylate R′ residue and hence creates a new structural type for this class. This effect can be demonstrated by the structure of $[Ph_2Sn(O_2CC_5H_4N\text{-}2)_2]$[240] where the nitrogen atom from the pyridine is coordinated to the tin atom. Only one of the oxygen atoms from the carboxylate is bonded to the tin as shown in Figure 3.5. The structure is monomeric, with the tin atom existing in a distorted octahedral geometry with the two oxygen atoms *trans* to each other.

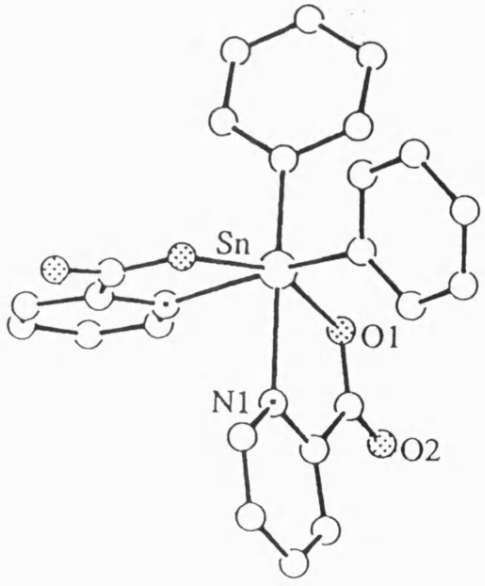

Figure 3.5 Molecular Structure of $[Ph_2Sn(O_2CC_5H_4N\text{-}2)_2]$[240]

Structural Type D is shown by the dimethyltin analogue of the compound described previously for the Type C motif. In $[Me_2Sn(O_2CC_5H_4N\text{-}2)_2]_n$ the pyridine-2-carboxylate ligands coordinate to the tin atom in different ways. The first uses all three donor atoms by chelating the tin atom via two oxygen and one nitrogen atom, and hence, unlike Type C, leads to the formation of a polymeric chain. The second ligand coordinates in an identical fashion to that exhibited by Type C. The tin atom is therefore seven coordinate and in a distorted pentagonal bipyramidal geometry, as shown by $[Me_2Sn(O_2CC_5H_4N\text{-}2)_2]_n$[241] (Figure 3.6).

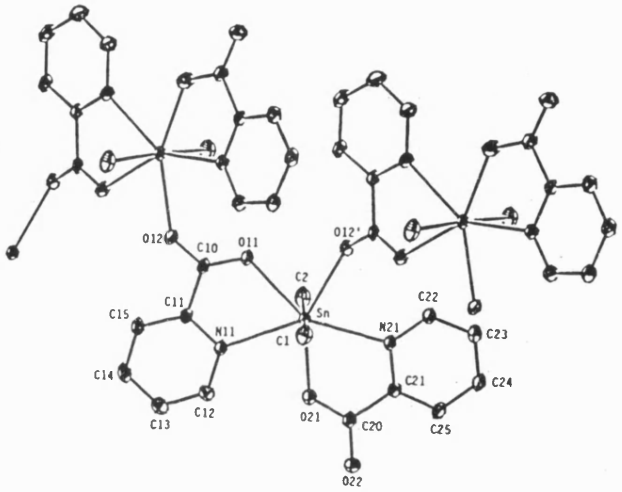

Figure 3.6 Molecular Structure of $[Me_2Sn(O_2CC_5H_4N\text{-}2)_2]_n$[241]

3.2.2.2 $[R_2Sn(O_2CR')_2L]$

There are relatively few examples of a diorganotin bis-carboxylate with a coordinated ligand. The apparently unique example of a monodentate ligand is illustrated by $[n\text{-}Bu_2Sn(O_2CCH_2C_6H_5)_2(OH_2)]$[242], as shown in Figure 3.7. The tin atom and the oxygen atom of the water molecule are situated on a crystallographic 2-fold axis in this structure, and the carboxylate ligands chelate the tin atom which forms a pentagonal plane about the tin atom. The two n-butyl groups occupy the axial positions, therefore creating a pentagonal bipyramidal geometry.

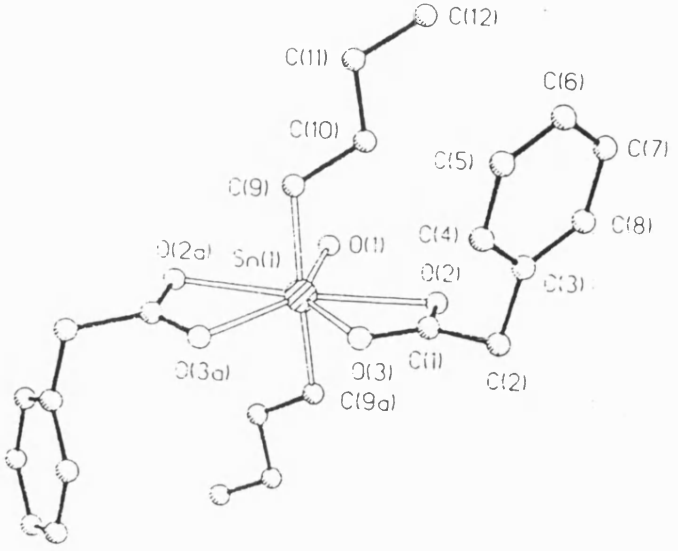

Figure 3.7 Molecular Structure of $[n\text{-}Bu_2Sn(O_2CCH_2C_6H_5)_2(OH_2)]$[242]

3.2.3 Triorganotin Carboxylates

There are a vast number of structural deviations known for the triorganotin derivatives. Examples of each class are given in Table 3.3.

Table 3.3 Structural Variations in Triorganotin Carboxylates

FORMULA	Variation	Example	Ref.
$[R_3Sn(O_2CR')]$	Type A[a]	$\{Ph_3Sn[O_2CC_6H_4(OH)\text{-}2]\}$	247
	Type B[b]	$[(c\text{-}C_6H_{11})_3Sn(O_2C\text{-}N\text{-}Me\text{-}3\text{-}indolylacetate)]$	248
	Type C[c]	$[n\text{-}Bu_3Sn(O_2CCH{=}CHC_6F_5)]$	249
$[R_3Sn(O_2CR')]_4$		$[n\text{-}Bu_3Sn(O_2CC_6H_3F_2)]_4$	250
$[R_3Sn(O_2CR')L]$		$[Me_3Sn(O_2CC_5H_4N\text{-}2)(OH_2)]$	251
$[R_3Sn(O_2CR'H)X]$		$[Ph_3Sn(O_2CC_5H_5N)(NCS)]$	252
$[R_3Sn(O_2CR')_2]^-$		$[Ph_3Sn(O_2CCF_3)_2]^-$	253
$[R_3Sn(O_2CR')_2SnR_3(L)]$		$[Ph_3Sn(O_2CC_6H_4\text{-}2\text{-}Cl)_2SnPh_3(OH_2)]$	254
$[R_3Sn(O_2CR')SnR_3]$		$[Ph_3Sn(O_2CC_6H_4\text{-}2\text{-}S)SnPh_3]$	255
$[(R_3Sn)_3(O_2C_2O_2)_2]^-$		$[Ph_3Sn)_3(O_2C_2O_2)_2]^-$	256
$[(R_3Sn)_4(O_2C_2O_2)_3L_2]^{2-}$		$[(n\text{-}Bu_3Sn)_4(O_2C_2O_2)_3(EtOH)_2]^{2-}$	257
$[(R_3Sn)_2(O_2R'O_2)]$	Type A[d]	$[Ph_3Sn(O_2CH(Ph)CH_2CO_2)SnPh_3]$	258
	Type B[e]	$[Ph_3Sn(O_2CCH_2CH(Me)CO_2SnPh_3]$	258
	Type C[f]	$[Me_3Sn(O_2CCH_2CO_2)SnMe_3]$	259
$[(R_3Sn)_2(O_2R'O_2)L]$		$\{[Ph_3Sn(O_2C(CH_2)_2CO_2)SnPh_3(dmf)]_2\}_n$	260
$[R_3Sn(O_2CR'CO_2)]^-$		$[n\text{-}Bu_3Sn(O_2C(C_5H_3N\text{-}2)CO_2)]^-$	261

[a] Monomeric tetrahedral with a monodentate carboxylate ligand. [b] Monomeric *cis*-trigonal bipyramidal with a bidentate chelating carboxylate ligand. [c] Polymeric *trans*-trigonal bipyramidal with bidentate bridging carboxylate ligands. [d] Dinuclear with two tin centres linked by the dicarboxylate ligand. [e] Linear polymer with tin atom in distorted *cis*-trigonal bipyramidal geometry. [f] 3-Dimensional polymer with tetradentate dicarboxylate ligands.

3.2.3.1 $[R_3Sn(O_2CR')]$

Triorganotin carboxylates of the general formula $[R_3Sn(O_2CR')]$ have been studied in this thesis and will therefore be discussed at greater length.

In the crystalline state, there are three possible structural modes for this class.

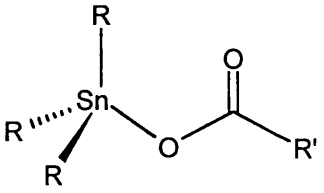

(XI)

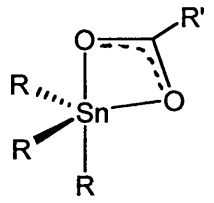

(XII)

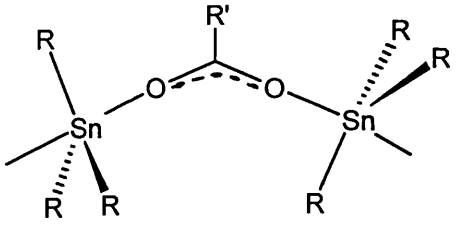

(XIII)

Structure (**XI**) incorporates a four-coordinate tin atom and features a monodentate carboxylate ligand. For structure (**XII**), a bidentate carboxylate ligand chelates the tin atom, which is now five-coordinate. In contrast to the monomeric structures depicted by (**XI**) and (**XII**), a polymeric structure is represented by (**XIII**). Here, the carboxylate ligands are bidentate bridging and the five-coordinate tin atoms exist in distorted trigonal bipyramidal geometries.

There are several factors which influence the structural variation adopted by the carboxylate. For example, organotin compounds with bulky R groups coordinated to tin would tend to favour the monomeric structures, whereas sterically less demanding R groups would lead to the formation of the polymeric arrangement. Electron-withdrawing R groups coordinated to tin would be expected to favour five-coordinate species as the acceptor character of the tin atom would be enhanced.

Although there are two monomeric variations, the known structures lie somewhere between (**XI**) and (**XII**). Examples which closely resemble that of structure (**XI**) are $Ph_3Sn[O_2CC_6H_4(OH)\text{-}2]$[247] and more recently, $(c\text{-}C_6H_{11})_3Sn[O_2C(CHS)_2NEt_2]$.[262] In these compounds, the tin atom is essentially four-

coordinate, distorted tetrahedral. This structural form can be identified by a long Sn-O(2) separation which is 3.071 Å in the case of $Ph_3Sn[O_2CC_6H_4(OH)\text{-}2]$,[247] (Figure 3.8) which is not indicative of a significant interaction.

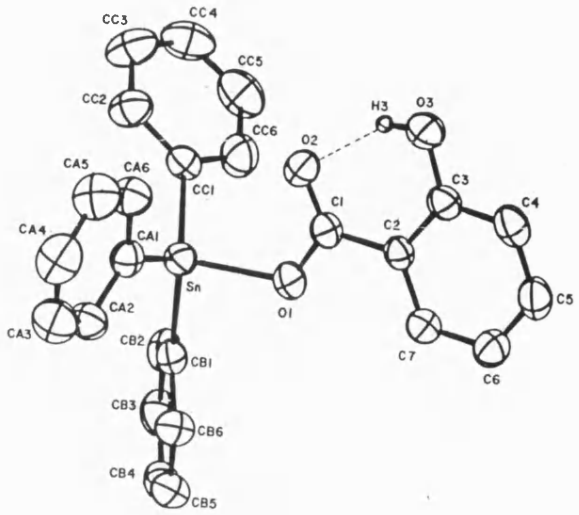

Figure 3.8 Molecular Structure of $Ph_3Sn[O_2CC_6H_4(OH)\text{-}2]$[247]

The limiting five-coordinate structure can be represented by $Ph_3Sn[(o\text{-}2\text{-hydroxy-}5\text{-methyl-phenylazo})benzoate]$[263] shown in Figure 3.9. Here, the tin atom exists in a distorted *cis*-trigonal bipyramidal geometry with the oxygen atoms occupying axial and equatorial positions. The two Sn-O bond distances of 2.070 and 2.463 Å indicate significant bonding interactions and therefore the tin atom must be thought of as being five coordinate.

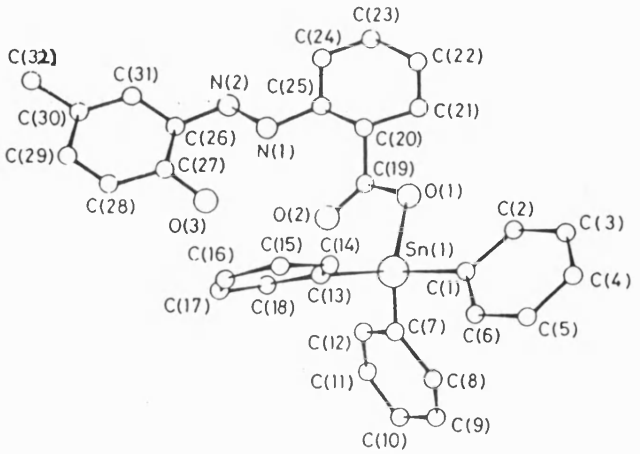

Figure 3.9 Molecular Structure of $Ph_3Sn[(o\text{-}2\text{-hydroxy-}5\text{-methyl-phenylazo})benzoate]$[263]

The compounds in the monomeric categories are characterised by relatively large tin-bound groups and frequently, but not exclusively, bulky carboxylate ligands.

By far the most common arrangement for the triorganotin carboxylates is the polymeric structure (**XIII**), which is best described as the *trans*-R_3SnO_2 type. The tin atoms in these structures exist in distorted trigonal bipyramidal environments with the three R groups defining the trigonal planes so that the C_3Sn groups are very nearly planar. The axial positions are occupied by the more electronegative oxygen atoms from the carboxylate ligands, and the polymeric arrangement is accomplished by the bidentate bridging action of the carboxylate ligands. The repeat distance in bridged triorganotin carboxylate polymers has been explored[264] and it is found that they always contain one short Sn-O(1) and one long Sn-O(2) bond.

There are an enormous number of examples of polymeric triorganotin carboxylates in the literature, but a typical structure can be illustrated by [*n*-$Bu_3Sn(O_2C$-$CH{=}CH$-$C_6F_5)$][249] (Figure 3.10).

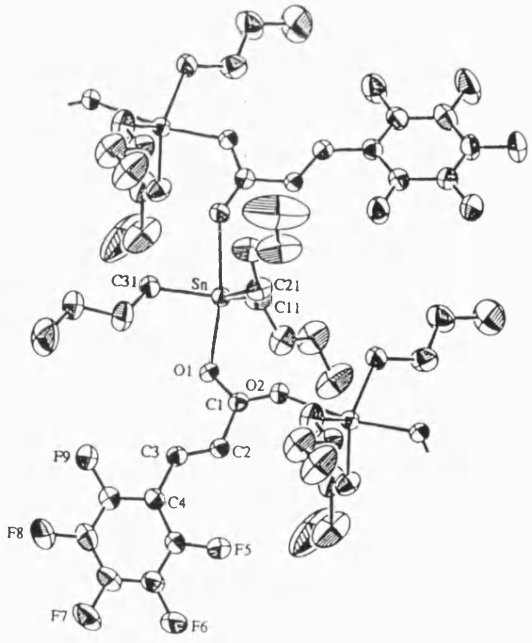

Figure 3.10 Molecular Structure of [*n*- $Bu_3Sn(O_2C$-$CH{=}CH$-$C_6F_5)$][249]

An extremely unusual structure has been found for [n-$Bu_3Sn(O_2CC_6H_3F_2)$] which is found to exist as a macrocyclic tetramer.[250] The structure is similar to that of the polymeric arrangement (**XIII**) but an infinite chain is not formed, and instead a finite tetramer as shown in Figure 3.11.

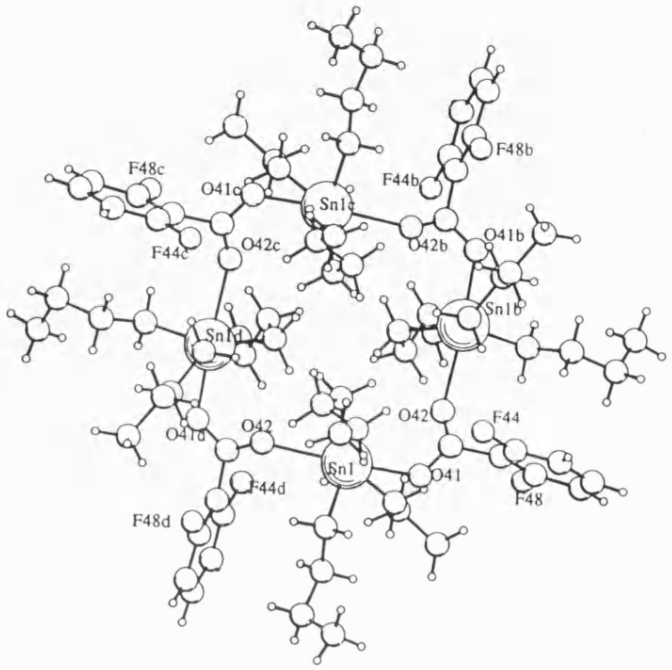

Figure 3.11 Molecular Structure of [n-$Bu_3Sn(O_2CC_6H_3F_2)$][250]

3.3 SYNTHETIC ROUTES

There are many synthetic routes available for the preparation of organotin carboxylates. In general, similar strategies are employed for mono-, di-, and triorganotin derivatives, with relatively simple synthetic methods available.

A good method for the synthesis of all classes of organotin carboxylates involves the reaction of the appropriate organotin chloride with a salt of the corresponding carboxylic acid. This reaction is always carried out in a polar solvent such as ethanol in order to achieve solubilisation of the salt. Examples are given for mono-,[224] di-,[238] and triorganotin[248] carboxylates respectively (Equations 3.2 - 3.4).

$$RSnCl_3 + 10R'CO_2M + 4H_2O \longrightarrow [(RSn(O)O_2CR')_2RSn(O_2CR')_3]_2 + 10MCl + 8HCl \quad [3.2]$$

$$R_2SnCl_2 + 2R'CO_2M \longrightarrow R_2Sn(O_2CR')_2 + 2MCl \quad [3.3]$$

$$R_3SnCl + R'CO_2M \longrightarrow R_3SnO_2CR' + MCl \quad [3.4]$$

M = Na, K, Ag

The second universal method involves the reaction of the appropriate organotin oxide with the corresponding carboxylic acid. Respective examples are given for the mono-, di-, and triorganotin carboxylates (Equations 3.5 - 3.8).

$$RSn(O)OH + 6R'CO_2H \longrightarrow [RSn(O)O_2CR']_6 + 6H_2O \quad [3.5]$$

$$RSn(O)OH + 10R'CO_2H \longrightarrow [(RSn(O)O_2CR')_2RSn(O_2CR')_3]_2 + 8H_2O \quad [3.6]$$

$$R_2SnO + 2R'CO_2H \longrightarrow R_2Sn(O_2CR')_2 + H_2O \quad [3.7]$$

$$(R_3Sn)_2O + 2R'CO_2H \longrightarrow 2R_3SnO_2CR' + H_2O \quad [3.8]$$

One diorganotin carboxylate [*n*-$Bu_2Sn(O_2CCH_2C_6H_5)_2(OH_2)$] has been prepared in which no solvent was used during the reaction.[242] In this case, the product was found to actually contain a coordinated water molecule showing the high acceptor character of the tin. More commonly, toluene[265-267] or benzene[268-269] can be used as solvents in which a Dean & Stark separator is used to remove the water liberated.

Although the two methods described above are commonly used, there are various alternative methods available which are specific for a certain class of carboxylate.

For the diorganotin carboxylates, a less frequently encountered synthesis involves the reaction of the diorganotin oxide with the appropriate anhydride.[270] This method is probably rarely used due to the limited number of commercially available anhydrides.

$$R_2SnO + (R'CO)_2O \longrightarrow R_2Sn(O_2CR')_2 \quad [3.9]$$

There are two alternative routes for the triorganotin derivatives. The first reacts the triorganotin hydroxide with the corresponding carboxylic acid to produce the carboxylate. A variety of solvents have been used for this synthetic route, including toluene,[248] ethanol,[271] and benzene.[272]

$$R_3SnOH + R'CO_2H \longrightarrow R_3SnO_2CR' + H_2O \qquad [3.10]$$

A more unusual method which also only appears for the triorganotin derivatives involves the reaction of the carboxylic acid with triorganotin acetate. This reaction can be undertaken in ethanol or toluene.[250]

$$R_3SnO_2CCH_3 + R'CO_2H \longrightarrow R_3SnO_2CR' + CH_3CO_2H \qquad [3.11]$$

3.4 RESULTS AND DISCUSSION

3.4.1 Synthesis

A series of fluorinated organotin carboxylates have been prepared with a variation in both the organic group R and the fluorinated component R′, which has enabled the effects of both constituents in the CVD process to be explored. The majority of compounds synthesised were triorganotin derivatives, which were usually obtained via the reaction of the triorganotin chloride and the sodium salt of the appropriate fluorinated carboxylic acid.

$$R_3SnCl + NaO_2CR' \xrightarrow{EtOH} R_3SnO_2CR' + NaCl \qquad [3.12]$$

R = Bu, R' = CF_3 (**6**), C_2F_5 (**7**), C_3F_7 (**8**)

R = Et, R' = CF_3 (**9**), C_2F_5 (**10**)

This method was very straightforward and proved to be highly successful. Due to the uncomplicated synthetic route, and ease of production of sufficient material for subsequent CVD testing, this method was chosen in all possible cases. Recrystallisation from 40°-60° petroleum ether yielded the compounds as colourless needles of a high purity and in yields of 23-60%, with tributyltin derivatives being recovered in higher quantities.

One triorganotin carboxylate was prepared by the alternative route of reacting bis(tributyltin) oxide with the fluorinated carboxylic acid. The water generated was removed by a Dean and Stark separator.

$$(Bu_3Sn)_2O + 2C_7F_{15}CO_2H \xrightarrow{\text{toluene}} 2Bu_3SnO_2CC_7F_{15} + H_2O \qquad [3.13]$$

(11)

To explore the effect of an additional fluorinated group in the precursor one diorganotin carboxylate was also prepared. The route chosen was the reaction between the diorganotin oxide and the corresponding fluorinated anhydride. This method was selected due to its known success for the equivalent hydrogenated analogue,[270] and the cheap availability of the trifluoroacetic anhydride.

$$Me_2SnO + (CF_3CO)_2O \xrightarrow{\text{no solvent}} Me_2Sn(O_2CCF_3)_2 \qquad [3.14]$$

(12)

The reaction had to be carried out in the strict absence of air due to the possible oxygen and moisture sensitivity of the product. A large excess of trifluoroacetic anhydride was used to encourage reaction, and theoretically absorb any moisture present. Very little solubilisation of the dimethyltin oxide was accomplished possibly due to the low boiling point of the anhydride (35°C). However, the reaction proved successful, and following the removal of the excess trifluoroacetic anhydride and subsequent sublimation of the product, a white solid was obtained. Although $Me_2Sn(O_2CCF_3)_2$ (**12**) could be obtained in powder form, a crystalline product could only be achieved as the hydrated

adduct $Me_2Sn(O_2CCF_3)_2(OH_2)$ (**13**). The attainment of both forms was shown conclusively by microanalysis as shown in Table 3.4.

Table 3.4 Analytical Data for Dimethyltin Bis-(trifluoroacetate) and its Monohydrate

COMPOUND	**Carbon Content (%)**		**Hydrogen Content (%)**	
	Calc.	Found	Calc.	Found
$Me_2Sn(O_2CCF_3)_2$ (**12**)	19.2	19.1	1.62	1.63
$Me_2Sn(O_2CCF_3)_2(OH_2)$ (**13**)	18.3	18.3	2.07	2.06

Substantial efforts to prepare a crystalline form of the anhydrous material were made via careful vacuum sublimation of the anhydrous powder, but the hydrated form was always the result. Hydrolysis of $Me_2Sn(O_2CCF_3)_2$ (**12**) to produce the monohydrate (**13**) was an unexpected outcome. The moisture sensitivity of the equivalent hydrogenated analogue $Me_2Sn(O_2CMe)_2$ is well documented,[235] but in this case the common distannoxane $\{[Me_2Sn(O_2CMe)]_2O\}_2$ is the resultant product. This demonstrates the extremely high acceptor character of the tin as there was no water involved in the reaction, either during the synthesis or the sublimation procedure. Also, the use of excess trifluoroacetic anhydride was unable to prevent the water incorporation. This high acceptor character displayed by the tin could be due to the electronegative CF_3 groups which would have enhanced the Lewis acidity of the tin atom.

3.4.1.1 Physical Properties

Table 3.5 lists the physical properties of the fluorinated organotin carboxylates synthesised.

Table 3.5 Physical Properties of the Fluorinated Organotin Carboxylates

COMPOUND		Appearance	Melting Point (°C)
$Bu_3SnO_2CCF_3$	**(6)**	Colourless Needles	49-52
$Bu_3SnO_2CC_2F_5$	**(7)**	Colourless Needles	64-66
$Bu_3SnO_2CC_3F_7$	**(8)**	Colourless Needles	58
$Et_3SnO_2CCF_3$	**(9)**	Colourless Needles	119
$Et_3SnO_2CC_2F_5$	**(10)**	Colourless Needles	94
$Bu_3SnO_2CC_7F_{15}$	**(11)**	Oil	-
$Me_2Sn(O_2CCF_3)_2$	**(12)**	Colourless Powder	140
$Me_2Sn(O_2CCF_3)_2(OH_2)$	**(13)**	Colourless Crystals	220

The vast majority of the compounds synthesised were crystalline solids with melting points rising with a decreasing size of the R group. For potential use as CVD precursors a low melting point is advantageous with liquid precursors preferred. However, the melting points of compounds **(6)** - **(12)** were not excessive, and did not pose a major problem for subsequent CVD testing. Due to the high melting point of compound **(13)**, the anhydrous material **(12)** was used for CVD screening.

3.4.2 Infra-red Spectroscopy

Infra-red spectroscopy is a very useful technique for the study of carboxylates due to the characteristic bands exhibited by the carboxylate group. It can therefore be used to good effect as a diagnostic tool to provide structural information regarding the bonding nature of the carboxylate group.

There are four distinct modes of coordination that can be determined by infra-red spectroscopy, ionic **(XIV)**, unidentate **(XV)**, bidentate chelating **(XVI)** and bidentate bridging **(XVII)**.

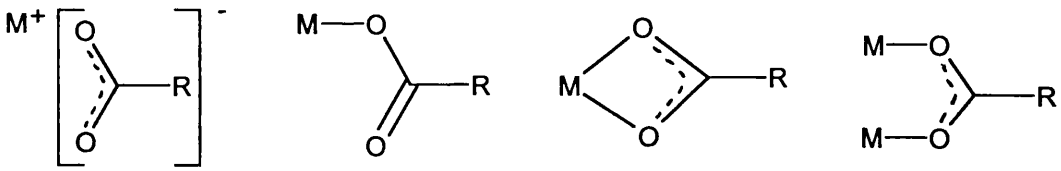

(XIV) (XV) (XVI) (XVII)

The unidentate carboxylate mode (**XV**) is substantially less symmetrical than the other three forms, which has consequences for its infra-red spectrum. Changes exhibited by the observed frequencies are normally compared to those of the ionic carboxylate (**XIV**), in which the carboxylate group is completely symmetrical.

Ionic carboxylates show no carbonyl band at about 1700 cm^{-1}, but depict characteristic bands in the range 1510-1650 cm^{-1} and 1280-1400 cm^{-1} representing the antisymmetric stretch $\nu_a(CO_2^-)$ and symmetric stretch $\nu_s(CO_2^-)$ respectively. Unidentate carboxylates show an increase in the antisymmetric stretching frequency together with a decrease in the symmetric stretching frequency. The reason for this dissimilarity is due to the break-down in equality of the carbonyl groups, which is unique for the unidentate mode of coordination. Therefore, a large splitting of the CO_2 stretching frequencies [$\Delta\nu = \nu_a(CO_2^-) - \nu_s(CO_2^-)$] is often an indication of monodentate coordination.

Bidentate carboxylate ligands have similar symmetry as ionic derivatives, so the CO_2 frequencies are very similar for the two modes. Although attachment of a heavy metal to each oxygen may cause some shifting of the frequencies, they are rather small. In general, bidentate chelating ligands exhibit a lower $\Delta\nu$ than bidentate bridging carboxylates, therefore in summary :

$$\Delta\nu \text{ (chelate)} < \Delta\nu \text{ (bridging)} \approx \Delta\nu \text{ (ionic)} << \Delta\nu \text{ (unidentate)}$$

Therefore, infra-red spectroscopy can be used to good effect to gain structural information as it is possible to distinguish between unidentate and bidentate carboxylate modes of coordination.

Examples of each mode of coordination are given in Table 3.6 showing typical values for $\Delta\nu$.

Table 3.6 Typical Values of $\Delta\nu$ for Each Mode of Coordination of the Carboxylate Group

MODE	**Example**	**$\Delta\nu$ (cm^{-1})**	**Ref.**
Ionic	NaO_2CCH_3	164	273
Unidentate	$CH_3CO_2CH_3$	523	274
Bidentate Chelating	$Na[UO_2(O_2CCH_3)_3]$	65	275
Bidentate Bridging	$[Cu_2(O_2CCH_3)_4].2H_2O$	185	276

Infra-red spectroscopy was performed on all compounds synthesised, with samples recorded as nujol mulls on NaCl plates. Table 3.7 shows the results obtained.

Table 3.7 Infra-red Data for the Fluorinated Organotin Carboxylates

COMPOUND		**$\nu_a(CO_2^-)$ (cm^{-1})**	**$\nu_s(CO_2^-)$ (cm^{-1})**	**$\Delta\nu$ (cm^{-1})**
$Bu_3SnO_2CCF_3$	**(6)**	1678	1447	231
$Bu_3SnO_2CC_2F_5$	**(7)**	1678	1424	254
$Bu_3SnO_2CC_3F_7$	**(8)**	1678	1418	260
$Et_3SnO_2CCF_3$	**(9)**	1653	1456	197
$Et_3SnO_2CC_2F_5$	**(10)**	1659	1462	197
$Bu_3SnO_2CC_7F_{15}$	**(11)**	1688	1466	222
$Me_2Sn(O_2CCF_3)_2(OH_2)$	**(13)**	1671	1453	218

All the results indicate that the triorganotin carboxylates are bidentate bridging (**XVII**), suggesting that they have all adopted the common *trans*-R_3SnX_2 arrangement (**IV**). This can be inferred from the relatively small values for $\Delta\nu$ indicating that there is little unidentate character. The values found for the tributyltin derivatives are larger than for the corresponding triethyltin carboxylates suggesting that the larger R groups create more unidentate character due to the increase in steric bulk. The positions of the two diagnostic stretching frequencies compare favourably with reported values for $Me_3SnO_2CCF_3$ which displays bands at 1680 cm^{-1} and 1435 cm^{-1} for $\nu_a(CO_2^-)$ and $\nu_s(CO_2^-)$ respectively,[277] and is polymeric (bridging carboxylate groups) in character.

Although attempts were made to obtain an infra-red spectrum for the anhydrous $Me_2Sn(O_2CCF_3)_2$ (**12**), they were unsuccessful. This could be inferred from presence of a large band at 3385 cm^{-1} indicating the presence of water. The values of 1671 cm^{-1} and 1453 cm^{-1} are very different than those reported for $Me_2Sn(O_2CMe)_2$ of 1607 cm^{-1} and 1380 cm^{-1}.[278] This suggests a totally different structure from the common Type A arrangement containing chelated carboxylates for $Me_2Sn(O_2CCF_3)_2(OH_2)$ (**13**) in the solid state. The value of 218 cm^{-1} for $\Delta\nu$ for the hydrated adduct suggests bidentate carboxylate groups which are bridging rather than chelating.

Following the apparent extreme moisture sensitivity of $Me_2Sn(O_2CCF_3)_2$ (**12**) and the difficulty in obtaining an infra-red spectrum, all analysis was initially collected for the hydrated adduct $Me_2Sn(O_2CCF_3)_2(OH_2)$ (**13**). Due to the stability of this compound it could safely be assumed that data obtained were reliable. Attempts to acquire analytical information for the anhydrous material (**12**) were subsequently performed, and any deviation from the data obtained for (**13**) indicated that analysis for (**12**) had been achieved.

3.4.3 Mössbauer Spectroscopy

All compounds were studied as solids at 78K; data are given in Table 3.8.

Table 3.8 Mössbauer Data for the Fluorinated Organotin Carboxylates

COMPOUND		Isomer Shift δ (mm s^{-1})	Quadrupole Splitting ΔE_Q (mm s^{-1})
$Bu_3SnO_2CCF_3$	**(6)**	1.51	4.06
$Bu_3SnO_2CC_2F_5$	**(7)**	1.52	4.12
$Bu_3SnO_2CC_3F_7$	**(8)**	1.52	4.05
$Et_3SnO_2CCF_3$	**(9)**	1.53	4.17
$Et_3SnO_2CC_2F_5$	**(10)**	1.54	4.12
$Bu_3SnO_2CC_7F_{15}$	**(11)**	1.53	4.07
$Me_2Sn(O_2CCF_3)_2$	**(12)**	1.47	4.36
$Me_2Sn(O_2CCF_3)_2(OH_2)$	**(13)**	1.30	3.85

All of the observed isomer shifts are consistent with organotin(IV) compounds as expected. The values obtained for the quadrupole splitting parameter can be used to determine the structural form adopted by the fluorinated organotin carboxylates. As mentioned previously (Section 1.10.1), certain values give a clear indication of the tin atom stereochemistry and this can be used to good effect in this study.

All of the values given by the triorganotin carboxylates are very high which is a clear indication of the *trans*-R_3SnX_2 arrangement (**IV**). The fact that the values exceed 4.00 mm s^{-1} can be explained by two factors. Firstly, a large difference in the two axial Sn-X bond lengths will lead to an increase in the observed quadrupole splitting parameter. More importantly, the difference in electronegativity between the axial and equatorial ligands produces a significantly increased quadrupole splitting. The electronegative equatorial fluorinated ligands are therefore responsible for the observation of the extremely large values of > 4.00 mm s^{-1}. The influence of the fluorinated ligands can be demonstrated by the difference in the quadrupole splittings observed for Me_3SnO_2CMe and $Me_3SnO_2CCF_3$. The reported value for Me_3SnO_2CMe is quoted as 3.68 mm s^{-1} with a much higher value of 4.22 mm s^{-1} found for

$Me_3SnO_2CCF_3$.[279] The two compounds adopt an identical polymeric structure (**IX**)[280] so the large difference can only be due to the electronegativity of the fluorinated ligand.

The Mössbauer data therefore confirm that the fluorinated triorganotin carboxylates have all adopted the polymeric *trans*-R_3SnX_2 arrangement (**IX**). This is consistent with the infra-red results, therefore concluding that the triorganotin derivatives have been produced with the most common structural form. This would be as expected as the groups contained are not necessarily bulky, but for CVD purposes monomeric compounds would have been preferential due to their enhanced volatility.

The value obtained for the anhydrous diorganotin carboxylate $Me_2Sn(O_2CCF_3)_2$ (**12**) can also be used to identify the structural mode adopted by this compound. A very high value of 4.36 mm s^{-1} suggests that the structure is the common *trans*-R_2SnX_4 form (**VIII**) with bidentate carboxylate groups. The large quadrupole splitting is again due to the large difference in electronegativity between the axial and equatorial ligands, which suggests that the carboxylates are in the equatorial positions and the R groups axial. It therefore appears that the anhydrous compound adopts the common Type A arrangement in the solid state with bidentate chelating carboxylates.

A much smaller quadrupole splitting of 3.85 mm s^{-1} was observed for the hydrated compound $Me_2Sn(O_2CCF_3)_2(OH_2)$ (**13**), which suggests a totally different structure for the adduct in the solid state. The lower value indicates a smaller difference in electronegativity between axial and equatorial ligands, and suggests an interesting structure for this compound.

3.4.4 NMR Spectroscopy

For all compounds synthesised, ^{1}H, ^{13}C and ^{119}Sn NMR spectroscopy studies were performed. Following the solid state analytical techniques of infra-red and Mössbauer spectroscopy, NMR studies could be used to obtain structural information of the carboxylates in solution.

3.4.4.1 ^{1}H and ^{13}C NMR Spectroscopy

Expected results were supplied by the proton and carbon-13 NMR studies. The R groups were shown clearly with their diagnostic chemical shifts, with predicted integration and multiplicities displayed by the proton spectra. However, there was an absence of observed resonances for the carbon atoms which contained the fluorines. The one bond tin-carbon coupling constants $^{1}J(^{13}C\text{-}^{119}Sn)$ could be extracted from the carbon-13 spectra for the triorganotin derivatives, and are shown in Table 3.9.

Table 3.9 $^{1}J(^{13}C\text{-}^{119}Sn)$ Coupling Constants for the Fluorinated Triorganotin Carboxylates

COMPOUND		**$^{1}J(^{13}C\text{-}^{119}Sn)$ (Hz)**
$Bu_3SnO_2CCF_3$	**(6)**	334
$Bu_3SnO_2CC_2F_5$	**(7)**	332
$Bu_3SnO_2CC_3F_7$	**(8)**	336
$Et_3SnO_2CCF_3$	**(9)**	322
$Et_3SnO_2CC_2F_5$	**(10)**	326
$Bu_3SnO_2CC_7F_{15}$	**(11)**	343

The values of approximately 330 Hz are indicative of four-coordinate tetrahedral triorganotin complexes which usually exhibit one bond tin-carbon coupling constants in the range 327 - 387 Hz.[216] Five-coordinate complexes would be expected to exhibit much larger values in the region of 442 - 509 Hz[216] due to the increase in *s*-character of the tin-carbon bonds. This suggests that the polymeric structures determined by Mössbauer spectroscopy have been broken up in solution to form monomeric entities with a reduction in coordination number from five to four. Such observations have previously been identified for trimethyltin haloacetates.[277]

As found for the infra-red spectroscopy, it was only possible to obtain NMR spectra for $Me_2Sn(O_2CCF_3)_2(OH_2)$ (**13**) due to the extreme moisture sensitivity of $Me_2Sn(O_2CCF_3)_2$ (**12**). Following the attainment of the spectra for (**13**), identical spectra were obtained for (**12**) showing that hydrolysis had occurred. The two bond tin-hydrogen coupling constant could be determined for this compound, and was found to have a value of 81 Hz. A C-Sn-C bond angle of 132.1° could be estimated by use of the equation derived to calculate this angle in methyltin compounds.[187] This compares to respective calculated values of 82.5 Hz and 135° for the hydrogenated analogue $Me_2Sn(O_2CMe)_2$,[235] which has been found to adopt the common Type A structural form with bidentate chelating carboxylates. The similarity in values obtained for the fluorinated derivative suggests that it adopted a similar structure in solution.

Therefore, the proton and carbon-13 NMR studies provided information regarding the R groups, and confirmed their presence in the correct ratios. Coupling constants could be used to good effect to decipher the structural form adopted in solution.

3.4.4.2 ^{119}Sn NMR Spectroscopy

The ^{119}Sn NMR studies provided structural information regarding the environment around the tin atom. All carboxylates were dissolved in deuterated chloroform and all triorganotin derivatives gave sharp singlets in the tin-119 spectra, showing that the compounds had been produced cleanly. Table 3.10 shows the observed chemical shifts for the fluorinated organotin carboxylates synthesised.

Table 3.10 ^{119}Sn Chemical Shifts for the Fluorinated Organotin Carboxylates

COMPOUND		Chemical Shift (ppm)
$Bu_3SnO_2CCF_3$	**(6)**	172.3
$Bu_3SnO_2CC_2F_5$	**(7)**	174.5
$Bu_3SnO_2CC_3F_7$	**(8)**	175.1
$Et_3SnO_2CCF_3$	**(9)**	164.7
$Et_3SnO_2CC_2F_5$	**(10)**	160.5
$Bu_3SnO_2CC_7F_{15}$	**(11)**	167.2
$Me_2Sn(O_2CCF_3)_2(OH_2)$	**(13)**	-139.4, -138.6

All of the triorganotin carboxylates exhibited large positive chemical shifts. This is consistent with a decrease in coordination number from five to four for the tin when dissolved in the NMR solvent. This reduction in coordination number can be explained by a break up of a polymeric arrangement to produce monomeric units, which is consistent with the information derived from the $^1J(^{13}C\text{-}^{119}Sn)$ coupling constants extracted from the carbon-13 NMR. The structure has therefore changed from a polymeric *trans*-R_3SnX_2 arrangement (**IX**) to a monomeric tetrahedral R_3SnX species (**I**) in solution.

As for the infra-red spectroscopy, it was found to be very difficult to obtain a spectrum for the anhydrous $Me_2Sn(O_2CCF_3)_2$ (**12**). The data given is therefore likely to be representative of the hydrated adduct (**13**). The spectrum displayed ^{119}Sn resonances at a much higher field due to the presence of an additional electronegative ligand as expected, which were found in the region characteristic of a diorganotin carboxylate.[281]

However, the observation of two resonances extremely close together was unexpected, as this suggested two similar tin environments in the compound. It was found to be quite difficult to dissolve the material so it could be feasible that small oligomers containing two tin environments were present in solution following partial

break up of a polymeric arrangement. Alternatively, it could be possible that both the anhydrous and hydrated forms were present in solution, resulting in two peaks, although this is very unlikely due to the extreme moisture sensitivity of the anhydrous material. The values at approximately -139 ppm are slightly further upfield from $Me_2Sn(O_2CMe)_2$ for which the resonance is displayed at -120 ppm.[244]

3.5 CRYSTAL STRUCTURES

3.5.1 Single Crystal X-Ray Structure Determination of $Et_3SnO_2CC_2F_5$ (10)

Crystallographic quality crystals of $Et_3SnO_2CC_2F_5$ (**10**), were obtained from slow evaporation of a saturated solution of 40°-60° petroleum ether at room temperature. The crystals were stable to light and to atmosphere, but data collection had to be carried out at 170 K due to the decay of the compound in the X-ray beam at room temperature. The structure is illustrated in Figure 3.12 with the polymeric arrangement shown in Figure 3.13. Relevant bond distances and angles are summarised in Tables 3.11 and 3.12 respectively, with further data provided in Appendix Two.

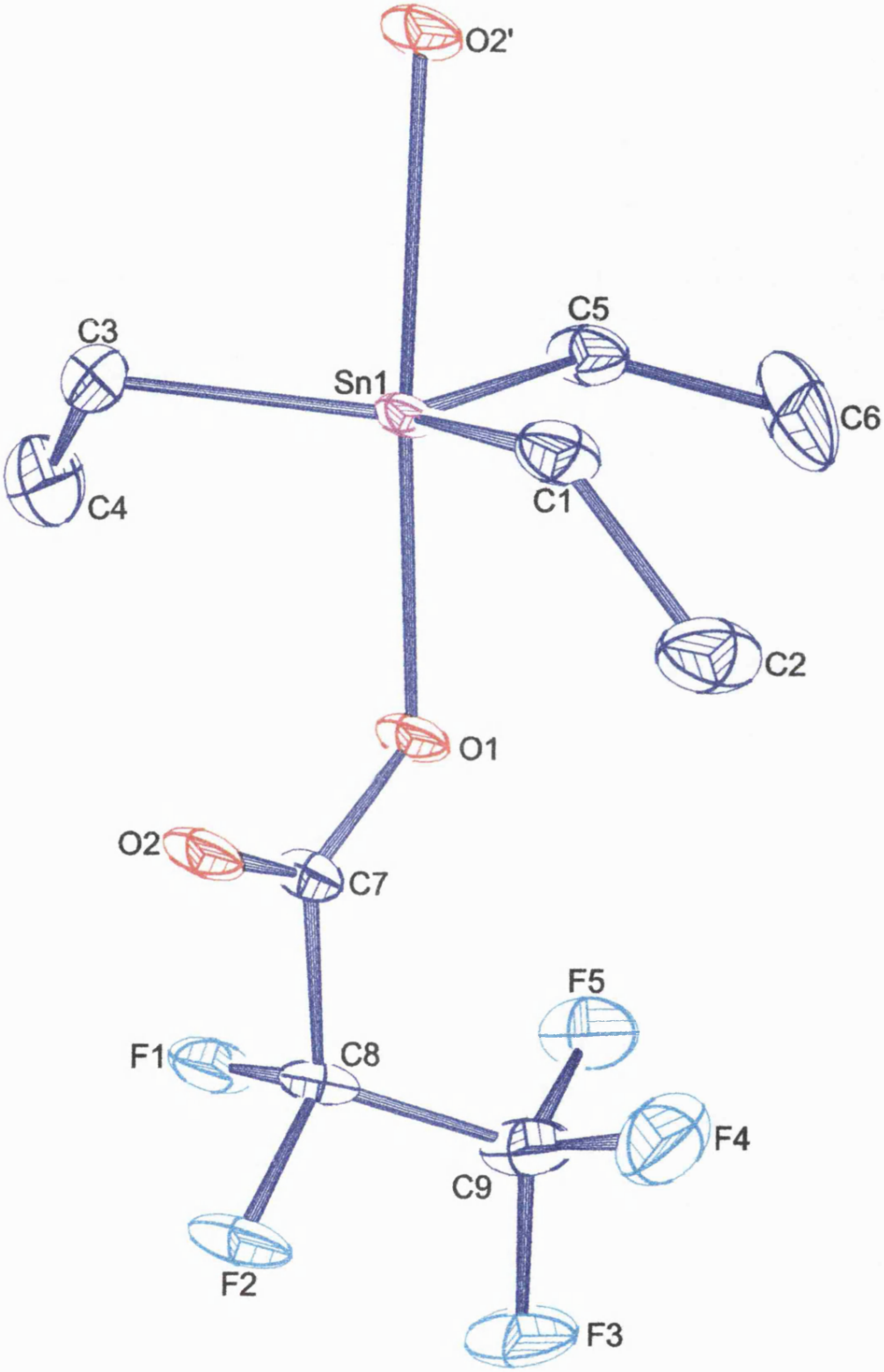

Figure 3.12 Molecular Structure of $Et_3SnO_2CC_2F_5$ (**10**)

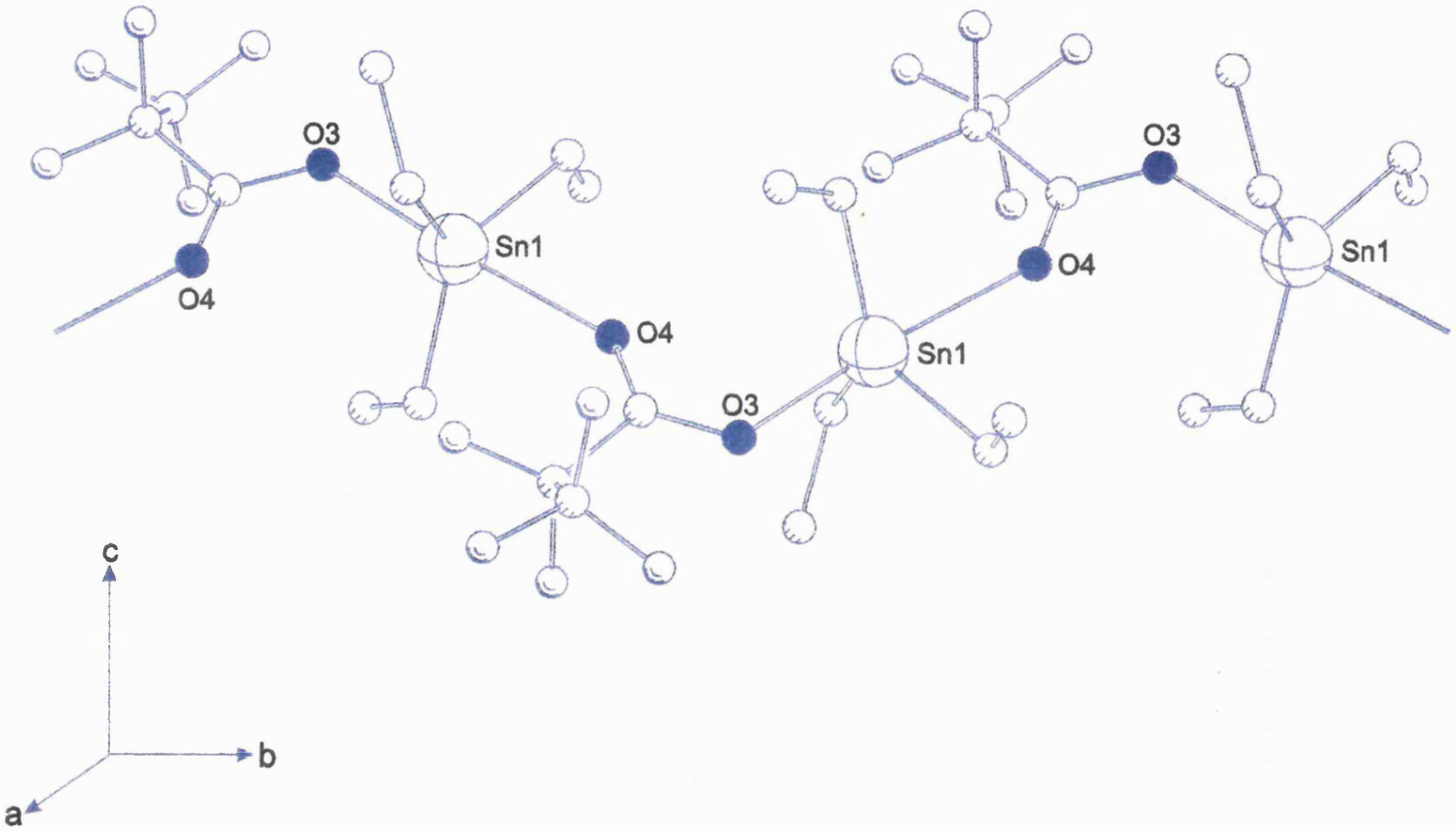

Figure 3.13 Polymeric Structure of $Et_3SnO_2CC_2F_5$ (**10**)

Table 3.11 Selected Bond Distances for $Et_3SnO_2CC_2F_5$ (**10**)

	Length (Å)		**Length (Å)**
Sn(1)-O(1)	2.218(4)	O(1)-C(7)	1.284(7)
Sn(1)-O(2)	2.481(4)	O(2)-C(7)	1.224(7)
Sn(1)-C(1)	2.119(6)	C(7)-C(8)	1.533(8)
Sn(1)-C(3)	2.137(7)	C(8)-C(9)	1.514(10)
Sn(1)-C(5)	2.119(6)		

Table 3.12 Selected Bond Angles for $Et_3SnO_2CC_2F_5$ (**10**)

	Angle (°)		**Angle (°)**
O(1)-Sn(1)-O(2′)	174.9(1)	C(1)-Sn(1)-C(5)	117.1(3)
O(1)-Sn(1)-C(1)	96.0(2)	C(3)-Sn(1)-C(5)	114.7(3)
O(1)-Sn(1)-C(3)	95.1(2)	Sn(1)-O(1)-C(7)	118.5(4)
O(1)-Sn(1)-C(5)	89.5(2)	C(7)-O(2)-Sn(1′)	144.0(4)
O(2′)-Sn(1)-C(1)	85.4(2)	O(1)-C(7)-O(2)	126.7(5)
O(2′)-Sn(1)-C(3)	87.9(2)	O(1)-C(7)-C(8)	112.8(5)
O(2′)-Sn(1)-C(5)	85.6(2)	O(2)-C(7)-C(8)	120.6(5)
C(1)-Sn(1)-C(3)	127.0(3)	C(7)-C(8)-C(9)	115.7(5)

The crystal structure as determined by single crystal X-ray diffraction is found to adopt the most common form for the triorganotin carboxylates, which confirms all of the evidence gained from infra-red, NMR and Mössbauer studies. The structure of triethyltin pentafluoropropionate consists of polymeric chains in which essentially planar triorganotin moieties are bridged by the bidentate carboxylate groups, therefore forming a slightly distorted *trans* trigonal bipyramidal geometry about the tin.

There are an enormous number of compounds reported with this structural form. Examples include $(PhCH_2)_3SnO_2CMe$,[158] $Bu_3SnO_2CCH{=}CHC_6F_5$,[249] $Ph_3Sn(o\text{-}ClC_6H_4CO_2)$,[254] and Ph_3SnO_2CH.[266]

The nature of the bridging is anisotropic, in which tin forms one short [Sn(1) - O(1) 2.218 Å] and one relatively long [Sn(1) - O(2) 2.481 Å] bond to oxygen. This is one of the reasons for the large quadrupole splitting value observed in the Mössbauer studies. These bond lengths are comparable to other Sn-O bonds found in typical polymeric triorganotin carboxylates, with short (2.12 - 2.246 Å) and long (2.24 - 2.65 Å) bonds, respectively.

The O(1)-Sn(1)-O(2) bond angle (174.9°) is also found to be comparable to other angles found in typical polymeric triorganotin carboxylates (168.6-178.7°). Compounds found with angles at the limiting range are $(PhCH_2)_3SnO_2CMe$ (168.6°)[158] and $[Ph_3Sn(O_2CCH_2SC_6H_3\text{-}2\text{-}N\text{-}6\text{-}N)]$ (178.7°).[282]

3.5.2 Single Crystal X-Ray Structure Determination of $Me_2Sn(O_2CCF_3)_2(OH_2)$ (13)

Crystallographic quality crystals of $Me_2Sn(O_2CCF_3)_2(OH_2)$ (**13**), were obtained by slow vacuum sublimation onto a cold finger. The crystals were found to be sensitive to air and moisture, and data collection was carried out at 170 K. The structure is illustrated in Figure 3.14 with the 3-dimensional lattice shown in Figure 3.15. Relevant bond distances and angles are summarised in Tables 3.13 and 3.14 respectively, with further data provided in Appendix Three.

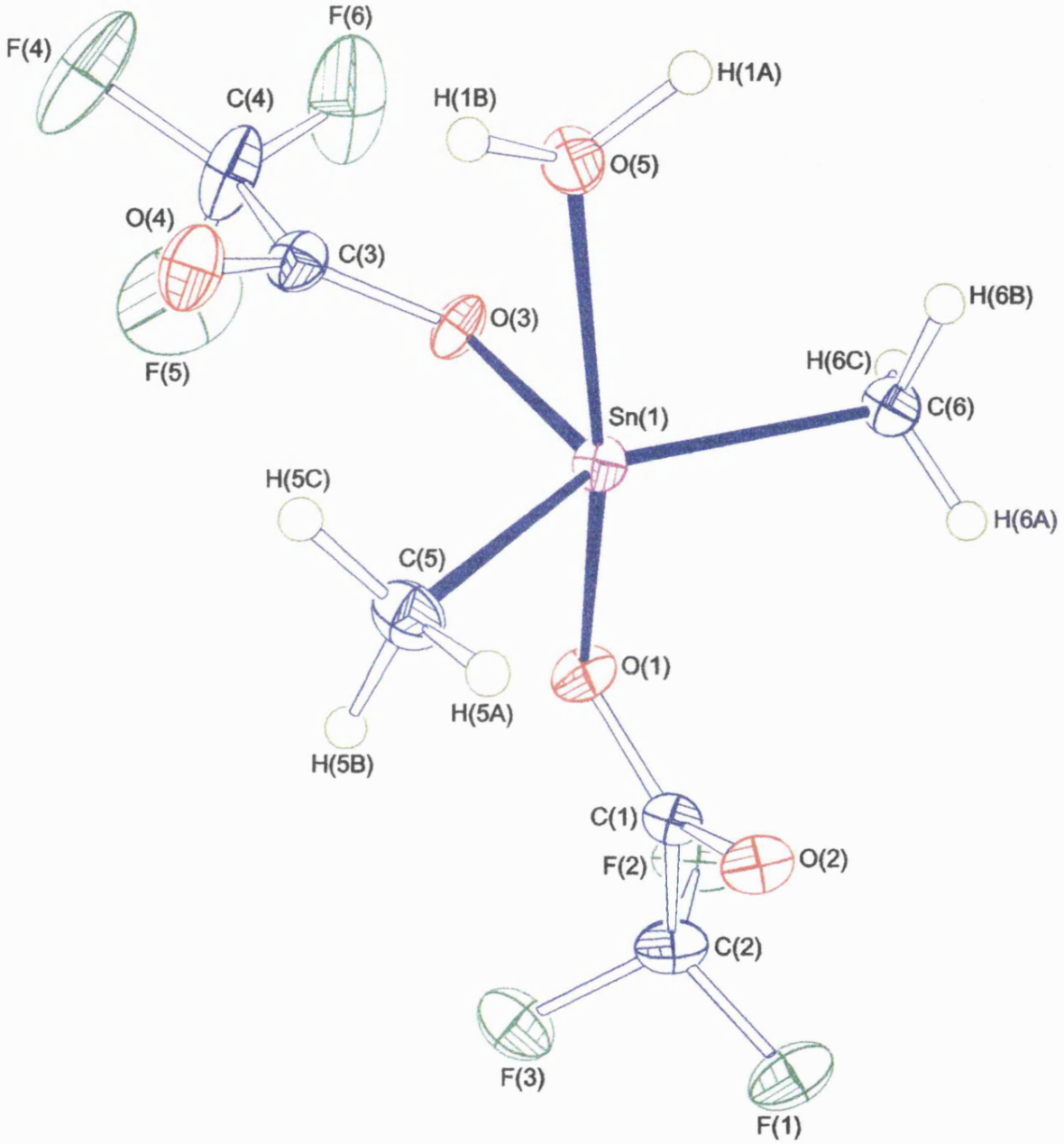

Figure 3.14 Molecular Structure of $Me_2Sn(O_2CCF_3)_2(OH_2)$ (**13**)

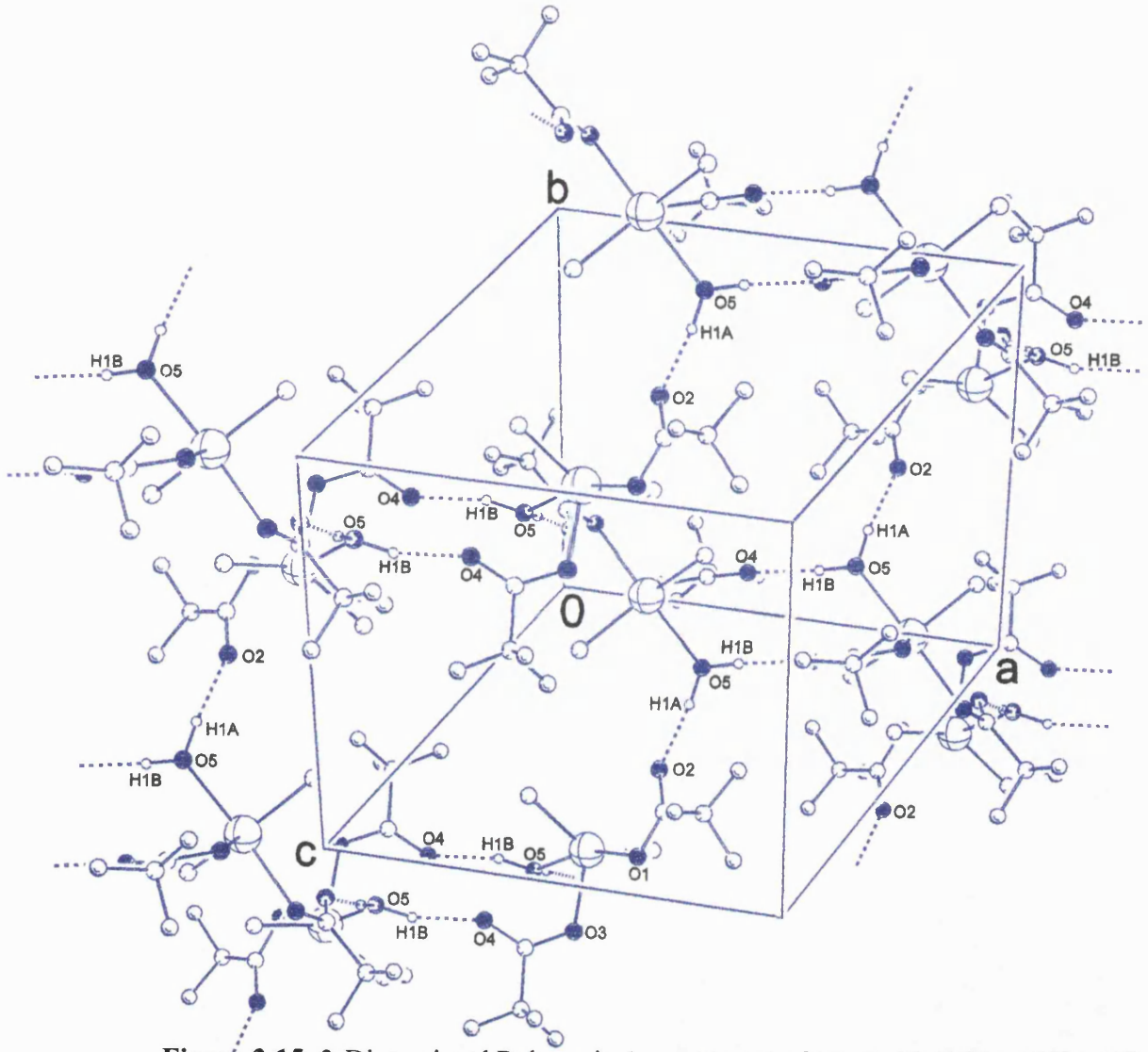

Figure 3.15 3-Dimensional Polymeric Arrangement of $Me_2Sn(O_2CCF_3)_2(OH_2)$ (**13**)

Table 3.13 Selected Bond Lengths for $Me_2Sn(O_2CCF_3)_2(OH_2)$ (**13**)

	Length (Å)		**Length (Å)**
Sn(1)-O(1)	2.205(3)	O(3)-C(3)	1.280(5)
Sn(1)-O(3)	2.082(3)	O(2)-C(1)	1.219(5)
Sn(1)-O(5)	2.238(3)	O(4)-C(3)	1.214(5)
Sn(1)-C(5)	2.102(4)	C(1)-C(2)	1.537(6)
Sn(1)-C(6)	2.098(4)	C(3)-C(4)	1.522(7)
O(1)-C(1)	1.271(5)		

Table 3.14 Selected Bond Angles for $Me_2Sn(O_2CCF_3)_2(OH_2)$ (**13**)

	Angle (°)		**Angle (°)**
O(1)-Sn(1)-O(5)	162.4(1)	O(3)-Sn(1)-C(5)	113.7(2)
O(1)-Sn(1)-C(5)	96.7(1)	O(3)-Sn(1)-C(6)	106.1(1)
O(1)-Sn(1)-C(6)	93.9(1)	C(5)-Sn(1)-C(6)	140.1(2)
O(1)-Sn(1)-O(3)	79.2(1)	Sn(1)-O(1)-C(1)	110.8(2)
O(5)-Sn(1)-C(5)	91.5(1)	Sn(1)-O(3)-C(3)	119.3(3)
O(5)-Sn(1)-C(6)	89.8(1)	O(1)-C(1)-O(2)	126.6(4)
O(5)-Sn(1)-O(3)	83.2(1)	O(3)-C(3)-O(4)	126.9(4)

The crystal structure as determined by single crystal X-ray diffraction was found to consist of a five-coordinate tin atom. The unit cell contains the two methyl groups and one unidentate carboxylate group in the three equatorial positions. The second carboxylate group is also bonded in a unidentate fashion in one of the axial locations, with the final axial position occupied by the oxygen of a coordinated water molecule. The geometry about the tin can therefore be described as distorted *cis*-R_2SnO_3 trigonal bipyramidal.

The presence of the carboxylate ligands in axial and equatorial positions could explain the smaller quadrupole splitting observed in the Mössbauer spectrum. This arrangement contains less electronegativity difference between the two locations resulting in a reduced quadrupole splitting compared to that observed for $Me_2Sn(O_2CCF_3)_2$ (**12**).

Due to the coordinated water molecule, the structure exhibits hydrogen bonding between the hydrogen atoms of the water molecule and the unbonded oxygen atoms of the carboxylate groups which creates a 3-dimensional polymeric lattice. It appears that the individual molecules dimerise through two related hydrogen bonds between the O(4) and H(1B) atoms. The 3-dimensional polymeric lattice is then constructed by single hydrogen bonds between the O(2) and H(1A) atoms which link the dimeric units. This polymeric structure could explain the observation of the two peaks displayed on the ^{119}Sn NMR spectrum.

It appears that there is only one other reported diorganotin carboxylate structure which contains a coordinated water molecule, that of $Bu_2Sn(O_2CCH_2C_6H_5)_2(OH_2)$.[242] However, the structure of this compound is very different and consists of a seven coordinate tin atom with *trans* C_2SnO_5 pentagonal bipyramidal geometry. This geometry is a result of the carboxylate groups bonding in a bidentate chelating fashion in two equatorial positions. The remaining equatorial site is occupied by the oxygen of the water molecule with the butyl groups in the two axial positions.

The attainment of the five-coordinate monohydrate, along with the other known structures, can be used to suggest a possible mechanism of hydrolysis for diorganotin carboxylates (Scheme 3.1). It completes the link between diorganotin carboxylates, the seven-coordinate monohydrate,[242] and the distannoxanes, the common products of hydrolysis.

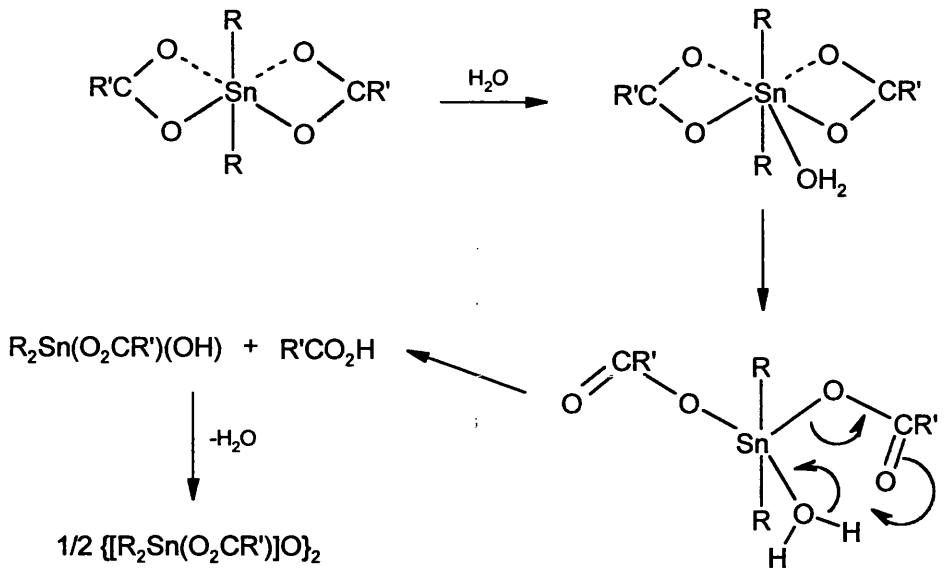

Scheme 3.1 Possible Mechanism of Hydrolysis of Diorganotin Carboxylates

Due to the apparently unique structure of $Me_2Sn(O_2CCF_3)_2(OH_2)$ it is not possible to make any comparisons of the geometry. However, there are certain observations which are of particular interest. Firstly, it can be seen that the bond to the oxygen of the water molecule (2.238 Å) is the longest of the three Sn-O bonds. Also, the bond angle found for C(5)-Sn(1)-C(6) of 140.1(2)° is a large deviation from an ideal angle of 120°. An increase in coordination number to six for the tin could have been expected with a gap created by an angle of this magnitude. This angle is much larger than the value of 132.1° predicted by NMR studies which suggests that the structure in solution is different to the one adopted in the solid state. Also, the unidentate nature of the carboxylate groups are evident by the short C=O (1.219 and 1.214 Å) and long C-O (1.271 and 1.280 Å) respective bond lengths, but were not clearly evident in the infra-red spectrum.

Although significant attempts to prepare the anhydrous form of dimethyltin bis(trifluoroacetate) as a crystalline material were performed through sublimation, only the hydrated form could be isolated.

3.6 CVD TESTING OF PRECURSORS

Suitable compounds were selected for CVD studies, with details of the apparatus given in Appendix Five. In all cases, the substrate used was 4 mm glass which was undercoated with a thin film of SiCO to act as a "blocking layer" to prevent sodium diffusion into the fluorine-doped tin oxide film. This Section gives details of the conditions used and results of the film analysis to identify the quality of the films and therefore allow an assessment of the potential of the fluorinated organotin carboxylates as single source precursors for the CVD of fluorine-doped tin oxide.

Compounds tested were (**6**) - (**8**), (**10**) and (**12**). This selection contained a variation of R group (Bu, Et and Me), fluorinated chain length (CF_3, C_2F_5 and C_3F_7), and number of fluorine-containing ligands (1 or 2). The effect of each variation could then be explored, hopefully enabling conclusions to be drawn regarding the ideal arrangement for a single source precursor. Due to the lower cost, availability and lower toxicity of the butyltin compounds, varying fluorine groups were investigated on the tributyltin carboxylates, before repeating the optimum arrangement with an alternative R group.

3.6.1 Deposition Conditions

The stainless steel bubbler was loaded with approximately 10 g of precursor, which was found to be a sufficient quantity for several runs. Due to the easier synthesis, the attainment of sufficient quantities of precursor was much improved from the perfluoroalkyltin compounds. More thorough screening could therefore be performed in an effort to identify the optimum set of conditions. Table 3.15 shows the deposition conditions that were used for each precursor.

Table 3.15 Conditions for the CVD of Fluorine-Doped Tin Oxide Using Fluorinated Organotin Carboxylates

PRECURSOR	**(6)**	**(7)**	**(8)**	**(10)**	**(12)**
Reactor Temperature (°C)	564	564	570	541	560
Bubbler Temperature (°C)	110	125	116	150	165
Heater Tapes (°C)	200	200	200	200	250
Diluent Flow ($Lmin^{-1}$)	3.00	3.00	3.00	2.75	2.75
Carrier Flow ($Lmin^{-1}$)	1.0	1.0	1.0	1.0	1.0
Oxygen Flow ($ccmin^{-1}$)	600	600	600	600	600
Run Time (min)	25	25	20	3	1.5

The conditions listed in Table 3.15 were found to produce good coatings of the appropriate thickness. As mentioned in Chapter Two, the appearance of the coating could be used as a good estimate of film thickness. It was often necessary to perform several runs in order to identify a set of conditions which resulted in the characteristic colour, but due to the relatively large quantities of material available, this task was much easier than for the perfluoroalkyltin precursors. All films adhered well to the glass, and could not be removed easily without relatively harsh treatment.

Although all of the triorganotin carboxylates were polymeric crystalline solids with melting points in the range 50-94°C, good volatility was achieved with bubbler temperatures approximately 60°C in excess of the melting points. The high temperature was necessary in order to break up the polymeric structure and achieve sufficient transfer of vaporised material to the reactor. Therefore, although initially unwanted, the polymeric nature of the precursors did not pose a major problem for CVD use as the melting points were not excessive.

The diorganotin carboxylate (**12**) with a melting point of 140°C only required a 25°C increase in bubbler temperature in order to grow a suitable film. This small

temperature rise was due to the sublimation of this compound, so a high rate of transport could easily be accomplished. A higher temperature for the heater tapes was required for this precursor in order to prevent premature sublimation in the pipework. Due to the high melting point of 220°C for the hydrated compound $Me_2Sn(O_2CCF_3)_2(OH_2)$ (**13**), it can be concluded that the CVD was performed on the anhydrous material (**12**) due to the production of a film from a bubbler temperature of 165°C.

Suitable gas flows were found to be fairly universal for all carboxylates tested. Slightly lower diluent flows were used for precursors (**10**) and (**12**), which can be explained by the smaller R groups and hence better mass transport of the material.

The reactor temperatures listed in Table 3.15 were found to produce good transparent films. Lower temperatures significantly decreased growth rates, with powdery deposits obtained at higher temperatures.

Films grown from the tributyltin carboxylates (**6**) - (**8**) were found to favour deposition at the front end of the substrate directly after the inlet, and only coated the first 5-6 cm of the glass. Films derived from the triethyltin carboxylate (**10**) and the dimethyltin carboxylate (**12**) had a much more uniform appearance and spanned the total length of the glass. This can be explained by a weaker tin-carbon bond in the longer hydrocarbon and therefore more rapid decomposition occurring. Also, the mechanism for the loss of the butyl ligands is easier than for the smaller organic groups of ethyl and methyl. Therefore, for a more uniform coating, small R groups appear to be preferential.

Although the melting points of the ethyl and methyltin compounds were higher than the butyltin compounds, the run times for the former were drastically reduced over the latter, which can be explained by a better mass transport of the smaller compounds. A greater concentration of precursors (**10**) and (**12**) was therefore achieved in the vapour phase, and hence the more rapid formation of a film of the appropriate thickness. Therefore, for large scale production where a high growth rate is vital, it would be advantageous to incorporate small R groups into the precursor.

3.6.2 Film Analysis

All coatings produced were subsequently analysed to determine which precursors had been successful in achieving a good fluorine-doped tin oxide film.

3.6.2.1 X-Ray Diffraction

Glancing Angle X-ray diffraction studies were performed to determine if the films were crystalline, and then confirm the film composition as tin oxide. All the samples showed preferred orientation and the diffraction patterns could be compared to standard tin oxide. As mentioned in Chapter Two, it has been shown that SnO_2 films grown along the (200) direction contain less structural defects,[114] so the percentage found with this orientation is calculated. For a random specimen of SnO_2 this ratio would be 7 %. From line broadening measurements of the (110) reflection it was possible to measure the approximate crystallite size of the samples. The X-Ray diffraction data are given in Table 3.16 showing the number of counts for each orientation, and a typical diffraction pattern is shown for $Bu_3SnO_2CC_2F_5$ (7) in Figure 3.16, this being representative of all samples. The top spectrum represents the sample, with the spectrum of standard tin oxide displayed below.

Scanning Electron Microscopy (SEM) was performed on the film deposited from $Bu_3SnO_2CC_2F_5$ (7) to show the surface of the film (Figure 3.17). The photographs clearly show the SiCO undercoat on which the fluorine-doped tin oxide film has subsequently been deposited.

Table 3.16 X-Ray Diffraction Data for the Organotin Carboxylates

PRECURSOR		**(6)**	**(7)**	**(8)**	**(10)**	**(12)**
(hkl)	Angle (°)					
(110)	26.6	513	175	165	145	127
(101)	33.9	221	332	316	302	154
(200)	37.9	673	566	340	254	21
(111)	39.0	0	0	0	0	0
(210)	42.6	27	27	27	28	0
(211)	51.7	457	537	500	481	154
(220)	54.8	98	40	29	31	3
(002)	57.8	0	0	0	0	0
(310)	61.9	109	122	85	75	19
(112)	64.7	0	27	0	0	0
(301)	66.0	82	66	37	28	9
Total Counts		2180	1893	1499	1344	488
(200) (Total as %)		30.9	29.9	22.7	18.9	4.2
Crystallite Size (Å)		320	193	183	151	*

* Could not be calculated

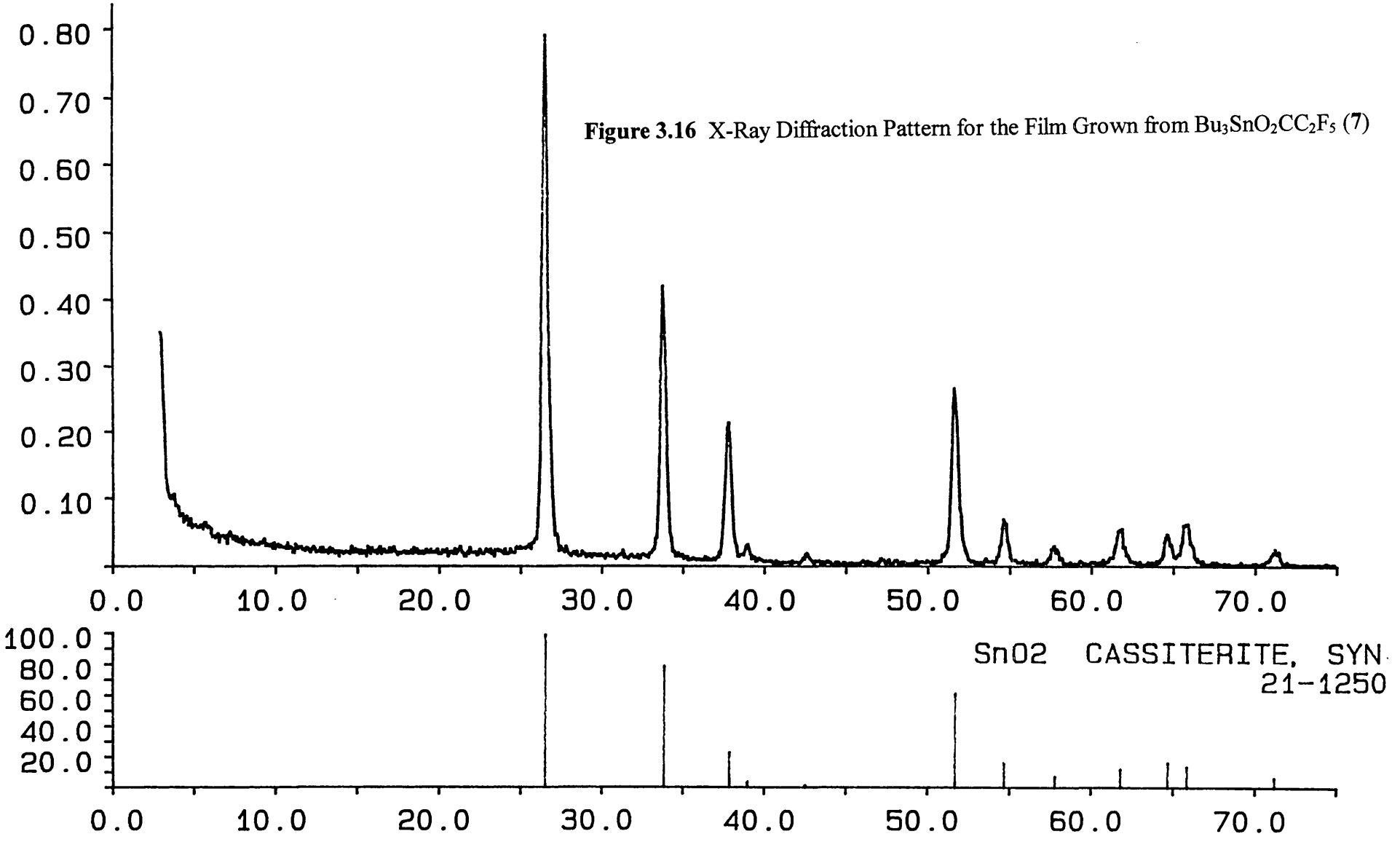

Figure 3.16 X-Ray Diffraction Pattern for the Film Grown from $Bu_3SnO_2CC_2F_5$ (7)

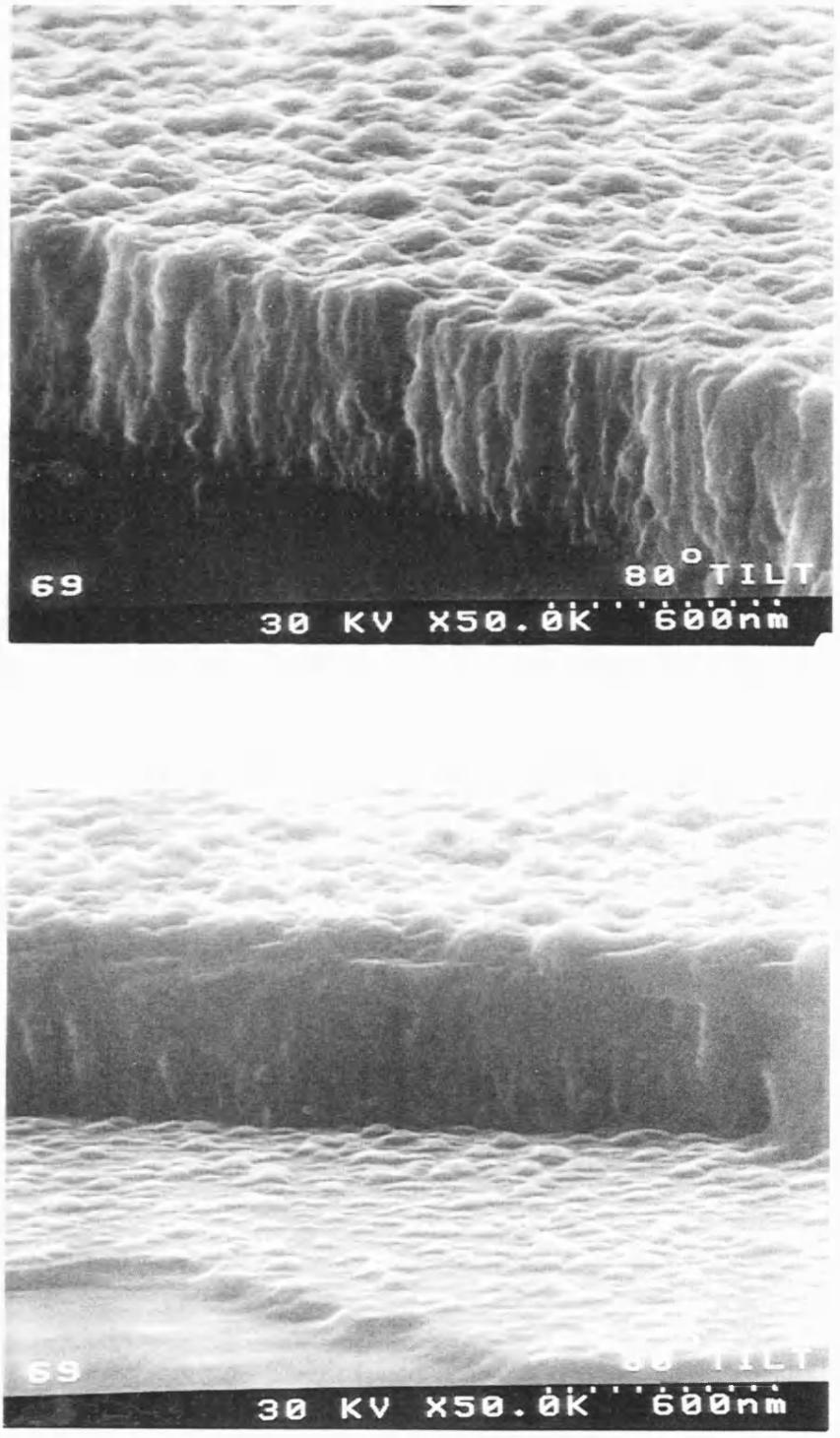

Figure 3.17 Scanning Electron Micrographs of Film Grown from $Bu_3SnO_2CC_2F_5$ (7)

It can be seen that all films provided a diffraction pattern and were therefore crystalline. The peak positions were consistent with those found for standard SnO_2, therefore confirming the expected film composition. For all carboxylates the preferred orientations were shown by the more intense (110), (101), (200) and (211) peaks. The proportions found for the (200) reflection were very high for the triorganotin carboxylates (**6**) - (**8**) and (**10**) and were well in excess of the 7% found for a random specimen of SnO_2, suggesting that the films contained less structural defects. The proportion for the diorganotin carboxylate (**12**) was very low at 4.2% showing that the films grown from the triorganotin derivatives appeared to be structurally favourable.

3.6.2.2 Film Properties

For all films, thickness, haze, emissivity, sheet resistance, resistivity and fluorine content were measured. The results of the analysis are given in Table 3.17.

Table 3.17 Analysis of Fluorine-Doped Tin Oxide Films from the Fluorinated Organotin Carboxylate Precursors

PRECURSOR	**(6)**	**(7)**	**(8)**	**(10)**	**(12)**	**Std[a]**
Thickness (Å)	3600	5150	3000	3470	2935	3000
Haze (%)	0.56	0.99	0.59	0.39	0.28	< 0.40
Emissivity	0.147	0.118	0.175	0.167	0.304	< 0.150
Sheet Resistance (Ω/□)	13	8	18	16	39	15
Resistivity ($\times 10^{-3}$ Ω cm)	0.46	0.43	0.54	0.54	1.13	0.50
Fluorine Content (atom%)	1.02	1.02	0.88	1.16	4.80	2.00

[a] Typical measurements for a good fluorine-doped tin oxide film derived from separate tin and fluorine sources

All precursors produced fluorine-doped tin oxide films showing that the fluorinated organotin carboxylates were capable of acting as single source precursors.

Reasonable success was achieved in trying to obtain films of approximately 3000 Å in thickness, showing that visual inspection of the film could be used as a good estimate of thickness. The thickness fluctuations produced variations in the film analysis as expected, with thicker films producing better emissivity and resistivity measurements, but higher haze. The electrical properties of the film grown from $Bu_3SnO_2CC_2F_5$ (**7**) were very good, which is likely to be due to its much higher thickness.

A significantly higher fluorine content was achieved from the diorganotin carboxylate, but the film properties were not enhanced by this additional dopant concentration. This shows that it was possible to overdope the film, as previously discussed in Chapter One (Section 1.6). The significantly inferior properties for precursor (**12**), especially emissivity and resistivity, could be linked to the X-ray diffraction results, where a very low proportion with the (200) orientation was determined. This could suggest that there were large structural defects in the film which resulted in the poor properties.

Another observation was that an increasing fluorinated chain length did not lead to an increase in the amount of incorporated fluorine into the film. The fluorine content for films grown from precursors (**6**) - (**8**) which contained an increasing number of fluorine atoms, was found to be almost identical, indicating that the fluorine was coming from a key position located on all three precursors. It therefore seems reasonable that the fluorines located on the first fluorinated carbon were the only effective dopants, and additional fluorine-loading did not, in this case, have the effect of increasing the resultant fluorine content of the tin oxide film.

It appears that the triorganotin carboxylates produce a consistent fluorine content of $\approx$ 1 atom%, which suggests a high level of active fluorine as this is a reasonably low dopant concentration for the level of resistivity achieved. From a comparison with a film produced from separate tin and fluorine precursors (Table 3.17, Std), it appears that this level could be close to the optimum as the film properties are very good. A variation in the R group doesn't seem to affect the film properties or amount of fluorine

incorporation enormously, but has quite a significant effect on the film uniformity and growth rate.

Studies have been performed on the thermal decomposition of $Bu_3SnO_2CCF_3$ (**6**) by FTIR in collaboration with P.G Harrison at the University of Nottingham.[218] Although no firm conclusions could be drawn from the investigation, it appears that the most likely decomposition pathway involves a radical reaction, with two mechanisms suggested (Scheme 3.2).

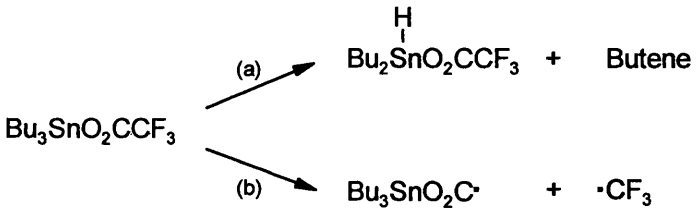

Scheme 3.2 Possible Decomposition Pathways for $Bu_3SnO_2CCF_3$ (**6**)

For the first possibility (a), the first step would be loss of butene to give the tin hydride. Loss of the hydrogen radical and abstraction of the CF_3 group of another molecule by this hydrogen radical would follow. Alternatively for mechanism (b), fission of the CF_3 group to yield a CF_3 radical which could abstract a hydrogen atom from a butyl group is equally likely. However, it should be noted that the reactor conditions (560°C) are completely different to those of a FTIR study (≈ 250°C), so decomposition pathways could vary considerably in each environment.

In conclusion, the films produced from the fluorinated triorganotin carboxylates were of a very high quality, with properties equalling those derived from separate tin and fluorine sources. Films grown from precursors (**6**), (**7**) and (**10**) were particularly encouraging, indicating that this group of compounds has a large potential for use as single source precursors for the CVD of fluorine-doped tin oxide. Overall, the triorganotin carboxylates were a much better group of precursors than the previous perfluoroalkyltin compounds due to easier synthetic routes, cheaper starting materials

and the production of better fluorine-doped tin oxide films. Therefore, the triorganotin carboxylates were extremely successful, from both synthetic and CVD points of view.

As there was a large difference in the quality of the films grown from each set of precursors it seems likely that the organotin carboxylates did not undergo a decarboxylation process as first envisaged. A R_3SnR' species was therefore unlikely to have been a dominant intermediate from which further decomposition occurred. If this decomposition pathway had been followed, similar properties could have been expected from the analysis of films derived from each set of precursor.

The harsh reactor conditions of $\approx$ 560°C would be likely to dictate the overall decomposition pathway followed. For example, although decarboxylation can occur at low temperatures of around 100-200°C, R groups will be largely unaffected at this temperature and the decomposition pathway would proceed via this route. However, at the elevated temperature of 560°C present in the CVD reactor, the R groups become vulnerable and decomposition mechanisms such as loss of butene become feasible. Such products could subsequently influence the overall decomposition mechanism followed. Therefore, the CVD process is extremely complicated due to the large number of possible decomposition mechanisms available at high temperature.

From the results obtained from the CVD of the fluorinated organotin carboxylates, it appears that to achieve a film with a high growth rate, good uniformity and a good overall set of properties, the precursor should be a triorganotin derivative with small R groups. Although organotin compounds containing smaller R groups such as ethyl are more expensive and have a higher level of toxicity, the benefits of low deposition times and superior film uniformity are very worthwhile.

3.7 EXPERIMENTAL

3.7.1 Preparation of Tributyltin Trifluoroacetate - $Bu_3SnO_2CCF_3$ (6)

Sodium trifluoroacetate (5.06 g, 37 mmol) in ethanol (100 ml) was added to a solution of tributyltin chloride (12.08 g, 37 mmol) in ethanol (75 ml). The mixture was refluxed for two hours before removing the solvent *in vacuo* to yield a white solid. This was recrystallised from 40° - 60° petroleum ether to yield white needles. The product was then dried under vacuum to give tributyltin trifluoroacetate (8.69 g, 58%), m.p. 49-52°C.

Analysis : Found (calc. for $C_{14}H_{27}F_3O_2Sn$) : C 41.8 (41.7)%; H 6.99 (6.77)%.

Mössbauer data ($mm\ s^{-1}$) : IS = 1.51; QS = 4.06.

^{119}Sn nmr [δ(ppm), $CDCl_3$ soln] : 172.3.

^1H nmr [δ(ppm), $CDCl_3$ soln] : 0.92 [9H, t, $CH_3(CH_2)_3$], $^3J(^1H\text{-}^1H)$ = 7 Hz; 1.38 [12H, m, C_4H_9]; 1.64 [6H, m, C_4H_9].

^{13}C nmr [δ(ppm), $CDCl_3$ soln] : 13.5 [$CH_3(CH_2)_3$]; 17.3 [$CH_3(CH_2)_2CH_2$]; 26.9 [$CH_3CH_2(CH_2)_2$]; 27.5 [$CH_3CH_2CH_2CH_2$]. $^1J(^{13}C\text{-}^{119}Sn)$ = 334 Hz. C-F carbon not observed.

IR data (NaCl plates, nujol mull, cm^{-1}) : 1721, 1678 [$\nu_a(CO_2^-)$], 1586, 1447 [$\nu_s(CO_2^-)$], 1206, 1160, 849, 793, 700, 675, 604.

3.7.2 Preparation of Tributyltin Pentafluoropropionate - $Bu_3SnO_2CC_2F_5$ (7)

The synthetic method described above for (**6**) was repeated using sodium pentafluoropropionate (6.16 g, 35 mmol) and tributyltin chloride (11.26 g, 35 mmol).

White needles of tributyltin pentafluoropropionate (9.07 g, 60%), m.p. 64-66°C were obtained.

Analysis : Found (calc. for $C_{15}H_{27}F_5O_2Sn$): C 40.0 (39.8)%; H 6.35 (6.02)%.

Mössbauer data (mm s^{-1}) : IS = 1.52; QS = 4.12.

^{119}Sn nmr [δ(ppm), $CDCl_3$ soln] : 174.5.

^{1}H nmr [δ(ppm), $CDCl_3$ soln] : 0.92 [9H, t, $CH_3(CH_2)_3$], $^3J(^1H\text{-}^1H)$ = 7 Hz; 1.37 [12H, m, C_4H_9]; 1.64 [6H, m, C_4H_9].

^{13}C nmr [δ(ppm), $CDCl_3$ soln] : 13.6 [$CH_3(CH_2)_3$]; 17.4 [$CH_3(CH_2)_2CH_2$]; 26.9 [$CH_3CH_2(CH_2)_2$]; 27.5 [$CH_3CH_2CH_2CH_2$]. $^1J(^{13}C\text{-}^{119}Sn)$ = 332 Hz. C-F carbons not observed.

IR data (NaCl plates, nujol mull, cm^{-1}) : 1678 [$\nu_a(CO_2^-)$], 1424 [$\nu_s(CO_2^-)$], 1329, 1292, 1221, 1169, 1078, 1034, 963, 880, 824, 702, 675.

3.7.3 Preparation of Tributyltin Heptafluorobutyrate - $Bu_3SnO_2CC_3F_7$ (**8**)

Sodium heptafluorobutyrate (9.38 g, 40 mmol) and tributyltin chloride (12.95 g, 40 mmol) were used in the methodology described for (**6**) to produce crystals of tributyltin heptafluorobutyrate (11.00 g, 55%), m.p. 58°C.

Analysis : Found (calc. for $C_{16}H_{27}F_7O_2Sn$) : C 38.2 (38.2)%; H 5.59 (5.42)%.

Mössbauer data (mm s^{-1}) : IS = 1.52; QS = 4.05.

^{119}Sn nmr [δ(ppm), $CDCl_3$ soln] : 175.1.

^{1}H nmr [δ(ppm), $CDCl_3$ soln] : 0.92 [9H, t, $CH_3(CH_2)_3$], $^{3}J(^{1}H\text{-}^{1}H)$ = 7 Hz; 1.36 [12H, m, C_4H_9]; 1.65 [6H, m, C_4H_9].

^{13}C nmr [δ(ppm), $CDCl_3$ soln]: 13.5 [$CH_3(CH_2)_3$]; 17.4 [$CH_3(CH_2)_2CH_2$]; 26.9 [$CH_3CH_2(CH_2)_2$]; 27.4 [$CH_3CH_2CH_2CH_2$]. $^{1}J(^{13}C\text{-}^{119}Sn)$ = 336 Hz. C-F carbons not observed.

IR data (NaCl plates, nujol mull, cm^{-1}) : 1678 [$\nu_a(CO_2^-)$], 1418 [$\nu_s(CO_2^-)$], 1275, 1190, 1086, 968, 934, 816, 673.

3.7.4 Preparation of Triethyltin Trifluoroacetate - $Et_3SnO_2CCF_3$ (9)

The method previously used to synthesise (**6**) was utilised. Sodium trifluoroacetate (1.36 g, 10 mmol) and triethyltin chloride (2.41 g, 10 mmol) were reacted to produce white crystals of triethyltin trifluoroacetate (0.72 g, 23%), m.p. 119°C.

Analysis : Found (calc. for $C_8H_{15}F_3O_2Sn$) : C 30.2 (30.1)%; H 4.82 (4.75)%.

Mössbauer data ($mm\ s^{-1}$) : IS = 1.53; QS = 4.17.

^{119}Sn nmr [δ(ppm), $CDCl_3$ soln] : 164.7.

^{1}H nmr [δ(ppm), $CDCl_3$ soln] : 1.34 [15H, m, C_2H_5].

^{13}C nmr [δ(ppm), $CDCl_3$ soln] : 8.88 [CH_3CH_2]; 9.54 [CH_3CH_2]. $^{1}J(^{13}C\text{-}^{119}Sn)$ = 322 Hz. C-F carbon not observed.

IR data (NaCl plates, nujol mull, cm^{-1}) : 1680, 1653 [$\nu_a(CO_2^-)$], 1590, 1456 [$\nu_s(CO_2^-)$], 1196, 1150, 1019, 959, 851, 795, 679.

3.7.5 Preparation of Triethyltin Pentafluoropropionate - $Et_3SnO_2CC_2F_5$ (10)

Sodium pentafluoropropionate (10.26 g, 55 mmol) and triethyltin chloride (13.36 g, 55 mmol) were used in the methodology described for (**6**) to form triethyltin pentafluoropropionate (9.08 g, 45%), m.p. 94°C as a crystalline material.

Analysis : Found (calc. for $C_9H_{15}F_5O_2Sn$) : C 29.3 (29.3)%; H 4.12 (4.10)%.

Mössbauer data (mm s^{-1}) : IS = 1.54; QS = 4.12.

^{119}Sn nmr [δ(ppm), $CDCl_3$ soln] : 160.5.

^{1}H nmr [δ(ppm), $CDCl_3$ soln] : 1.33 [15H, m, C_2H_5].

^{13}C nmr [δ(ppm), $CDCl_3$ soln] : 8.89 [CH_3CH_2]; 9.45 [CH_3CH_2]. $^{1}J(^{13}C\text{-}^{119}Sn)$ = 326 Hz. C-F carbons not observed.

IR data (NaCl plates, nujol mull, cm^{-1}) : 1659 [$\nu_a(CO_2^-)$], 1462 [$\nu_s(CO_2^-)$], 1426, 1335, 1219, 1171, 1038, 1017, 957, 826, 677.

3.7.6 Preparation of Tributyltin Pentadecafluorooctanoate - $Bu_3SnO_2CC_7F_{15}$ (11)

Pentadecafluorooctanoic acid (1.77 g, 4 mmol) in toluene (100 ml) was added to bis(tributyltin) oxide (1.19 g, 2 mmol) and the mixture refluxed for two hours. The water formed was azeotropically removed using a Dean and Stark apparatus. The solvent was removed *in vacuo* to leave the title compound as an oily semi-solid material (1.02 g, 36%).

Analysis : Found (calc. for $C_{20}H_{27}F_{15}O_2Sn$) : C 33.9 (34.2)%; H 3.88 (3.87)%.

Mössbauer data (mm s^{-1}) : IS = 1.53; QS = 4.07.

^{119}Sn nmr [δ(ppm), $CDCl_3$ soln] : 167.2.

^{1}H nmr [δ(ppm), $CDCl_3$ soln] : 0.92 [9H, t, $CH_3(CH_2)_3$], $^{3}J(^{1}H\text{-}^{1}H)$ = 7 Hz; 1.38 [12H, m, C_4H_9]; 1.65 [6H, m, C_4H_9].

^{13}C nmr [δ(ppm), $CDCl_3$ soln] : 13.4 [$CH_3(CH_2)_3$]; 17.5 [$CH_3(CH_2)_2CH_2$]; 26.9 [$CH_3CH_2(CH_2)_2$]; 27.5 [$CH_3CH_2CH_2CH_2$]. $^{1}J(^{13}C\text{-}^{119}Sn)$ = 343 Hz. C-F carbons not observed.

IR data (NaCl plates, nujol mull, cm^{-1}) : 1688 [$\nu_a(CO_2^-)$], 1466 [$\nu_s(CO_2^-)$], 1362, 1242, 1140, 1106, 1020, 667.

3.7.7 Preparation of Dimethyltin Bis-(trifluoroacetate) - $Me_2Sn(O_2CCF_3)_2$ (12)

1M sodium hydroxide was added to dimethyltin dichloride (25.00 g, 110 mmol) in distilled water (100 ml) until pH 9 was achieved, quantitatively precipitating dimethyltin oxide. The oxide was collected by filtration, washed several times with distilled water, then dried in an oven overnight.

Dimethyltin oxide (6.00 g, 36 mmol) and a large excess of trifluoroacetic anhydride (20.00 ml, 140 mmol) were refluxed for three hours, then the excess anhydride distilled off under a nitrogen atmosphere to leave a white solid. This solid was subsequently sublimed under reduced pressure to yield the product as a white crystalline material (11.10 g, 82%), sublimation temp. 80°C/1.5mm, m.p. 140°C.

Analysis : Found (calc. for $C_6H_6F_6O_4Sn$) : C 19.1 (19.2)%; H 1.63 (1.62)%.

Mössbauer data ($mm\ s^{-1}$) : IS = 1.47; QS = 4.36.

3.7.8 Preparation of Dimethyltin Bis-(trifluoroacetate) Monohydrate - $Me_2Sn(O_2CCF_3)_2(OH_2)$ (13)

The title compound was obtained following recrystallisation of (**12**) from chloroform, m.p. 220°C.

Analysis : Found (calc. for $C_6H_8F_6O_5Sn$) : C 18.3 (18.3)%; H 2.07 (2.06)%.

Mössbauer data (mm s^{-1}) : IS = 1.30; QS = 3.85.

^{119}Sn nmr [δ(ppm), $CDCl_3$ soln] : -139.4; -138.6.

^{1}H nmr [δ(ppm), $CDCl_3$ soln] : 1.25 [s, $(CH_3)_2Sn$]; $^{2}J(^{1}H\text{-}^{119}Sn)$ = 81 Hz.

^{13}C nmr [δ(ppm), $CDCl_3$ soln] : 5.8 [$(CH_3)_2Sn$]; 116.5 [$Sn(O_2CCF_3)_2$]; 163.0 [$Sn(O_2CCF_3)_2$].

^{19}F nmr [δ(ppm), $CDCl_3$ soln] : -75.6 [$Sn(O_2CCF_3)_2$].

IR data (NaCl plates, nujol mull, cm^{-1}) : 3386, 1671 [$\nu_a(CO_2^-)$], 1453 [$\nu_s(CO_2^-)$], 1202, 1146, 855, 789.

Chapter Four

Organotin Alkoxides

4.1 INTRODUCTION

Alkoxides are an important class of compound for this study because they have a major use as precursors to oxide films. There are several books[283] and reviews[284-285] available which describe the entire field of alkoxide chemistry.

For the production of tin oxide films, tin alkoxides have been utilised in the hope that the metal-oxygen bond in the precursor will be maintained during processing. This strategy has been successful, both for CVD[16] and sol-gel techniques.[95-98,286] In general, metal alkoxides are much more commonly used for sol-gel processing due to their facile hydrolysis to produce the metal oxide. They have been utilised to good effect in the production of tin oxide films, and their diversity is illustrated by their ability to deposit more complex materials such as hybrid inorganic-organic materials[287] and heterometallic oxides.[288]

Fluorocarbon derivatives of metal alkoxides are attractive precursors for CVD processing because of their volatility which is generally greater than that of their hydrocarbon analogues. This increased volatility may be due to intermolecular repulsions between the many fluorine lone pairs, or alternatively, the low polarisability of the fluorine may reduce the van der Waals attractive forces. The electron withdrawing fluorinated groups also lower the basicity of the alkoxide oxygens which reduces their tendency to polymerise. The enhanced volatility achieved by the fluorinated component has been shown by a variety of fluorinated derivatives, for example, in sodium and thallium fluoroalkoxide compounds.[289] Studies have also been performed on sodium and zirconium fluoroalkoxides in an attempt to correlate the enhanced volatility with structure.[290]

Although the attractive property of enhanced volatility can be achieved by the incorporation of fluorine into the alkoxide precursor, it has also been found to cause fluorine incorporation into the resultant oxide film, often an undesired effect. This is due to the short M···F contacts which can be present in fluorinated alkoxide arrangements.

Fluorine incorporation can be obtained from compounds even if there is a considerable distance between the metal and the fluorine in the precursor. This effect is highlighted by certain sodium and zirconium fluoroalkoxides in which the fluorine is positioned four bonds away (Figure 4.1).

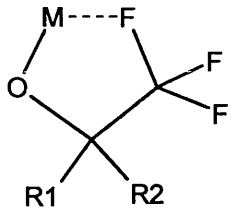

Figure 4.1 Metal-Fluorine Association in Alkoxides

Using such compounds, metal fluoride and not oxide films were unexpectedly obtained, with NaF and ZrF_4 films deposited respectively.[291]

Therefore, although fluorine transfer has been unwelcome in some cases, this phenomenon is extremely encouraging for this study. The fluorinated organotin alkoxides could consequently be a very attractive group of precursor due to the enhanced volatility and good chance of fluorine incorporation into the film.

4.1.1 Advantages and Disadvantages

There are a number of advantages for organotin alkoxides as single source precursors for the CVD of fluorine-doped tin oxide.

(i) *Fluorine incorporation is known to occur in certain instances from the use of fluoroalkoxides as CVD precursors.*
(ii) *They should have a good level of volatility.*
(iii) *They are likely to be liquids.*

There are, however, a number of disadvantages for this class of precursor.

(i) *Organotin alkoxides are sensitive to moisture and carbon dioxide, therefore creating some handling difficulties.*

(ii) *There is a restricted choice of possible starting materials, therefore limiting the composition of the resultant alkoxides.*

The main reason for choosing organotin fluoroalkoxides as the next group of precursors was due their known viability as CVD precursors for the production of tin oxide films, and the good chance of fluorine incorporation due to the observation of metal fluoride films from the CVD of other metallic fluoroalkoxides.

This chapter will briefly describe the structural chemistry and various synthetic routes currently known for this class of compound. The introduction will be followed by details of the synthesis, characterisation and CVD testing of a series of novel organotin fluoroalkoxides produced for this thesis. Throughout this chapter the carbon adjacent to the oxygen atom will be referred to as the β-position and the second carbon the γ-position with respect to the tin.

4.2 STRUCTURAL CHEMISTRY

There are a wide variety of organotin(IV) alkoxides known, a reasonable number of which are solid compounds, although the majority are liquids.[292] The structural change exhibited by the organotin alkoxides in the series $R_nSn(OR')_{4-n}$ can be exemplified by the butyltin derivatives for which ^{119}Sn NMR data can be used to decipher the structure adopted in solution.[137] Tributyltin alkoxides Bu_3SnOR' are all liquids and are believed to exist as tetrahedral monomers at room temperature, while dibutyltin dialkoxides $Bu_2Sn(OR')_2$ are monomeric when a sterically bulky group such as ^tBu prevents dimerisation. Butyltin trialkoxides $BuSn(OR')_3$ are probably six coordinate with octahedral geometry with small R′ groups, but monomeric if sterically bulky groups are involved, for example $BuSn(O^tBu)_3$.

Relatively few tin alkoxide crystal structures have appeared in the literature, and usually consist of compounds containing four tin-oxygen bonds. An example is given by $Sn(O^tBu)_4$ which displays tetrahedral geometry (Figure 4.2).[293]

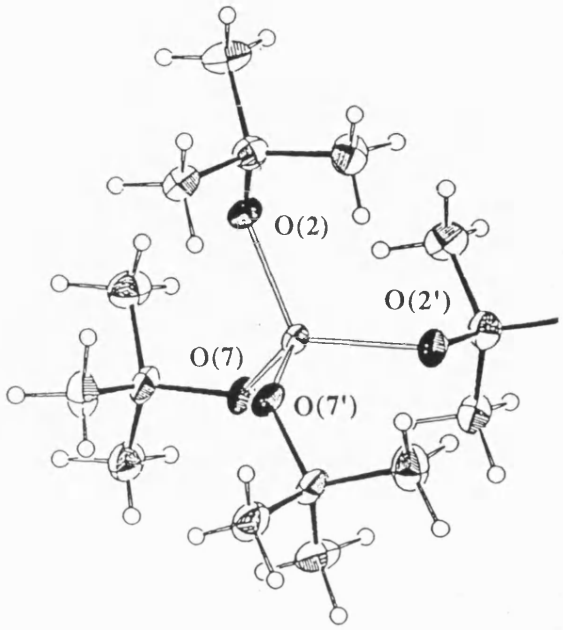

Figure 4.2 Molecular Structure of $Sn(O^tBu)_4$[293]

A very different structure has been determined for the corresponding tetraisopropoxide derivative. The crystal structure is found to contain a coordinated alcohol molecule which leads to the formation of a dimer $[Sn(O^iPr)_4 \cdot HO^iPr]_2$.[293] The structure can be described as distorted edge-shared, bi-octahedral containing two doubly bridged isopropoxide ligands, with four terminal alkoxide ligands (two bonded to each tin) in the same plane and four other ligands perpendicular to this plane (two on each metal) that are involved in hydrogen bonding. The two isopropoxide ligands and two coordinated isopropanol ligands that are involved in hydrogen bonding create a significant deviation from octahedral geometry about tin (Figure 4.3).

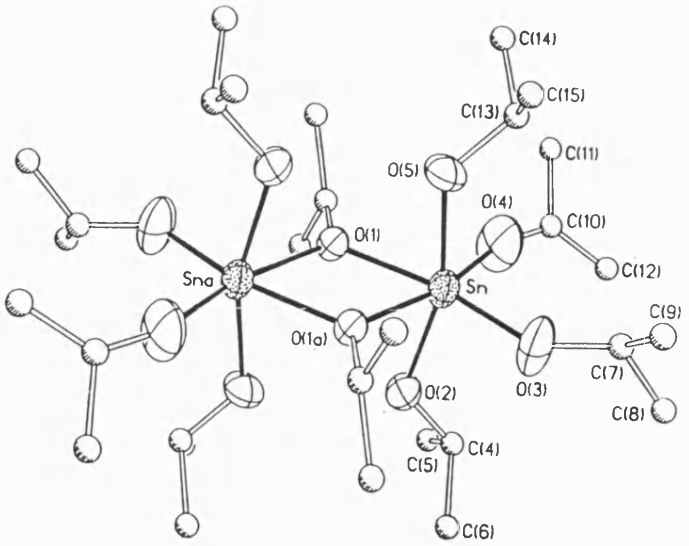

Figure 4.3 Molecular Structure of $[Sn(O^iPr)_4 \cdot HO^iPr]_2$[293]

A dimeric structure has also been found for $^iPrSn(O^iPr)_3$ in the solid state due to association.[294] The structure contains a four-membered Sn-O framework with distorted trigonal bipyramidal geometry about the tin (Figure 4.4).

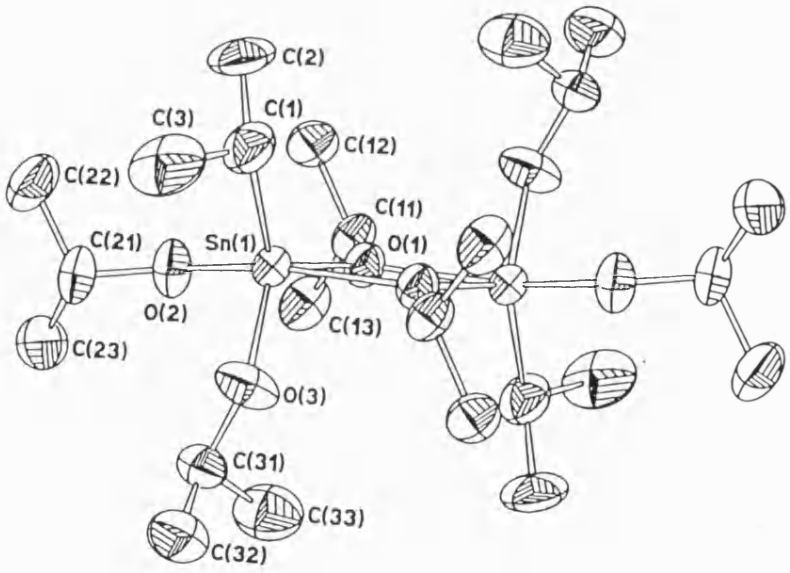

Figure 4.4 Molecular Structure of $^iPrSn(O^iPr)_3$[294]

Another example of a tin fluoroalkoxide containing four tin-oxygen bonds is given by $Sn[OCH(CF_3)_2]_4(HNMe_2)_2$ which is a volatile solid and its use as a CVD precursor has previously been discussed (Chapter One, Section 1.6).[116] This molecule is shown to have octahedral geometry with *trans*-amine ligands (Figure 4.5).

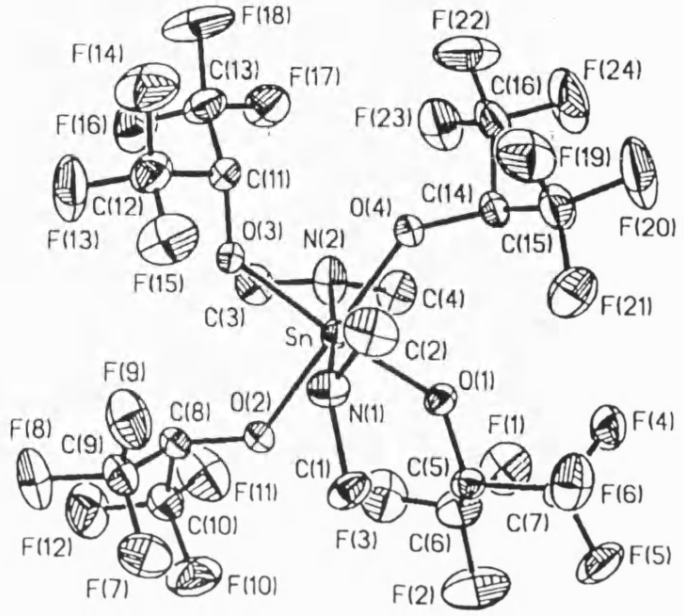

Figure 4.5 Molecular Structure of $Sn[OCH(CF_3)_2]_4(HNMe_2)_2$[116]

An example of a compound containing one Sn-O bond is given by $[Me_3SnOC(CF_3)_2]_2C_6F_4$ which contains the expected four coordinate tin.[192] However, the structure contains highly flattened Me-Sn-Me bond angles, resulting in appreciable deviation from ideal tetrahedral geometry (Figure 4.6). The Sn(1)-O(1)-C(4) angle is quite large at 138.4° and the trimethyltin groups are bent away from the two trifluoromethyl groups in order to minimise electronic/steric repulsions. There are two Sn-F intramolecular contacts per tin atom which result from a fluorine atom of one of the propylidine CF_3 groups Sn(1)-F(51) and from one of the aromatic fluorine atoms Sn(1)-F(9). The CF_3 group not involved with intramolecular bonding plays an important role in forming intermolecular Sn-F contacts Sn(1)-F(62). The geometry about the tin can be described as pseudo trigonal bipyramidal.

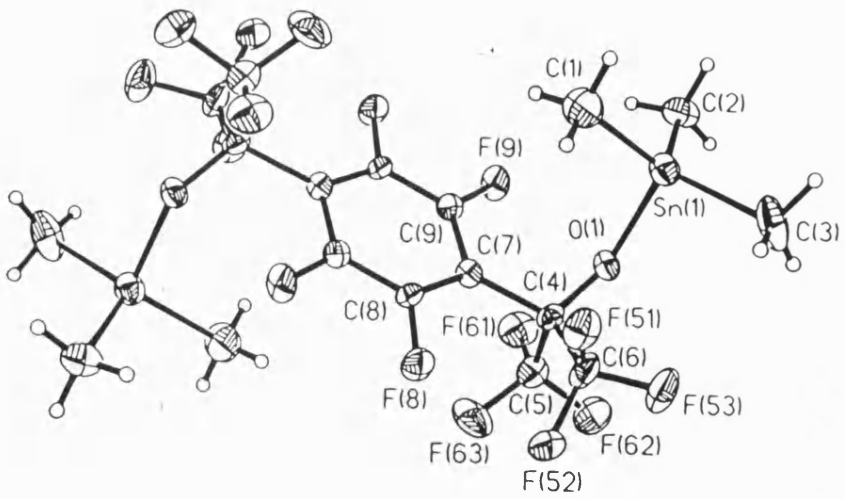

Figure 4.6 Molecular Structure of $[Me_3SnOC(CF_3)_2]_2C_6H_4$[192]

4.3 SYNTHETIC ROUTES

There are a number of relatively simple methods available for the synthesis of organotin alkoxides.[295] The best established method is that in which an organotin chloride is treated with the appropriate sodium alkoxide, usually in the parent alcohol or ether as the solvent. The sodium chloride which is formed is filtered or centrifuged off, and the alkoxide is recovered by distillation or recrystallisation. The filtration must be carried out in the absence of air due to the sensitivity of the alkoxides to moisture and carbon dioxide which can sometimes create difficulties as the sodium chloride can be finely divided. This method can be used for the preparation of organotin trialkoxides $RSn(OR')_3$,[296] diorganotin dialkoxides $R_2Sn(OR')_2$[292] and triorganotin alkoxides R_3SnOR'[292] (Equations 4.1 - 4.3).

$$3NaOR' + RSnCl_3 \xrightarrow{\text{benzene}} RSn(OR')_3 + 3NaCl \qquad [4.1]$$

$$2NaOR' + R_2SnCl_2 \xrightarrow[\text{or } Et_2O]{R'OH} R_2Sn(OR')_2 + 2NaCl \qquad [4.2]$$

$$NaOR' + R_3SnCl \xrightarrow[\text{or } Et_2O]{R'OH} R_3SnOR' + NaCl \qquad [4.3]$$

A more convenient route to the trialkyltin alkoxides which avoids a difficult filtration is the azeotropic dehydration of a mixture of the appropriate alcohol and the corresponding bis(trialkyltin) oxide in benzene or toluene.[295] This route is only available for alcohols with a boiling point in excess of approximately 90°C.

$$2R'OH + (R_3Sn)_2O \xrightarrow{\text{toluene}} 2R_3SnOR' + H_2O \qquad [4.4]$$

If the alcohol is more volatile, the dialkyl carbonate can be used instead.[295]

$$(R'O)_2CO + (R_3Sn)_2O \longrightarrow R_3SnOR' + R_3SnOCO_2R' \xrightarrow{-CO_2} 2R_3SnOR' \qquad [4.5]$$

The reactions shown by Equations 4.4 and 4.5 are most effective for the preparation of trialkyltin alkoxides.

A good method for the preparation of cyclic alkoxides is the reaction between alkyltin hydrides and unsaturated alcohols to give the alkoxides and molecular hydrogen.[297]

$$R_2SnH_2 + CH_2{=}CHCH_2OH \longrightarrow \text{ 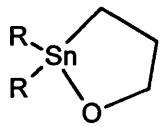 } + H_2 \qquad [4.6]$$

Organotin alkoxides can also be formed by the addition of the Sn-H bond or activated Sn-C, Sn-O or Sn-N bonds to the carbonyl groups of aldehydes and ketones. The Sn-H additions can be catalysed by azobis-isobutyronitrile (AIBN) or by $ZnCl_2$, involving attack at oxygen by a radical or an electrophilic tin species, respectively. An example of such a reaction is given in Equation 4.7.

$$Et_3SnH + Me_2CHCHO \xrightarrow{\text{AIBN}} Et_3SnOCH_2CHMe_2 \qquad [4.7]$$

Another route to the organotin trialkoxides involves the alcoholysis of the appropriate alkyltin tris(diethylamide) which is rapid and exothermic at room temperature.[298]

$$RSn(NEt_2)_3 + 3R'OH \longrightarrow RSn(OR')_3 + 3Et_2NH \qquad [4.8]$$

4.4 RESULTS AND DISCUSSION

4.4.1 Synthesis

A series of organotin alkoxides have been prepared with a variation in the fluorinated component, which has enabled the effect of different fluorine arrangements to be explored. All alkoxides synthesised were triorganotin derivatives with butyl as the organic group, Bu_3SnOR', which was due to the cheap availability and lower degree of toxicity of the butyltin starting materials. As determined by the results of the CVD analysis of the perfluoroalkyltin compounds and organotin carboxylates in Chapters Two and Three respectively, the choice of R group had been found to have little effect on the properties of the fluorine-doped tin oxide film deposited. Therefore, the effect of the fluorinated component could be determined with butyl groups as the R groups, before exploring the effect on film uniformity and growth rates with alternative R groups, if sufficiently encouraging film properties were achieved. It would also appear from results quoted earlier (Chapters Two and Three) that a triorganotin compound containing one fluorinated ligand would be the best formulation as superior results had already been achieved from precursors containing this arrangement.

Two methods were utilised for the preparation of the tributyltin alkoxides which both used fluoroalcohols as the fluorine containing source. The method chosen was dependent on the boiling point of the fluoroalcohols. With lower boiling alcohols the common method of using the sodium alkoxide to react with the organotin chloride was utilised. The appropriate sodium alkoxide was formed by reaction of the fluorinated

alcohol with sodium hydride, then subsequent reaction with tributyltin chloride yielded the target tributyltin fluoroalkoxide. An excess of the sodium alkoxide was required to ensure complete reaction, and prevent contamination of the product with unreacted tributyltin chloride. Separation of this mixture would have been difficult due to similar boiling points for the two tributyltin compounds. Diethyl ether was used as the solvent to prevent unnecessary wastage of the sometimes expensive fluoroalcohols.

$$NaH + R'OH \xrightarrow{Et_2O} R'ONa + H_2 \qquad [4.9]$$

$$R'ONa + Bu_3SnCl \xrightarrow{Et_2O} Bu_3SnOR' + NaCl \qquad [4.10]$$

R' = $CH(CF_3)_2$ (**14**), CH_2CF_3 (**15**), $CH_2C_2F_5$ (**16**)

This method was extremely successful, and, following distillation under reduced pressure, all compounds were produced as colourless liquids in a very high yield (75-93%). Care had to be taken to carry out all manipulations in a nitrogen atmosphere due to the slight moisture sensitivity of the alkoxide products. Minor difficulties were encountered during the filtration of the liberated sodium chloride due to the very fine nature of the precipitate, however successful separation could be achieved with a canula filter.

For alcohols with boiling points in excess of 90°C, the alternative method of reacting the fluorinated alcohol with bis(tributyltin) oxide was utilised. The reaction was carried out in toluene and the water formed removed azeotropically using a Dean and Stark separator.

$$(Bu_3Sn)_2O + 2R'OH \xrightarrow{toluene} 2Bu_3SnOR' + H_2O \qquad [4.11]$$

R' = $CH_2(CF_2)_3CF_2H$ (**17**), CH_2CH_2F (**18**)

This method was also very successful and avoided the need for an awkward filtration. Following distillation under reduced pressure, colourless liquids were obtained in yields of 69-79%.

The composition of the fluorinated tributyltin alkoxides was restricted by the choice of fluorinated alcohols commercially available. There were no alcohols with fluorine atoms on the carbon atom adjacent to the oxygen, therefore alkoxides containing fluorines in the β-position could not be prepared. The composition of the fluorinated alkoxides may therefore not have been ideal as precursors for the CVD of fluorine-doped tin oxide if the β-fluoride elimination is indeed an important process.

4.4.2 Mössbauer Spectroscopy

All compounds were studied as frozen liquids at 78K, data are given in Table 4.1.

Table 4.1 Mössbauer Data for the Fluorinated Organotin Alkoxides

COMPOUND		**Isomer Shift** δ **(mm s^{-1})**	**Quadrupole Splitting** ΔE_Q **(mm s^{-1})**
$Bu_3SnOCH(CF_3)_2$	**(14)**	1.36	2.81
$Bu_3SnOCH_2CF_3$	**(15)**	1.34	2.56
$Bu_3SnOCH_2C_2F_5$	**(16)**	1.30	2.52
$Bu_3SnOCH_2(CF_2)_3CF_2H$	**(17)**	1.34	2.54
$Bu_3SnOCH_2CH_2F$	**(18)**	1.28	2.38

All of the observed isomer shifts are consistent with organotin(IV) compounds as expected. The values obtained for the quadrupole splitting parameter do not provide a conclusive determination of the structure adopted by the fluorinated tributyltin alkoxides in the solid state. This is due to the similarity in the observed quadrupole splitting range for the two possibilities of tetrahedral (1.00 - 2.40 mm s^{-1}) and *cis*-trigonal bipyramidal

(1.70 - 2.40 mm s^{-1}) geometries. Tetrahedral compounds Bu_3SnOR' (**XVIII**) would arise from the existence of monomeric entities, with a *cis*-trigonal bipyramidal arrangement $Bu_3Sn(OR')_2$ (**XIX**) caused by the association of monomeric units to form a dimeric structure.

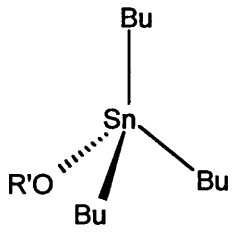

(**XVIII**)

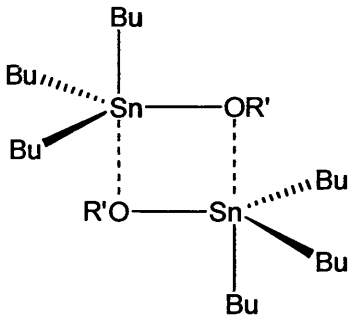

(**XIX**)

The observation of relatively high quadrupole splitting values which exceed 2.40 mm s^{-1} can be explained by the influence of the electronegative fluorine atoms which cause additional asymmetry of the electronic field gradient around the tin. The effect of the fluorines present on the first fluorinated carbon atom is clearly demonstrated by the series of compounds synthesised for this thesis. For example, $Bu_3SnOCH(CF_3)_2$ (**14**) which contains the largest number of fluorines in this position exhibits a very high value of 2.81 mm s^{-1}. At the other end of the scale, $Bu_3SnOCH_2CH_2F$ (**18**) with a single fluorine atom in the same location has the lowest value of 2.38 mm s^{-1}. It can also be observed that the series of compounds (**15**) - (**17**) have very similar values for the quadrupole splitting parameter which can be explained by the presence of two fluorines on the first fluorinated carbon in all three compounds.

The values determined for the alkoxides synthesised are consistent with reported values for other non-fluorinated tributyltin alkoxides.[299] For example, the value for Bu_3SnOEt is quoted as 2.11 mm s^{-1}, and the higher values found for the fluorinated compounds prepared for this study can be explained by the influence of the electronegative fluorinated ligand.

High quadrupole splitting values in the range 2.81 - 3.09 mm s^{-1} have been reported for trialkyltin methoxides and phenoxides which are markedly higher than would be expected for tetrahedral monomers in the solid state.[299] Therefore, the significantly lower values found for the fluorinated alkoxides in this study suggests that they are more likely to adopt this latter geometry in the solid state, and dimerisation appears unlikely.

4.4.3 NMR Spectroscopy

For all compounds synthesised, ^{1}H, ^{13}C, ^{19}F and ^{119}Sn NMR spectroscopy studies were performed.

4.4.3.1 ^{1}H, ^{13}C and ^{19}F NMR Spectroscopy

Expected results were observed in the proton and carbon-13 NMR studies, with resonances due to the butyl groups displayed clearly. Both spectra showed diagnostic chemical shifts for the butyl groups, with predicted integration and multiplicities evident in the proton spectra. Characteristic coupling between hydrogen and fluorine atoms could also clearly be seen in the proton NMR spectra. The one bond tin-carbon coupling constants $^{1}J(^{13}C\text{-}^{119}Sn)$ could be extracted from the carbon-13 spectra, and are shown in Table 4.2.

Table 4.2 $^{1}J(^{13}C\text{-}^{119}Sn)$ Coupling Constants for the Fluorinated Organotin Alkoxides

COMPOUND		**$^{1}J(^{13}C\text{-}^{119}Sn)$ (Hz)**
$Bu_3SnOCH(CF_3)_2$	**(14)**	364
$Bu_3SnOCH_2CF_3$	**(15)**	358
$Bu_3SnOCH_2C_2F_5$	**(16)**	358
$Bu_3SnOCH_2(CF_2)_3CF_2H$	**(17)**	357
$Bu_3SnOCH_2CH_2F$	**(18)**	347

The magnitudes of the coupling constants for all compounds are in the appropriate region for four-coordinate tributyltin species, which are usually found in the range 327-387 Hz.[216] Very similar values were obtained for compounds **(15)** - **(17)** which all possess fully fluorinated arrangements in the γ-position. A slightly higher value was observed for $Bu_3SnOCH(CF_3)_2$ **(14)** which can be explained by the presence of an additional CF_3 group in the γ-position which leads to a slightly higher covalent character of the Sn-Bu bond and hence a stronger demand for 5*s*(Sn) character. Similarly, a slightly lower coupling constant is observed for $Bu_3SnOCH_2CH_2F$ **(18)** due to the presence of only one electronegative fluorine atom in this location.

The fluorine-19 NMR spectra displayed clear resonances for all the fluorine atoms contained on the alkoxide ligands, and confirmed the presence of the appropriate ligand.

4.4.3.2 ^{119}Sn NMR Spectroscopy

The ^{119}Sn NMR studies provided information regarding the environment around the tin atom. This analytical technique was found to be an extremely useful tool to ensure the absence of any unreacted tributyltin chloride [$\delta(^{119}Sn)$ = 156 ppm] in the isolated product. All fluorinated tributyltin alkoxides were run as solutions in deuterated chloroform and all gave one signal showing that each compound had been produced cleanly. Data are shown in Table 4.3.

Table 4.3 ^{119}Sn NMR Data for the Fluorinated Organotin Alkoxides

COMPOUND		Chemical Shift (ppm)
$Bu_3SnOCH(CF_3)_2$	**(14)**	151.9
$Bu_3SnOCH_2CF_3$	**(15)**	133.7
$Bu_3SnOCH_2C_2F_5$	**(16)**	132.4
$Bu_3SnOCH_2(CF_2)_3CF_2H$	**(17)**	133.9
$Bu_3SnOCH_2CH_2F$	**(18)**	114.2

A similar pattern was shown by the ^{119}Sn chemical shifts to that which had previously been observed for the Mössbauer and $^1J(^{13}C\text{-}^{119}Sn)$ coupling constant data. Again, the highest value was shown for $Bu_3SnOCH(CF_3)_2$ **(14)** and the lowest for $Bu_3SnOCH_2CH_2F$ **(18)** with little deviation observed for the series **(15)** - **(17)**.

Certain organotin alkoxides are known to undergo association in solution resulting in the formation of dimeric arrangements (**XIX**). All fluorinated tributyltin alkoxides displayed large positive chemical shifts which indicates tetrahedral monomers in solution, which is consistent with the information gained from the $^1J(^{13}C\text{-}^{119}Sn)$ coupling constants. Dimerisation would be indicated by a chemical shift much further upfield. For example, monomeric $Bu_2Sn(O^tBu)_2$ displays a ^{119}Sn chemical shift at -34 ppm, with an upfield shift at -165 ppm observed for dimeric $Bu_2Sn(OMe)_2$.[137]

In general, the dimeric arrangement is more commonly found for compounds containing relatively small ligands, with sterically bulky alkoxide groups preventing the formation of this structure. The larger downfield shift observed for $Bu_3SnOCH(CF_3)_2$ **(14)** suggests a lower degree of association for this branched compound which is unsurprising due to the higher steric bulk of the alkoxide ligand. Also, the electron withdrawing effect of the fluorinated alkoxide ligands would be expected to lower the basicity of the alkoxide oxygens which reduces the probability of bridging. The

observation of the largest downfield shift for $Bu_3SnOCH(CF_3)_2$ (**14**) which contains the most electronegative ligand is consistent with this hypothesis.

The large positive values obtained for the fluorinated tributyltin alkoxides are consistent with previously reported values for unfluorinated triorganotin alkoxides. For example, a ^{119}Sn chemical shift of +129 ppm has been found for Me_3SnOMe which is four-coordinate in solution.[300]

4.5 CVD TESTING OF PRECURSORS

All compounds (**14**) - (**18**) were subsequently tested as CVD precursors, with details of the apparatus provided in Appendix Five. Care had to be taken during the loading of the precursors into the bubbler assembly due to the moisture sensitivity of the materials. In all cases, the substrate used was 4 mm glass which had been undercoated with a thin film of SiCO to act as a "blocking layer" to prevent sodium diffusion into the fluorine-doped tin oxide film. This section gives details of the CVD conditions used and results of the film analysis to identify the quality of the films, and therefore allow an assessment of the potential of the fluorinated organotin alkoxides as single source precursors for the CVD of fluorine-doped tin oxide.

4.5.1 Deposition Conditions

All precursors were tested with oxygen gas present in the reactor. To see if a tin oxide film could be produced by maintaining the oxygen present in the alkoxide precursor, one compound (**18**) was tested with no oxygen gas in the reactor. Table 4.4 shows the deposition conditions that were used for each precursor.

Table 4.4 Conditions for the CVD of Fluorine-Doped Tin Oxide Using Fluorinated Organotin Alkoxides

PRECURSOR	**(14)**	**(15)**	**(16)**	**(17)**	**(18)**	**(18)**[a]
Reactor Temperature (°C)	554	554	554	544	554	467
Bubbler Temperature (°C)	98	111	112	106	128	128
Heater Tapes (°C)	200	200	200	200	200	200
Diluent Flow ($Lmin^{-1}$)	2.75	2.75	2.75	2.75	2.75	2.75
Carrier Flow ($Lmin^{-1}$)	1.0	1.2	1.0	1.0	1.2	1.2
Oxygen Flow ($ccmin^{-1}$)	600	600	600	600	600	0
Run Time (min)	25	30	30	20	20	35

[a] No oxygen used during deposition.

As for the perfluoroalkyltin compounds and the organotin carboxylates, attempts were made to deposit a film of approximately 3000 Å in thickness. Several runs were performed to try to obtain a film exhibiting the characteristic purple/green fringe which was indicative of the required thickness. However, although several attempts were made and long run times used as shown in Table 4.4, this target could not always be achieved.

The reactor temperatures listed in Table 4.4 were found to produce good transparent films for all precursors when oxygen gas was present in the reactor. All films were found to adhere well to the glass substrate, and could not be removed without relatively harsh treatment.

However, the film that had been deposited with no oxygen gas present during the deposition process was extremely powdery and could easily be wiped from the glass. Although a large variety of conditions were tried in an attempt to obtain a hard, transparent coating, only powdery deposits could be achieved. A lower reactor temperature was found to produce a slight improvement in the film quality, but it was

concluded that oxygen gas was essential in the production of a hard transparent tin oxide film.

As all compounds were liquids, it was hoped that low bubbler temperatures would be sufficient to achieve a good transport of material in the vapour phase. However, as found with the perfluoroalkyltin compounds, reasonably high temperatures were again required, suggesting that the alkoxides were not remarkably volatile. It was generally found that a slightly lower temperature was required for precursors containing more fluorine atoms. For example, $Bu_3SnOCH(CF_3)_2$ (**14**) required a bubbler temperature of 98°C, while $Bu_3SnOCH_2CH_2F$ (**18**) was found to require a much higher bubbler temperature of 128°C. This demonstrates a higher volatility for compounds with increasing fluorine incorporation which is due to weaker intermolecular interactions caused by the minimising of dipole-dipole interactions between molecules.

As all precursors were liquids, heater tapes could be maintained at 200°C as there were no problems with possible condensation of precursors within the pipework. Suitable gas flows were also found to be fairly universal for all precursors.

Very long run times were required, which was expected as all precursors contained butyl groups bonded to tin. As found from the perfluoroalkyltin compounds and the organotin carboxylates in Chapters Two and Three respectively, the incorporation of smaller R groups into the precursor leads to vastly diminished run times, so it can quite safely be assumed that this would also be the case for the alkoxides. The long run times for the tributyltin alkoxides can be explained by a slow mass transport of material and hence a low concentration of precursor in the vapour phase during deposition.

As found with the two previous classes of compound in which butyl was used as the R group, the tributyltin alkoxides were found to favour deposition at the front end of the substrate directly after the inlet, and only coated the first 5 - 6 cm of the glass. Rapid decomposition occurred due to a weak tin-carbon bond and a facile β-hydride elimination mechanism for this group. It could be suggested that improved film

uniformity would arise from the incorporation of smaller R groups into the precursor, as previously found for the perfluoroalkyltin compounds and the fluorinated organotin carboxylates.

4.5.2 Film Analysis

All coatings produced were subsequently analysed to determine which precursors had been successful in achieving a good fluorine-doped tin oxide film.

4.5.2.1 X-Ray Diffraction

Glancing Angle X-Ray diffraction studies were performed to determine if the films were crystalline, and then confirm the film composition as tin oxide. All the samples showed preferred orientation and were compared to a standard sample of SnO_2. As previously mentioned in Chapter Two, SnO_2 films grown along the (200) direction are believed to contain less structural defects and therefore exhibit better properties.[114]

As a means of expressing the degree of orientation, the peak counts of each SnO_2 reflection were summed and a ratio of the peak counts of the (200) reflection to the summed total expressed as a percentage. It should be noted that for a random specimen of SnO_2 the value of this ratio would be 7%. From line broadening measurements of the (110) reflection it was possible to measure the approximate crystallite size of the samples. A representative crystallite size of 132 Å was measured for the film deposited from $Bu_3SnOCH(CF_3)_2$ (**14**). The X-Ray diffraction data are given in Table 4.5 showing the number of counts for each orientation, and a diffraction pattern for $Bu_3SnOCH(CF_3)_2$ (**14**) illustrated in Figure 4.7. The top spectrum represents the sample (**14**), with the spectrum of standard tin oxide displayed below.

Scanning Electron Microscopy (SEM) was performed to show the surface of the film deposited from $Bu_3SnOCH(CF_3)_2$ (**14**) (Figure 4.8). The photographs clearly show the SiCO undercoat and the crystalline SnO_2 film which has subsequently been deposited.

Table 4.5 X-Ray Diffraction Data for the Fluorinated Organotin Alkoxides[a]

PRECURSOR		**(14)**	**(15)**	**(17)**	**(18)**
(hkl)	Angle (°)				
(110)	26.6	174	71	75	886
(101)	33.9	233	32	24	16
(200)	37.9	328	18	11	73
(111)	39.0	0	0	0	0
(210)	42.6	0	0	0	7
(211)	51.7	390	51	43	208
(220)	54.8	33	0	3	50
(002)	57.8	0	0	0	0
(310)	61.9	92	7	0	50
(112)	64.7	0	0	0	0
(301)	66.0	36	3	3	24
Total Counts		1285	182	159	1313
(200) (Total as %)		25.5	9.9	6.7	5.5

[a] **(16)** = Amorphous

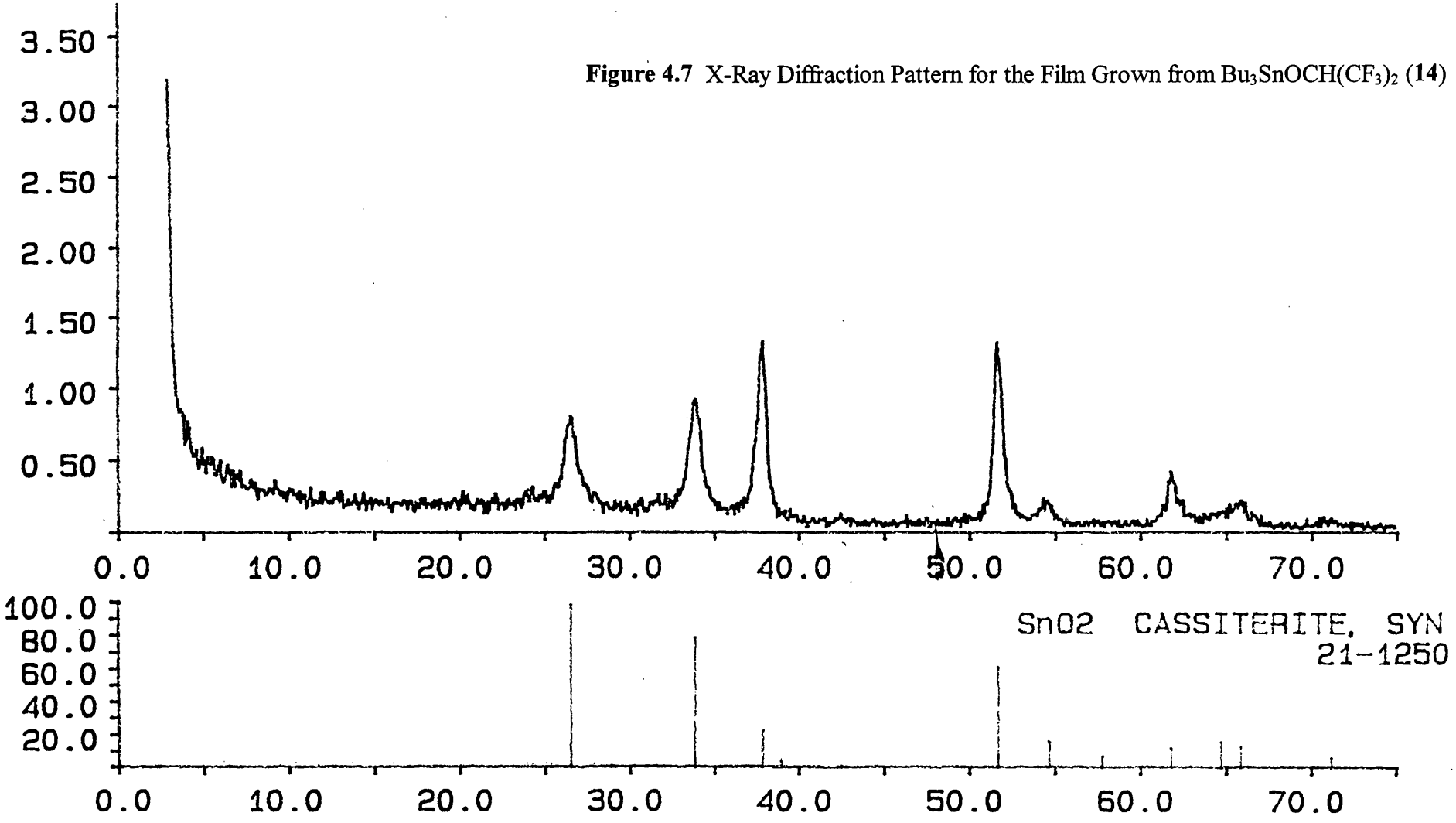

Figure 4.7 X-Ray Diffraction Pattern for the Film Grown from $Bu_3SnOCH(CF_3)_2$ (**14**)

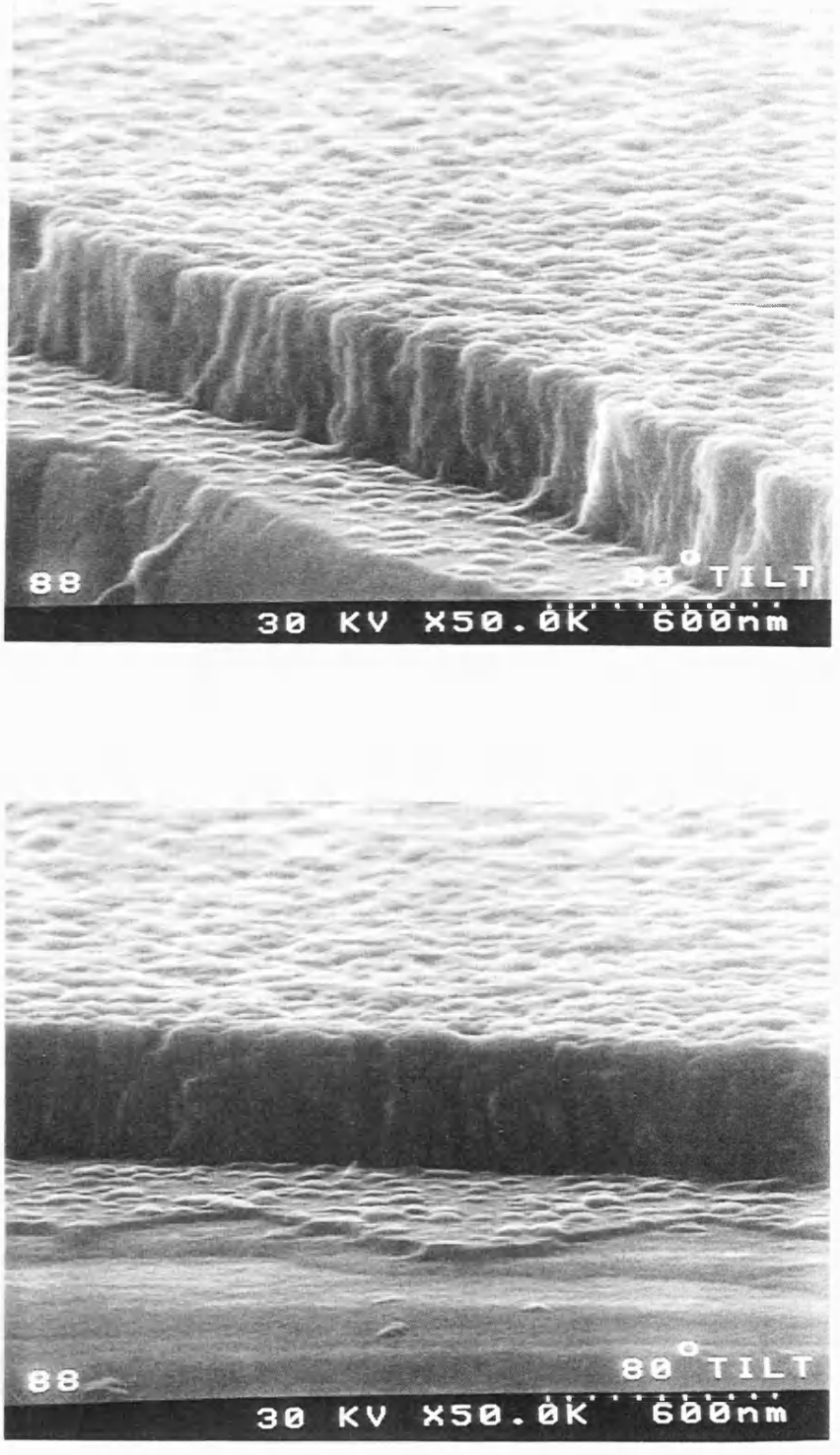

Figure 4.8 Scanning Electron Micrographs of the Film from $Bu_3SnOCH(CF_3)_2$ **(14)**

It can be seen that the films deposited from precursors (**14**), (**15**), (**17**) and (**18**) provided a diffraction pattern and were therefore crystalline. The peak positions were consistent with those found for standard tin oxide, therefore confirming the expected film composition. Due to the low counts generally found, preferred orientations were difficult to determine, but were generally found to be the (110), (101), (200) and (211) planes. Only the film grown from precursor (**14**) was found to contain a proportion for the (200) reflection of over 7% and was found to contain a very high proportion of 25.5% which suggests few structural defects. The films deposited from the other precursors contained a very small percentage of counts from the (200) plane which indicates the presence of large structural defects in the films. The film grown from precursor (**16**) did not produce a diffraction pattern and was therefore of an amorphous nature.

4.5.2.2 Film Properties

For all films deposited in the presence of oxygen gas, thickness, haze, emissivity, sheet resistance, resistivity and fluorine content were measured. The results of the analysis are given in Table 4.6.

Table 4.6 Analysis of Fluorine-Doped Tin Oxide Films from Fluorinated Organotin Alkoxide Precursors

PRECURSOR	**(14)**	**(15)**	**(16)**	**(17)**	**(18)**	**Std.**[a]
Thickness (Å)	3750	1815	1460	2910	2410	3000
Haze (%)	0.74	0.54	0.27	0.61	0.42	< 0.40
Emissivity	0.278	0.813	0.829	0.889	0.358	< 0.150
Sheet Resistance (Ω/□)	38	915	1035	220	54	15
Resistivity ($\times 10^{-3}$ Ω cm)	1.42	16.60	15.13	6.40	1.30	0.50
Fluorine Content (atom%)	0.64	0.10	< 0.03	0.14	1.52	2.00

[a] Typical measurements for a good fluorine-doped tin oxide film derived from separate tin and fluorine sources.

It can be seen that films of the required 3000 Å were not achieved for precursors (**15**) and (**16**). Despite the reasonable quantities of around 10 g of each precursor, high bubbler temperatures and long run times, the films were rather thin. However, following analysis of the two films in question it can clearly be seen that the film properties are very poor with extremely high emissivity and resistivity measurements. The fluorine contents of both films are very low which explains the poor properties and also the difficulty in obtaining a good quality X-ray diffraction pattern. The fluorine content of < 0.03% determined for the film grown from precursor (**16**) shows that this compound in particular did not perform as a single source precursor for the CVD of fluorine-doped tin oxide. Following the disappointing results from precursors (**15**) and (**16**) it was thought unnecessary to perform additional runs in an attempt to attain films of the desired thickness.

An unusual pattern can be observed from the fluorine contents determined for the films. It can be seen that precursors (**15**), (**16**) and (**17**) achieved very little fluorine incorporation and hence extremely poor film properties. The arrangements of the fluorinated alkoxide ligands are very similar in these three precursors with a linear chain containing an increasing number of fluorine atoms in the fashion CF_3 (**15**), C_2F_5 (**16**) and $(CF_2)_3CF_2H$ (**17**) respectively. The common feature of the three compounds is the $Bu_3SnOCH_2CF_2$ segment, and it can be concluded that the presence of additional fluorine in the ligand did not have a positive effect on the amount of resultant fluorine deposited in the doped tin oxide film.

To explain the very low fluorine incorporation into the films, it seems likely that the decomposition pathway involved the loss of the fluorinated ligand in such a way as to prevent effective fluorine transfer to the tin during the CVD process. There are two feasible explanations for this. One explanation could be that the electron withdrawing effect of the fluorinated alkoxide ligands caused a weakening of the Sn-O bond. This could therefore have influenced the breaking of this bond and a resultant decomposition pathway which prevented the desired Sn/F association. Such a process is shown in Scheme 4.1.

$$Bu_3SnOR' \xrightarrow{\text{- butene}} HSnOR' \xrightarrow{O_2} SnO_2 + HOR'$$

Scheme 4.1 Possible Decomposition Pathway for the Fluorinated Tributyltin Alkoxides

The second explanation for the low fluorine incorporation could be that a β-hydride elimination was more favourable than a γ-fluoride elimination which resulted in hydrogen incorporation instead of the desired fluorine transfer (Figure 4.9).

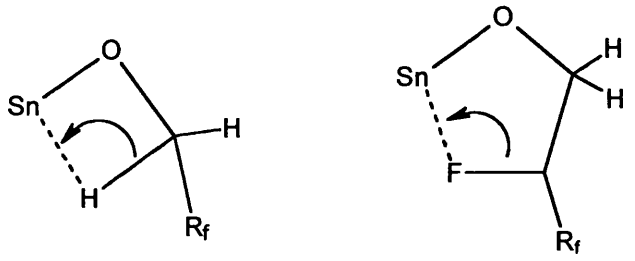

(a) β-Hydride (b) γ-Fluoride

Figure 4.9 β-Hydride and γ-Fluoride Eliminations

A β-hydride elimination would explain the low fluorine levels determined for precursors (**15**) - (**17**) which all contained β-hydrogens and γ-fluorines. If this was indeed the case, this suggests that the presence of hydrogens on the first carbon atom is significant and fluorines would be required in this location in order to achieve fluorine transfer to the tin during the CVD process. Therefore, the presence of fluorine atoms in this position would be expected to give the corresponding β-fluoride elimination and the target fluorine-doped tin oxide film. However, the synthesis of such compounds would be extremely difficult due to the absence of commercially available fluorinated alcohols with fluorines in the desired location.

A higher fluorine content of 0.64 atom% was achieved from $Bu_3SnOCH(CF_3)_2$ (**14**) which resulted in much improved film properties, although they were still considerably poorer than those found for the standard film deposited by the dual source method. It therefore seems possible that a different mechanism was in operation for this branched precursor, as some fluorine incorporation was achieved. The presence of only

one hydrogen atom on the first carbon could have been significant, and it could be possible that this resulted in less hydrogen incorporation into the film than occurred for precursors (**15**) - (**17**). The branched fluorine arrangement appeared to be a more favourable configuration than the linear fluorinated alkoxide ligands present in precursors (**15**) - (**17**).

A very interesting observation can be made from the fluorine content determined for the film deposited from $Bu_3SnOCH_2CH_2F$ (**18**), in which 1.52 atom% was measured. This increased fluorine content resulted in improved film properties as expected, although they were still inferior to the properties of the standard film grown from the dual source precursors. However, the film derived from precursor (**18**) was relatively thin at 2410 Å and a thicker film would be expected to exhibit improved properties which may be close to the standard.

From the large difference in the fluorine contents found for the films deposited from $Bu_3SnOCH_2CF_3$ (**15**) and $Bu_3SnOCH_2CH_2F$ (**18**), it seems extremely likely that a different decomposition mechanism was in operation for the two precursors. It appears that the presence of three fluorine atoms on the fluorinated alkoxide ligand actually had a detrimental effect on the mechanism of fluorine transfer to the tin during the CVD process. To achieve a reasonably high fluorine content of 1.52 atom%, it seems that the single fluorine atom in precursor (**18**) was in an effective location for transfer. It therefore seems that the decomposition mechanism for precursor (**15**) involved the production of a stable species containing the CF_3 moiety which was lost from the reactor without any fluorine transfer occurring. Fluorine transfer from precursor (**18**) appears to be a more favourable process so it seems likely that the two precursors generate different decomposition products. The enhanced electronegativity of the CF_3 group on precursor (**15**) over CH_2F present on precursor (**18**) could have promoted a weaker Sn-O bond which resulted in the breaking of this bond as previously discussed (Scheme 4.1).

From the results obtained from the perfluoroalkyltin compounds and the fluorinated organotin carboxylates in Chapters Two and Three respectively, it had been found that better film uniformity and vastly decreased run times could be accomplished

from precursors containing small R groups such as ethyl and methyl. However, the use of such constituents had been found to have little effect on the resultant film properties exhibited. Therefore, following the disappointing film analyses obtained from the fluorinated tributyltin alkoxides, it was deemed unnecessary to try any compounds containing the smaller R groups.

In conclusion, the films produced from the organotin alkoxides were very disappointing, with generally very little fluorine incorporation achieved. Modest results were obtained from only one compound, $Bu_3SnOCH_2CH_2F$ (**18**) which suggests that fewer fluorine atoms in these precursors is a more favourable arrangement. It appears that the presence of hydrogen atoms on the first carbon could be significant as the majority of the precursors with this arrangement achieved very little fluorine incorporation into the film. Consequently, the replacement of the hydrogen atoms with fluorines could be effective, although synthesis of such compounds would be very difficult.

There are two compounds which would be interesting for this study. The first is $R_3SnOC(CF_3)_3$ because it contains no β-hydrogens, therefore eliminating the possibility of a β-hydride elimination resulting in preferential hydrogen transfer. However, the fluorinated alcohol which would be required as the starting material is available at a very high cost which would make the production of a sufficient quantity for CVD testing very expensive. The second compound which would be interesting is $Sn(OR_f)_4$ as there are no R groups present which could influence the overall decomposition pathway followed. However, the synthesis of such compounds is difficult due to the extreme air sensitivity of compounds containing four alkoxide ligands and the difficulty in the isolation of a pure product. Therefore, the two possible mechanisms which are thought to be responsible for the low fluorine incorporation in the films grown in this study could be investigated by the testing of such compounds as those described above. However, the synthesis and handling of such derivatives is met with a certain degree of difficulty.

Therefore, despite the observation of effective fluorine transfer from other metallic fluoroalkoxides, this did not appear to be the case for the equivalent organotin

compounds. Overall, the fluorinated organotin alkoxides do not appear to be a good group of single source precursors for the CVD of fluorine-doped tin oxide.

4.6 EXPERIMENTAL

4.6.1 Preparation of Tributyltin Hexafluoroisopropoxide - $Bu_3SnOCH(CF_3)_2$ (14)

Sodium hydride (1.00 g, 42 mmol) was suspended in dry ether (60 ml), and hexafluoroisopropyl alcohol (3.67 g, 22 mmol) added dropwise. After gas evolution had ceased the solution was stirred for a further 30 mins and the excess sodium hydride separated by a canula transfer of the soluble material to a clean vessel in the strict absence of air. Tributyltin chloride (7.08 g, 22 mmol) was then added dropwise to the filtrate and a white precipitate rapidly formed. The mixture was subsequently refluxed for one hour, cooled and the soluble material separated by a second canula transfer. The solvent was removed *in vacuo* and the residue distilled under reduced pressure to yield the product as a colourless oil (7.70 g, 93%), b.p. 105°C/1.0 mm.

Analysis : Found (calc. for $C_{15}H_{28}F_6OSn$) : C 39.7 (39.4)%; H 6.30 (6.45)%.

Mössbauer data ($mm\ s^{-1}$) : IS = 1.36; QS = 2.81.

^{119}Sn nmr [δ(ppm), $CDCl_3$ soln] : 151.9.

^1H nmr [δ(ppm), $CDCl_3$ soln] : 0.92 [9H, t, $CH_3(CH_2)_3$], $^3J(^1H\text{-}^1H)$ = 7 Hz; 1.26 [6H, m, C_4H_9]; 1.34 [6H, m, C_4H_9]; 1.58 [6H, m, C_4H_9]; 4.40 [1H, sept, $Bu_3SnOCH(CF_3)_2$], $^3J(^1H\text{-}^{19}F)$ = 6 Hz.

^{13}C nmr [δ(ppm), $CDCl_3$ soln] : 13.5 [$CH_3(CH_2)_3$]; 15.8 [$CH_3(CH_2)_2CH_2$]; 27.0 [$CH_3CH_2(CH_2)_2$]; 27.4 [$CH_3CH_2CH_2CH_2$]. $^1J(^{13}C\text{-}^{119}Sn)$ = 364 Hz. C-F carbons not observed.

IR data (NaCl plates, liquid film, cm^{-1}) : 1466, 1418, 1370, 1289, 1186, 1098, 1078, 891, 858, 747, 687, 666.

4.6.2 Preparation of Tributyltin Trifluoroethoxide - $Bu_3SnOCH_2CF_3$ (15)

The same method as for (**14**) was used. Sodium hydride (2.40 g, 100 mmol) and trifluoroethanol (7.00 g, 70 mmol) were reacted together, followed by the addition of tributyltin chloride (11.50g, 35 mmol). The product was isolated as a colourless oil (9.50 g, 81%), b.p. 100°C/1.0 mm.

Analysis : Found (calc. for $C_{14}H_{29}F_3OSn$) : C 44.0 (43.2)%; H 7.83 (7.53)%.

Mössbauer data ($mm\ s^{-1}$) : IS = 1.34; QS = 2.56.

^{119}Sn nmr [δ(ppm), $CDCl_3$ soln] : 133.7.

^1H nmr [δ(ppm), $CDCl_3$ soln] : 0.92 [9H, t, $CH_3(CH_2)_3$], $^3J(^1H\text{-}^1H)$ = 7 Hz; 1.19 [6H, m, C_4H_9]; 1.36 [6H, m, C_4H_9]; 1.61 [6H, m, C_4H_9]; 4.01 [2H, q, CH_2CF_3], $^3J(^1H\text{-}^{19}F)$ = 9 Hz.

^{13}C nmr [δ(ppm), $CDCl_3$ soln] : 13.6 [$CH_3(CH_2)_3$]; 15.2 [$CH_3(CH_2)_2CH_2$]; 27.2 [$CH_3CH_2(CH_2)_2$]; 27.8 [$CH_3CH_2CH_2CH_2$]; 64.4 [CH_2CF_3]. $^1J(^{13}C\text{-}^{119}Sn)$ = 358 Hz. C-F carbon not observed.

^{19}F nmr [δ(ppm), $CDCl_3$ soln] : -77.7 [t, CH_2CF_3], $^3J(^{19}F\text{-}^1H)$ = 9 Hz.

4.6.3 Preparation of Tributyltin Pentafluoropropoxide - $Bu_3SnOCH_2C_2F_5$ (16)

This was prepared as for (**14**) using sodium hydride (1.64 g, 70 mmol) and pentafluoro-1-propanol (5.13 g, 34 mmol). The sodium alkoxide was subsequently reacted with tributyltin chloride (10.20 g, 31 mmol) and the product isolated by

distillation under reduced pressure to yield a colourless oil (10.20 g, 75%), b.p. 102°C/1.0 mm.

Analysis : Found (calc. for $C_{15}H_{29}F_5OSn$) : C 41.9 (41.0)%; H 7.27 (6.67)%.

Mössbauer data (mm s^{-1}) : IS = 1.30; QS = 2.52.

^{119}Sn nmr [δ(ppm), $CDCl_3$ soln] : 132.4.

^{1}H nmr [δ(ppm), $CDCl_3$ soln] : 0.92 [9H, t, $CH_3(CH_2)_3$], $^3J(^1H\text{-}^1H)$ = 7 Hz; 1.18 [6H, m, C_4H_9]; 1.33 [6H, m, C_4H_9]; 1.60 [6H, m, C_4H_9]; 4.10 [2H, t, $CH_2CF_2CF_3$], $^3J(^1H\text{-}^{19}F)$ = 14 Hz.

^{13}C nmr [δ(ppm), $CDCl_3$ soln] : 13.6 [$CH_3(CH_2)_3$]; 15.2 [$CH_3(CH_2)_2CH_2$]; 27.2 [$CH_3CH_2(CH_2)_2$]; 27.8 [$CH_3CH_2CH_2CH_2$]; 63.8 [$CH_2C_2F_5$]. $^1J(^{13}C\text{-}^{119}Sn)$ = 358 Hz. C-F carbons not observed.

^{19}F nmr [δ(ppm), $CDCl_3$ soln] : -126.4 [m, $CH_2CF_2CF_3$], $^3J(^{19}F\text{-}^1H)$ = 14 Hz; -83.7 [m, $CH_2CF_2CF_3$].

4.6.4 Preparation of Tributyltin Octafluoropentoxide - $Bu_3SnOCH_2(CF_2)_3CF_2H$ (17)

Bis(tributyltin) oxide (11.44 g, 19 mmol) and a slight excess of octafluoro-1-pentanol (10.00 g, 43 mmol) were dissolved in dry toluene (100 ml) and refluxed for two hours. The water formed was removed azeotropically using a Dean and Stark apparatus. The toluene was then removed *in vacuo* to yield a yellow oil which was distilled under reduced pressure to give the product as a colourless oil (13.70 g, 69%), b.p. 130°/1.0 mm.

Analysis : Found (calc. for $C_{17}H_{30}F_8OSn$) : C 39.4 (39.2)%; H 5.94 (5.81)%.

Mössbauer data (mm s^{-1}) : IS = 1.34; QS = 2.54.

^{119}Sn nmr [δ(ppm), $CDCl_3$ soln] : 133.9.

^{1}H nmr [δ(ppm), $CDCl_3$ soln] : 0.92 [9H, t, $CH_3(CH_2)_3$], $^{3}J(^{1}H\text{-}^{1}H)$ = 7 Hz; 1.19 [6H, m, C_4H_9]; 1.35 [6H, m, C_4H_9]; 1.60 [6H, m, C_4H_9]; 4.12 [2H, t, $CH_2(CF_2)_3CF_2H$], $^{3}J(^{1}H\text{-}^{19}F)$ = 9 Hz; 6.14 [1H, tt, $CH_2(CF_2)_3CF_2H$], $^{2}J(^{1}H\text{-}^{19}F)$ = 52 Hz, $^{3}J(^{1}H\text{-}^{19}F)$ = 6 Hz.

^{13}C nmr [δ(ppm), $CDCl_3$ soln] : 13.5 [$CH_3(CH_2)_3$]; 15.0 [$CH_3(CH_2)_2CH_2$], $^{1}J(^{13}C\text{-}^{119}Sn)$ = 357 Hz; 27.1 [$CH_3CH_2(CH_2)_2$]; 27.7 [$CH_3CH_2CH_2CH_2$]; 63.6 [t, $CH_2(CF_2)_3CF_2H$], $^{2}J(^{13}C\text{-}^{19}F)$ = 24 Hz; 107.8 [tt, $CH_2CF_2(CF_2)_3H$]; $^{2}J(^{13}C\text{-}^{19}F)$ = 254 Hz, $^{3}J(^{13}C\text{-}^{19}F)$ = 30 Hz; 110.3 [m, $CH_2CF_2CF_2(CF_2)_2H$]; 111.3 [m, $CH_2(CF_2)_2CF_2CF_2H$]; 116.7 [tt, $CH_2(CF_2)_3CF_2H$], $^{2}J(^{13}C\text{-}^{19}F)$ = 254 Hz, $^{3}J(^{13}C\text{-}^{19}F)$ = 30 Hz.

^{19}F nmr [δ(ppm), $CDCl_3$ soln] : -138.4 [m, $CH_2(CF_2)_2CF_2CF_2H$]; -131.5 [m, $CH_2CF_2CF_2(CF_2)_2H$]; -127.1[m, $CH_2CF_2(CF_2)_3H$]; -122.7 [m, $CH_2(CF_2)_3CF_2H$].

IR data (NaCl plates, liquid film, cm^{-1}) : 1466, 1248, 1189, 1127, 1073, 1044, 974, 895, 812, 756, 644, 604.

4.6.5 Preparation of Tributyltin Fluoroethoxide - $Bu_3SnOCH_2CH_2F$ (18)

The synthetic method for (17) was followed using bis(tributyltin) oxide (16.69 g, 28 mmol) and a slight excess of 2-fluoroethanol (4.91 g, 77 mmol). A colourless oil was obtained (15.70 g, 79%), b.p. 130°C/1.0 mm.

Analysis : Found (calc. for $C_{14}H_{31}FOSn$) : C 47.7 (47.6)%; H 8.89 (8.87)%.

Mössbauer data ($mm\ s^{-1}$) : IS = 1.28; QS = 2.38.

^{119}Sn nmr [δ(ppm), $CDCl_3$ soln] : 114.2.

^{1}H nmr [δ(ppm), $CDCl_3$ soln] : 0.92 [9H, t, $CH_3(CH_2)_3$], $^{3}J(^{1}H\text{-}^{1}H)$ = 7 Hz; 1.15 [6H, m, C_4H_9]; 1.34 [6H, m, C_4H_9]; 1.61 [6H, m, C_4H_9]; 3.90 [2H, dt, CH_2CH_2F], $^{3}J(^{1}H\text{-}^{19}F)$ =

30 Hz, $^{3}J(^{1}H\text{-}^{1}H)$ = 4 Hz; 4.45 [2H, dt, CH_2CH_2F], $^{2}J(^{1}H\text{-}^{19}F)$ = 48 Hz, $^{3}J(^{1}H\text{-}^{1}H)$ = 4 Hz.

^{13}C nmr [δ(ppm), $CDCl_3$ soln] : 13.4 [$CH_3(CH_2)_3$]; 14.6 [$CH_3(CH_2)_2CH_2$]; 27.0 [$CH_3CH_2(CH_2)_2$]; 27.7 [$CH_3CH_2CH_2CH_2$]; 65.2 [CH_2CH_2F]; 85.6 [CH_2CH_2F]. $^{1}J(^{13}C\text{-}^{119}Sn)$ = 347 Hz.

^{19}F nmr [δ(ppm), $CDCl_3$ soln] : -75.6 [CH_2CH_2F].

IR data (NaCl plates, liquid film, cm^{-1}) : 1464, 1418, 1377, 1364, 1341, 1121, 1074, 1015, 895, 858, 770, 689, 596.

Conclusions

5 CONCLUSIONS

Three classes of fluorinated organotin compounds have been investigated as potential single source precursors for the CVD of fluorine-doped tin oxide. Compounds synthesised have been fully characterised and CVD deposition experiments have been conducted in order to assess their suitability. These conclusions aim to compare and contrast the three classes of compound prepared in Chapters Two to Four and identify the major points discovered. Selected results from the CVD experiments are collected in Table 5.1, which represent the best results obtained from each class.

In terms of the ease of preparation, cost, and handling, the triorganotin carboxylates were extremely favourable. The starting materials were readily available at low cost and syntheses succeeded in relatively high yield, which enabled facile production of sufficient quantities for adequate CVD testing. The only drawback of the carboxylates was that they were all solids which lowered their volatility.

On the other hand, both the perfluoroalkyltin compounds and the organotin alkoxides were found to involve some synthetic difficulties. The perfluoroalkyltin compounds were very difficult to prepare, with long synthetic methods and very low yields. Starting materials were also very expensive which made the production of sufficient quantities for subsequent CVD testing a difficult task. However, once obtained, the compounds were all liquids and very stable which were attractive properties for CVD in terms of volatility and ease of handling. The organotin alkoxides were relatively simple to prepare and yields were very high so large quantities could be obtained comparatively easily. However, the alkoxides were sensitive to moisture which created some handling difficulties.

In terms of the CVD testing itself, all compounds were found to produce tin oxide films without the need for excessive bubbler temperatures. Therefore, the solid carboxylates did not present any insuperable problems in terms of volatility, and good transport in the vapour phase could be achieved. All films were found to adhere well to

the glass substrate and could not be removed easily. One major discovery was that compounds containing small R groups (*e.g.* ethyl) achieved films of a superior uniformity and run times were significantly reduced. However, precursors containing methyl or ethyl as the R group have a higher degree of toxicity and are also more expensive to prepare. Compounds containing more fluorinated ligands were also found to be more volatile due to the weaker intermolecular interactions caused by the minimising of dipole-dipole interactions between molecules.

In terms of the quality of the films produced, a large variation was found in the three classes of precursors investigated. Table 5.1 shows selected results from the film analysis in order for direct comparisons to be made.

Table 5.1 Selected Film Analysis of Fluorine-Doped Tin Oxide Films from Fluorinated Organotin Precursors

PRECURSOR	**(1)**	**(6)**	**(12)**	**(17)**	**(18)**	**Std.**[a]
Thickness (Å)	3795	3600	2935	2910	2410	3000
Haze (%)	0.64	0.56	0.28	0.61	0.42	< 0.40
Emissivity	0.220	0.147	0.304	0.889	0.358	< 0.150
Sheet Resistance	22	13	39	220	54	15
Resistivity ($\times 10^{-3}$ Ω cm)	0.85	0.46	1.13	6.40	1.30	0.50
Fluorine Content (atom%)	1.48	1.02	4.80	0.14	1.52	2.00

[a] Typical measurements for a good fluorine-doped tin oxide film derived from separate tin and fluorine sources.

Overall, the triorganotin carboxylates were the best group of precursors in terms of the quality of the films deposited. $Bu_3SnO_2CCF_3$ (**6**) is a representative sample which produced a fluorine-doped tin oxide film with properties rivalling those obtained from dual source methods.

Reasonable success was achieved in the attempt to produce films of the target 3000 Å when sufficient quantities of material were available. In general, thickness fluctuations resulted in a variation in the film properties as expected. Thicker coatings exhibited better resistivity and emissivity, but resulted in a deterioration in haze. Thin films displayed the exact opposite, with films of the target 3000 Å producing the best overall set of properties without the significant deterioration in any specific characteristic.

All perfluoroalkyltin compounds and fluorinated organotin carboxylates produced fluorine-doped tin oxide films thus achieving the project objective. The fluorinated organotin alkoxides were not as successful, with very low fluorine incorporation achieved from most precursors tried. $Bu_3SnOCH_2(CF_2)_3CF_2H$ (**17**) is a representative sample in which very little fluorine was measured and which thus resulted in very poor film properties. The film deposited from $Bu_3SnOCH_2CH_2F$ (**18**) exhibited the best properties but was atypical of the alkoxide group.

In general, relatively low levels of fluorine incorporation were found from the single source precursors. The one diorganotin carboxylate tried, $Me_2Sn(O_2CCF_3)_2$ (**12**) was found to achieve a much higher dopant level (4.8 atom%) but this high level was not found to enhance the film properties. All other precursors achieved much lower fluorine levels of around 1 atom% which suggests that fluorine transfer was not facile in the harsh CVD conditions of ≈ 560°C. The fact that the properties of the films deposited from the triorganotin carboxylates rivalled those of a film grown by dual source methods suggests that the single source precursors achieved a higher level of *active fluorine*. It appears that the triorganotin carboxylates were capable of depositing films exhibiting the same properties but containing half as much fluorine.

A significant discovery was that additional fluorine loading on the precursor did not generally lead to an increase in the resultant fluorine found in the tin oxide film. Longer fluorinated chains on the ligand appeared to have minimal effect on the quantity of fluorine transferred to the tin during the CVD process. This suggests that there was one carbon in the ligand from which all the fluorine was transferred. Considering that

the same level of fluorine was achieved from $Bu_3SnO_2CCF_3$ (**6**) as $Bu_3SnO_2CC_3F_7$ (**8**), it can be suggested that only the first fluorine-bearing carbon was an effective location.

Overall, very encouraging results were obtained from the fluorinated organotin compounds, as it proved that it was possible to achieve a fluorine-doped tin oxide film from a single source precursor. Particular success was achieved from the triorganotin carboxylates which produced films with properties rivalling those for a film grown from dual source methods. From all the results obtained, it appears that the best arrangement for a single source precursor is a triorganotin carboxylate with a short fluorinated carboxylate ligand. To enable short run times and superior film uniformity, small alkyl groups such as methyl or ethyl should be incorporated.

Further work could serve to improve the quality of the films produced from the three classes of compound tried. It must be noted that the CVD testing performed in this study was merely for screening purposes, and significant improvements could be possible with more thorough testing to optimise the deposition conditions. Additional research into the potential of the organotin alkoxides could be performed in an attempt to locate a position on the precursor which would lead to effective fluorine transfer. As mentioned in Chapter Four, two interesting compounds would be $R_3SnOC(CF_3)_3$ and $Sn(OR_f)_4$ as they consist of very different arrangements to the compounds tested in this study. Also, due to the encouraging results obtained from the alkoxide containing a single fluorine atom $Bu_3SnOCH_2CH_2F$ (**18**), it could be interesting to try a similar fluorine arrangement on a successful precursor such as a carboxylate or a perfluoroalkyltin compound.

A very interesting possibility could be the testing of a precursor which already contains a Sn-F bond to see if it is maintained during the CVD process, and lead to a film with a very high fluorine content. However, volatility problems could be encountered with such compounds as tin fluorides generally exhibit very high melting points due to their tendency to polymerise. An example of a possible precursor of this nature could be $Bu_2[Me_2N(CH_2)_3]SnF$ which would be expected to form a five coordinate tin atom due to interaction between the tin and the nitrogen atom of the amine ligand. Such an arrangement could prevent polymerisation and hence improve the volatility.

Other further work could be the synthesis and testing of new classes of precursors, for example organotin β-diketonates.

Appendices

APPENDIX ONE

Starting Materials

Organotin Reagents

Tributyltin chloride, dibutyltin dichloride, dimethyltin dichloride and bis(tributyltin) oxide were purchased from Aldrich and used without further purification. Butyltin trichloride and triethyltin chloride were prepared according to literature methods,[292] in which the appropriate tetraorganotin is initially synthesised and subsequently reacted with tin tetrachloride in the appropriate ratio (Equations A.1 - A.3).

$$RBr + Mg \longrightarrow RMgBr \qquad [A.1]$$

$$4RMgBr + SnCl_4 \longrightarrow R_4Sn \qquad [A.2]$$

$$(4\text{-}n)R_4Sn + nSnCl_4 \longrightarrow R_{(4-n)}SnCl_n \qquad [A.3]$$

Fluorinated Reagents

Fluorinated iodides were purchased from Aldrich and distilled prior to use. Sodium trifluoroacetate, pentadecafluorooctanoic acid, trifluoroacetic anhydride and all fluorinated alcohols were also purchased from Aldrich and used without further purification. Sodium pentafluoropropionate and sodium heptafluorobutyrate were purchased from Fluorochem and used without further purification.

Other Reagents and Solvents

Isopropyl chloride, magnesium turnings and sodium hydride were purchased from Aldrich. Diethyl ether and toluene were distilled over sodium/benzophenone prior to use. Ethanol was used without distillation.

APPENDIX TWO

Crystallographic Analysis and Structural Refinement of $Et_3SnO_2CC_2F_5$ (10)

A crystal of approximate dimensions 0.2 x 0.2 x 0.2 mm was used for data collection.

Crystal data: $C_9H_{15}F_6O_2Sn$, $M = 368.9$, monoclinic, $a = 8.057(1)$, $b=10.406(2)$, $c = 16.254(3)$Å, $\beta = 99.65(1)^{\circ}$, $U = 1343.5$ Å^3, space group $P2_1/c$, $Z = 4$, $D_c = 1.82$ gcm^{-3}, (μMo-K_α) = 1.95 mm^{-1}, $F(000) = 720$. Crystallographic measurements were made at 170° K on a CAD4 automatic four-circle diffractometer in the range $2\leq\theta\leq24°$. Data (2100 reflections) were corrected for Lorentz and polarization and also for absorption.[301] (Max. and Min absorption corrections; 0.839, 0.434 respectively).

In the final least squares cycles all atoms were allowed to vibrate anisotropically. Hydrogen atoms were included at calculated positions where relevant.

Examination of the lattice structure revealed that it is dominated by linear polymers along the *b* axis. Typically, Sn1 of the molecule as presented bonds to O2 of the lattice neighbour generated via the symmetry operator *-x 0.5+y,0.5-z*, effectively completing the slightly distorted trigonal bypyramidal geometry about the metal atom.

The solution of the structure (SHELX86)[302] and refinement (SHELX93)[303] converged to a conventional [i.e. based on 1504 reflections with $F_o>4\sigma(F_o)$] $R1=0.0369$ and $wR2=0.0923$. Goodness of fit = 1.033. The max. and min. residual densities were 0.70 and -0.84Å^{-3} respectively. The asymmetric unit (shown in Fig. 3.12), along with the labelling scheme used was produced using ORTEX.[304] Final fractional atomic co-ordinates and isotropic thermal parameters, bond distances and angles are given in Tables A2.2 and A2.3 respectively. Tables of anisotropic temperature factors are available as supplementary data.

Table A2.1 Crystal Data and Structure Refinement for (**10**)

Identification code	95KCM2
Empirical formula	$C_9 H_{15} F_5 O_2 Sn$
Formula weight	368.90
Temperature	170(2)° *K*
Wavelength	0.70930 Å
Crystal system	Monoclinic
Space group	$P2_1/c$
Unit cell dimensions	a = 8.0570(10)Å α= 90°
	b = 10.406(2)Å β= 99.65(1)°
	c = 16.254(3)Å γ= 90°
Volume	1343.5(4) $Å^3$
Z	4
Density (calculated)	1.824 Mg/m^3
Absorption coefficient	1.949 mm^{-1}
F(000)	720
Crystal size	2.0 x 2.0 x 5.0 mm
Theta range for data collection	2.33 to 23.94 deg.
Index ranges	0<=h<=9; -11<=k<=0; -18<=l<=18
Reflections collected	2263
Independent reflections	2100 [R(int) = 0.0650]
Absorption correction	DIFABS
Max. and min. transmission	0.839 and 0.434
Refinement method	Full-matrix least-squares on F
Data / restraints / parameters	2100 / 0 / 158
Goodness-of-fit on F2	1.033
Final R indices [I>2sigma(I)]	$R1$ = 0.0369 w$R2$ = 0.0923
R indices (all data)	$R1$ = 0.0656 w$R2$ = 0.0992
Largest diff. peak and hole	0.701 and -0.842 $e.Å^{-3}$
Weighting scheme	calc w=1/[σ2(Fo^2)+(0.0661P)^2+0.0000P] where P=(Fo^2+2Fc^2)/3
Extinction coefficient	0.0000(4)
Extinction expression	Fc^*=kFc[1+0.001x$Fc^2\lambda^3$/sin(2θ)]$^{-1/4}$

Table A2.2 Atomic Coordinates (x 10^4) and Equivalent Isotropic Displacement Parameters ($Å^2$ x 10^3) for (10).

U(eq) is defined as one third of the trace of the orthogonalized Uij tensor.

Atom	**x**	**y**	**z**	**U(eq)**
Sn(1)	344(1)	125(1)	2062(1)	26(1)
F(1)	226(5)	-3651(3)	234(2)	46(1)
F(2)	1521(5)	-4788(3)	1267(2)	43(1)
F(3)	3576(6)	-4402(4)	243(3)	57(1)
F(4)	4293(5)	-3150(4)	1299(3)	57(1)
F(5)	3063(6)	-2381(4)	123(3)	54(1)
O(1)	1138(6)	-1461(4)	1303(3)	32(1)
O(2)	414(6)	-2970(4)	2162(3)	36(1)
C(1)	2092(8)	-286(6)	3157(4)	37(1)
C(2)	3687(10)	-988(7)	3059(5)	51(2)
C(3)	-2270(8)	-362(7)	1822(5)	42(2)
C(4)	-2881(10)	-727(8)	917(5)	60(2)
C(5)	1095(9)	1470(6)	1217(5)	43(2)
C(6)	2964(11)	1650(9)	1293(6)	70(3)
C(7)	941(8)	-2624(5)	1533(4)	27(1)
C(8)	1442(8)	-3616(5)	921(4)	31(1)
C(9)	3115(10)	-3384(6)	639(5)	43(2)

Table A2.3 Bond Lengths [Å] and Angles [deg] for (**10**)

Sn(1)-C(5)	2.119(6)	C(5)-Sn(1)-O(2)#1	85.6(2)
Sn(1)-C(1)	2.119(6)	C(1)-Sn(1)-O(2)#1	85.4(2)
Sn(1)-C(3)	2.137(7)	C(3)-Sn(1)-O(2)#1	87.9(2)
Sn(1)-O(1)	2.218(4)	O(1)-Sn(1)-O(2)#1	174.93(14)
Sn(1)-O(2)#1	2.481(4)	C(7)-O(1)-Sn(1)	118.5(4)
F(1)-C(8)	1.358(7)	C(7)-O(2)-Sn(1)#2	144.0(4)
F(2)-C(8)	1.340(7)	C(2)-C(1)-Sn(1)	117.8(5)
F(3)-C(9)	1.325(7)	C(4)-C(3)-Sn(1)	112.7(5)
F(4)-C(9)	1.330(8)	C(6)-C(5)-Sn(1)	114.9(5)
F(5)-C(9)	1.335(8)	O(2)-C(7)-O(1)	126.7(5)
O(1)-C(7)	1.284(7)	O(2)-C(7)-C(8)	120.6(5)
O(2)-C(7)	1.224(7)	O(1)-C(7)-C(8)	112.8(5)
O(2)-Sn(1)#2	2.481(4)	F(2)-C(8)-F(1)	107.3(5)
C(1)-C(2)	1.510(10)	F(2)-C(8)-C(9)	106.8(5)
C(3)-C(4)	1.519(10)	F(1)-C(8)-C(9)	108.2(5)
C(5)-C(6)	1.502(11)	F(2)-C(8)-C(7)	109.9(5)
C(7)-C(8)	1.533(8)	F(1)-C(8)-C(7)	108.7(5)
C(8)-C(9)	1.514(10)	C(9)-C(8)-C(7)	115.7(5)
		F(3)-C(9)-F(4)	108.6(6)
C(5)-Sn(1)-C(1)	117.1(3)	F(3)-C(9)-F(5)	107.5(5)
C(5)-Sn(1)-C(3)	114.7(3)	F(4)-C(9)-F(5)	107.9(6)
C(1)-Sn(1)-C(3)	127.0(3)	F(3)-C(9)-C(8)	110.9(6)
C(5)-Sn(1)-O(1)	89.5(2)	F(4)-C(9)-C(8)	109.6(5)
C(1)-Sn(1)-O(1)	96.0(2)	F(5)-C(9)-C(8)	112.3(6)
C(3)-Sn(1)-O(1)	95.1(2)		

Symmetry transformations used to generate equivalent atoms:

#1 -x,y+1/2,-z+1/2 #2 -x,y-1/2,-z+1/2

Table A2.4 Anisotropic Displacement Parameters ($Å^2$ x 10^3) for (**10**).

The anisotropic displacement factor exponent takes the form:

$$-2\,pi^2\,[\,h^2\,a^*\,2\,U_{11} + ... + 2\,h\,k\,a^*\,b^*\,U_{12}\,]$$

Atom	U_{11}	U_{22}	U_{33}	U_{23}	U_{13}	U_{12}
Sn(1)	26(1)	27(1)	27(1)	0(1)	5(1)	0(1)
F(1)	47(3)	40(2)	45(3)	-11(2)	-6(2)	3(2)
F(2)	66(3)	29(2)	37(2)	5(2)	13(2)	7(2)
F(3)	68(3)	58(2)	50(3)	-6(2)	25(2)	22(2)
F(4)	37(3)	81(3)	54(3)	-9(2)	7(2)	9(2)
F(5)	62(3)	55(2)	54(3)	9(2)	30(2)	6(2)
O(1)	38(3)	28(2)	32(3)	1(2)	7(2)	1(2)
O(2)	46(3)	27(2)	37(3)	2(2)	12(2)	0(2)
C(1)	38(4)	37(3)	35(4)	3(3)	2(3)	2(3)
C(2)	50(5)	53(4)	42(4)	-3(3)	-12(4)	13(3)
C(3)	30(4)	49(4)	46(4)	-5(3)	6(3)	3(3)
C(4)	41(5)	73(5)	62(6)	-6(4)	-2(4)	-6(4)
C(5)	52(5)	36(3)	45(4)	2(3)	23(4)	-1(3)
C(6)	63(6)	88(6)	61(6)	3(5)	17(5)	-45(5)
C(7)	29(3)	31(3)	21(3)	-1(2)	0(3)	0(2)
C(8)	36(4)	33(3)	23(3)	0(2)	0(3)	6(3)
C(9)	46(5)	47(4)	38(4)	1(3)	13(4)	11(3)

Table A2.5 Hydrogen Coordinates (x 10^4) and Isotropic Displacement Parameters (A^2 x 10^3) for (**10**).

Atom	x	y	z	U(eq)
H(1A)	2410(8)	521(6)	3438(4)	45
H(1B)	1516(8)	-791(6)	3524(4)	45
H(2A)	4375(33)	-1098(47)	3596(6)	76
H(2B)	4293(36)	-498(27)	2706(28)	76
H(2C)	3407(10)	-1815(23)	2812(32)	76
H(3A)	-2466(8)	-1075(7)	2177(5)	50
H(3B)	-2920(8)	365(7)	1965(5)	50
H(4A)	-2726(70)	-14(21)	563(6)	90
H(4B)	-4054(20)	-947(56)	843(9)	90
H(4C)	-2250(51)	-1451(37)	773(12)	90
H(5A)	654(9)	1194(6)	653(5)	51
H(5B)	588(9)	2294(6)	1303(5)	51
H(6A)	3190(11)	2348(39)	942(30)	105
H(6B)	3462(15)	877(22)	1124(36)	105
H(6C)	3434(16)	1841(58)	1862(9)	105

APPENDIX THREE

Crystallographic Analysis and Structural Refinement of $Me_2Sn(O_2CCF_3)(OH_2)$ (13)

A crystal of approximate dimensions 0.2 x 0.2 x 0.2 mm was used for data collection.

Crystal data: $C_6 H_8 F_6 O_5 Sn$, M = 392.81, Monoclinic , a = 10.8330(10), b = 11.436(2), c = 10.893(2) Å , a = 90, b = 107.810(10), g = 90°, U = 1284.8(3) $Å^3$, space group $P2_1/n$, Z = 4, D_c = 2.031 gcm^{-3}, (mMo-K_a) = 2.072 mm^{-1}, F(000) = 752. Crystallographic measurements were made at 170(2)° K on a CAD4 automatic four-circle diffractometer in the range 2<q<23°. Data (1883 reflections) were corrected for Lorentz and polarization but not for absorption.

In the final least squares cycles all atoms were allowed to vibrate anisotropically. Hydrogen atoms were included at calculated positions where relevant, except for the bound water protons (H1A and H1B) which were located and refined at a fixed distance of 0.98Å from the parent atom, O5.

The supramolecular structure for this compound is dominated by polymeric sheets of molecules. Lattice neighbours which straddle inversion centres 'dimerise' as a consequence of hydrogen-bonding between O4 and H1B. Typically, H1B in the asymmetric as presented, interacts with O4 of the molecule generated via the transformation *1-x, -y, -z.* [H1B-O4, 1.79(3) Å; O5-H1B-O4, 165(5)°]

These 'dimers' are then interlinked, to form 2-dimensional sheets as a result of further intermolecular hydrogen-bonding between H1A and O2. In particular, H1A (as presented) bonds to O2 of the molecule generated by the symmetry transformation *0.5-x, -0.5+y, 0.5-z.* [H1A-O2, 1.74(3) Å; O5-H1A-O2, 171(6)°]

The solution of the structure (SHELX86)[302] and refinement (SHELX93)[303] converged to a conventional [i.e. based on 1547 with *Fo*>4s(*Fo*)] *R1* = 0.0231 and *wR2* = 0.0561. Goodness of fit = 1.147. The max. and min. residual densities were 0.854 and -0.452eÅ^{-3} respectively. The asymmetric unit (shown in Fig. 3.14), along with the labelling scheme used was produced using ORTEX.[304] Final fractional atomic co-ordinates and isotropic thermal parameters, bond distances and angles are given in Tables A3.2 and A3.3 respectively. Tables of anisotropic temperature factors are available as supplementary data.

Table A3.1 Crystal Data and Structure Refinement for (**13**)

Identification code	96KCM3
Empirical formula	$C_6 H_8 F_6 O_5 Sn$
Formula weight	392.81
Temperature	170(2)°K
Wavelength	0.70930 A
Crystal system	Monoclinic
Space group	$P2_1/n$
Unit cell dimensions	a = 10.833(1)Å
	b = 11.436(2)Å β= 107.81(1)°
	c = 10.893(2)Å
Volume	1284.8(3) $Å^3$
Z	4
Density (calculated)	2.031 Mg/m^3
Absorption coefficient	2.072 mm^{-1}
F(000)	752
Crystal size	0.2 x 0.2 x 0.2 mm
Theta range for data collection	2.32 to 22.93°
Index ranges	-11<=h<=0; -12<=k<=0; -11<=l<=11
Reflections collected	1883
Independent reflections	1777 [R(int) = 0.0259]
Refinement method	Full-matrix least-squares on F^2
Data / restraints / parameters	1777 / 2 / 174
Goodness-of-fit on F^2	1.147
Final R indices [I>2σ(I)]	R1 = 0.0231 wR2 = 0.0561
R indices (all data)	R1 = 0.0314 wR2 = 0.0605
Largest diff. peak and hole	0.854 and -0.452 $eÅ^{-3}$
Weighting scheme	calc $w=1/[\sigma^2(Fo^2)+(0.0279P)^2+3.2487P]$ where $P=(Fo^2+2Fc^2)/3$
Extinction coefficient	0.0039(4)
Extinction expression	$Fc^*=kFc[1+0.001xFc^2\lambda^3/\sin(2\theta)]^{-1/4}$

Table A3.2 Atomic Coordinates (x 10^4) and Equivalent Isotropic Displacement Parameters ($Å^2$ x 10^3) for (**13**).

U(eq) is defined as one third of the trace of the orthogonalized Uij tensor.

Atom	**x**	**y**	**z**	**U(eq)**
Sn(1)	2418(1)	825(1)	990(1)	18(1)
O(1)	666(3)	1797(2)	-93(3)	23(1)
O(2)	1075(3)	2888(2)	1677(3)	24(1)
O(3)	1839(3)	-130(3)	-718(3)	23(1)
O(4)	3680(3)	210(3)	-1175(3)	32(1)
O(5)	3998(3)	-514(3)	1553(3)	25(1)
F(1)	-1198(3)	3953(2)	746(3)	39(1)
F(2)	-1810(2)	2585(2)	-657(3)	41(1)
F(3)	-633(3)	3989(2)	-977(3)	40(1)
F(4)	2970(3)	-1303(4)	-3097(3)	76(1)
F(5)	1255(4)	-336(4)	-3516(3)	92(1)
F(6)	1375(4)	-1842(4)	-2448(4)	89(2)
C(1)	418(4)	2607(4)	595(4)	19(1)
C(2)	-830(4)	3289(4)	-70(4)	27(1)
C(3)	2616(4)	-233(4)	-1392(4)	24(1)
C(4)	2084(5)	-991(5)	-2586(5)	43(1)
C(5)	3758(4)	2156(4)	995(4)	26(1)
C(6)	1517(4)	36(4)	2230(4)	21(1)

Table A3.3 Bond Lengths [Å] and Angles [deg] for (**13**)

Sn(1)-O(3)	2.082(3)	O(3)-Sn(1)-O(5)	83.24(11)
Sn(1)-C(6)	2.098(4)	C(6)-Sn(1)-O(5)	89.80(14)
Sn(1)-C(5)	2.102(4)	C(5)-Sn(1)-O(5)	91.45(14)
Sn(1)-O(1)	2.205(3)	O(1)-Sn(1)-O(5)	162.35(11)
Sn(1)-O(5)	2.238(3)	C(1)-O(1)-Sn(1)	110.8(2)
O(1)-C(1)	1.271(5)	C(3)-O(3)-Sn(1)	119.3(3)
O(2)-C(1)	1.219(5)	O(2)-C(1)-O(1)	126.6(4)
O(3)-C(3)	1.280(5)	O(2)-C(1)-C(2)	119.5(4)
O(4)-C(3)	1.214(5)	O(1)-C(1)-C(2)	114.0(3)
F(1)-C(2)	1.320(5)	F(1)-C(2)-F(2)	108.1(4)
F(2)-C(2)	1.330(5)	F(1)-C(2)-F(3)	107.7(3)
F(3)-C(2)	1.338(5)	F(2)-C(2)-F(3)	106.9(3)
F(4)-C(4)	1.298(6)	F(1)-C(2)-C(1)	112.2(3)
F(5)-C(4)	1.355(7)	F(2)-C(2)-C(1)	112.1(3)
F(6)-C(4)	1.276(6)	F(3)-C(2)-C(1)	109.6(4)
C(1)-C(2)	1.537(6)	O(4)-C(3)-O(3)	126.9(4)
C(3)-C(4)	1.522(7)	O(4)-C(3)-C(4)	119.6(4)
		O(3)-C(3)-C(4)	113.5(4)
O(3)-Sn(1)-C(6)	106.12(14)	F(6)-C(4)-F(4)	113.0(5)
O(3)-Sn(1)-C(5)	113.7(2)	F(6)-C(4)-F(5)	103.0(5)
C(6)-Sn(1)-C(5)	140.1(2)	F(4)-C(4)-F(5)	103.8(4)
O(3)-Sn(1)-O(1)	79.15(11)	F(6)-C(4)-C(3)	114.7(4)
C(6)-Sn(1)-O(1)	93.86(14)	F(4)-C(4)-C(3)	112.7(4)
C(5)-Sn(1)-O(1)	96.71(14)	F(5)-C(4)-C(3)	108.4(5)

Table A3.4 Anisotropic Displacement Parameters ($Å^2 \times 10^3$) for (**13**).

The anisotropic displacement factor exponent takes the form:

$-2\ pi^2\ [\ h2\ a^*\ 2\ U11 + ... + 2\ h\ k\ a^*\ b^*\ U12\ ]$

Atom	**U11**	**U22**	**U33**	**U23**	**U13**	**U12**
Sn(1)	13(1)	20(1)	19(1)	0(1)	3(1)	-1(1)
O(1)	18(2)	25(2)	23(2)	-4(1)	1(1)	4(1)
O(2)	19(2)	23(2)	24(2)	-5(1)	0(1)	2(1)
O(3)	13(1)	32(2)	22(2)	-8(1)	6(1)	-1(1)
O(4)	20(2)	47(2)	31(2)	-4(2)	10(1)	-5(2)
O(5)	15(2)	31(2)	28(2)	9(1)	7(1)	4(1)
F(1)	30(1)	41(2)	42(2)	-10(1)	5(1)	14(1)
F(2)	19(1)	30(2)	58(2)	-6(1)	-9(1)	-1(1)
F(3)	39(2)	35(2)	39(2)	15(1)	2(1)	7(1)
F(4)	45(2)	123(3)	65(2)	-58(2)	28(2)	-7(2)
F(5)	82(3)	129(4)	42(2)	-20(2)	-16(2)	20(3)
F(6)	128(4)	84(3)	77(3)	-54(2)	64(3)	-67(3)
C(1)	16(2)	18(2)	23(2)	1(2)	3(2)	-2(2)
C(2)	23(2)	23(2)	30(3)	-5(2)	0(2)	0(2)
C(3)	17(2)	30(2)	24(2)	1(2)	5(2)	4(2)
C(4)	31(3)	68(4)	35(3)	-20(3)	18(3)	-10(3)
C(5)	21(2)	23(2)	33(3)	3(2)	7(2)	-4(2)
C(6)	15(2)	23(2)	24(2)	1(2)	6(2)	-2(2)

Table A3.5 Hydrogen Coordinates (x 10^4) and Isotropic Displacement Parameters ($Å^2$ x 10^3) for (**13**)

Atom	**x**	**y**	**z**	**U(eq)**
H(1A)	4065(53)	-1060(39)	2223(41)	51(16)
H(1B)	4814(32)	-306(44)	1529(47)	40(14)
H(5A)	4105(21)	2465(17)	1851(7)	39
H(5B)	3331(8)	2770(12)	419(21)	39
H(5C)	4450(15)	1843(7)	716(27)	39
H(6A)	1207(24)	630(4)	2686(20)	31
H(6B)	2130(8)	-453(19)	2837(17)	31
H(6C)	800(17)	-431(19)	1736(5)	31

APPENDIX FOUR

Instrumentation

Microanalysis

Carbon and hydrogen were analysed for using a Carlo-Erba Strumentazione E. A. mod 1106 microanalyser operating at 500°C. Results were calibrated against an acetanilide [$PhNHC(O)CH_3$] standard.

Infra-red Spectrometry

Infra-red spectra were recorded as nujol (liquid paraffin) mulls or liquid films between NaCl plates. Measurements were taken using a Nicolet 510P Fourier Transform spectrometer within the range 4000 - 600 cm^{-1} with a medium slit width and a peak resolution of 4.0 cm^{-1}.

Mössbauer Spectra

Mössbauer spectra were recorded on a Constant Acceleration Mössbauer Spectrometer (Cryophysics) fitted with a 10 mCi calcium metastannate-119m source (Amersham Int.) and operated in sawtooth mode. Spectra were run at 78K with liquid nitrogen as the cooling source. Samples were run as finely ground powders or frozen liquids. Isomer shifts are relative to SnO_2.

^1H and $^{13}C\{^1H\}$ Nuclear Magnetic Resonance Spectroscopy

Proton and carbon-13 NMR spectra were recorded using either Jeol JNM-GX-270FT (270 MHz) or Jeol EX-400 (400 MHz) Fourier Transform spectrometers using $SiMe_4$ as an internal reference.

^{19}F and ^{119}Sn Nuclear Magnetic Resonance Spectroscopy

Fluorine-19 and tin-119 NMR spectra were recorded on a Jeol EX400 (400 MHz) Fourier Transform spectrometer. Chemical shifts [$\delta(^{19}F)$] are relative to $CFCl_3$, and chemical shifts [$\delta(^{119}Sn)$] are relative to $SnMe_4$.

X-Ray Diffraction (XRD)

Samples of coating for XRD were of approximate dimensions 1.5 × 2.0 cm. The X-ray diffraction equipment consisted of a Philips PW1130 generator operating at 45 kV and 40 mA to power a copper long fine focus X-ray tube. A PW 1820 goniometer fitted with "thin film optics" and proportional X-ray detector was used. The non focusing thin film optics employed a ¼ degree primary beam slit to irradiate the specimen at a fixed incident angle of 1.5°. Diffraction radiation from the sample was collimated with a flat plate collimator and passed through a Graphite flat crystal monochromator to isolate diffracted Copper Kα peaks onto the detector. The equipment was situated in a total enclosure to provide radiation safety for the highly collimated narrow beams of X-rays. Data was acquired by a PW1710 microprocessor and processed using Philips APD VMS software on a Micro VAX computer. Crystalline phases were identified from the International Centre for Diffraction Data (ICDD) database held on CD-ROM. Crystallite size was determined from line broadening using the Scherrer equation. The instrumental effect was removed using the NIST SRM660 lanthanum hexaboride standard. These operating conditions were used in preference to conventional Bragg-Brentano optics for thin films to give an order of magnitude increases count rates from a fixed volume of coating with little contribution from the substrate.

Film Thickness

The thickness of the films were determined by etching a thin strip of the films with zinc powder and 50% HCl solution. This created a step in the film which was measured with a Dektak stylus technique.

Haze

A sample of coated glass approximately 3 cm × 3 cm was cleaned using iso-propanol and allowed to dry to remove dust from the surface of the glass, prior to analysis. The haze was then measured on a Pacific Scientific Hazeguard meter and the sample is measured with a barium fluoride detector. The calculation of haze is carried out by measurement of the specular light and diffusive light. The specular light is defined as light transmitted straight through the sample within ± 2.5° of normal incidence and the diffusive light is defined as light scattered beyond 2.5°. The initial measurement is carried out with the specular detector slot closed, and therefore a value for the sum of the specular light and the diffusive light is obtained. The specular light slot is then opened and a measurement of the diffusive light is obtained.

$$\% \text{ Haze} = [\text{Diffusive Light} / (\text{Diffusive} + \text{Specular Light})] \times 100$$

Emissivity

Initially, infra-red reflectance spectra were measured using a 2 beam Perkin Elmer 883 machine. The spectra were measured against a rhodium mirror standard. Emissivity data were then calculated from this infra-red reflectance spectra using the formula[305] :

$$Emissivity = 1 - \frac{\int_{5\mu}^{50\mu} R_\lambda P_\lambda d\lambda}{\int_{5\mu}^{50\mu} P_\lambda d\lambda}$$

i.e. Integral of total emittance between 5 and 50 μm divided by the integral from 5 - 50 μm of the total emittance of a blackbody at room temperature.

Sheet Resistance

Firstly, a scribed circle was made in the film to electrically isolate the area to be analysed. Sheet resistance was then measured with a four point probe and corrected using a conversion factor, the value being dependent on the diameter of the scribed circle.

Resistivity

Knowing the sheet resistance and the film thickness, the resistivity was determined by the following equation.

$$\text{Resistivity } (\Omega \text{ cm}) = \text{Sheet resistance } (\Omega/\square) \times \text{Thickness (cm)}$$

X-Ray Fluorescence (XRF)

The apparatus used for XRF was a Philips PW1400 machine fitted with a Scandium Target X-ray tube. The penetration depth achieved was between 9 and 10 microns, so the result obtained was throughout the thickness of the coating. The analysis was performed on approximately 1 square inch of material.

APPENDIX FIVE

CVD Reactor

The CVD apparatus used in this study has been assembled as a general screening rig for use with this and various other projects. The entire system consists of a horizontal cold wall reactor with associated gas lines and electrical heater controls. The reactor contains two separate systems, a heated bubbler assembly encased in an oven, and also ultrasonic nebuliser equipment. Screening tests for this project have exclusively utilised the heated bubbler assembly. A schematic of the relevant apparatus is shown in Figure A5.1. Detailed diagrams of the heated bubbler assembly and the CVD reactor are shown in Figures A5.2 and A5.3 respectively.

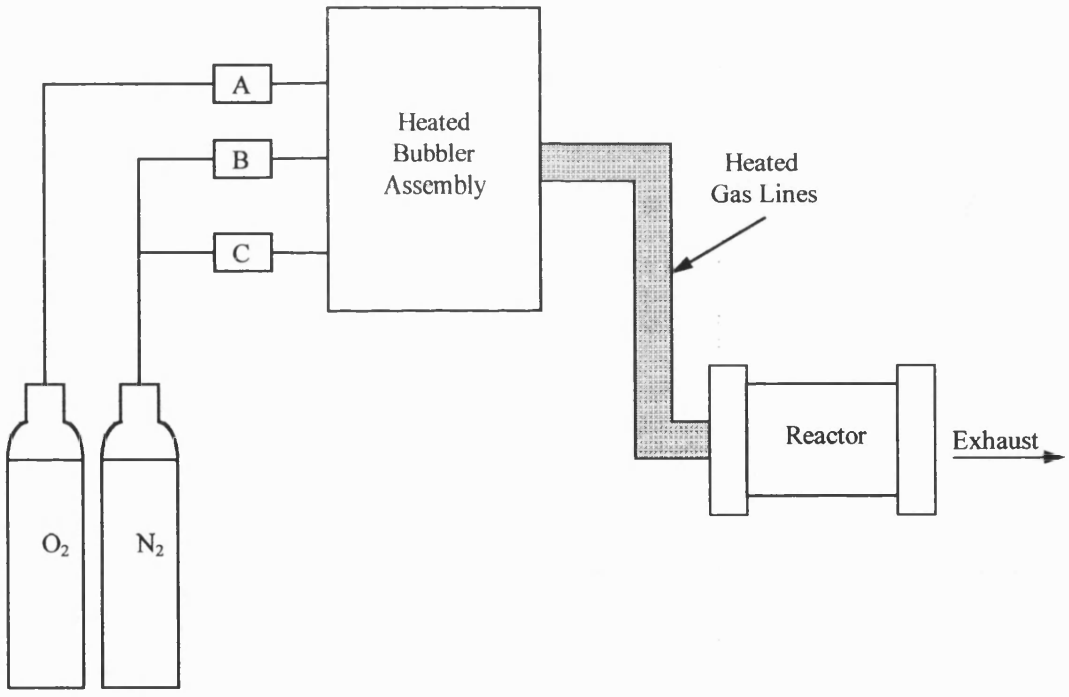

Figure A5.1 Schematic Representation of the CVD Reactor

A = Oxygen Flow Control, B = Diluent Flow Control, C = Carrier Flow Control.

The precursor was heated in a stainless steel bubbler which was encased in an oven. The temperature of the precursor could be measured accurately by a thermocouple which was positioned inside the bubbler. The pipework inside the oven contained a by-pass system which enabled the gas flows and temperatures to be set before the nitrogen carrier gas flow was turned to the bubbler to transport the vaporised precursor. A schematic of the bubbler assembly is shown in Figure A5.2.

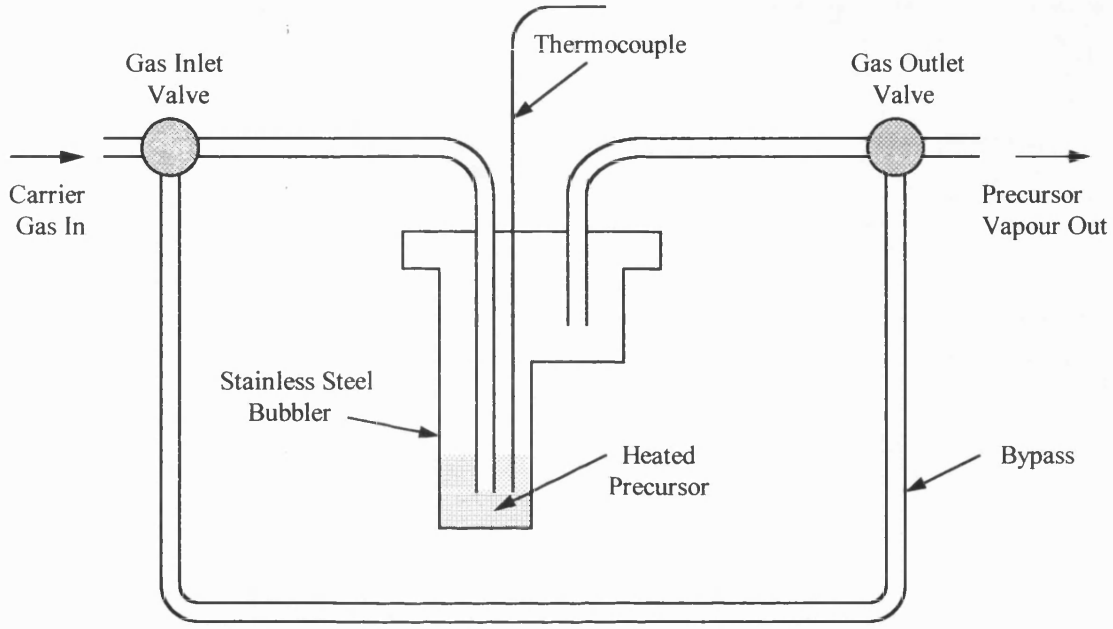

Figure A5.2 Schematic of the Bubbler Assembly

The bubbler was designed in such a way as to maximise the level of liquid contained. This prevented the need for vast quantities of precursor and made deposition experiments possible with relatively small quantities of material.

Following the turning of the valves to direct the gas flow to the bubbler, the precursor was swept from the bubbler and then mixed with nitrogen diluent and oxygen before being transported from the oven. The mixture was then transported along the heated external pipework to the CVD reactor. Before the vapour reached the CVD reactor, it passed through a baffle to promote laminar flow. A schematic of the reactor is shown in Figure A5.3.

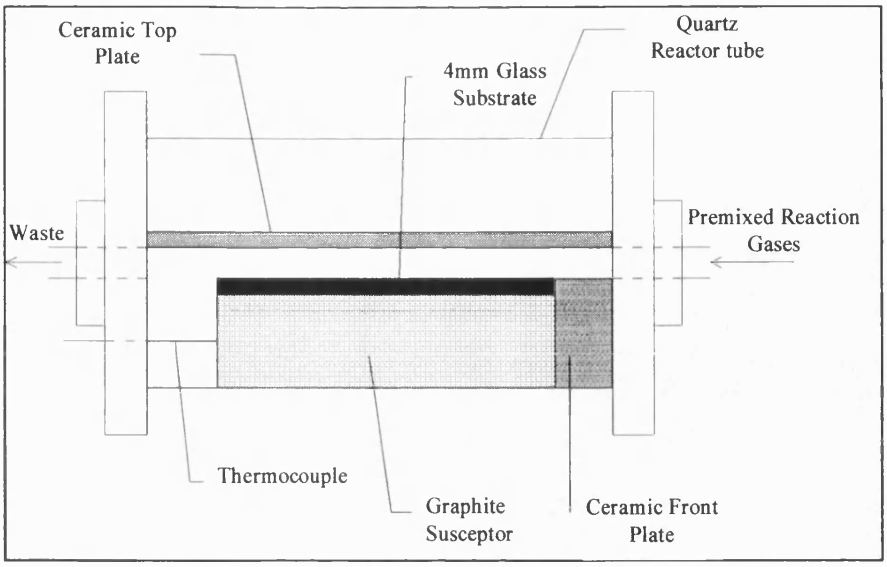

Figure A5.3 Schematic of the CVD Reactor Chamber

After passing through the baffle, the precursor vapour was passed directly into the reactor chamber which is 8 mm high, 40 mm wide and 300 mm long. The ceiling tile and walls consist of silica plates. The glass substrate is positioned upon a large graphite susceptor which is heated by three Watlow firerod cartridge heaters. The temperature of the graphite block is maintained by a Watlow series 965 controller which monitors the temperature by means of thermocouples positioned inside the block. The graphite susceptor is held inside a large silica tube (330 mm long, 100 mm diameter) suspended between stainless steel flanges upon which many of the electrical and gas line fittings are fixed. Air-tight seals are provided by "Viton" O-rings.

Substrate Preparation Procedure

All of the glass substrates were cleaned in an identical manner prior to use. The cleaning routine was as follows:

(i) The glass was washed thoroughly with tap water.

(ii) The glass was then washed thoroughly with copious amounts of distilled water.

(iii) The substrate was finally washed with a generous amount of isopropyl alcohol (IPA) and allowed to drain.

The glass was always prepared immediately prior to a deposition experiment to ensure as clean a substrate surface as possible. Following preparation and subsequent film deposition, the glass was handled very carefully and always outside of the deposition area.

Following the completion of the screening of each precursor, the bubbler and pipework were thoroughly cleaned to prevent unwanted contamination in films deposited from subsequent precursors.

APPENDIX SIX

Numerical Index of Compounds Prepared in this Thesis

(1) $Bu_3SnC_4F_9$

(2) $Bu_2Sn(C_4F_9)_2$

(3) $BuSn(C_4F_9)_3$

(4) $Bu_3SnC_6F_{13}$

(5) $Et_3SnC_4F_9$

(6) $Bu_3SnO_2CCF_3$

(7) $Bu_3SnO_2CC_2F_5$

(8) $Bu_3SnO_2CC_3F_7$

(9) $Et_3SnO_2CCF_3$

(10) $Et_3SnO_2CC_2F_5$

(11) $Bu_3SnO_2CC_7F_{15}$

(12) $Me_2Sn(O_2CCF_3)_2$

(13) $Me_2Sn(O_2CCF_3)_2(OH_2)$

(14) $Bu_3SnOCH(CF_3)_2$

(15) $Bu_3SnOCH_2CF_3$

(16) $Bu_3SnOCH_2C_2F_5$

(17) $Bu_3SnOCH_2(CF_2)_3CF_2H$

(18) $Bu_3SnOCH_2CH_2F$

References

REFERENCES

1. K. L. Chopra, S. Major and D. K. Pandya, *Thin Solid Films*, **102**, 1 (1983).
2. A. L. Dawar and J. C. Joshi, *J. Mater. Sci.*, **19**, 1 (1984).
3. B. G. Lewis and D. M. Moffatt, *Glass*, **4**, 537 (1996).
4. Z. M. Jarzebski and J. P. Marton, *J. Electrochem. Soc.*, **123**, 199C, 299C, 333C (1976).
5. I. I. Popova, M. G. Michailov, V. K. Gueorguiev and A. Shopov, *Thin Solid Films*, **186**, 107 (1990).
6. D. Fröhlich, R. Kenklies and R. Helbig, *Phys. Rev. Lett.*, **41**(25), 1750 (1978).
7. A. F. Carroll and L. H. Slack, *J. Electrochem. Soc.*, **123**, 1889 (1976).
8. Y-J Lin and C-J Wu, *Surf. Coat. Technol.*, **88**, 239 (1996).
9. T. D. Senguttuvan and L. K. Malhotra, *Thin Solid Films*, **289**, 22 (1996).
10. J. C. McAteer, *J. Chem. Soc., Faraday Trans.*, **75**, 2768 (1979).
11. Y. Takahashi and Y. Wada, *J. Electrochem. Soc.*, **137**(1), 267 (1990).
12. J. Kane, H. P. Schweizer and W. Kern, *J. Electrochem. Soc.*, **123**, 270 (1976).
13. T. P. Chow, M. Ghezzo and B. J. Baliga, *J. Electrochem. Soc.*, **129**, 1040 (1982).
14. S. R. Vishwakarma, J. P. Upadhyay and H. C. Prasad, *Thin Solid Films*, **176**, 99 (1989).
15. J. P. Upadhyay, S. R. Vishwakarma and H. C. Prasad, *Thin Solid Films*, **169**, 195 (1989).
16. D. J. Houlton, A. C. Jones, P.W. Haycock, E. W. Williams, J. Bull and G. W. Critchlow, *Chem. Vap. Deposition*, **1**(1), 26 (1995).
17. R. G. Egdell, A. Gulino, C. Rayden, G. Peacock and P. A. Cox, *J. Mater. Chem.*, **5**(3), 499 (1995).
18. M. Mizuhashi, Y. Gotoh and K. Adachi, *Jpn. J. Appl. Phys.*, **27**(11), 2053 (1988).
19. A. K. Saxena, R. Thangaraj, S. P. Singh and O. P. Agnihotri, *Bull. Mater. Sci.*, **8**(3), 315 (1986).

20. A. K. Saxena, R. Thangaraj, S. P. Singh and O. P. Agnihotri, *Thin Solid Films*, **131**, 121 (1985).

21. K. H. Yoon and J. S. Song, *Solar Energy Mater. Solar Cells*, **28**, 317 (1993).

22. H. L. Ma, D. H. Zhang, S. Z. Win, S. Y. Li and Y. P. Chen, *Solar Energy Mater. Solar Cells*, **40**, 371 (1996).

23. C. Tan, Y. Xia, Y. Chen, S. Li, J. Liu, X. Liu, B. Xu, J. Li and W. Cao, *J. Appl. Phys.* **73**(9), 4266 (1993).

24. T. Ishida, O. Tabata, J. Park, S. H. Shin, H. Magara, S. Tamura, S. Mochizuki and T. Mihara, *Thin Solid Films*, **281-282**, 228 (1996).

25. J. Proscia and R. G. Gordon, *Thin Solid Films*, **214**, 175 (1992).

26. T. Maruyama and K. Tabata, *J. Appl. Phys.*, **68**(8), 4282 (1990).

27. C. Agashe, B. R. Marathe, M. G. Takwale and V. G. Bhide, *Thin Solid Films*, **164**, 261 (1988).

28. D. R. Acosta, E. P. Zironi, E. Montoya and W. Estrada, *Thin Solid Films*, **288**, 1 (1996).

29. H. H. Afify, R. S. Momtaz, W. A. Badawy and S. A. Nasser, *J. Mater. Sci. Mater. in Electronics*, **2**, 40 (1991).

30. S. Major, M. C. Bhatnager, S. Kumar and K. L. Chopra, *J. Vac. Sci. Technol. A*, **6**(4), 2415 (1988).

31. A. K. Abass and M. T. Mohammad, *J. Appl. Phys.*, **59**(5), 1641 (1986).

32. C. Agashe and B. R. Marathe, *J. Phys.D: Appl. Phys.*, **26**, 2049 (1993).

33. C. Agashe, M. G. Takwale, B. R. Marathe and V. G. Bhide, *Solar Energy Mater.*, **17**, 99 (1988).

34. J. Bruneaux, H. Cachet, M. Froment and A. Messad, *Thin Solid Films*, **197**, 129 (1991).

35. J. P. Upadhyay, S. R. Vishwakarma and H. C. Prasad, *Thin Solid Films*, **167**, L7 (1988).

36. E. Shanthi, A. Banerjee, V. Dutta and K. L. Chopra, *J. Appl. Phys.*, **53**(3), 1615 (1982).

37. C. Agashe and S. S. Major, *J. Mater. Sci. Lett.*, **15**, 497 (1996).

38. P. Thilakan and J. Kumar, *Thin Solid Films*, **292**, 50 (1997).

39. J. C. C. Fan and J. B. Goodenough, *J. Appl. Phys.*, **48**(8), 3524 (1977).

40. W. T. Pawlewicz, I. B. Mann, W. H. Lowdermilk and D. Milam, *Appl. Phys. Lett.*, **34**(3), 196 (1979).

41. X. W. Sun, H. C. Huang and H. S. Kwok, *Appl. Phys. Lett.*, **68**(19), 2663 (1996).

42. T. J. Vink, M. H. F. Overwijk and W. Walrave, *J. Appl. Phys.*, **80**(7), 3734 (1996).

43. M. Rottmann, H. Hennig, B. Ziemer, R. Kalähne and K. H. Heckner, *J. Mater. Sci.*, **31**, 6495 (1996).

44. Y. Shigesato, S. Takaki and T. Haranoh, *J. Appl. Phys.*, **71**(7), 3356 (1992).

45. Y. Shigesato and D. C. Paine, *Appl. Phys. Lett.*, **62**(11), 1268 (1993).

46. R. Nomura, K. Konishi and H. Matsuda, *J. Electrochem. Soc.*, **138**, 631 (1991).

47. C. G. Granqvist, *Thin Solid Films*, **193**, 730 (1990).

48. B. Karlsson, E. Valkonen, T. Karlsson and C-G. Ribbing, *Thin Solid Films*, **86**, 91 (1981).

49. R. B. Nikodem, *J. Vac. Sci. Technol. A*, **10**(4), 1884 (1992).

50. B. Buffat, *J. De Physique IV*, **2**, C2-11 (1992).

51. P. F. Gerhardinger and R. J. McCurdy, *Mat. Res. Soc. Symp. Proc.*, **426**, 399 (1996).

52. D. J. Brinker, E. Y. Wang, W. H. Wadlin and R. N. Legge, *J. Electrochem. Soc.*, **128**, 1968 (1981).

53. S. K. Das and G. C. Morris, *J. Appl. Phys.*, **73**(2), 782 (1993).

54. R. Brendel, R. B. Bergmann, P. Lölgen, M. Wolf and J. H. Werner, *Appl. Phys. Lett.*, **70**(3), 390 (1997).

55. T. Takamoto, E. Ikeda, H. Kurita and M. Ohmori, *Appl. Phys. Lett.*, **70**(3), 381 (1997).

56. H. Pink, L. Treitinger and L. Vité, *Jpn. J. Appl. Phys.*, **19**(3), 513 (1980).

57. J. F. McAleer, P. T. Moseley, J. O. W. Norris, D. E. Williams and B. C. Tofield, *J. Chem. Soc., Faraday Trans. I*, **84**(2), 441 (1988).

58. N. Bârsan and A. Tomescu, *Thin Solid Films*, **259**, 91 (1995).

59. C. S. Rastomjee, R. S. Dale, R. J. Schaffer, F. H. Jones, R. G. Egdell, G. C. Georgiadis, M. J. Lee, T. J. Tate and L. L. Cao, *Thin Solid Films*, **279**, 98 (1996).

60. S. G. Ansari, S. W. Gosavi, S. A. Gangal, R. N. Karekar and R. C. Aiyer, *J. Mater. Sci. Mater in Electronics*, **8**, 23 (1997).

61. M. Ippommatsu and H Sasaki, *J. Electrochem. Soc.*, **136**, 2123 (1989).

62. T. Suzuki, T. Yamazaki, H. Yoshioka and K. Hikichi, *J. Mater. Sci.*, **23**, 1106 (1988).

63. T. W. Capehart and S. C. Chang, *J. Vac. Sci. Technol.*, **18**(2), 393 (1981).

64. M. Ando, S. Suto, T. Suzuki, T. Tsuchida, C. Nakayama, N. Miura and N. Yamazoe, *J. Mater. Chem.*, **4**(4), 631 (1994).

65. S-S Park and J. D. Mackenzie, *Thin Solid Films*, **274**, 154 (1996).

66. J. Zhang, B. K. Miremadi and K. Colbow, *J. Mater. Sci. Lett.*, **13**, 1048 (1994).

67. G. Hass, J. B. Heaney and A. R. Toft, *Appl. Optics*, **18**(10), 1488 (1979).

68. C. Tatsuyama and S. Ichimura, *Jpn. J. Appl. Phys.*, **15**, 843 (1976).

69. J. P. Fillard and J. C. Manifacier, *Jpn. J. Appl. Phys.*, **9**, 1012 (1970).

70. J. L. Vossen, *Physics of Thin Films*, **9**, 1 (1977).

71. K. K. Schuegraf, *Handbook of Thin-Film Deposition Processes and Techniques*, Noyes Publications (1988).

72. J. T. Spencer, *Progress in Inorganic Chemistry*, **41**, 145 (1994).

73. K. F. Jenson and W. Kern, *Thin Film Processes II*, Academic Press (1991).

74. M. J. Hampden-Smith and T. T. Kodas, *Chem. Vap. Deposition*, **1**(1), 8 (1995).

75. T. T. Kodas and M. J. Hampden-Smith, *The Chemistry of Metal CVD*, VCH, Weinheim (1994).

76. J. M. Blocher, *Thin Solid Films*, **77**, 51 (1981).

77. O. A. Harizanov, K. A. Gesheva and P. L. Stefchev, *Ceramics International*, **22**, 91 (1996).

78. M. Kojima, H. Kato, A. Imai and A. Yoshida, *J. Appl. Phys.*, **64**(4), 1902 (1988).

79. R. N. Ghoshtagore, *J. Electrochem. Soc.*, **125**, 110 (1978).

80. K. H. Kim and J. S. Chun, *Thin Solid Films*, **141**, 287 (1986).

81. G. Sanon, R. Rup and A. Mansingh, *Thin Solid Films*, **190**, 287 (1990).

82. K. Tokita and F. Okada, *J. Appl. Phys.*, **80**(12), 7073 (1996).

83. W. Kulisch, M. Witt, H. J. Frenck and R. Kassing, *Materials Science and Engineering A*, **140**, 715 (1991).

84. A. I. Ivashchenko, E. V. Karyaev, I. V. Khoroshun, G. A. Kiosse, V. T. Moshnyaga and P. A. Petrenco, *Thin Solid Films*, **263**, 122 (1995).

85. M. Di Giulio, D. Manno, G. Micocci, R. Rella, P. Siciliano and A. Tepore, *Solar Energy Mater. Solar Cells*, **31**, 235 (1993).

86. T. Minami, H. Nanto and S. Takata, *Jpn. J. Appl. Phys.*, **27**(3), L287 (1988).

87. T. K. S. Wong and W. K. Man, *Thin Solid Films*, **287**, 45 (1996).

88. C. Kaito and Y. Saito, *J. Crystal Growth*, **79**, 403 (1986).

89. W. M. Sears and M. A. Gee, *Thin Solid Films*, **165**, 265 (1988).

90. P. Grosse, F. J. Schmitte, G. Frank and H. Köstlin, *Thin Solid Films*, **90**, 309 (1982).

91. J. Sanz-Maudes and T. Rodríguez, *Thin Solid Films*, **69**, 183 (1980).

92. M. Miki-Yoshida and E. Andrade, *Thin Solid Films*, **224**, 87 (1993).

93. G. Gordillo, L. C. Moreno, W. de la Cruz and P. Teheran, *Thin Solid Films*, **252**, 61 (1994).

94. T. Karlsson, A. Roos and C-G. Ribbing, *Solar Energy Mater.*, **11**, 469 (1985).

95. S-S. Park and J. D. Mackenzie, *Thin Solid Films*, **258**, 268 (1995).

96. J. P. Chatelon, C. Terrier, E. Bernstein, R. Berjoan and J. A. Roger, *Thin Solid Films*, **247**, 162 (1994).

97. T. M. Racheva and G. W. Critchlow, *Thin Solid Films*, **292**, 299 (1997).

98. D. C. Bradley, *Chem. Rev.*, **89**, 1317 (1989).

99. F. Maury, *Chem. Vap. Deposition*, **2**(3), 113 (1996).

100. K. H. Yoon and J. S. Song, *Thin Solid Films*, **224**, 203 (1993).

101. A. Smith, J-M. Laurent, D. S. Smith, J-P. Bonnet and R. R. Clemante, *Thin Solid Films*, **266**, 20 (1995).

102. D. C. Bradley, *Polyhedron*, **13**(8), 1111 (1994).

103. L. M. Atagi and D. M. Hoffman, *Chem. Mater.*, **6**, 360 (1994).

104. C. G. Borman and R. G. Gordon, *J. Electrochem. Soc.*, **136**, 3820 (1989).

105. S. K. Ghandhi, R. Siviy and J. M. Borrego, *Appl. Phys. Lett.*, **34**(12), 833 (1979).

106. C. F. Wan, R. D. McGrath, W. F. Keenan and S. N. Frank, *J. Electrochem. Soc.*, **136**, 1459 (1989).

107. A. G. Zawadzki, C. J. Giunta and R. G. Gordon, *J. Phys. Chem.*, **96**, 5364 (1992).

108. C. J. Giunta, D. A. Strickler and R. G. Gordon, *J. Phys. Chem.*, **97**, 2275 (1993).

109. J. Kane, H. P. Schweizer and W. Kern, *J. Electrochem. Soc.*, **122**, 1144 (1975).

110. F. Caillard, A. Smith and J-F. Baumard, *Thin Solid Films*, **208**, 4 (1992).

111. I. Yagi, E. Ikeda and Y. Kuniya, *J. Mater. Res.*, **9**(3), 663 (1994).

112. T. Maruyama and T. Morishita, *Thin Solid Films*, **251**, 19 (1994).

113. T. Maruyama and Y. Ikuta, *Solar Energy Mater. Solar Cells*, **28**, 209 (1992).

114. D. Bélanger, J. P. Dodelet, B. A. Lombos and J. I. Dickson, *J. Electrochem. Soc.*, **132**, 1398 (1985).

115. S. Suh and D. M. Hoffman, *Inorg. Chem.*, **35**, 6164 (1996).

116. S. Suh, D. M. Hoffman, L. M. Atagi, D. C. Smith, J-R. Liu and W-K. Chu, *Chem. Mater.*, **9**, 730 (1997).

117. H. O. Pierson, *Handbook of Chemical Vapour Deposition*, Noyes Publications.

118. A. I. Ivahchenko, G. A. Kiosse, I. Y. Maronchuk, V. V. Popushoi and I. V. Khoroshun, *Inorganic Materials*, **30**, 801 (1994).

119. H. C. Clark, R. J. O'Brien and J. Trotter, *J. Chem. Soc. A*, 2332 (1964).

120. D. Tudela, E. Gutiérrez-Puebla and A. Monge, *J. Chem. Soc., Dalton Trans.*, 1069 (1992).

121. S. Calogero, P. Ganis, V. Peruzzo, G. Tagliavini and G. Valle, *J. Organomet. Chem.*, **220**, 11 (1981).

122. H. Reuter and H. Puff, *J. Organomet. Chem.*, **379**, 223 (1989).

123. S. S. Al-Juaid, S. M. Dhaher, C. Eaborn, P. B. Hitchcock and J. D. Smith, *J. Organomet. Chem.*, **325**, 117 (1987).

124. A. Miehr, O. Ambacher, W. Rieger, T. Metzger, E. Born and R. A. Fisher, *Chem. Vap. Deposition*, **2**(2), 51 (1996).

125. R. Nomura, K. Miyawaki, T. Toyosaki and H. Matsuda, *Chem. Vap. Deposition*, **2**(5), 174 (1996).

126. J. Cheon, D. S. Talaga and J. I. Zink, *J. Am. Chem. Soc.*, **119**, 163 (1997).

127. G. Shang, K. Kunze, M. J. Hampden-Smith and E. N. Duesler, *Chem. Vap. Deposition*, **2**(9), 242 (1996).

128. M. Bochmann, *Chem. Vap. Deposition*, **2**(3), 85 (1996).

129. P. O'Brien and R. Nomura, *J. Mater. Chem.*, **5**(11), 1761 (1995).

130. R. A. Baldwin, E. E. Foos, R. L. Wells, P. S. White, A. L. Rheingold and G. P. A. Yap, *Organometallics*, **15**, 5035 (1996).

131. P. Doppelt and T. H. Baum, *Chem. Mater.*, **7**(12), 2217 (1995).

132. S-G. Shyu, J-S. Wu, S-H. Chuang, K-M. Chi and Y-S. Sung, *J. Chem. Soc., Chem. Commun.*, 2239 (1996).

133. P. G. Harrison, *Chemistry of Tin*, Blackie (1989).

134. A. K. Sawyer, *Organotin Compounds*, (1972).

135. M. Pereyre, J-P. Quintard and A. Rahm, *Tin in Organic Synthesis*, Butterworths (1987).

136. A. G. Davies, *Organotin Chemistry*, Wiley-VCH (1997).

137. A. G. Davies and P. J. Smith, *Comprehensive Organometallic Chemistry*, 519, Pergamon Press (1982).

138. P. G. Harrison, *Comprehensive Coordination Chemistry*, Volume 3, 183, Pergamon Press (1987).

139. A. G. Davies, *Comprehensive Organometallic Chemistry*, Volume 2, 355 Pergamon Press (1994).

140. E. W. Abel, *Comprehensive Inorganic Chemistry*, Volume 2, 43, Pergamon Press (1975).

141. D. E. Goldberg, P. B. Hitchcock, M. F. Lappert, K. M. Thomas, A. J. Thorne, Fjeldberg, A. Haaland and B. E. R. Schilling, *J. Chem. Soc., Dalton Trans.*, 2387 (1986).

142. M. Weidenbruch, H. Kilian, M. Stürmann, S. Pohl, W. Saak, H. Marsmann, D. Steiner and A. Berndt, *J. Organomet. Chem.*, **530**, 255 (1997).

143. P. C. Chieh and J. Trotter, *J. Chem. Soc. A*, 911 (1970).

144. M. Bilayet Hossain, J. L. Lefferts, K. C. Molloy, D. Van der Helm and J. J. Zuckerman, *Inorganica Chimica Acta*, **36**, L409 (1979).

145. R. R. Holmes, S. Shafieezad, J. M. Holmes and R. O. Day, *Inorg. Chem.*, **27**, 1232 (1988).

146. W. A. Schenk, A. Khadra and C. Burschka, *J. Organomet. Chem.*, **468**, 75 (1994).

147. G. K. Sandhu, N. Sharma and E. R. T. Tiekink, *J. Organomet. Chem.*, **371**, C1 (1989).

148. D. V. Naik and W. R. Scheidt, *Inorg. Chem.*, **12**, 272 (1973).

149. P. G. Harrison and K. Molloy, *J. Organomet. Chem.*, **152**, 53 (1978).

150. S. S. Al-Juaid, M. Al.Rawi, C. Eaborn, P. B. Hitchcock and J. D. Smith, *J. Organomet. Chem.*, **446**, 161 (1993).

151. R. A. Howie, J-N. Ross and J. L. Wardell, *Acta Cryst.*, **C50**, 229 (1994).

152. R. A. Howie and J. L. Wardell, *Acta Cryst.*, **C52**, 1424 (1996).

153. J. S. Tse, M. J. Collins, F. L. Lee and E. J. Gabe, *J. Organomet. Chem.*, **310**, 169 (1986).

154. A. Rauk, L. C. Allen and K. Mislow, *J. Am. Chem. Soc.*, **94**, 3035 (1972).

155. R. Hoffman, J. M. Howell and E. L. Muetterties, *J. Am. Chem. Soc.*, **94**, 3047 (1972).

156. R. S. Berry, *J. Chem. Phys.*, **32**, 933 (1960).

157. P. G. Harrison, K. Lambert, T. J. King and B. Majee, *J. Chem. Soc., Dalton Trans.*, 363 (1983).

158. N. W. Alcock and R. E. Timms, *J. Chem. Soc. A*, 1873 (1968)

159. R. Hulme, *J. Chem. Soc.*, 1524 (1963).

160. V. G. Kumar Das, L K. Mun, C. Wei, S. J. Blunden and T. C. W. Mak, *J. Organomet. Chem.*, **322**, 163 (1987).

161. B. Salgado, E. Freijanes, A. Sánchex González, J. S. Casas, J. Sordo, U. Cassellato and R. Graziani, *Inorganica Chimica Acta*, **185**, 137 (1991).

162. D. Dakternieks, G. Dyson, K. Jurkschat, R. Tozer and E. R. T. Tiekink, *J. Organomet. Chem.*, **458**, 29 (1993).

163. E. G. Martinez, A. Sánchez Gonzalez, A. Macias, M. V. Castaño, J. S. Casas and J. Sordo, *J. Organomet. Chem.*, **385**, 329 (1990).

164. F. Caruso, D. Leonesi, F. Marchetti, E. Rivarola, M. Rossi, V. Tomov and C. Pettinari, *J. Organomet. Chem.*, **519**, 29 (1996).

165. E. O. Schlemper, *Inorg. Chem.*, **6**, 2012 (1967).

166. S. W. Ng, V. G. Kumar Das, B. W. Skelton and A. H. White, *J. Organomet. Chem.*, **377**, 221 (1989).

167. V. G. Kumar Das, L. K. Mun, C. Wei and T. C. W. Mak, *Organometallics*, **6**, 10 (1987).

168. B. K. Nicholson, *J. Organomet. Chem.*, **265**, 153 (1984).

169. J. S. Casas, E. E. Castellano, F. J. García Barros, A. Sánchez, A. Sánchez González, J. Sordo and J. Zukerman-Schpector, *J. Organomet. Chem.*, **519**, 209 (1996).

170. E. Kellö, V. Vrábel, J. Holecek and J. Sivý, *J. Organomet. Chem.*, **493**, 13 (1995).

171. R. Allmann, R. Hohlfeld, A. Waskowska and J. Lorberth, *J. Organomet. Chem.*, **192**, 353 (1980).

172. N. A. Alcock and J. F. Sawyer, *J. Chem. Soc., Dalton Trans.*, 1090 (1977).

173. E. Maslowsky, *Vibrational Spectra of Organometallic Compounds*, Wiley Interscience (1977).

174. J. E. Stewart, *Infrared Spectroscopy*, Marcel Dekker Inc. (1970).

175. S. A. Richards, *Laboratory Guide to Proton NMR Spectroscopy*, Blackwell Scientific Publications (1988).

176. F. W. Wehrli, A. P. Marchand and S. Wehrli, *Interpretation of Carbon 13-NMR Spectra*, John Wiley & Sons (1988).

177. R. H. Herber, *Chemical Mössbauer Spectroscopy*, Plenum Press (1984).

178. *The Mössbauer Effect and its Application in Chemistry*, Advances in Chemistry Series, American Chemical Society (1967).

179. R. V. Parish, *Progr. Inorg. Chem.*, **15**, 101 (1972).

180. J. J. Zuckerman, *Adv. Organomet. Chem.*, **9**, 21 (1970).

181. L. A. Hobbs and P. J. Smith, *J. Organomet. Chem.*, **206**, 59 (1981).

182. G. M. Bancroft, V. G. Kumar Das, T. K. Sham and M. G. Clark, *J. Chem. Soc. Chem. Commun.*, 236 (1974).

183. T. K. Sham and G. M. Bancroft, *Inorg. Chem.*, **14**, 2281 (1975).

184. R. K. Harris and B. E. Mann, *NMR and the Periodic Table*, Academic Press (1979).

185. J. Mason, *Multinuclear NMR*, Plenum Press (1987).

186. J. Holecek and A. Lycka, *Inorg. Chim. Acta*, **118**, L15 (1986).

187. T. P. Lockhart and W. F. Manders, *Inorg. Chem.*, **25**, 892 (1986).

188. H. C. Clark, N. Cyr and J. H. Tsai, *Can. J. Chem.*, **45**, 1073 (1967).

189. R. E. Banks, B. E. Smart and J. C. Tatlow, *Organofluorine Chemistry, Principles and Commercial Applications*, Plenum Press (1994).

190. T. Umemoto, *Chem. Rev.*, **96**, 1757 (1996).

191. J. L. Kiplinger, T. G. Richmond and C. E. Osterberg, *Chem. Rev.*, **94**, 373 (1994).

192. A. Vij, R. L. Kirchmeier, R. D. Willett and J. M. Shreeve, *Inorg. Chem.*, **33**, 5456 (1994).

193. S. H. Strauss, *Chem. Rev.*, **93**, 927 (1993).

194. H. D. Kaesz, J. R. Phillips and F. G. A. Stone, *J. Am. Chem. Soc.*, **82**, 6228 (1960).

195. W. R. Cullen, J. R. Sams and M. C. Waldman, *Inorg. Chem.*, **9**, 1682 (1970).

196. F. G. A. Stone and P. M. Treichel, *Chem. Ind.*, 837 (1960).

197. D. Seyferth and F. Richter, *J. Organomet. Chem.*, **499**, 131 (1995).

198. H. Uno, Y. Shiraishi and H. Suzuki, *Bull. Chem. Soc. Jpn.*, **62**, 2636 (1989).

199. H. C. Clark and C. J. Willis, *J. Am. Chem. Soc.*, **82**, 1888 (1960).

200. D. J. Burton and Z-Y. Yang, *Tetrahedron*, **48**, 189 (1992).

201. D. Seyferth, G. Raab and K. A. Brändle, *J. Org. Chem.*, **26**, 2934 (1961).

202. O. R. Pierce, A. F. Meiners and E. T. McBee, *J. Am. Chem. Soc.*, **75**, 2516 (1953).

203. H. Gilman, *J. Organomet. Chem.*, **100**, 83 (1975).

204. D. D. Denson, C. F. Smith and C. Tamborski, *J. Fluorine Chem.*, **3**, 247 (1973/74).

205. D. P. Curran and S. Hadida, *J. Am. Chem. Soc.*, **118**, 2531 (1996).

206. K. Kawakami and H. G. Kuivila, *J. Org. Chem.*, **34**, 1502 (1969).

207. J. Burdon, P. L. Coe, I. B. Haslock and R. L. Powell, *Chem. Commun*, 49 (1996).

208. L. J. Krause and J. A. Morrison, *J. Chem. Soc., Chem. Commun.*, 671 (1980).

209. T. Kitazume and N. Ishikawa, *Chem. Lett.*, 1337 (1981).

210. W. T. Miller and R. J. Burnard, *J. Am. Chem. Soc.*, **90**, 7367 (1968).

211. W. T. Miller, R. H. Snider and R. J. Hummel, *J. Am. Chem. Soc.*, **91**, 6532 (1969).

212. B. L. Dyatkin, B. I. Martynov, L. G. Martynova, N. G. Kizim, S. R. Sterlin, Z. A. Stumbrevichute and L. A. Fedorov, *J. Organomet. Chem.*, **57**, 423 (1973).

213. R. R. Burch and J. C. Calabrese, *J. Am. Chem. Soc.*, **108**, 5359 (1986).

214. R. V. Parish and R. H. Platt, *Chem. Commun.*, 1118 (1968).

215. R. V. Parish and R. H. Platt, *J. Chem. Soc.A*, 2145 (1969).

216. M. Nádvorník, J. Holecek, K. Handlír and A. Lycka, *J. Organomet. Chem.*, **275**, 43 (1984).

217. R. Eujen, N. Jahn and U. Thurmann, *J. Organomet. Chem.*, **465**, 153 (1994).

218. P. G. Harrison and D. Jollie, Unpublished Results.

219. G. B. Deacon and G. J. Farquharson, *J. Organomet. Chem.*, **135**, 73 (1977).

220. J. E. Connett and G. B. Deacon, *J. Chem. Soc. C*, 1058 (1966).

221. E. R. T. Tiekink, *Applied Organometallic Chemistry*, **5**, 1 (1991).

222. E. R. T. Tiekink, *Trends in Organometallic Chemistry*, **1**, 71 (1994).

223. R. O. Day, V. Chandrasekhar, K. C. Kumara Swamy, J. M. Holmes, S. D. Burton and R. R. Holmes, *Inorg. Chem.*, **27**, 2887 (1988).

224. R. R. Holmes, C. G. Schmid, V. Chandrasekhar, R. O. Day and J. M. Holmes, *J. Am. Chem. Soc.*, **109**, 1408 (1987).

225. V. Chandrasekhar, R. O. Day and R. R. Holmes, *Inorg. Chem.*, **24**, 1970 (1985).

226. V. Chandrasekhar, C. G. Schmid, S. D. Burton, J. M. Holmes, R. O. Day and R. R. Holmes, *Inorg. Chem.*, **26**, 1050 (1987).

227. T. Birchall and J. P. Johnson, *Can. J. Chem.*, **60**, 934 (1982).

228. F. E. Smith, R. C. Hynes, T. T. Ang, L. E. Khoo and G. Eng, *Can. J. Chem.*, **70**, 1114 (1992).

229. T. P. Lockhart, *Organometallics*, **7**, 1438 (1988).

230. D. W. Allen, I. W. Nowell, J. S. Brooks and R. W. Clarkson, *J. Organomet. Chem.*, **219**, 29 (1981).

231. V. B. Mokal, V. K. Jain and E. R. T. Tiekink, *J. Organomet. Chem.*, **431**, 283 (1992).

232. I. W. Nowell, J. S. Brooks, G. Beech and R. Hill, *J. Organomet. Chem.*, **244**, 119 (1983).

233. N. W. Alcock and S. M. Roe, *J. Chem. Soc., Dalton Trans.*, 1589 (1989).

234. E. R. T. Tiekink, M. Gielen, A. Bouhdid, M. Biesemans and R. Willem, *J. Organomet. Chem.*, **494**, 247 (1995).

235. T. P. Lockhart, W. F. Manders and E. M. Holt, *J. Am. Chem. Soc.*, **108**, 6611 (1986).

236. C. S. Parulekar, V. K. Jain, T. K. Das, A. R. Gupta, B. F. Hoskins and E. R. T. Tiekink, *J. Organomet. Chem.*, **372**, 193 (1989).

237. S-G. Teoh, S-H. Ang, E-S. Looi, C-A. Keok, S-B. Teo and H-K. Fun, *J. Organomet. Chem.*, **527**, 15 (1997).

238. T. S. Basu Baul and E. R. T. Tiekink, *Acta Cryst.*, **C52**, 1959 (1996).

239. F. Mistry, S. J. Rettig, J. Trotter and F. Aubke, *Acta Cryst.*, **C46**, 2091 (1990).

240. M. Gielen, M. Bouâlam and E. R. T. Tiekink, *Main Group Metal Chem.*, **16**, 251 (1993).

241. T. P. Lockhart and F. Davidson, *Organometallics*, **6**, 2471 (1987).

242. S. W. Ng, W. Chen, A. Zainudin, V. G. Kumar Das, W-H. Yip, R-J. Wang and T. C. W. Mak, *J. Cryst. Spectro. Res.*, **21**, 39 (1991).

243. C. D. Garner, B. Hughes and T. J. King, *J. Chem. Soc., Dalton Trans.*, 562 (1975).

244. T. P. Lockhart, J. C. Calabrese and F. Davidson, *Organometallics*, **6**, 2479 (1987).

245. A. Meriem, R. Willem, J. Meunier-Piret and M. Gielen, *Main Group Metal Chem.*, **12**, 187 (1989).

246. F. Huber, H. Preut, E. Hoffman and M. Gielen, *Acta Cryst.*, **C45**, 51 (1989).

247. J. F. Vollano, R. O. Day, D. N. Rau, V. Chandrasekhar and R. R. Holmes, *Inorg. Chem.*, **23**, 3153 (1984).

248. K. C. Molloy, T. G. Purcell, M. F. Mahon and E. Minshall, *Applied Organometallic Chemistry*, **1**, 507 (1987).

249. R. Willem, A. Bouhdid, M. Biesemans, J. C. Martins, D. de Vos, E. R. T. Tiekink and M. Gielen, *J. Organomet. Chem.*, **514**, 203 (1996).

250. M. Gielen, A. E. Khloufi, M. Biesemans, F. Kayser, R. Willem, B. Mahieu, D. Maes, J. N. Lisgarten, L. Wyns, A. Moreira, T. K. Chattopadhay and R. A. Palmer, *Organometallics*, **13**, 2849 (1994).

251. P. G. Harrison and R. C. Philips, *J. Organomet. Chem.*, **182**, 37 (1979).

252. E. J. Gabe, F. L. Lee, L. E. Khoo and F. E. Smith, *Inorg. Chim. Acta.*, **112**, 41 (1986).

253. S. W. Ng and V. G. Kumar Das, *Acta. Cryst.*, **C53**, 212 (1997).

254. R. R. Holmes, R. O. Day, V. Chandrasekhar, J. F. Vollano and J. M. Holmes, *Inorg. Chem.*, **25**, 2490 (1986).

255. S. W. Ng, K. L. Chin, C. Wei, V. G. Kumar Das and T. C. W. Mak, *J. Organomet. Chem.*, **365**, 207 (1989).

256. S. W. Ng and V. G. Kumar Das, *J. Organomet. Chem.*, **456**, 175 (1993).

257. S. W. Ng, V. G. Kumar Das, M. B. Hossain, F. Goerlitz and D. Van der Helm, *J. Organomet. Chem.*, **390**, 19 (1990).

258. A. Samuel-Lewis, P. J. Smith, J. H. Aupers, D. Hampson and D. C. Povey, *J. Organomet. Chem.*, **437**, 131 (1992).

259. U. Schubert, *J. Organomet. Chem.*, **155**, 285 (1978).

260. S. W. Ng and V. G. Kumar Das, *Acta. Cryst.*, **C49**, 754 (1993).

261. S. W. Ng, V. G. Kumar Das and E. R. T. Tiekink, *J. Organomet. Chem.*, **403**, 111 (1991).

262. S. W. Ng and V. G. Kumar Das, *Acta Cryst.*, **C53**, 548 (1997).

263. P. G. Harrison, K. Lambert, T. J. King and B. Majee, *J. Chem. Soc., Dalton Trans.*, 363 (1983)

264. S. W. Ng, C. Wei and V. G. Kumar Das, *J. Organomet. Chem.*, **345**, 59 (1988).

265. S-G. Teoh, E-S. Looi, S-B. Teo and S-W. Ng, *J. Organomet. Chem.*, **509**, 57 (1996).

266. K. C. Molloy, K. Quill and I. W. Nowell, *J. Chem. Soc., Dalton Trans.*, 101 (1987).

267. K. C. Molloy, S. J. Blunden and R. Hill, *J. Chem. Soc., Dalton Trans.*, 1259 (1988).

268. S. P. Narula, S. Kaur, R. Shankar, S. K. Bharadwaj and R. K. Chadha, *J. Organomet. Chem.*, **506**, 181 (1996).

269. Q. Xie, Z. Yang and L. Jiang, *Main Group Metal Chemistry*, **19**, 509 (1996).

270. Y. Maeda and R. Okawara, *J. Organomet. Chem.*, **10**, 247 (1967).

271. S. W. Ng, V. G. Kumar Das, F. Van Meurs, J. D. Schagen and L. H. Straver, *Acta Cryst.*, **C45**, 570 (1989).

272. P. J. Smith, R. O. Day, V. Chandrasekhar, J. M. Holmes and R. R. Holmes, *Inorg. Chem.*, **25**, 2495 (1986).

273. K. Ito and H. J. Bernstein, *Can. J. Chem.*, **34**, 170 (1956).

274. M. Kato, H. B. Jonassen and J. C. Fanning, *Chem. Rev.*, **64**, 99 (1964).

275. H. Koyama and Y. Saito, *Bull. Chem. Soc. Jpn.*, **27**, 113 (1954).

276. J. N. van Niekerk and F. R. L. Schoening, *Acta Cryst*, **6**, 227 (1953).

277. E. V. Van den Berghe, G. P. Van der Kelen and J. Albrecht, *Inorg. Chim. Acta*, **2**, 89 (1968).

278. Y. Maeda, C. R. Dillard and R. Okawara, *Inorg. Nucl. Chem. Letters*, **2**, 197 (1966).

279. C. Poder and J. R. Sams, *J. Organomet. Chem.*, **19**, 67 (1969).

280. H. Chih and B. R. Penfold, *J. Cryst. Mol. Struct.*, **3**, 285 (1973).

281. S. Holecek, M. Nádvorník, K. Handlír and M. A. Lycka, *J. Organomet. Chem.*, **315**, 299 (1986).

282. S. W. Ng, V. G. Kumar Das, W. H. Yip and T. C. W. Mak, *J. Cryst. Spectro. Res.*, **23**, 441 (1993).

283. D. C. Bradley, R. C. Mehrotra and D. P. Gaur, *Metal Alkoxides*, Academic Press (1978).

284. R. C. Mehrotra, A. Singh and S. Sogani, *Chem. Rev.*, **94**, 1643 (1994).

285. W. A. Herrmann, N. W. Huber and O. Runte, *Angew. Chem. Int. Ed. Engl.*, **34**, 2187 (1995).

286. C. D. Chandler, C. Roger and M. J. Hampden-Smith, *Chem. Rev.*, **93**, 1205 (1993).

287. U. Schubert, N. Hüsing and A. Lorenz, *Chem. Mater.*, **7**, 2010 (1995).

288. C. K. Narula, A. Varshney and U. Riaz, *Chem. Vap. Deposition*, **2**(1), 13 (1996).

289. J. A. Samuels, E. B. Lobkovsky, W. E. Streib, K. Folting, J. C. Huffman, J. W. Zwanziger and K. G. Caulton, *J. Am. Chem. Soc.*, **115**, 5093 (1993).

290. J. A. Samuels, K. Folting, J. C. Huffman and K. G. Caulton, *Chem. Mater.*, **7**, 929 (1995).

291. J. A. Samuels, W-C. Chiang, C-P. Yu, E. Apen, D. C. Smith, D. V. Baxter and K. G. Caulton, *Chem. Mater.*, **6**, 1684 (1994).

292. R. K. Ingham, S. D. Rosenberg and H. Gilman, *Chem. Rev.*, **60**, 459 (1960).

293. M. J. Hampden-Smith, T . A. Wark, A. Rheingold and J. C. Huffman, *Can. J. Chem.*, **69**, 121 (1991).

294. H. Reuter and D. Schröder, *J. Organomet. Chem.*, **455**, 83 (1993).

295. A. G. Davies, D. C. Kleinschmidt, P. R. Palan and S. C. Vasishtha, *J. Chem. Soc* (C), 3972 (1971).

296. D. P. Gaur, G. Srivastava and R. C. Mehrotra, *J. Organomet. Chem.*, **63**, 221 (1973).

297. M. Massol, J. Barrau, J. Satgé and B. Bouýssieres, *J. Organomet. Chem.*, **80**, 47 (1974).

298. J. D. Kennedy, W. McFarlane, P. J. Smith, R. F. M. White and L. Smith, *J. Chem. Soc., Perkin Trans. II*, 1785 (1973).

299. P. J. Smith, R. F. M. White and L. Smith, *J. Organomet. Chem.*, **40**, 341 (1972).

300. J. D. Kennedy, *J. Chem. Soc., Perkin Trans. II*, 242 (1977).

301. N. Walker and D. Stewart, *Acta Cryst.*, **A39**, 158 (1983).

302. G. M. Sheldrick, *Acta Cryst.*, **A46**, 467 (1990).

303. G. M. Sheldrick, *J. Appl.Cryst.*, 1995 (In Preparation).

304. P. McArdle, *J. Appl. Cryst.*, **27**, 438 (1994).

305. M. Bass, *Handbook of Optics Vol. 2 (2nd Edition)*, McGraw Hill Inc.(1995).